University of Alberta

Characterization of an Athabasca oil sand ore and process streams

©

by

Heather Anne Welling Kaminsky

A thesis submitted to the Faculty of Graduate Studies and Research
in partial fulfillment of the requirements for the degree of

Doctor of Philosophy
in
Materials Engineering

Department of Chemical and Materials Engineering

Edmonton, Alberta
Fall 2008

Library and
Archives Canada

Published Heritage
Branch

395 Wellington Street
Ottawa ON K1A 0N4
Canada

Bibliothèque et
Archives Canada

Direction du
Patrimoine de l'édition

395, rue Wellington
Ottawa ON K1A 0N4
Canada

Your file Votre référence
ISBN: 978-0-494-46342-0
Our file Notre référence
ISBN: 978-0-494-46342-0

NOTICE:
The author has granted a non-exclusive license allowing Library and Archives Canada to reproduce, publish, archive, preserve, conserve, communicate to the public by telecommunication or on the Internet, loan, distribute and sell theses worldwide, for commercial or non-commercial purposes, in microform, paper, electronic and/or any other formats.

The author retains copyright ownership and moral rights in this thesis. Neither the thesis nor substantial extracts from it may be printed or otherwise reproduced without the author's permission.

AVIS:
L'auteur a accordé une licence non exclusive permettant à la Bibliothèque et Archives Canada de reproduire, publier, archiver, sauvegarder, conserver, transmettre au public par télécommunication ou par l'Internet, prêter, distribuer et vendre des thèses partout dans le monde, à des fins commerciales ou autres, sur support microforme, papier, électronique et/ou autres formats.

L'auteur conserve la propriété du droit d'auteur et des droits moraux qui protège cette thèse. Ni la thèse ni des extraits substantiels de celle-ci ne doivent être imprimés ou autrement reproduits sans son autorisation.

In compliance with the Canadian Privacy Act some supporting forms may have been removed from this thesis.

While these forms may be included in the document page count, their removal does not represent any loss of content from the thesis.

Conformément à la loi canadienne sur la protection de la vie privée, quelques formulaires secondaires ont été enlevés de cette thèse.

Bien que ces formulaires aient inclus dans la pagination, il n'y aura aucun contenu manquant.

Canada

Portions of this thesis have been published in:

Kaminsky, H.A.W., Etsell, T. H., Ivey, D.G., & Omotoso, O. (2006). Fundamental Particle Size of Clay Minerals in Athabasca Oil Sands Tailings.*Clay Science 12* (supplement 2), 217–222

Kaminsky, H.A.W., Etsell, T.H., Ivey, D.G., & Omotoso, O. (2008). Characterization of heavy minerals in the Athabasca oil sands. *Minerals Engineering, 21*(4), 264-271.

Kaminsky, H.A.W., Etsell, T.H., Ivey, D.G., & Omotoso, O. (2008). Distribution of clay minerals in the process streams produced by the extraction of bitumen from Athabasca oil sands. *Canadian Journal of Chemical Engineering, in press.*

Abstract

The production of bitumen from oil sands via the hot water extraction process consumes a significant amount of water and produces a significant amount of mineral wastes. Understanding the mineralogy of each waste stream and how it derives from the parent ore is important in designing processes to mitigate both water consumption and waste production. Furthermore, an understanding of the mineralogy may help recover valuable mineral components such as zircon, ilmenite, and rutile from the waste streams.

This dissertation investigated a single ore and detailed how the minerals partitioned to the froth and tailings streams after batch extraction. Size separation, X-ray diffraction combined with quantification by the Rietveld method, and X-ray fluorescence analysis were used to provide a detailed breakdown of how minerals are affected by the hot water extraction process. Key results showed that the primary froth was enriched in chlorite, kaolinite, iron oxide-hydroxides, zircon, and titanium oxides compared with the other streams. On the other hand, the middlings stream was enriched in all the clay minerals, and especially in illite-smectite. Also of interest was the observation that the majority of the titanium and iron in all streams was found in the <45μm size fraction (fines).

Further characterization was performed on the clay size (<0.2 μm and 0.2–2 μm) fractions of each stream, as well as on the heavy minerals (>2.8 g/cm^3) present in the coarse size fractions (>45 μm) of the froth and tailings. TEM analysis of the clay size fractions revealed that the average fundamental thickness of the illite particles was 4 nm

for both the froth and middlings streams. The thickness distribution of illite in the froth stream showed a bimodal distribution, while thickness distribution of the illite in the middlings was more uniform. SEM analysis of the heavy minerals revealed that titanium minerals are often intergrown with quartz. The titanium minerals exhibited an iron content range from a few percent to stoichiometric ilmenite. TEM analysis of a titanium particle with an intermediate iron content (often referred to as leucoxene), revealed a heterogeneous mixture of rutile closely intergrown with fine hematite platelets and pseudobrookite

Acknowledgements

There are many people who have helped me in the journey of my dissertation. First, I would like to thank the people who provided me with various data: Sola Adeyinka for Mastersizer results, Pat Munoz for TG-EG results, Wally Friesen for the first set of TG results, Ali Hooshiar for the last set of clay TEM images, Peter Uhlik and Ali Hooshiar for CHNS results, and Brad Helm at the RCMP forensics lab for micro-XRD and micro-XRF results.

Second, I would like to thank the wonderful technicians who taught me how to obtain my own data: Greg Popowich, Julie Qian, Tina Barker, Andree Koenig, Tammy Parker, Michelle Morin, and Benham Namsechi.

Third, I would like to thank my wonderful WISEST students who have helped me conduct my work: Allison DeMan, Jenn Fiske, Jessica Gosslein, Alyssa Shinbine, and Jenny Thompson. Their enthusiasm and interest helped keep me motivated throughout this project. I also would like to thank the WISEST program for giving me the opportunity to have such wonderful helpers for 6 weeks every summer, and for paying their way.

Fourth I would like to thank my fellow graduate students whose camaraderie made graduate school a good place to be, and whose questions often lead the way for new insights into my data. In particular, I would like to thank Ali Hooshiar, Patrick Kerr,

Peter Uhlik, and Christine Siebel who are/were the best office/lab mates a person could wish for.

Fifth, I would like to thank my supervisors, Doug Ivey, Tom Etsell, and Dipo Omotoso. Their guidance and insistence on excellence helped me reach my potential.

I also would like to thank the National Sciences and Engineering Research Council of Canada (NSERC) and the Oil Sands Tailings Research Facility for funding my work.

Finally, I would like to thank my husband Kurtis, whose love and support mean the world to me. I cannot imagine doing this without him.

Table of Contents

1 Introduction to Alberta's Oil Sands 1
  1.1 Oil sands processing 1
    1.1.1 Terminology used in oil sands processing 4
    1.1.2 Effect of mineralogy on extraction 5
    1.1.3 Oil sands tailings management 6
  1.2 Oil sands mineralogy 7
    1.2.1 Heavy minerals in the oil sands 12
    1.2.2 Clay minerals in the oil sands 15
  1.3 Titanium mineralogy 19
  1.4 Clay and clay mineralogy 20
    1.4.1 Definitions of clays and clay minerals 20
    1.4.2 Clay mineral structure 22
    1.4.3 Classification of clay minerals 26
      1.4.3.1 Common polytypes of mica 27
      1.4.3.2 Reichweite ordering 28
      1.4.3.3 Isomorphous substitution 29
      1.4.3.4 Mixed-layer minerals 30
    1.4.4 Structure of clay minerals important in the oil sands 30
    1.4.5 Fundamental particle theory 32
    1.4.6 Formation of mixed layered clay minerals 32
      1.4.6.1 Structure of mica 32
      1.4.6.2 Structure of hydrous mica 33
      1.4.6.3 Mica-vermiculite 34
      1.4.6.4 Structure of vermiculite and smectite 35
      1.4.6.5 Illite-smectite from smectite or from mica 35

1.4.6.6 Formation of kaolinite-smectite 35

1.4.7 Important clay properties 35

1.4.7.1 Charge distribution 35

1.4.7.2 Cation exchange capacity (CEC) 37

1.4.7.3 Clay activity 38

1.5 Characterization techniques 38

1.5.1 Elemental compositional analysis 39

1.5.2 Structural analysis 42

1.5.2.1 Rietveld method 43

1.5.2.2 TEM analysis of clay minerals 45

2 Mass and Mineral Balances around Extraction 47

2.1 Materials and methods 47

2.1.1 Sample selection 47

2.1.2 Warm water extraction 47

2.1.3 Dean Stark extraction 48

2.1.4 Size separation 49

2.1.4.1 Dispersion 49

2.1.4.2 Sieving 51

2.1.4.3 Separation clay size samples from sub-sieve samples 52

2.1.5 X-ray diffraction 54

2.2 Quantitative analysis using the Rietveld procedure 55

2.2.1 Elemental analysis using X-ray fluorescence spectrometry 57

2.3 Results and discussion 58

2.3.1 Warm water extraction 58

2.3.2 Particle size distribution of process solids 60

2.3.3 Element balances 63

2.3.4 Mineral identification 65

2.3.5 Mineral quantification 69
2.3.6 Mineral balances 69
2.3.6.1 Clay minerals 69
2.3.6.2 Other silicates 70
2.3.6.3 Zircon 71
2.3.6.4 Titanium-bearing minerals 71
2.3.6.5 Iron bearing minerals 72
2.3.7 Comparisons between XRF and XRD results 73
2.4 Conclusions 75
3 Characterization of Oil Sands Clays 77
3.1 Materials and methods 78
3.1.1 Separation of clay minerals and elemental analysis 78
3.1.2 X-ray diffraction analysis 78
3.1.2.1 Random powder mounts 79
3.1.2.2 Preparation of oriented clay slides 79
3.1.2.3 Pretreatments 80
3.1.2.4 Preparation of clay quantitative standard 82
3.1.2.5 X-ray diffraction data collection 83
3.1.2.6 Quantification of clay minerals 83
3.1.2.6.1 NEWMOD™ modeling 85
3.1.2.6.2 TOPAS™ modelling of NEWMOD™ profiles 86
3.1.2.6.3 TOPAS™ modelling of sample profiles 87
3.1.2.6.4 Determination of degree of interstratification 88
3.1.2.7 Surface area determination 90
3.1.2.7.1 Crystallite size determination 90

3.1.2.7.2 Definition of LVol-IB in TOPAS™ 90

3.1.2.7.3 Fundamental thickness determination 91

3.1.2.7.4 Mean crystallite area, volume, mass, and surface area 92

3.1.2.7.5 Total stream surface area 93

3.1.2.7.6 Limitations of surface area analysis by XRD 93

3.1.3 Methylene blue adsorption test 94
3.1.4 TEM analysis 96
3.1.5 Thermogravimetric analysis 96
3.2 Results 98

3.2.1 Particle size distribution 98
3.2.2 Clay mass balance 101
3.2.3 Elements mass balance 101
3.2.4 Identification of clay minerals 103
3.2.4.1 Mineral identification of 0.2–2μm samples & <2 μm secondary froth

103

3.2.4.2 Mineral identification of <0.2 μm samples 105

3.2.4.3 Differences between process streams 106

3.2.5 Quantification of clay minerals 107
3.2.5.1 Determination of degree of interstratification 107

3.2.5.2 Quantification of clay minerals 108

3.2.5.2.1 Comparison with source clay quantitative standard 112

3.2.6 Clay activity 113
3.2.6.1 Methylene blue analysis 113

3.2.6.2 Surface area estimation by XRD 114

3.2.7 Thermogravimetric analysis 115
3.2.8 Particle morphology by TEM 118

3.2.9 Fundamental particle thickness 122
3.2.10 Charge distribution — TEM-EDX results 128
3.3 Discussion 133
3.4 Conclusions 136
4 Characterization of the Coarse Solids in the Athabasca Oil Sands 138
4.1 Introduction 138
4.2 Materials and methods 138
4.2.1 Thermogravimetric analysis 139
4.2.2 Density separation 139
4.2.3 SEM analysis 141
4.2.4 XRD analysis 143
4.2.4.1 Micro-XRD analysis 143
4.2.5 TEM analysis 144
4.3 Results and discussion 145
4.3.1 TG analysis 145
4.3.2 Analysis of the effectiveness of density separation 149
4.3.3 Analysis of XRF results of coarse solids 154
4.3.4 SEM analysis 158
4.3.4.1 Sub samples from sieved coarse solids 158
4.3.4.2 Sub-samples of heavy mineral fraction 161
4.3.4.2.1 Froth heavies 161
4.3.4.2.2 Comparison of heavy particles in the froth and tailings streams .. 169
4.3.5 Analysis of heavy mineral fraction of froth solids by XRD and XRF 175
4.3.6 Micro-XRD analysis of “leucoxene” particle 177
4.3.7 TEM analysis of “leucoxene” particle 178
4.4 Conclusions 197
4.4.1 Characteristic differences between heavy minerals in froth and tailings 197

4.4.2 Degree of liberation of the valuable minerals 198
4.4.3 Association of Fe with valuable minerals 199
4.4.4 Association of silicon and aluminum with valuable minerals 200
4.4.5 Association of calcium with valuable minerals 201
5 Conclusions and Future Work 202
5.1 Conclusions 202
5.1.1 Secondary resource potential 202
5.1.2 Process management 205
5.2 Future Work 205
5.2.1 Secondary resource potential 206
5.2.2 Process management 207
6 References 209
Appendix A 231
Appendix B 304
General Notes on Uncertainty analysis 304
Uncertainty in Methylene Blue Analysis 304
Uncertainty in Modelled values – peak area, peak position, crystallite size 306
Uncertainty in % Smectite calculations 306
Uncertainty in Quantification 307
Uncertainty in XRD Surface area calculations 307
Uncertainty in TEM Particle size and % Smectite calculations 309
Combining data 310
Appendix C- Visual basic modules used for solving diffraction patterns 311
Multiple Pattern Solver 313
Allowed reflection checker 322
Smallest planes checker 331
Plotable pattern checker 339
Zone axes type definer 340

List of Figures

Figure 1: Schematic of the hot water extraction process. 3

Figure 2: Particle size ranges in soils. 21

Figure 3: Schematics of silicon tetrahedron and aluminum octahedron. 23

Figure 4: Side and top view of a tetrahedral sheet. 24

Figure 5: Types of octahedral sheets. 24

Figure 6: Trans orientation for octahedral sheets; black circles represent hydroxyl ions, M are cation sites, and V are vacant sites. The mirror plane formed is indicated with the dashed line. 26

Figure 7: Schematic of ideal mica. The triangles with the purple dots represent silicon tetrahedra while the triangles with the blue dots represent aluminum tetrahedra. The rectangles with the blue dots represent aluminum octahedra. The green dots represent oxygen ions and the orange dots represent hydroxyl ions. The pink circles represent potassium ions. 33

Figure 8: Schematic of hydrous mica. The yellow triangles represent silicon tetrahedra, the purple triangles represent aluminum tetrahedra and the purple squares represent aluminum octahedra. 34

Figure 9: Charge distribution and schematic of pyrophyllite. The triangles with the purple dots represent silicon tetrahedra. The rectangles with the blue dots represent aluminum octahedra. The green dots represent oxygen ions and the orange dots represent hydroxyl ions. 36

Figure 10: Charge distribution and schematic of kaolinite.[13] The triangles with the purple dots represent silicon tetrahedra while the triangles with the blue dots represent aluminum tetrahedra. The rectangles with the blue dots represent aluminum octahedra. The green dots represent oxygen ions and the orange dots represent hydroxyl ions. 37

Figure 11: Sample preparation of XRD slides to minimize preferred orientation. a) XRD slide is placed into a small aluminum pan. b) Using a 400 μm sieve, the sample is sieve mixed, and micronized sample is deposited onto the XRD slide. c) A flat edge is used to scrape the excess powder off the slide and create a flat sample. 55

Figure 12 :Particle size distribution of process streams. 61

Figure 13: Particle size distribution for <0.2 μm. 99

Figure 14: Particle size distribution for the 0.2–2 micron streams. 101

Figure 15: XRD trace for calcium saturated, ethylene glycol solvated <0.2 μm oil sands sample. 110

Figure 16: XRD trace for calcium saturated, ethylene glycol solvated 0.2–2 μm oil sands samples. 111

Figure 17: TEM bright field (BF) image of 0.2 to 2 μm middlings sample showing iron-rich particles. A SAD pattern from the circled region is shown in the inset (JEOL 2010)[20] 121

Figure 18: EDX spectrum from iron-rich particles circled in Figure 17 (JEOL 2010). . 121

Figure 19: HRTEM image of an illite particle in the 0.2 to 2 μm middlings. A SAD pattern is included in the insert showing the 1nm d-spacing characteristic of illite (JEOL 2010) 123

Figure 20: Image showing typical particles in <0.2-μm middlings sample (JEOL 2010) 124

Figure 21: HRTEM image of 0.2-2 μm middlings sample showing regions with inconsistent layer spacings (JEOL 2010). 126

Figure 22: Thickness distribution of particles from HRTEM images. (JEOL 2010) 128

Figure 23: Typical false-colour image of >106 μm froth sample showing purple (quartz), red (feldspars), mottled yellow (inter grown quartz with heavy minerals), and yellow particles (heavy minerals) (Hitachi S-2700). 142

Figure 24: SEM image of "leucoxene" particle showing location of FIB sections. 145

Figure 25: TG curves for froth solids. Temperaures at peak mass loss rate are shown on the figure. 147

Figure 26: TG curves for middlings solids. Temperaures at peak mass loss rate are shown on the figure. 148

Figure 27: TG curves for tailings solids. Temperaures at peak mass loss rate are shown on the figure. 149

Figure 28: Area fraction by phase contrast in coarse fractions of froth solids and tailings. 160

Figure 29: Mottled iron-rich particle. Yellow areas are iron-rich and purple areas are silica. 160

Figure 30: Mottled titanium-rich particle. Yellow areas are rich in titanium, purple areas are silica. 161

Figure 31: Typical backscattered SEM image from primary froth heavies. 161

Figure 32: Iron, silicon, and titanium X-ray maps of an area of froth heavies. 165

Figure 33: Higher magnification image of particle 1 in Figure 32 one showing contrast differences. 166

Figure 34: Distribution of iron in iron-titanium oxides, the grey area indicates the range of Fe/(Fe+Ti) ratios expected for rutile (<0.1), pseudorutile (0.25–0.35) and ilmenite (0.45–0.55). 167

Figure 35: XRD traces of heavy fraction of primary froth. 176

Figure 36: Micro-XRD pattern from "leucoxene" particle. 178

Figure 37: EDX spectra from taken from two regions in FIB Section 1. These regions correspond to Areas 1 and 2 labelled in Figure 39 (JEOL 2010). 179

Figure 38: Pattern ABC is the typical matrix diffraction pattern from the circled region of FIB Section 1 shown in Figure 39, and is comprised of three overlapped patterns A, B and C. Pattern A is rutile $[0\bar{1}0]$, Pattern B is hematite [100], and Pattern C is hematite $[\bar{1}00]$ (JEOL 2200 FS) 181

Figure 39: HAADF- STEM image of "leucoxene" particle showing three distinct regions. The dark spots shown in the micrograph are pores while the bright streaks are areas that were found to be rich in iron (FEI Tecnai F20). 182

Figure 40: Close up HAADF STEM image of Area 1 from Figure 39 and an X-ray line scan of the streaked region. (FEI Tecnai F20). 183

Figure 41: TEM bright field image of streaked region shown in Figure 40, the dark regions indicate areas of strong amplitude contrast due to either increase mass/thickness or due to a strongly diffracting region. The bright regions are areas where the electrons passed through the sample with very little energy loss – characteristic of small pores in the sample. (FEI Tecnai F20). 184

Figure 42: TEM bright field image showing border of Section 1 Area 2 (left) and Section 1 Area 3 (right). (JEOL 2010) 185

Figure 43: TEM bright field image of Section 1 Area 2 from Figure 39 showing two apparently different regions in the matrix, labelled A and B. (JEOL 2010)........... 186

Figure 44: EDX spectra showing differences in composition between points A and B in Figure 43 187

Figure 45: Diffraction pattern from region A in Figure 43, which is consistent with pseudobrookite zone type <141>. 187

Figure 46: HAADF STEM image of FIB Section 2 from the "leucoxene" particle showing an inhomogeneous mixture of regions (FEI Technai F20)....................... 189

Figure 47: EDX spectra of Area 1 from FIB Section 2 (FEI Tecnai F20)...................... 190

Figure 48: Diffraction patterns A, B, and C, were obtained from Area 1 in Figure 46 and correspond with either brookite or anatase (indexed as anatase). Pattern A is consistent with anatase zone type <553> or brookite zone type <103>. Pattern B is consistent with anatase zone type <151> or brookite zone type <156>. Pattern C is consistent with either anatase zone type <131> or brookite zone type <312>. Pattern D is from Area 2 in Figure 46 and shows an overlap with pattern C (blue dots) and pseudobrookite zone type <212> shown with red labels (FEI Tecnai F20). 191

Figure 49: Dark field image showing TiO particles (bright) in anatase matrix (FEI Tecnai F20). 192

Figure 50: Diffraction pattern from FIB Section 2 Area 3, matching rutile [103] (JEOL 2010). 193

Figure 51: EDX spectra from Areas 3 and 4 as labelled on Figure 46 (JEOL 2010). 193

Figure 52: Diffraction patterns from FIB Section 2-Area 4 . Pattern A is from at zero tilt, showing a pattern consistent with rutile $[0\bar{1}0]$, the boxes show how extra spots could be derived from a shift of the most intense spots of the main pattern. Pattern B shows the same area after tilting. Pattern C shows how the Pattern B is comprised of four overlayed patterns. Patterns D-F show the simulated diffraction patterns for rutile $[0\bar{1}0]$ (D), hematite [100] (E) and hematite $[\bar{1}00]$ (F) using Single Crystal™. 195

List of Tables

Table 1: Minerals reported in the oils sands literature 8

Table 2: Means and ranges of principal minerals reported by Bayliss and Levison (1976) 11

Table 3: Important heavy minerals in Athabasca oil sands 14

Table 4: Summary of literature on the clay mineralogy of the Athabasca oil sands 17

Table 5: Lattice parameters of the six titanium oxides found in oil sands 20

Table 6: Radius ratio and coordination number of common cations 22

Table 7: Relationship between radius ratio and coordination number 23

Table 8: AIPEA classification of clay minerals (Bailey, 1980) 27

Table 9: Structure of important clay minerals 31

Table 10: Typical properties of important clay minerals 31

Table 11: Compositional techniques and their properties 41

Table 12: Mass balances of bitumen, solids, and water around extraction 59

Table 13: Analysis of mass losses during sample preparation 60

Table 14: Distribution of sand, fines, clays and ultrafine clays around extraction 62

Table 15: Distribution of particle sizes in sand fractions around extraction 63

Table 16: Qualitative XRD analysis of run 2 samples 67

Table 17: Qualitative XRD analysis of run 3-5 tailings and middlings 68

Table 18: Qualitative XRD analysis of run 3-5 Froth streams 68

Table 19: Modelling parameters for NEWMOD^{TM} models 86

Table 20: Particle size distribution numbers for d_{10}, d_{50}, and d_{90} 99

Table 21: Mass balance of fines, clays, and ultrafine clays around extraction 101

Table 22: Element balance for ultrafine (<0.2 μm) clay fraction 102

Table 23: Element balance for clay size (<2 μm) fraction 103

Table 24: Degree of interstratification (% smectite) for illite-smectite and kaolinite-smectite in oil sands streams 108

Table 25: Clay mineral composition of the clay size fractions (wt%) 109

Table 26: Distribution of non-clay minerals in the clay fraction of the oil sands 112

Table 27: Quantitative clay standard analysis 112

Table 28: Clay activity results 114

Table 29: TG results 116

Table 30: C, H, N, S determination 117

Table 31: Length and width measurement for dispersed particles in primary froth and middlings samples 119

Table 32: Crystallite size (thickness) measurements for different clay minerals as determined by XRD 120

Table 33: Particle thickness measurements by XRD and HRTEM 122

Table 34: Percent expandability of illite and kaolinite in the <0.2 μm middlings sample 125

Table 35: Average particle thickness and d-spacings for particles observed in HRTEM 127

Table 36: Counts of particles containing iron and potassium (all STEM results) 129

Table 37: Counts of particles containing iron and potassium (STEM results from pure clay areas) 129

Table 38: Counts of particles containing iron and potassium (all EM results) (JEOL 2022 FS) 130

Table 39: Counts of particles containing iron and potassium (EM results from pure clay areas) (JEOL 2022 FS) 130

Table 40: Average EDX results for 0.2–2 μm middlings and primary froth particles, as determined in EM mode (JEOL 2022 FS) 131

Table 41: EM mode EDX results for 0.2–2 μm middlings and primary froth classified by type (JEOL 2022 FS) 131

Table 42: Layer charge calculations for 0.2–2 μm primary froth illite particles 132

Table 43: Layer charge calculations for 0.2–2 μm middlings illite particles 133

Table 44: LST separations of R3-5 solids 150

Table 45: Overall EDX analysis of samples before and after LST separation (wt%) 151

Table 46: Evaluation of LST separation – SEM/EDX results 153

Table 47: Evaluation of LST separation – XRF/XRD results 153

Table 48 XRF analysis results from froth samples (wt%) 156

Table 49: XRF results for tailings samples 157

Table 50: Chemical assays of selected Syncrude and Suncor samples, summarized from MDA study (Alberta Chamber of Resources, 1996) 158
Table 51: Criteria used for classification of particles by EDX 162
Table 52: Criteria used for classification of particle liberation 163
Table 53: Degree of liberation of various minerals in the froth heavies indicated by the percentage of particles in each class 163
Table 54: Contamination levels in liberated valuable minerals of heavy froth solids.... 168
Table 55: Particle breakdown in SEM/EDX analysis 169
Table 56: Compositional variation in pyrite particles among samples 170
Table 57: Compositional variation in siderite particles among samples 171
Table 58: Compositional variation in rutile particles among samples 172
Table 59: Compositional variation in "leucoxene" particles among samples 172
Table 60: Contamination by various elements in well liberated particles as determined by EDX 173
Table 61: Degree of liberation of potentially valuable minerals 173
Table 62: XRF results from primary froth heavies 175
Table 63: Quantitative XRD results from primary froth heavies 177
Table A–1: XRF analysis results from froth samples 231
Table A–2: XRF results for tailings samples 232
Table A–3: XRF results for ore samples 233
Table A–4: Element balance for <0.2 µm size fraction 234
Table A–5: Element balance for 0.2-2 µm size fraction 235
Table A–6: Element balance for <2 µm size fraction 236
Table A–7: Element balance for 2-45 µm size fraction 237
Table A–8: Element balance for <45 µm size fraction 238
Table A–9: Element balance for >45 µm size fraction 239
Table A–10: Element balance for 45-106 µm size fraction 240
Table A–11: Element balance for >106 µm size fraction 241
Table A–12: Total element balance around extraction 242
Table A–13: Silicon balance around extraction 243
Table A–14: Aluminum balance around extraction 244

Table A–15: Iron balance around extraction 245
Table A–16: Potassium balance around extraction 246
Table A–17: Magnesium balance around extraction 247
Table A–18: Titanium balance around extraction 248
Table A–19: Zirconium balance around extraction 249
Table A–20: Calcium balance around extraction 250
Table A–21: Chlorine balance around extraction 251
Table A–22: Sodium balance around extraction 252
Table A–23: Chromium balance around extraction 253
Table A–24: Copper balance around extraction 254
Table A–25: Phosphorous balance around extraction 255
Table A–26: Manganese balance around extraction 256
Table A–27: Zinc balance around extraction 257
Table A–28: XRD results that best match XRF results for ore and froth samples 258
Table A–29: XRD results that best match XRF results for middlings and tailings samples 259
Table A–30: XRD results based on the average of all refined data for non-clay size fractions of ore and froth samples 260
Table A–31: XRD results based on the average of all refined data for non-clay size fractions of middlings and tailings samples 261
Table A–32: XRD results for clay fractions of oil sands streams 262
Table A–33: Abbreviations used in mineral balance tables 263
Table A–34: Mineral balance around extraction for <0.2 μm size fraction 264
Table A–35: Mineral balance around extraction for 0.2-2 μm size fraction 265
Table A–36: Mineral balance around extraction for <2 μm size fraction 266
Table A–37: Mineral balance around extraction for 2-45 μm size fraction 267
Table A–38: Mineral balance around extraction for <45 μm size fraction 268
Table A–39: Mineral balance around extraction for >45 μm size fraction 269
Table A–40: Mineral balance around extraction for 45-106 μm size fraction 270
Table A–41: Mineral balance around extraction for >106 μm size fraction 271
Table A–42: Mineral balance around extraction for sum of all size fractions 272

Table A–43: Anatase balance around extraction 273
Table A–44: Ankerite balance around extraction 274
Table A–45: Brookite balance around extraction 275
Table A–46: Chlorite balance around extraction 276
Table A–47: Illite balance around extraction 277
Table A–48: Illite-Smectite balance around extraction 278
Table A–49: Ilmenite balance around extraction 279
Table A–50: Kaolinite balance around extraction 280
Table A–51: Kaolinite-smectite balance around extraction 281
Table A–52: Lepidocrocite balance around extraction 282
Table A–53 Microcline balance around extraction 283
Table A–54: Plagioclase Oligoclase balance around extraction 284
Table A–55: Pyrite balance around extraction 285
Table A–56: Quartz balance around extraction 286
Table A–57: Rutile balance around extraction 287
Table A–58: Schorl balance around extraction 288
Table A–59: Siderite balance around extraction 289
Table A–60: Zircon balance around extraction 290
Table A–61: Total clay balance around extraction 291
Table A–62: Total titanium mineral balance around extraction 292
Table A–63: Total feldspar balance around extraction 293
Table A–64: Total iron bearing mineral balance around extraction 294
Table A–65: Comparisons of elemental compositions from XRF and XRD for the <0.2 µm size fraction 295
Table A–66: Comparisons of elemental compositions from XRF and XRD for the 0.2-2 µm size fraction 296
Table A–67: Comparisons of elemental compositions from XRF and XRD for the <2 µm size fraction 297
Table A–68: Comparisons of elemental compositions from XRF and XRD for the 2-45 µm size fraction 298

Table A–69: Comparisons of elemental compositions from XRF and XRD for the <45 µm size fraction 299

Table A–70: Comparisons of elemental compositions from XRF and XRD for the >45 µm size fraction 300

Table A–71: Comparisons of elemental compositions from XRF and XRD for the 45-106 µm size fraction 301

Table A–72: Comparisons of elemental compositions from XRF and XRD for the >106 µm size fraction 302

Table A–73: Comparisons of elemental compositions from XRF and XRD around extraction 303

Table C- 1: Mineral phases tested and their structural information 311

1 Introduction to Alberta's Oil Sands

Oil is a major industry in Alberta, providing thousands of direct jobs and millions of dollars of royalties to the government. With the depletion of conventional reserves, Alberta's oil sands are playing an ever-increasing role in this industry. From 1990 to 2002 the oil sands contributed over 2.8 billion dollars in royalties to the province (Alberta Department of Energy, 2003).

There are three main oil sands deposits in Alberta, located near Peace River, Athabasca, and Cold Lake. The largest of the deposits is the Athabasca deposit, containing approximately three quarters of Alberta's oil sands reserves (Zhao et al., 2001).

Alberta's oil sands deposits represent the second largest reserve of oil in the world, with established reserves estimated at 28.3 billion cubic meters (178 billion barrels) (National Energy Board, 2004). These reserves are in the form of oil sands, comprised of 55–80% inorganic materials (primarily quartz), 4–18% bitumen, and 2–15% water (Kasperski, 2001). This composition makes the recovery of oil from oil sands a considerably more challenging prospect than the recovery of oil from conventional crude reserves.

1.1 Oil sands processing

Oil sands are currently treated in two ways: open pit mining or in situ production. Open pit mining is applicable anywhere the overburden is less than 75 m (National Energy Board, 2004). According to Alberta Economic Development, "Alberta oil sands production figures for 2002 indicate that mining operations accounted for approximately two-thirds (540,000 bpd) of the total, with in situ operations accounting for one-third (284,000 bpd)" (Alberta Economic Development, 2004). Open pit mining follows the general procedure developed by Karl Clark, where hot water and caustic (NaOH) are added to the ore, and the slurry is agitated in order to produce a separable froth. In the hot water extraction process, water at 80°C with a pH of approximately 8.5 is mixed with the ore in order to create a slurry wherefrom the bitumen can be removed by froth flotation. This is a fairly efficient process, with recoveries often exceeding 90% (Chalaturnyk et al., 2002). More recently, the hot water process has been modified to a warm-water hydro transport process, where the ore is conditioned in a pipeline with warm water (45°C to 55°C) at a pH between 7 and 8.5 prior to froth separation. A generalized process flow sheet for the warm-water extraction process used in open pit mining is shown in Figure 1 (Omotoso, 2003). This dissertation is concerned solely with the mineralogy of the different streams produced by this modified warm water extraction process.

The efficiency of extraction is dependent on several factors (Kasperski, 2001), including the water chemistry, mineralogy of the ore, and bitumen chemistry (Munoz et al., 2003). For further details, the reader is referred to the review article by Masliyah et al. on the hot water extraction process (Masliyah et al., 2004).

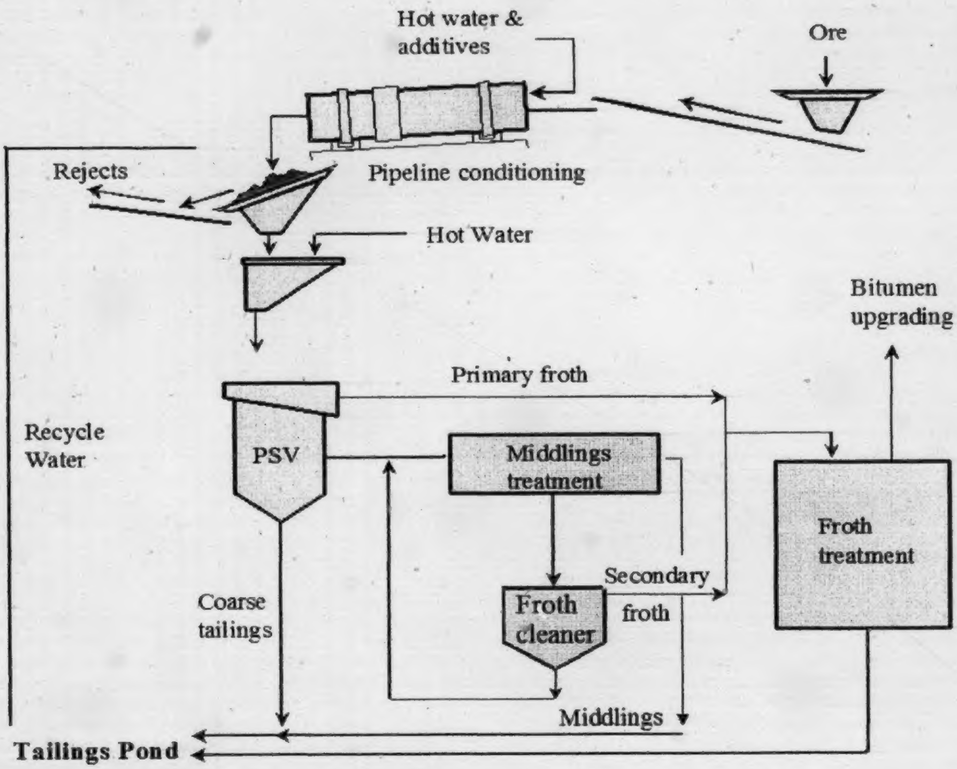
Hot water &
additives
Ore
Pipeline conditioning
Rejects
Hot Water
Bitumen
upgrading
Primary froth
Recycle
Water
PSV
Middlings
treatment
Froth
treatment
Secondary
froth
Coarse
tailings
Froth
cleaner
Middlings
Tailings Pond

Figure 1: Schematic of the hot water extraction process[1].

Unfortunately, the extraction process is very water-intensive; for every barrel (0.16 m^3) of oil produced, two tonnes of ore and 2.6 m^3 of water are required (Western Oil Sands, 2002, MacKinnon, 1989). Approximately 2 m^3 of water is eventually recovered as free recycled water. Ultimately, each tonne of ore generates about 0.25 m^3 of waste called mature fine tailings or MFT (MacKinnon, 1989), which is a mixture of water, residual organics (bitumen, tightly bound organics, and solvents), and fines (<44 μm fraction). It takes approximately ten years for the fines to settle to about 30 wt% solids (MacKinnon,

---

[1] **Provided by O. Omotoso,**

1989). The solids content remains at this level when the pond is active and increases to about 50 wt% solids when the pond becomes inactive. Currently over 400 million cubic meters of MFT is stored in tailings ponds. At the current production rate, this is expected to grow to over billion cubic metres by 2020 (Chalaturnyk et al. 2002). The close proximity of the tailings ponds to the Athabasca River requires that the ponds be monitored and maintained for decades after mine closure to prevent discharge into the river. This build-up of tailings, therefore, represents a potential environmental liability.

1.1.1 Terminology used in oil sands processing

An oil sands ore has many descriptors. By far the most common descriptor attached to an ore is its grade. A high-grade ore is considered to contain more than 10% bitumen, a mid-grade ore contains 8–10% bitumen, and a low-grade ore contains less than 8% bitumen (Kasongo, 2006). Another common descriptor is the percentage of the fines (<44 μm) material contained in the ore. A high-fines ore contains >18% fines while a low-fines ore contains <6% fines (Kasperski, 2001). A final descriptor is how the ore behaves in the extraction process (processability). Processability is measured by how much bitumen is recovered in the froth. A "good processing" ore will have a "good recovery" of bitumen in the froth (>80% primary recovery and >90% total recovery) (Kasperski, 2001). Froth quality and settling behaviour are also sometimes considered as factors in processability, but most processability curves report recovery only. A "high quality" froth will contain about 66% bitumen, 25% water, and 9% solids or a 7:1 bitumen to solids ratio (Kasperski, 2001). It should be noted that although these terms (high grade, good recovery, good processing, and high froth quality) are universally used, they are not universally defined. The definitions provided here are operational definitions provided from examining instances where an ore is said to exhibit one or more of these qualities.

1.1.2 Effect of mineralogy on extraction

Over the years a general trend has been observed: as the clay content of an ore increases, the bitumen recovery from that ore decreases (Liu et al., 2004). It has also been shown that the addition of montmorillonite and calcium ions have a synergistic effect in decreasing bitumen recovery whereas the addition of other clay minerals (kaolinite and illite) did not have such an impact on recovery (Kasongo et al., 2000). Further work by Wallace et al. (2004) showed a relationship between increased soluble potassium and decreased bitumen recovery that points to degraded illite having a negative impact on recovery. Finally, work by Tu et al. (2005) showed the ultrafine (<0.3μm) clays may be responsible for the gelation and sludging behaviour of some ores, which negatively affects bitumen recovery and tailings management. These studies underscore the importance of characterizing the clay minerals in the oil sands, as they all indicate that the clay activity of the ore is the largest predictor of poor recovery. In other words, an increased surface area (decreased particle size), an increase in surface charge (i.e. degraded illite/smectite), and an asymmetric particle shape all increase the yield strength of a slurry of particles (Brenner, 1974), (Scales, 2008), thereby making bitumen flotation more difficult.

1.1.3 Oil sands tailings management

In recognition of the hazards of the oil sands tailings, a great deal of research has been done both to minimize the production of tailings and to look at ways of dealing with the current tailings problems. Kim Kasperski wrote an excellent review in 1992 on the properties and treatment of oil sands tailings, which succinctly summarizes most of the tailings treatment options up to 1992.

For the fine tailings stream, the current EUB approved tailings management scheme, designed to return the tailings containment areas to a dry landscape, involves combining mature fine tailings with the coarser cyclone underflow tailings and gypsum to produce a consolidated tailings stream that settles to ~ 60% solids within a matter of weeks as opposed to years. Chalaturnyk et al. (2002) proposed a variation of this process using lime and CO_2 instead of gypsum. This modification drastically changed the structure of the consolidated tailings, which in turn improved the water release rate from the tailings. Unfortunately, the reasons for the change in structure are not fully understood, making it difficult to optimize the process.

The coarse solids, which make up the bulk of the tailings, are primarily used for the building of containment ponds and for the coarse component of consolidated tailings. In addition to these mundane roles, the portion of the coarse solids coming from the froth treatment tailings have been shown to contain enriched levels of titanium and zirconium bearing minerals (Ityokumbol et al., 1987), (Owen and Tipman, 1999), (Majid and Sparks, 1999). According to the Mineral Development Agreement (MDA) study (Alberta

Chamber of Resources, 1996), the froth treatment tailings contain an average of 11.5% TiO_2 and 3.4% $ZrSiO_4$. At 2005 production levels of ~ 272 million barrels of bitumen per year, this translates to a potential 700 kt/year of TiO_2 and 200 kt/year of $ZrSiO_4$ (Whitcomb and Associates, 2005). With the planned expansion of bitumen production, this potential is expected to grow to 1050 kt/year of TiO_2 and 300kt/year of $ZrSiO_4$. This represents a significant proportion of the world demand for TiO_2, which was 4.7 Mt in 2003 (Whitcomb and Associates, 2005).

Considering both heavy mineral recovery and tailings consolidation, a fundamental understanding of the oil sands mineralogy and tailings mineralogy is required in order to fully realize the potential of this resource.

1.2 Oil sands mineralogy

The mineralogy of the oil sands is very complex, as evidenced by the sheer number of possible minerals identified by workers in the area. To date over 90 mineral species have been identified as being present either in the oil sands deposits or as products of hydrothermal alteration of the oil sands. To further complicate matters, many of these minerals are polymorphs, end members of a series of minerals, unofficial minerals, or just poorly characterized. For example: anatase, rutile, and brookite are all polymorphs of one another, all having the same chemical composition (TiO_2) but completely different structures. (Deer et al., 1966). Albite is a member of the feldspar ternary system $NaAlSi_3O_8$- $KAlSi_3O_8$- $CaAl_2$ Si_2O_8 (Deer et al., 1966). "Members of the series between $NaAlSi_3O_8$ and $KAlSi_3O_8$ are called alkali feldspars, and those between $NaAlSi_3O_8$ and

$CaAl_2$ Si_2O_8 plagioclase feldspars" (Deer et al., 1966, pp 282). Due to the difficulty in distinguishing unique members of a continuous series, only the end members of a series are recognized minerals. Therefore the mention of albite in the oil sands may mean that any of the alkali feldspars or plagioclase feldspars could be present (although it is more commonly associated with the plagioclase feldspars). Related to this problem of continuous series of minerals is the problem posed by leucoxene – an alteration product of ilmenite. Leucoxene is not a recognized mineral; however, it is a very common "mineral" found in the oil sands literature. Basically, leucoxene is cited in the oil sands literature whenever there is a titanium mineral containing more iron than the TiO_2 polymorphs and that is not one of the recognized iron-based titanium minerals (i.e., ilmenite or pseudobrookite). Finally, there are the clay minerals which are not well characterized and may have structure that are extremely sensitive to environmental conditions. Conditions such as humidity and the presence of mono and divalent cations make swelling clay minerals difficult to identify. Table 1 lists the non-clay minerals identified as present in the oil sands and the study in which they were identified.

Table 1: Minerals reported in the oils sands literature

Mineral Class	Mineral Group	Mineral Name Mentioned	Chemical Formula	Ref.
Carbonate	Calcite	Siderite	$FeCO_3$	Hepler & Hsi (1989)
Carbonates	Calcite	Calcite	$CaCO_3$	Hepler & Hsi (1989)
Carbonates	Aragonite	Cerussite	$PbCO_3$	Alberta Chamber of Resources (1996)
Carbonates	Dolomite	Dolomite	$CaMg(CO_3)_2$	Hepler & Hsi (1989)
Carbonates	Calcite	Magnesite	$MgCO_3$	Bichard (1987)
Elements		Gold	Au	Alberta Chamber of Resources (1996)
Elements		Tungsten	W	Alberta Chamber of Resources (1996)
Oxides and Hydroxides		Anatase	TiO_2	Alberta Chamber of Resources (1996)
Oxides and Hydroxides		Baddeleyite	ZrO_2	Alberta Chamber of Resources (1996)
Oxides and Hydroxides		Boehmite	AlO(OH)	Hepler & Hsi (1989)
Oxides and Hydroxides		Brookite	TiO_2	

Mineral Class	Mineral Group	Mineral Name Mentioned	Chemical Formula	Ref.
Oxides and Hydroxides	Brucite	Brucite	$Mg(OH)_2$	Hepler & Hsi (1989)
Oxides and Hydroxides	Rutile	Cassiterite	SnO_2	Alberta Chamber of Resources (1996)
Oxides and Hydroxides	Hematite	Corundum (Alumina)	Al_2O_3	Kotlyar et al. (1990)
Oxides and Hydroxides	Diaspore	Diaspore	$AlO(OH)$	Hepler & Hsi (1989)
Oxides and Hydroxides		Gibbsite	$Al(OH)_3$	Hepler & Hsi (1989)
Oxides and Hydroxides	Diaspore	Goethite (Limonite)	$FeO(OH)$	Bichard (1987)
Oxides and Hydroxides	Hematite	Hematite	Fe_2O_3	Hepler & Hsi (1989)
Oxides and Hydroxides	Spinel	Hercynite	$FeAl_2O_4$	Alberta Chamber of Resources (1996)
Oxides and Hydroxides	Hematite	Ilmenite	$FeTiO_3$	Bichard (1987)
Oxides and Hydroxides		Ixiolite	$(Nb, Ta)_2O_6$	Alberta Chamber of Resources (1996)
Oxides and Hydroxides		Leucoxene		Ciu et al. (2003)
Oxides and Hydroxides	Periclase	Lime	CaO	Kotlyar et al. (1990)
Oxides and Hydroxides	Spinel	Magnetite	Fe_3O_4	Hepler & Hsi (1989)
Oxides and Hydroxides		Pseudobrookite	Fe_2TiO_5	Kramers & Brown, 1975
Oxides and Hydroxides		Pseudorutile	$Fe_2Ti_3O_9$	Ityokumbol et al. (1987)
Oxides and Hydroxides	Rutile	Rutile	TiO_2	Bichard (1987)
Oxides and Hydroxides	Spinel	Spinel	$MgAl_2O_4$	Bichard (1987)
Oxides and Hydroxides		Uraninite	UO_2	Alberta Chamber of Resources (1996)
Oxides and Hydroxides	Periclase	Wustite	FeO	Hepler & Hsi (1989)
Phosphates	Apatite	Apatite	$Ca_5(PO4)_3(OH,F,Cl)$,	Bichard (1987)
Phosphates	Monazite	Brabantite	$CaThPO_4$	Alberta Chamber of Resources (1996)
Phosphates	Monazite	Monazite	$(Ce, La, Th, Nd, Y)PO_4$	Alberta Chamber of Resources (1996)
Phosphates		Pyromorphite	$Pb_5(PO_4)_3Cl$	Alberta Chamber of Resources (1996)
Phosphates	Zenotime	Xenotime	YPO_4	Alberta Chamber of Resources (1996)
Silicate	Mica	Paragonite	$NaAl_3Si_3O_{10}(OH)_2$	Hepler & Hsi (1989)
Silicate	Sepiolite	Sepiolite	$Mg_4Si_6O_9(OH)_{14}$	Hepler & Hsi (1989)
Silicates	Feldspars	Albite	$NaAlSi_3O_8$	Hepler & Hsi (1989)
Silicates		Amorphous Silica	SiO_2	Hepler & Hsi (1989)
Silicates	Zeolites	Analcime	$NaAlSi_2O_5(OH)_2$	Hepler & Hsi (1989)
Silicates		Andalusite	Al_2SiO_5	Hepler & Hsi (1989)
Silicates	Feldspars	Anorthite	$CaAl_2\ Si_2O_8$	Hepler & Hsi (1989)
Silicates	Mica	Biotite	$K(Mg,Fe)_3(Al,Fe)Si_3O_{10}(F, OH)_2$	Hepler & Hsi (1989)
Silicates	Chloritoid	Chloritoid	$Fe_{2+}1.2Mg_{0.6}Mn_{2+}0.2A_{14}Si_2O_{10}(OH)_4$	Bichard (1987)

Mineral Class	Mineral Group	Mineral Name Mentioned	Chemical Formula	Ref.
Silicates	Serpentine	Clinochrysotile	$Mg_3Si_2O_5(OH)_4$	Hepler & Hsi (1989)
Silicates	Epidote	Clinozoisite	$Ca_2Al_3Si_3O_{12}(OH)$	Hepler & Hsi (1989)
Silicates	Tourmaline	Elbaite		Bichard (1987)
Silicates	Epidote	Epidote	$Ca_2(Al, Fe)_3(SiO_4)_3(OH)$	Bichard (1987)
Silicates	Mica	Glauconite	$(K,Na)(Al,Fe,Mg)_2(Al,Si)_4O_{10}(OH)_2$	Hepler & Hsi (1989)
Silicates	Nepheline	Kalsilite	$KAlSiO_4$	Hepler & Hsi (1989)
Silicates		Kyanite	$Al_2\ SiO_5$	Bichard (1987)
Silicates	Zeolites	Laumontite	$CaAl_2Si_4O_8(OH)_8$	Hepler & Hsi (1989)
Silicates	Lawsonite	Lawsonite	$CaAl_2Si_2O_6(OH)_4$	Hepler & Hsi (1989)
Silicates	Feldspars	Microcline	$KAl\ Si_3O_8$	Hepler & Hsi (1989)
Silicates	Mica	Muscovite	$KAl_3Si_3O_{10}(OH)_2$	Hepler & Hsi (1989)
Silicates	Feldspathoid	Nepheline	$NaAlSiO_4$	Hepler & Hsi (1989)
Silicates	Zeolites	Phillipsite	$KAlSi_2O_6.4H_20$	Hepler & Hsi (1989)
Silicates	Quartz	Quartz	SiO_2	Hepler & Hsi (1989)
Silicates		Samarskite	$(Y,U)Nb_2O_6$	Alberta Chamber of Resources (1996)
Silicates		Sillimanite	$Al_2\ SiO_5$	Bichard (1987)
Silicates		Staurolite	$Fe_2Al_9Si_4O_{22}(OH)_2$	Bichard (1987)
Silicates	Pyrophyllite-talc	Talc	$Mg_3Si_4O_{10}(OH)_2$	Hepler & Hsi (1989)
Silicates	Zircon	Thorite	$ThSiO_4$	Alberta Chamber of Resources (1996)
Silicates	Titanite	Titanite (Sphene)	$CaTiSiO_5$	Bichard (1987)
Silicates	Analcime	Wairakite	$CaAl_2Si_2Si_4O_{10}(OH)_4$	Hepler & Hsi (1989)
Silicates	Pyroxenoid	Wollastonite	$CaSiO_3$	Hepler & Hsi (1989)
Silicates	Zircon	Zircon	$ZrSiO_4$	Bichard (1987)
Silicates	Epidote	Zoisite	$Ca_2Al_3(SiO_4)_3(OH)$	Bichard (1987)
Silicates	Amphibole		$XY_2Z_5(Si, Al, Ti)_8O_2\ 2(OH, F)_2$	Bichard (1987)
Silicates	Garnet		$(Ca,Fe,Mn,Mg)_3(Al,Fe,Cr,Ti)_2(SiO_4)_3$	Bichard (1987)
Sulfates	Alunite	Alunite	$KAl_3(SO4)_2(OH)_6$	Hepler & Hsi (1989)
Sulfates		Anhydrite	$CaSO_4$	Hepler & Hsi (1989)
Sulfates	Barite	Barite	$BaSO_4$	Alberta Chamber of Resources (1996)
Sulfates		Gypsum	$CaSO_4.2H_2O$	Hepler & Hsi (1989)
Sulfates	Melanterite	Melanterite	$FeSO_4.7H_2O$	Hepler & Hsi (1989)
Sulfides	Pentlandite	Pentlandite	$(Ni,Co)_9S_8$	Alberta Chamber of Resources (1996)
Sulfides	Pyrite	Pyrite	FeS_2	Hepler & Hsi (1989)
Sulfides		Pyrrhotite	FeS	Hepler & Hsi (1989)
Sulfides	Sphalerite	Sphalerite	ZnS	Alberta Chamber of Resources (1996)
Sulfides	Tetrahedrite	Tetrahedrite	$Cu_{12}Sb_4S_{13}$	Alberta Chamber of Resources (1996)
Sulphides		Acanthite	AgS	Alberta Chamber of Resources (1996)
Sulphides		Chalcocite	Cu_2S	Alberta Chamber of Resources (1996)
Sulphides	Chalcopyrite	Chalcopyrite	$CuFeS_2$	Alberta Chamber of Resources (1996)
Sulphides	Galena	Galena	PbS	Alberta Chamber of Resources (1996)
Sulphides	Marcasite	Marcasite	FeS_2	Bayliss & Levinson (1976)

In addition to the difficulties in identifying the different minerals present in the oil sands, it is clear that the oil sands themselves are highly heterogeneous. An idea of the variability of the data available on the mineralogy of the oil sands is best demonstrated by the statistical summary of the principal minerals found in the 1976 mineralogical review by Bayliss and Levison (Table 2). In this study, the major mineral fraction was found to be quartz, but the quartz content ranged between 17% and 98%, underscoring the extreme variability of the samples.

Table 2: Means and ranges of principal minerals reported by Bayliss and Levison (1976)

		McMurray		Clearwater		Bluesky/ Gething		Wabiskaw		Grand Rapids		Clearwater / Grand Rapids	
		247 Samples		15 Samples		32 Samples		15 Samples		6 Samples		15 Samples	
		$\bar{X}$	Range	$\bar{X}$	Range	$\bar{X}$	Range	$\bar{X}$	Range	$\bar{X}$	Range	$\bar{X}$	Range
% of Total Minerals	Quartz	80	41-97	63	21-87	69	17-92	81	57-96	66	55-87	75	30-98
	Potash Feldspar	2	0-16	6	0-42	2	0-7	4	T-20	10	0-30	7	0-19
	Plagioclase	0.1	0-8	3	0-11	N		1	0-6	12	0-41	7	0-27
	Calcite	0.2	0-28	4	0-12	0.5	0-5	0.9	0-9	0.3	0-2	0.1	0-2
	Dolomite	0.4	0-9	4	0-13	5	0-4	1	0-7	N		0.6	0-5
	Siderite	1	0-20	2	0-4	N		0.3	0-2	3	0-15	N	
	Pyrite/Marcasite	0.4	0-10	5	0-45	6	0-62	1	0-4	1	0-8	0.1	0-2
	Kaolinite	9	1-27	5	0-19	15	4-27	7	2-18	4	2-7	3	0-11
	Mica	1	0-8	T	0-2	0.3	0-4	0.8	0-2	0.2	0-1	0.5	0-3
	Illite	4	T-10	6	1-15	3	T-11	3	T-9	3	1-10	3	T-13
	Chlorite	N		0.3	T-4	N		0.1	0-1	N		1	T-7
	Montmorillonite	N		1	T-7	N		N		N		3	0-17
% of Total Clay Minerals	Kaolinite	65	28-90	39	0-67	85	47-94	74	57-85	54	40-78	52	0-91
	Illite	31	7-54	44	29-66	13	6-35	24	14-38	36	16-60	25	7-42
	Chlorite	0.8	0-18	6	1-15	0.9	0-18	2	0-5	5	0-9	8	2-25
	Montmorillonite	0.2	0-7	11	2-26	0.3	0-3	0.6	0-5	5	0-11	15	0-42
	Mixed-Layer Clays[2]	3	0-26	N		0.7	0-4	N		N		N	
	Kaolinite/Illite Ratio	2	0.2-11	0.9	0-2	7	1-15	3	2-6	2	0.7-5	2	0-9

T = Trace, N= Not Detected

---

[2] illite-smectite, chlorite-illite-smectite, chlorite-vermiculite, chlorite-illite-vermiculite

1.2.1 Heavy minerals in the oil sands

In the context of oil sands minerals, "heavy" minerals are generally considered to be anything with a density of 2.9 g/cm^3 or greater. This cut-off eliminates quartz and clay minerals, but still leaves a large list of minerals to be considered. The most relevant minerals in this category are the titanium-bearing, the zirconium-bearing, and the rare-earth-bearing minerals. These minerals are all important from the point of view of economic potential.

Currently, Titanium Corporation is piloting the production of zircon, ilmenite (60–65% TiO_2), and "leucoxene" (70–84% TiO_2) concentrates from the tailings (Titanium Corporation, 2007). For leucoxene and ilmenite streams, the goal is to sell these concentrates as a feed material for production of titanium pigments via the chloride or chloride-ilmenite process. The chloride process uses chlorine to produce volatile titanium tetrachloride, which can be re-oxidized into pure TiO_2 and recyclable chlorine (Lynd & Lefond, 1983), (Chachula, 2002). The typical grade of feed for the chloride process is a concentrate with over 85 wt% TiO_2 (Lynd & Lefond, 1983). The amount of chlorine lost depends on the level of iron and other contaminants present in the ore. Thus, the lower the amount of iron contained in the concentrate, the more valuable it will be for this process. The chloride-ilmenite process is similar but can handle ores much richer in iron (60-70% TiO_2) (Office of Solid Waste, 1995), (Lynd & Lefond, 1983). Several studies have attempted to achieve better separation of the TiO_2, but they have always had a problem with iron contamination (Coward and Oxenford, 1997).

As evidenced from the contamination problems experienced by Coward, Oxenford, and others, iron-bearing minerals present in the oil sands are also important to consider, as they may interfere with the recovery of the other, more economically valuable minerals. Table 3 lists the most important heavy minerals in each category present in the oil sands, their density, and their chemical formulae.

Table 3: Important heavy minerals in Athabasca oil sands[3]

Importance	Mineral Name	Class	Density	Chemical Formula
Zirconium bearing	Zircon	Silicates	4.6	$ZrSiO_4$
	Baddeleyite	Oxides and Hydroxides	5.5	ZrO_2
Titanium bearing	Sphene (Titanite)	Silicates	3.3	$CaTiSiO_5$
	Anatase	Oxides and Hydroxides	3.8	TiO_2
	Brookite	Oxides and Hydroxides	3.9	TiO_2
	Rutile	Oxides and Hydroxides	4.2	TiO_2
	Pseudobrookite	Oxides and Hydroxides	4.4	Fe_2TiO_5
	Pseudorutile	Oxides and Hydroxides	4.0	$Fe_2Ti_3O_9$
	Ilmenite	Oxides and Hydroxides	4.5	$FeTiO_3$
	Leucoxene		4.5	$xFe_2O_3 \cdot yTiO_2$
Rare earth bearing	Thorite	Silicates	4.1	$ThSiO_4$
	Xenotime	Phosphates	4.4	YPO_4
	Monazite	Phosphates	4.6	$(Ce, La, Th, Nd, Y)PO_4$
	Brabantite	Phosphates	4.72	$CaThPO_4$
Iron bearing	Epidote	Silicates	3.3	$Ca_2(Al, Fe)_3(SiO_4)_3(OH)$
	Siderite	Carbonate	3.9	$FeCO_3$
	Limonite (Goethite)	Oxides and Hydroxides	4	$FeO(OH) \cdot nH_2O$
	Pyrrhotite	Sulfides	4.6	FeS
	Marcasite	Sulfides	4.8	FeS_2
	Magnetite	Oxides and Hydroxides	5.1	Fe_3O_4
	Pyrite	Sulfides	5.1	FeS_2
	Hematite	Oxides and Hydroxides	5.3	Fe_2O_3
	Wustite	Oxides	5.88	FeO

---

[3] Table compiled from webmineral.com and mineralgalleries.com

Another interesting property of the heavy minerals in the oil sands is their relative polarity (i.e., degree of hydrophobicity). According to Wills's textbook on mineral processing (Wills, 1997, pp. 261), pyrite and siderite are more hydrophobic than either rutile, ilmenite, hematite, or magnetite, which are, in turn, more hydrophobic than zircon and quartz. Zircon is approximately as hydrophobic as quartz. This is interesting, because the zircon is found to be preferentially enriched to the froth (Ityokumbol et al., 1987), while the quartz and feldspar minerals remain in the coarse tailings. Based on their respective levels of hydrophobicity zircon should remain in the tailings along with the quartz. This indicates that something in the oil sands extraction system is interacting with the zircon to make it prefer the bitumen phase over the water phase.

1.2.2 Clay minerals in the oil sands

The clay mineralogy of the Athabasca oil sands has been studied fairly extensively and most studies agree that the major minerals are kaolinite and illite, as shown in Table 4. These findings led to the prediction that the oil sands tailings should have a fairly low surface area and low cation exchange capacity, but it has been demonstrated that this is not the case. Consequently, much work has been done to try and answer the question of why the fine tailings exhibit the high surface area, cation exchange capacity (CEC), and gelation capacity that have been observed.

Initially, the most prevalent theory to explain the discrepancy in tailings properties was that there must be significant amounts of discrete montmorillonite (smectite) in the tailings. This theory has been largely disproved, because the majority of the studies have found no evidence of discrete smectite (Table 4). Some of the mineralogical studies have also found significant quantities of amorphous iron and silica fine solids (Kotlyar et al., 1990). The studies have asserted that these amorphous fine solids are responsible for the extra surface area and CEC. However, results from Omotoso et al. (2002) indicate that this fraction probably does not contribute significantly to the surface area and CEC, at least in the middlings fraction. Finally, there is the issue of the mixed layer clay minerals. Several studies (Smith and Ng, 1993), (Ignasiak et al.,1983), (Dusseault et al., 1989), (Bayliss and Levison, 1976), have found evidence of mixed-layer clay minerals with some swelling characteristics (<50% swelling characteristics) present in the oil sands. These clay minerals include kaolinite-smectite and illite-smectite. The presence of these swelling clay minerals is able to explain the poor settling behaviour of the oil sands tailings; however, these clay minerals are often overlooked or are simply lumped together with illite and kaolinite. These swelling mixed layer clay minerals lack distinct 3-D structures. There is some disagreement about whether the swelling characteristics are caused by the presence of distinct smectite layers or by fine kaolin and illite particles, whose charge distribution has been altered slightly at the particles' surfaces; both result in swelling behaviour consistent with smectite, as per the fundamental particle theory (Nadeau et al., 1984).

Table 4: Summary of literature on the clay mineralogy of the Athabasca oil sands

Authors	Reported mineralogy of clay (<2 µm) fraction	Sample source and stream investigated
Bayliss & Levinson (1976)	kaolinite, illite, up to 10% mixed layers, up to 6% chlorite and up to 1% montmorillonite	247 core ore samples
Camp (1976 a, b)	kaolinite, illite, mixed-layer clays, chlorite & smectite	ore and fine tailings
Yong & Sethi (1978)	kaolinite, illite, mixed-layer clays, chlorite & smectite, up to 4% amorphous Fe_2O_3	Suncor pond fine tailings
Kessick (1979)	kaolinite, illite	extraction tailings
Dusseault & Scafe (1979)	illite, kaolinite, vermiculite, illite-vermiculite, kaolinite-vermicuilite	outcrop and borehole ore samples in McMurray formation
Roberts et al. (1980)	kaolinite, illite, 0.9–3% smectite, 1–6% chlorite, 0.1–6% mixed-layer clays	Suncor pond fine tailings
Ignasiak et al. (1983)	kaolinite, illite/smectite (<10% smectite interlayers)	froth solids
Kotlyar et al. (1984)	kaolinite, illite	ore & froth solids
Kotlyar et al. (1985)	kaolinite, illite	froth solids
Ignasiak et al. (1985)	kaolinite, illite, trace amounts of chlorite and smectite in some samples	ore
Scott et al. (1985)	kaolinite and illite, trace quantities of smectite, vermiculite, chlorite and mixed-layer clays	ore & fine tailings
Kotlyar et al. (1987)	kaolinite, illite, up to 90% amorphous minerals	ore
Dusseault et al. (1989)	kaolinite, illite, smectites, vermiculites, mixed-layer clays	ore samples from various formations
Kotlyar et al. (1990)	kaolin, illite, up to 92% poorly crystalline minerals (allophane?)	Syncrude estuarine and marine ore
Ripmeester et al. (1993)	kaolinite, illite, trace amounts of smectites	fine tailings
Kotlyar et al. (1993)	kaolinite, illite, trace amounts of smectite and vermiculite	Suncor fine tailings
Cloutis et al. (1995)	kaolinite, illite	oil sand samples from Syncrude and Suncor leases
Kotlyar et al. (1995)	kaolinite, illite	Suncor fine tailings
Dudas, M.J (1998)	kaolinite, hydrous mica	5 fine tailings samples from Suncor, Syncrude and Oslo
Omotoso et al. (2002)	kaolinite, illite, mixed layer clays (kaolinite-smecite/illite-smectite)	mature fine tailings from Syncrude and Suncor ponds
Omotoso et al. (2004)	kaolinite, illite, mixed layer clays (kaolinite-smectite/illite smectite) and chlorite (in some samples)	mature fine tailings from Syncrude pond, thickener overflow and froth tailings
Wallace et al. (2004)	kaolinite, "degraded illite"	ore samples

Authors	Reported mineralogy of clay (<2 µm) fraction	Sample source and stream investigated
Omotoso et al. (2006)	kaolinite, illite, mixed layer clays (kaolinite-smecite/illite-smectite), trace amounts of discrete smectite in marine ores	61 ore samples, 22 froth samples, 54 tailings samples from 3 different leases
Mercier et al. (2008)	kaolinite, illite	Syncrude fine tailings

1.3 Titanium mineralogy

There are six titanium oxide minerals that have been found in the oil sands: rutile, anatase, brookite, pseudobrookite, pseudorutile, and ilmenite. The crystal structure and chemical of each phase is shown in Table 5. Rutile, anatase, and brookite are polymorphs having the chemical formula TiO_2 with rutile being the most common polymorph. Iron substitution in all of these structures is extremely limited. Ilmenite, pseudorutile, and pseudobrookite all contain iron. Pseudobrookite is the phase with the highest iron content. Pseudobrookite has a range of compositions between Fe_2TiO_5 and $FeTi_2O_5$ (Bowles, 1988). Ilmenite contains approximately equal amounts of ferrous iron and titanium. Because the structure of ilmenite is very similar to that of hematite, "natural ilmenites can take up to 6% Fe_2O_3 into solid solution" (Deer et al., 1966, pp 412). Complete solubility between the two minerals has been found at higher temperatures (Deer et al., 1966). Pseudorutile is thought to derive from ilmenite via electrochemical corrosion where the ferrous iron is oxidized to ferric iron in the presence of oxygenated water (Grey & Reid, 1975). In addition one third of the iron is removed by diffusion during this process. Further iron removal from pseudorutile is thought to proceed via dissolution of the pseudorutile and the reprecipitation of TiO_2 in the form of rutile (Grey & Reid, 1975). This process is thought to account for the majority of ilmenite alteration, however, pseudobrookite and anatase have also been found in altered ilmenite deposits (Karkhanavala et al., 1959)

Table 5: Lattice parameters of the six titanium oxides found in oil sands

Mineral (formula)	**a (nm)**	**b (nm)**	**c (nm)**	**α (°)**	**β (°)**	**γ (°)**	**Volume ($nm^3 x 10^{-3}$)**	**Spacegroup**
Anatase (TiO_2)	0.379	0.379	0.951	90	90	90	136.3	$I4_1$/amd (141)
Brookite (TiO_2)	0.918	0.545	0.515	90	90	90	257.4	Pbca (61)
Ilmenite ($FeTiO_3$)	0.509	0.509	1.409	90	90	120	316.8	R-3 (148)
Pseudobrookite (Fe_2TiO_5 to $FeTi_2O_5$)	0.98	0.998	0.373	90	90	90	364.7	Cmcm (63)
Pseudorutile ($Fe_2Ti_3O_9$)	1.438	1.438	0.462	90	90	120	828	$P6_322$ (182)
Rutile (TiO_2)	0.459	0.459	0.296	90	90	90	62.4	$P4_2$/mnm (136)

1.4 Clay and clay mineralogy

1.4.1 Definitions of clays and clay minerals

Clays have been used by man for millennia, but it was only recently that they have been studied and classified. As such, the term *clay* is rather difficult to define precisely because it has been used in many different ways. The two most common usages of the word *clay* are as a rock term describing a "natural, earthy, fine grained material which develops plasticity[4] when mixed with a limited amount of water" (Grim, 1968) and as a particle-size term describing the finest particles. The upper limit of "finest particles" is a matter of some debate—the largest upper limit being around 4 μm "equivalent spherical diameter"[5]. The most common definition of a clay particle is a particle that is less than 2 µm equivalent spherical diameter. Figure 2 shows the standard particle sizes defining the terms *clay*, *silt*, *sand*, and *gravel*. Because this definition of clay is based solely on particle size, the "clay fraction" may contain fine materials other than clay minerals, such as rock flour and fine metal oxides.

---

[4] Plasticity – the property of a material that when deformed under pressure will retain the deformed shape when the applied pressure is removed.

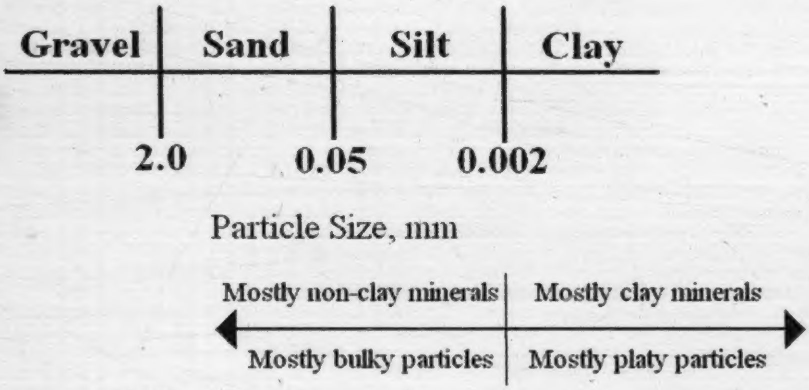
Gravel
Sand
Silt
Clay
2.0
0.05
0.002
Particle Size, mm
Mostly non-clay minerals
Mostly clay minerals
Mostly bulky particles
Mostly platy particles

Figure 2: Particle size ranges in soils.[6]

Clay minerals are typically concentrated in the clay fraction of a soil or an ore. According to the AIPEA nomenclature committee:

> "Clay minerals belong to the family of phyllosilicates and contain continuous two-dimensional tetrahedral sheets of composition T_2O_5 (T = Si, Al, Be, ...) with tetrahedra linked by sharing three comers of each, and with the fourth corner pointing in any direction. The tetrahedral sheets are

---

[5] Equivalent spherical diameter- the diameter of a spherical particle with the same settling behavior.

[6] Compiled from the US department of Agriculture particle size definitions found in Fang (1991), pp 89.

linked in the unit structure to octahedral sheets, or to groups of coordinated cations, or individual cations."(Bailey, 1980, pp 2)

Generally, clay minerals are concentrated in the clay fraction of the soil. However, just as not all clay-sized materials are clay minerals, not all clay minerals are clay sized.

1.4.2 Clay mineral structure

The main building blocks of clay minerals are tetrahedral and octahedral sheets (Pauling, 1930). Tetrahedra and octahedra are the geometrical shapes used to describe how oxygen atoms cluster around a central cation. The bigger the cation, the more oxygen atoms can fit around it, and so the more points in the shape. The ratio of cation radius to oxygen or anion radius determines the coordination number and geometry (Callister, 2000). Table 6 provides the radius ratio for common cations, while Table 7 gives the radius ratios characteristic of the various geometries available (Dudas, 1995).

Table 6: Radius ratio and coordination number of common cations

Ion	Ionic Radius (nm)	Radius Ratio Cation/oxygen	Coordination number
Si^{4+}	0.041	0.29	4
Al^{3+}	0.05	0.36	6, 4
Li^{+}	0.06	0.43	6
Fe^{3+}	0.064	0.46	6
Mg^{2+}	0.065	0.46	6
Ti^{4+}	0.068	0.49	6
Fe^{2+}	0.076	0.54	6
Zr^{4+}	0.08	0.57	6,8
Na^{+}	0.095	0.68	8
Ca^{2+}	0.099	0.71	8
Sr^{2+}	0.113	0.81	8
K^{+}	0.133	0.95	8, 12, (14)
Rb^{+}	0.148	1.06	12, (14)
Cs^{+}	0.169	1.21	12, (14)

Table 7: Relationship between radius ratio and coordination number

Radius of Cation to Anion	Coordination Number	Geometry
0.15–0.22	3	Triangle
0.22–0.41	4	Tetrahedron
0.41–0.73	6	Octahedron
0.73–1.00	8	Cube
>1	12	Dodecahedron

As evident in Table 6, silicon has a coordination number of four, corresponding to a tetrahedral shape. Similarly magnesium has a coordination number of six corresponding to an octahedral shape. Aluminum can either have a coordination number or four or six, meaning it can form either tetrahedra or octahedra. Schematic representations of a silicon tetrahedron and an aluminum octahedron are shown in Figure 3 (Cooper et al., 2005).

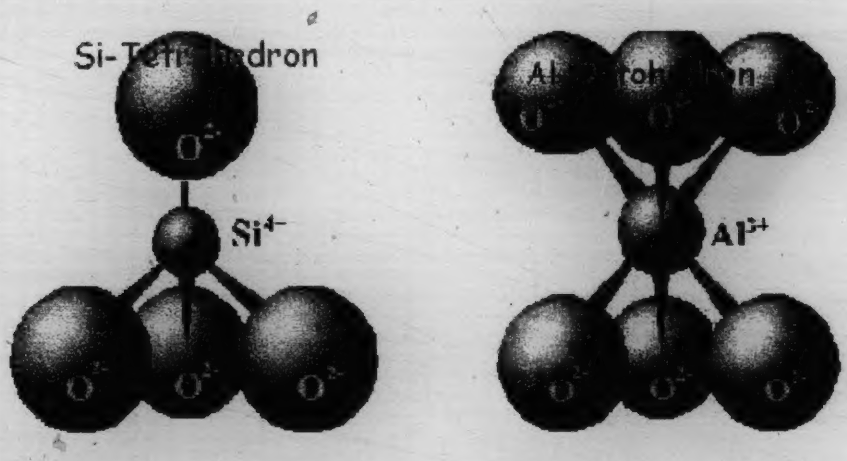

Figure 3: Schematics of silicon tetrahedron and aluminum octahedron.[7]

When there are many tetrahedra present, they arrange themselves in a hexagonal pattern (Pauling, 1930) as shown in Figure 4 (Thomas, 2004). This combination of tetrahedra is known as a tetrahedral sheet. Similarly, when many octahedra join they form an octahedral sheet. Within an octahedral sheet there are three cation positions. When the cation is divalent (e.g., Mg^{2+}) all three positions are filled, and the sheet is called a trioctahedral sheet. When the cation is trivalent (e.g., Al^{3+}), however, only two out of every three positions are filled, leading to a dioctahedral sheet. Figure 5 shows a schematic of typical dioctahedral and trioctahedral sheets (Schroeder, 2008).

---

[7] (Cooper et al., 2005).

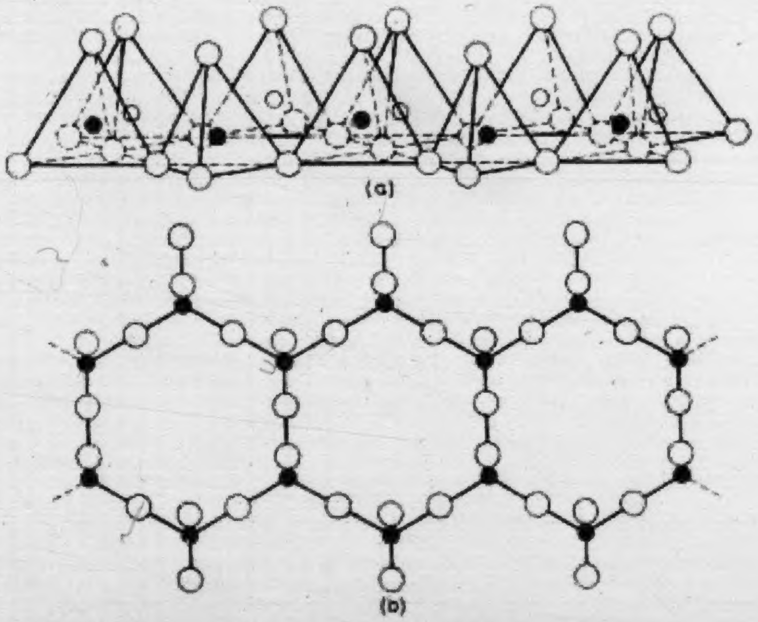

Figure 4: Side and top view of a tetrahedral sheet.[8]

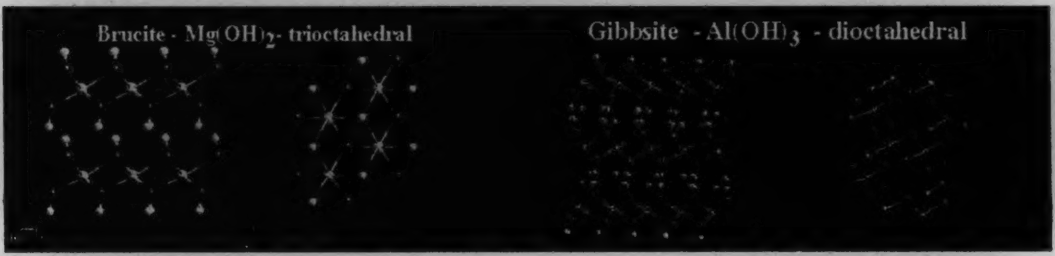
Brucite - Mg(OH)2- trioctahedral
Gibbsite - Al(OH)3 - dioctahedral

Figure 5: Types of octahedral sheets. [9]

---

[8] (Thomas, 2004)

In dioctahedral sheets, only two out of the possible three octahedral sites are occupied by cations. This means that the three-fold symmetry within a sheet is removed. The selection of occupied sites relative to the hydroxyl groups determines whether any additional symmetry is present. If the empty site is situated such that it lines up with the hydroxyl groups, then a mirror plane forms as an additional symmetry element. Such a situation is called the trans-vacant orientation, because the two occupied sites are on opposite sides of the hydroxyl ions from each other. This arrangement is shown in Figure 6 (Sainz-Diaz et al., 2001). When the cations are on the same side relative to the hydroxyl ions, the arrangement is called cis-vacant.

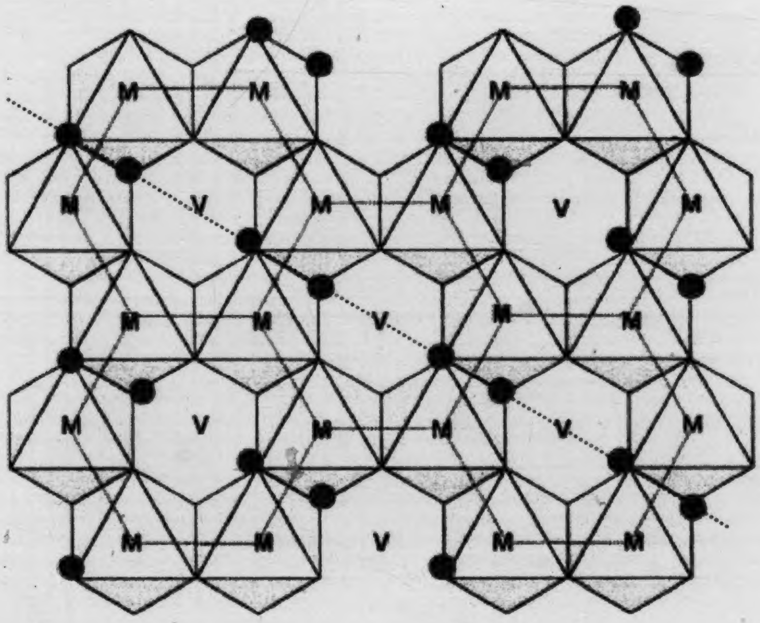

---

[9] (Schroeder, 2008)

Figure 6: Trans orientation for octahedral sheets; black circles represent hydroxyl ions, M are cation sites, and V are vacant sites. The mirror plane formed is indicated with the dashed line.[10]

1.4.3 Classification of clay minerals

Like many other minerals, clay minerals are classified based on their unit structure. For clay minerals, the unit structure is made up of octahedral and tetrahedral sheets joined together in layers with a gap or interlayer between layers. There are four main unit structure groupings: 1:1 layering of tetrahedral and octahedral sheets; 2:1 layering, with two tetrahedral sheets sandwiching the octahedral sheet; 2:1:1 layering, with two tetrahedral sheets sandwiching the octahedral sheet and another octahedral sheet where the interlayer would normally be. The fourth category is for amorphous clay minerals, which do not have a distinct long-range order in their layering.

Clay minerals are further classified by the layer charge (or charge per formula unit) and the type of octahedral layer (dioctahedral or trioctahedral). The charge per formula unit arises when isomorphous substitutions of the cations occur. The amount and type of substitution will determine the total charge generated in the tetrahedral and octahedral layers. Any charge generated in these layers must then be balanced by the interlayer. Thus, a negative charge can be balanced by having a positive ion such as potassium sit inside the interlayer. Table 8 shows the accepted classification scheme as submitted by the AIPEA nomenclature committee to the International Mineralogical Association (Bailey, 1980, pp 1). A more detailed classification of the mica group and kaolinite group of minerals are found in Rieder et al. (1998) and Guggenheim et al. (1997), respectively.

---

[10] (Sainz-Diaz et al., 2001)

Table 8: AIPEA classification of clay minerals (Bailey, 1980)

Layer Type	**Interlayer Material (x=layer charge per formula unit)**	**Group**	**Ocathedral Character**	**Species**
1:1	None or H_2O only (x~0)	Serpentine-kaolin	Trioctahedral	Lizardite, berthierine, amesite, crondstedtite, nepouite, kellyite, fraipontite, brindleyite
			Dioctahedral	Kaolinite, dickite, nacrite, halloysite
2:1	None (x~0)	Talc-pyrophyllite	Trioctahedral	Talc, willemseite, kerolite, pimelite
			Dioctahedral	Pyrophyllite, ferripyrophyllite
	Hydrated exchangeable cations (x~0.2–0.6)	Smectite	Trioctahedral	Saponite, hectorite, sauconite, stevensite, swinefordite
			Dioctahedral	Montmorillonite, beidellite, nontronite, volkonskoite
	Hydrated exchangeable cations (x~0.6-0.9)	Vermiculite	Trioctahedral	Trioctahedral vermiculite
			Dioctahedral	Dioctahedral vermiculite
	Non-hydrated monovalent cations (x~0.6–1.0)	True (flexible) mica	Trioctahedral	Biotite, phlogopite, lepidolite,
			Dioctahedral	Muscovite, illite, glauconite, celadonite, paragonite
	Non-hydrated divalent cations (x~1.8–2.0)	Brittle Mica	Trioctahedral	Clintonite, kinoshitalite, bityite, anandite
			Dioctahedral	Margarite
	Hydroxide sheet (x=variable)	Chlorite	Trioctahedral	Clinochlore, chamosite, pennantite, nimite, baileychlore
			Dioctahedral	Donbassite
			Di-trioctahedral	Cookeite, sudoite

1.4.3.1 Common polytypes of mica

There are three common polytypes in mica: 1M, $2M_1$, and 3T; there are two rarer polytypes 2Or and $2M_2$ (Radoslovich, 1959), (Moore & Reynolds, 1997). The 1M polytype is a monoclinic structure made up of a single 2:1 layer that is repeatedly stacked, with no rotation between stacks. The $2M_1$ polytype is a monoclinic unit cell made up of two 2:1 layers, because the layers are rotated ±120° with respect to each other. In other words, if the first layer is at 0°, the second will be at 120°, and the third layer will be a repeat of the 0° layer. The 3T polytype is a trigonal unit cell, formed because each layer is rotated 120° from the one below, therefore increasing the symmetry of the system. The rare polytype 2Or is an orthorhombic unit cell formed similarly to the $2M_1$ structure, but where the rotation is 180° instead of 120°. Finally, the $2M_2$ unit cell is like the $2M_1$, but with 60° rotations instead of 120°. No other rotations are allowed in mica, the K^+ sites must line up, and, therefore, no turbostratic stacking occurs in micas. (Moore & Reynolds, 1997).

1.4.3.2 Reichweite ordering

Reichweite is a system of describing the degree of ordering in an interstratified or mixed-layer structure (i.e., a structure where there are multiple layer types being stacked, rather than a single type being stacked with different rotations) (Moore and Reynolds, 1997). Reichweite is defined as the "reach back" or influence that one layer has on the surrounding layers. For R0 there is no influence of one layer type on the layers next to it; therefore, the stacking is random. For R1 there is perfect ordering, indicating that all of the minor component layers must be separated by at least one of the major component layers. An illite(50)-smectite with R1 ordering, would imply that an illite layer always follows a smectite layer and vice versa. An illite(70)-smectite with R1 ordering, would imply that a smectite layer is always preceded and followed by at least one illite layer, but it says nothing about the number of illite layers stacked next to each other. R3 ordering means that there is an influence of three, so if one layer is known then so are the next three; the stacking sequence of this type for illite-smectite is ISII. R2 ordering has also been predicted, but there is debate as to whether or not it exists. If it does, it would mean that knowing one layer would provide knowledge for the next two layers.

1.4.3.3 Isomorphous substitution

Two types of substitution occur in clay minerals: substitution in the octahedral layer and substitution in the tetrahedral layer. Atoms with a coordination number of four can substitute in the tetrahedral layer. Atoms with a coordination number of six can substitute in the octahedral layer. As shown in Table 6, Al^{3+} is the ion that substitutes for Si^{4+} in the tetrahedral layer, because it can have a tetrahedral or an octahedral coordination. Since they are not the same valence, a substitution of Al^{3+} for Si^{4+} causes a net negative charge to form on the layer. This is an example of a permanent charge and is generally the main source of cation exchange capacity in clay minerals. Many more types of cations can substitute into the octahedral layer. If the substitution is of the same charge, then no net charge develops; however, these substitutions also involve a change in cation size, which, in turn, disturbs the spacing of atoms within a layer. Finally, cations can be replaced with vacancies that cause a negative charge to form on the layer and cause adjustment of the atomic spacing within a layer.

1.4.3.4 Mixed-layer minerals

Mixed-layer minerals are minerals where the interlayer or layer type differs within the mineral (Srodon, 1999). Mixed layer minerals are not currently part of the AIPEA classification or naming scheme (except for the occasional regularly interstratified mineral), because the precise nature of these minerals is not clear. When naming mixed-layer minerals, the minerals are named by the mineral types of the two components; the mineral with the smallest d-spacing is named first (Srodon, 1999). The surface area and cation exchange capacities of these minerals are similar to a mixture of the mixed layer minerals. However, other geotechnical properties are very different from those predicted from a physical mixture of minerals, indicating that the mixed-layer minerals do indeed form a unique structure.

1.4.4 Structure of clay minerals important in the oil sands

As shown in Table 4, the major clay minerals in the oil sands are kaolinite and illite, with minor amounts of smectite (montmorillonite/beidellite), vermiculite, chlorite, and mixed-layer clay minerals. Unfortunately, this covers a fairly large range of clay minerals, since smectite, chlorite, and vermiculite are all group names, and "mixed layer" clay minerals are not well characterized. Table 9 summarizes the typical structure of ideal specimens of each group, and Table 10 (Mitchell, 1976) summarizes some of the typical properties of specimens in each group. These properties are not necessarily representative of the properties for all clay minerals of each type, because large variations in isomorphous substitution can exist within each group, leading to a blurring of the division in the classification scheme.

Table 9: Structure of important clay minerals

Name	Formula/Unit Cell **Tetrahedral Cations** *Octahedral Cations* Interlayer Molecules/Cations	**Isomorphous substitution**	**Interlayer bond**
Kaolin	$\mathit{Al_4}\ \mathbf{Si_4}O_{10}\ (OH)_8$	little	hydrogen: strong
Illite	$\underline{(K_x)}\ \mathit{(Al,Fe^{3+})_4}(\mathbf{Si_{8-x}, Al_x})O_{20}(OH_4)$	Some Si always replaced by Al, balanced by K fixed in the interlayer	K ions: strong bond
Montmorillonite	$\underline{(K,Na)_{x+y}}\ \mathit{[(Al, Fe^{3+})_{4-y},(Mg,Fe^{2+})_y]}\ (\mathbf{Si_{8-x}, Al_x})\ O_{20}(OH_4)$	Mg for Al net charge ~ 0.66/unit cell	O-O : very weak
Vermiculite	$\underline{(K,Na)_{x-y}}\ (\mathbf{Si_{8-x}, Al_x})\ O_{20}(OH_4)$	Al for Si net charge of 1 to 1.4/unit cell	weak
Chlorite	$\underline{[(Al_{x+y},Mg_{6-x-y})(OH)_{12}]}\mathit{[(Mg,Fe^{2+})_{6-y},(Al, Fe^{3+})_y]}\ (\mathbf{Si_{8-x}, Al_x})\ O_{20}(OH_4)$	Al for Si in 2:1 layer, Al for Mg in interlayer	

Table 10: Typical properties of important clay minerals[11]

Name	**Basal Spacing (nm)**	**Shape**	**Cation Exchange Capacity (meq/100 g)**	**Specific Gravity**	**Surface Area (m^2/g)**
Kaolin	0.72	6 sided flakes	3–15	2.6–2.68	10–20
Illite	1	Flakes	10–40	2.6–3.0	65–100
Montmorillonite	0.96	Flakes	80–150	2.35–2.7	50–120 external 700–840 total
Vermiculite	1.05-1.4	Flakes	100–150		40–80 external, 870 total
Chlorite	1.4	Flakes	10–40	2.6–2.96	

---

[11] Compiled from Mitchell (1976), pp 44-45

1.4.5 Fundamental particle theory

The fundamental particle theory, originally proposed by Nadeau et al. (1984), explains the existence of mixed layer minerals (specifically illite-smectite and chlorite-smectite) as "aggregates of fundamental particles." (Nadeau et al., 1984, pp 1) Furthermore, Nadeau et al. explained that mixed layering is observed in highly illitic (>50% illite) mixed-layer minerals (i.e., illite/smectite). This is really just an indication of interparticle diffraction between very thin illite particles, where the terminal layers of the illite acted like smectite, ultimately allowing swelling between the illite particles. Minerals with more smectite are considered to have individual smectite layers as well as individual illite layers.

The fundamental particle theory has stirred up a great deal of controversy in the clay science community. Several papers on this topic include Tettenhorst & Roberson (1973), Srodon (1980), Nadeau et al. (1984b), Nadeau (1985), Ahn & Peacor (1986), Klimentidis & Mackinnon (1986), Srodon & Elsass (1994), Sucha et al. (1996).

1.4.6 Formation of mixed layered clay minerals

1.4.6.1 Structure of mica

Mica has a 2:1 layer structure with an ideal net negative charge of -1. This charge is generated by the substitution of aluminum for ¼ of the silicon in the tetrahedral layers. Because the charge is located in the tetrahedral layer, the charge is very localized. Consequently, it is balanced by a small cation with a charge of +1. Potassium easily balances the charge and fits perfectly into the honeycomb structure (Grim, 1962) of the tetrahedral sheet. Therefore, the interlayer bond is quite strong. Figure 7 shows a schematic of the charge distribution over the various layers. Illite is a derivative of the mica structure.

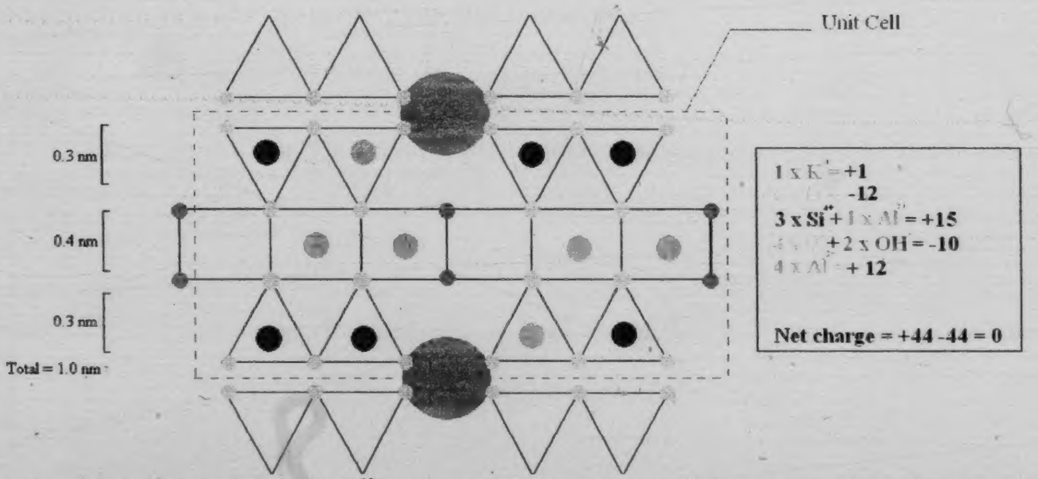

Figure 7: Schematic of ideal mica.[12] **The triangles with the purple dots represent silica tetrahedra, while the triangles with the blue dots represent alumina tetrahedra. The rectangles with the blue dots represent aluminum octahedra. The green dots represent oxygen ions and the orange dots represent hydroxyl ions. The pink circles represent potassium ions.**

1.4.6.2 Structure of hydrous mica

During weathering, the potassium ions on the edges of the mica particle may be removed (Fanning et al., 1989), (Wallace et al., 2004). Since the layer charge has not changed, this results in a residual charge that needs to be balanced with another cation. Generally, this means a replacement of the potassium with cations such as calcium or magnesium. These are cations with sizes different from potassium, that do not fit neatly into the tetrahedral sheet structure. The edges of the particle are now at a slightly different d-spacing than the main mineral (Figure 8). These edges give the particle a very slight capacity for expansion.

---

[12] Based on Mitchell (1976).

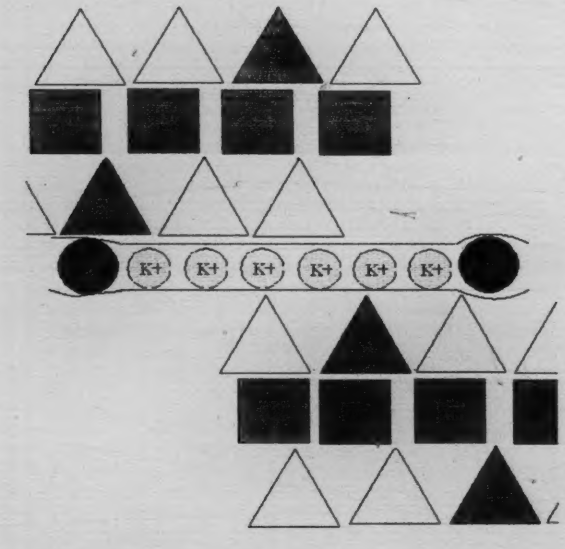

Figure 8: Schematic of hydrous mica. The yellow triangles represent silica tetrahedra, the purple triangles represent alumina tetrahedra and the purple squares represent aluminum octahedra.

1.4.6.3 Mica-vermiculite

Depotassification can continue until an entire layer of potassium has been removed from the mica (Fanning et al., 1989). This results in one entire layer being expandable. This process can continue to give increasing numbers of expandable layers. If it continues to the point where all of the potassium has been removed, the result is a "soil vermiculite." It should be noted that this depotassification of mica is most common in biotite (a trioctahedral mineral) (Fanning et al., 1989).

1.4.6.4 Structure of vermiculite and smectite

If depotassification is accompanied by a reduction in the net negative charge on the layer, then the structure can change from a soil vermiculite to a true vermiculite, or even a smectite, depending on the degree of negative charge reduction.

1.4.6.5 Illite-smectite from smectite or from mica

Illite-smectite can arise from the depotassification and negative charge reduction of mica as explained above. Alternatively, illite-smectite can form from smectite; the exact mechanism is a subject for debate, but the theory that is currently consistent with the data is that smectite is dissolved and reacts with potassium to provide the elements necessary for the formation of new illite particles (Srodon, 1999).

1.4.6.6 Formation of kaolinite-smectite

Kaolinite-smectite is thought to evolve from smectite, possibly by the dissolution of smectite in the presence of excess aluminum, with new kaolinite crystals forming either within the smectite crystals or outside the smectite crystals (Srodon, 1999).

1.4.7 Important clay properties

1.4.7.1 Charge distribution

The charge distribution of ideal pyrophyllite and kaolinite are shown in Figure 9 and Figure 10 respectively. The ideal charge distribution has the negatively charged oxygen atoms on the outside of the particle, with the positive cations towards the inside. This balanced charge distribution will change if isomorphous substitution occurs in the mineral. For instance, when substitution occurs in the tetrahedral sheet, the negative charge generated is close to the surface of the clay mineral so that its effect will be quite strong and localized near the area of the substitution (Mitchell, 1976), such as in muscovite (Figure 7). In order to balance this charge, the interlayer cations will tend to cluster near the area of substitution (as is the case with K in illite). Octahedral substitution, on the other hand, occurs within the centre of a clay mineral, and so generates a more diffuse negative charge on the surface of the clay mineral (Mitchell, 1976). Consequently, the interlayer cations are more diffusely spread in the interlayer.

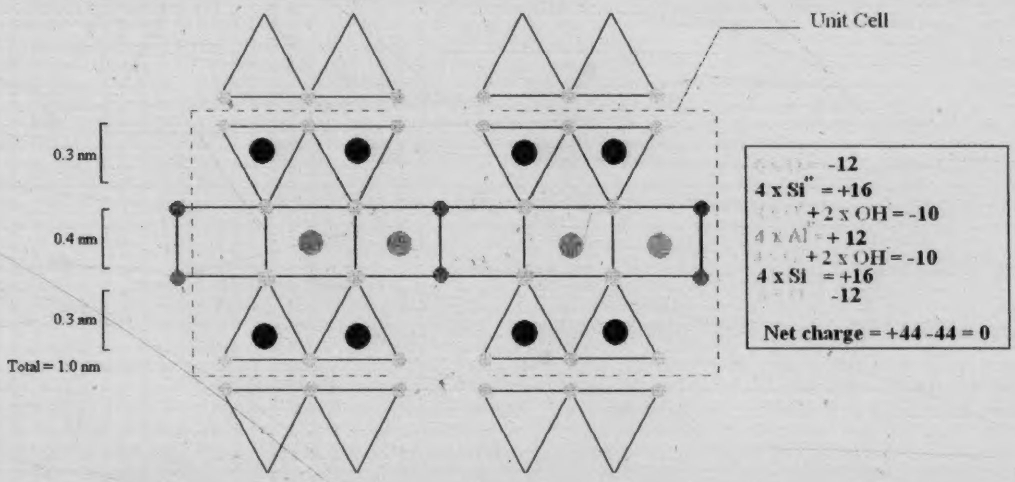

Figure 9: Charge distribution and schematic of pyrophyllite.[13] The triangles with the purple dots represent silica tetrahedra. The rectangles with the blue dots represent alumina octahedra. The green dots represent oxygen ions and the orange dots represent hydroxyl ions.

---

[13] Based on Mitchell (1976)

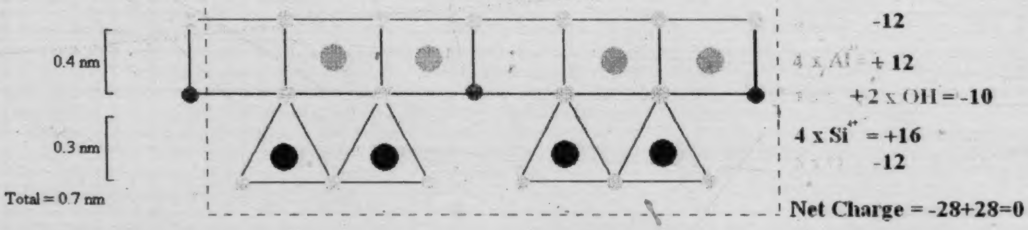

Figure 10: Charge distribution and schematic of kaolinite.[13] The triangles with the purple dots represent silica tetrahedra, while the triangles with the blue dots represent alumina tetrahedra. The rectangles with the blue dots represent aluminum octahedra. The green dots represent oxygen ions and the orange dots represent hydroxyl ions.

1.4.7.2 Cation exchange capacity (CEC)

In most clay minerals, the cations in the interlayer that balance the net charge on the clay mineral, due to isomorphous substitution, are exchangeable. The notable exception to this occurs for illite and other true micas where the charge is balanced by potassium in the interlayer. The potassium ion is the right size to fit between the oxygen atoms that make up the base of a tetrahedron in the tetrahedral sheet (Mitchell, 1976). This excellent fit, combined with the local charge created by tetrahedral substitution, ensures that the potassium is tightly bound within the structure and is not exchangeable. Clay minerals also have exchangeable cations at the edges of the minerals, where broken bonds leave an unbalanced charge (Mitchell, 1976). The total CEC of a clay mineral is the milliequivalents of exchangeable cations in the interlayer plus the milliequivalents of cations that associate with the edges of the crystal. Clay minerals without an accessible interlayer have much lower CEC than clay minerals with an exchangeable interlayer.

1.4.7.3 Clay activity

In geotechnical terms, activity is defined as the plasticity index (PI) divided by the clay fraction (Day, 2006, pp 4.1) or

$$A = \frac{PI}{clay\ fraction} \qquad \textbf{Equation 1}$$

The clay fraction is the dry weight of the soil sample having an equivalent spherical diameter < 2 μm.

The plasticity index increases as cation exchange capacity and surface area increases. Therefore, sometimes the clay activity is simply given as the cation exchange capacity/clay content (Olson et al., 2000).

1.5 Characterization techniques

There are several characterization techniques used in this work to examine the oil sands minerals. Elemental composition is determined using energy-dispersive X-ray spectroscopy (EDX) analysis and X-ray fluorescence spectroscopy (XRF). Structural composition of minerals is determined by electron diffraction (ED) and X-ray diffraction (XRD), with quantitative X-ray analysis performed using the Reitveld method. Information on morphology and interactions between minerals is obtained using optical and electron microscopy (both transmission (TEM) and scanning (SEM)). Information on chemical stability and degree of organics present is obtained by thermogravimetric analysis (TGA). Clay activity is measured by methylene blue analysis. The purpose of the following sections is to highlight the principles behind each technique, the reasons each was chosen, and the limitations of each.

1.5.1 Elemental compositional analysis

There are many different techniques available to assess the elemental composition of a sample. Table 11 outlines some of the more popular techniques, the main principles behind them, and their major disadvantages. Two of the most popular techniques are EDX and XRF. In this thesis, reference to EDX applies solely to its implementation in an electron microscope (SEM-EDX and TEM-EDX). Both techniques take advantage of the fact that each element will give off a unique energy profile when the electrons within the element decay from a higher energy orbital to replace an electron removed from a lower energy orbital. In EDX, an electron beam is used to excite the electrons within a sample to a higher energy state, and subsequently, the energies of the characteristic X-rays emitted by the sample are measured (typically by a solid state detector). In XRF, an X-ray beam is used to excite the electrons and generate the characteristic X-rays.

EDX was chosen for this thesis because it is easiest to use in conjunction with electron microscopy and it can be used to determine the composition of small particles or areas within a sample, as well as the bulk composition. Most of the other techniques do not have this ability and generally only produce information about the bulk sample, which is not useful for highly inhomogeneous samples like the oil sands. The major disadvantage of EDX is that light elements (atomic number less than 11) produce very few characteristic X-rays but produce mainly Auger electrons instead (fluorescence yield increases with increasing atomic number). Therefore, it is difficult to obtain an accurate composition for these elements. XRF was chosen because it is widely available, non destructive, relatively accurate, and it can test for a wide range of elements. Like any spectroscopic technique, quantitative analysis requires development of a calibration standard from fundamental parameters or by using standard reference materials.

Table 11: Compositional techniques and their properties

Technique Name	Basic Principle used	Major Disadvantage	Required Sample
Energy Dispersive X-ray (EDX)	Electron excitation	light elements difficult to detect and quantify, peak overlaps can be a major problem	Small solid sample, further sample prep dictated by type of microscope the technique is used with
Inductively Coupled Plasma-Atomic Emission Spectrosopy (ICP-AES)	Electron excitation	Sample must be in solution,	Liquid solution
X-ray flourescence spectroscopy (XRF)	Electron excitation	Less sensitive to lighter elements	As received solid, liquid or suspension. Better quantitative results achieved from homogenous samples
Atomic Absorption (AA)	Electron excitation	Sample must be in solution, one element at a time	Liquid solution
Emission Spectrogaphic Analysis (Sparking)	Electron excitation	Spectral overlap, standards required	Solid sample, remove grease and other debris on surface of metals if bulk composition is desired
Particle-induced X-ray emission (PIXE)	Electron excitation	Protons are difficult to focus, expensive set up	As received solid. Size limited to size of detection chamber.
Wavelength Dispersive Electron Microprobe Analysis (WDX)	Electron excitation	Smaller range, precise orientation requirements, large size	Small solid sample, further sample prep dictated by type of microscope the technique is used with.
Auger Electrons	Electron excitation	Beam damage, peak overlap, sample charging	Solid samples, size limited to size of microscope chamber, samples should be minimally conductive to prevent charging
X-ray absorption spectroscopy (XAS)	Electron excitation	Spectral overlap	Uniform samples, either solid or liquid. Solids are best analyzed as thin foils or pellets.
Electron Energy Loss Spectroscopy (EELS)	Electron excitation	sample must be electron transparent	electron transparent solid
Inductive Coupled Plasma -Mass Spectroscopy (ICP-MS)	ion charge/mass ratio	Sample must be vaporized or in solution.	Liquid solution or solids that have been vaporized by a laser
Instrumental neutron activation analysis (INAA)	nuclear excitation	Limited to solids and liquids, requires neutron source, very specialized equipment and personal required. Long testing times.	As received solid or liquid, gases absorbed on inert support. Non-destructive technique
Classical Chemical Analysis	Reaction chemistry	Different test must be designed for each element/compound.	Variable -generally solution

1.5.2 Structural analysis

The principle behind X-ray diffraction and electron diffraction is ultimately the same: diffraction. The difference between the two techniques lies in the type of radiation diffracted. X-ray and electron diffraction is similar to diffraction of light in that a diffraction pattern is a pattern formed from the constructive interference of scattered waves of electromagnetic radiation. With X-ray and electron diffraction the coherent radiation source is scattered by the electron cloud surrounding an atom. After scattering the beam splits into multiple paths. When constructive interference occurs between two or more scattered beams diffraction is said to have occurred. Mathematically diffraction will occur if the path difference between the two beams is equivalent to a whole number n of wavelengths (λ) of the beams. In a crystal which is supposed to be comprised of parallel planes of atoms the path difference is equal to twice the spacing between planes (d) times the sine of the angle between the incident beam and the planes of atoms (θ). This is known as Bragg's law which is given in equation form as:

$$n\lambda = 2d\sin\theta \qquad \textbf{Equation 2}$$

Diffraction will only occur if the wavelength of the diffracted beam is on the same order of magnitude as the interplanar distance (d). Since the interference of the radiation depends on the placement of atoms within the structure, as well as the relative angle of the light relative to the object (Bragg angle), one can determine the placement of the atoms if the angle of diffraction is known. In electron diffraction, the diffraction angle is very small and the constructive interference shows up as spots in the back focal plane. These spots can be indexed by comparing them with known patterns, and the plane types and orientations can subsequently be determined. If the sample is polycrystalline, the spots will blur into rings. One can generate similar patterns from XRD, but generally XRD involves changing the angle between the X-ray source and the sample (Bragg angle) to excite different planes. Constructive interference will occur for a particular plane at a particular angle, resulting in a series of characteristic peaks with respect to the angle of incidence.

In addition to being able to determine the interplanar distance, diffraction experiments can take advantage of differences in scattering strength between atoms to determine the position of different types of atoms within a structure. The strength with which an atom scatters radiation is given by it's atomic scattering factor (*f*) and is proportional to it's atomic number. A thorough treatment of diffraction and atomic scattering factors can be found in Cullity (1978).

1.5.2.1 Rietveld method

The major drawback of XRD data is that the most interesting problems involve mixtures of materials or involve materials that are difficult to grow as a single crystal. This means that most XRD data is from polycrystalline samples. The Rietveld method (Rietveld, 1969) helps overcome the largest obstacle in XRD interpretation of powder diffraction data — namely peak overlap. A complete description of the Rietveld method is found in "The Rietveld Method" edited by R.A. Young (1995). The Rietveld method is a method of whole pattern profile refinement using a non-linear curve fitting algorithim; the method attempts to model an XRD or neutron diffraction pattern based on a theoretical understanding of the structure of the material being analyzed and the optics of the analytical equipment. This modeled pattern is compared with the experimental pattern, and further refinements in the model are made until an acceptable agreement between the experimental and measured patterns have been obtained. The final model is then assumed to be an accurate model of the sample, and provides information such as the lattice parameters and positions of atoms within the phase. The process is similar for a mixtures of phases, where instead of a single structure being added, the structures for all identified minerals in the mixture are included in the refinement, and the refinement adjusts a scaling factor which is proportional to the quantity of each phase present. Once the modeling is complete, these scaling factors can be converted to give a weight percentage of each component according to Equation 3.

$$wt\% = \frac{SZMV}{\sum_i S_i Z_i M_i V_i} \qquad \textbf{Equation 3}$$

S is the scale factor, Z is the number of formula units in a unit cell, M is the mass of the formula unit and V is the unit cell volume. (Hill & Howard, 1987). To improve the accuracy of the refinements a known quantity of a well ordered known material may be added to the mixture of phases to provide an internal standard. It is important to realize that, like all numerical methods, proper assumptions are vital in obtaining useful results. There are other profile refinement techniques that use geometric functions rather than known structures to model the different phases present. Langford and Louër provide a good review of powder diffraction and quantitative refinement techniques in their 1996 article.

1.5.2.2 TEM analysis of clay minerals

Sample preparation is the key to achieving good TEM results. Clay minerals have some particular characteristics that must be taken into account when preparing them: they are insulators, they contain water in the interlayers which can dehydrate in the column and they are ceramic in nature, so they are generally resistant to corrosive attack (limiting the possibility for chemical polishing/preparation).

The characteristic spacing of most clays is dependent on the material in its interlayer. For this reason all specimens prepared for the TEM should be homoionic (have only one type of cation present in the interlayer). This is most easily done by repeatedly washing clay powders with 0.5 M or 1.0 M solutions of NaCl, CaCl or LiCl and then washing with distilled water to remove the excess chloride. The washings may be done with the aid of dialysis to help retain the very fine size fraction.

Another concern for TEM analysis is the tendency of samples to loose the water in their interlayers due to the combination of the high vacuum environment and beam damage. Several chemical treatments have been developed to try and improve sample stability in the beam. All the chemical treatments are essentially variations on a theme – full rehydration of the clay in distilled water, replacement of the water with methanol or another type of alcohol and then replacement of the methanol by a low viscosity resin. The benefits of these techniques is that the resin does not evaporate as easily in the beam as water does and so swelling clays can be easily distinguished from non-swelling clays. Unfortunately, the resin may not evenly swell the layers nor will the configuration be the same as if there is water in the system instead of the resin.

Some good papers on sample preparation of clay minerals for TEM analysis are: Buseck & Iijima (1974), Lee et al. (1984), Vali & Koster (1986), Kim et al., 1995) and Gillot et al. (2000).

Even if the samples have been well prepared, TEM analysis of the clay minerals is no easy task. O'Keefe et al. (1978) and Guthrie & Veblen (1989) demonstrate in their simulations just how difficult it can be to interepret HRTEM images of clay minerals.

2 Mass and Mineral Balances around Extraction

One of the principal aims of this research was to determine how different minerals, elements, and size fractions partition during the warm water extraction process.

2.1 Materials and methods

2.1.1 Sample selection

Ore from Suncor NIS upset 44G + clay was selected for this study. This ore represented a good processing ore (i.e., >90% recovery of bitumen into the froth) with a mid–low bitumen content (8%) and excess clay in the form of included clay lenses. This ore was chosen so that a large amount of clay material would be present in the fine fraction to allow for better clay identification.

2.1.2 Warm water extraction

Six 500 g samples of the ore were separated from a 20 L pail of frozen, homogenized ore. The ore was mined and then frozen to slow the aging of the bitumen which influences the processability of the ore (Mikula et al., 2003). The samples were obtained using a quartering/mixing, technique to ensure uniform samples. One of the six samples was kept aside for bitumen, water, and solids determination by Dean Stark extraction. The other five samples were processed in a batch-extraction unit (BEU) using the CANMET extraction protocol. The CANMET BEU is a modification of the Syncrude hot water BEU, designed to mimic hydrotransport conditioning. The batch extraction process involved mixing 500 g of ore with 200 g of Devon tap water at 50°C for 20 minutes with a mixer rotating at 1200 rpm. After the 20 minute conditioning, an additional 850 g of Devon tap water at 50°C was added to the unit. The mixing speed was reduced to 800 rpm and air was pumped through the mixing rotor at a rate of 3.9 mL/s. Mixing took place for ten minutes. During this process bitumen that loosened from the sand and clay floated to the top of the separation vessel. At this point the mixing and air flow were stopped, and the surface froth was scooped off the surface as the primary froth fraction. Mixing at 800 rpm and an air flow at 3.9 mL/s was resumed for an additional five minutes. This additional mixing allowed more froth to float to the surface. At the end of the five minutes of additional mixing, the secondary froth was scooped off. After the removal of the secondary froth, a drain at the bottom of the vessel was opened allowing the remaining water/clay/bitumen mixture to drain into a two litre bucket. The walls and impeller of the unit were washed with distilled water to remove any loose material. The wash water was allowed to run through the drain and join the remaining slurry. The slurry was stirred for 30 s to re-suspend any settled particles and was then allowed to settle for two minutes. The portion still in suspension was decanted into another bucket. The fraction which settled is the tailings, and the fraction still in suspension after the short settling is the middlings (fine tailings).

2.1.3 Dean Stark extraction

After extraction, the samples from each stream and the retained ore sample were sent to Maxxam Analytics for Dean Stark extraction. To reduce sample loss in the Dean Stark thimbles, the primary froth samples from batch extraction runs 3–5 were combined, as were the secondary froth samples.

Dean Stark analysis is a method used to quantitatively determine the bitumen, solids, and water content of a given sample by extraction with toluene (Bulmer & Starr, 1979). In this analysis the sample is placed in the thimble of a modified soxhlet extractor[14], and toluene is heated so that the vapours wash over the sample, thereby separating the water and bitumen from the solids. The solids remain in the thimble, and any solids that pass through the thimble into the boiling flask are removed from the bitumen/toluene phase by centrifugation at high speed or filtration. The extraction is complete when there is a clear colorless drip of toluene from the bottom of the thimble, and the glassware is 'dry', indicating that all of the water from the sample has been collected in the water trap (Barber, 2004).

2.1.4 Size separation

2.1.4.1 Dispersion

The bitumen-free, dry solids obtained by Maxxam's Dean Stark procedure were homogenized by lightly crushing the samples with a mortar and pestle to break up any agglomerations. The middlings samples were not as completely disaggregated as desired, as evidenced by the appearance of agglomerates in the >250 μm fraction after sieving.

---

[14] For a description of a soxhlet extractor see Jensen, W. B. (2007). The Origin of the Soxhlet Extractor. Journal of Chemical Education, 84 (12), 1913.

These agglomerates, however, were still relatively small and difficult to see or break up while crushing. The agglomerates were broken up, as much as possible, by water squirted from a deionized water bottle during sieving. Due to the presence of these agglomerates in the middlings, a small 400 μm sieve was used to check the crushed particles for residual agglomerates when crushing the ore sample. During homogenization, the solids from runs 3–5 middlings were combined into a single middlings stream. The froth samples had been combined during extraction.

Dispersion of the samples was done after homogenization. The middlings & tailings streams were separated into two parts per sample to reduce spillage during dispersion. Glass jars 500mL in size were used to contain the samples. To disperse the samples, the jars were shaken, stirred using a metal rod, and then ultrasonicated in a bath for at least one hour with breaks for stirring and shaking. The run 4–5 tailings, the runs 3–5 froth samples, and the ore samples were subjected to a powerful hand-held mixer for approximately 1–2 minutes. Magnetic stirring rods were not used, to avoid any possible preferential removal of magnetic particles from the solids. The froth solids were initially quite hydrophobic, and as such, took some time to disperse. They were left sitting overnight in water. A small amount of foaming was noted on the tailings samples. Dispersion was determined to be sufficient by the presence of streaming birefringence in the samples and the absence of solids remaining at the bottom of the beaker during stirring.

2.1.4.2 Sieving

Sieving for all samples from run 2, the middlings from runs 3–5 and the tailings from run 3 was done using 60, 140 and 325 mesh cascade sieves and deionized water. The cascade sieves were cleaned as well as possible by flushing and brushing with tap water and then with deionized water before and after each run. A spray bottle was used during sieving to break up agglomerates and to attempt to obtain complete separation. The sieving was stopped when the water appeared relatively clear out the bottom of the tray.

Sieving for the remaining samples used a Ro-Tap[15] with deionized water. This process seemed much more contained and made it much easier to recover the solids. A small amount from run 5 tailings was spilt, but, otherwise, recoveries were excellent. Deionized water was added in increments of ~ 50–100 mL per minute of tapping. The tapping/shaking went on for about 18–20 min. The runs were deemed complete when the effluent was clear. This method used more water than the cascade sieve, though this may have been due to inexperience. However, this method seemed to significantly reduce the risk of contamination from the cascade bench and sample loss.

Sieved weights, for sieve-sized solids, were obtained by drying the sample on the sieve and subtracting the weight of the cleaned, dried sieve. The sub-sieve sample was collected in plastic buckets, which were weighed prior to sieving and then weighed again while full of the effluent. The effluent from each sample was mixed, and a sub sample taken to determine percent solids. From the percent solids, the total sub-sieve mass was calculated for each sample. The three tailings samples from runs 3–5 were combined by particle size at this stage.

---

[15] For a description of a Ro-Tap mechanical mixer see: McKetta, J. (Ed.). (1985). Particle size measurement techniques. In *Encyclopedia of chemical processing and design.* pp 91

2.1.4.3 Separation clay size samples from sub-sieve samples

Clay minerals (especially mixed layer minerals) are generally concentrated in the clay-sized fraction of an ore, which is defined by most workers as the <2 μm fraction. The <2 μm fraction is actually the <2 μm equivalent-spherical-diameter fraction; in other words, the fraction which has a free settling velocity equivalent to a sphere with a diameter of 2 μm. This, consequently, is the fraction of interest in oil sands clay research. The initial size separation was performed by wet sieving to remove the coarse (> 44 μm) fraction. The clays were then isolated from the fines by centrifuging. Centrifuging time is calculated as shown in Equation 4 (Geankoplis, 1993).

$$t = \frac{18\mu}{\omega^2(\rho_s - \rho)d^2}\ln\frac{r_2}{r1}\varepsilon \times 10^{-(1-\varepsilon)}$$

Equation 4

where t is the settling time of the particle, μ is the dynamic viscosity of the fluid, ω is the radial velocity of the centrifuge, ρ is the liquid density, ρ_s is the particle density, d is the particle diameter, r_2 is the radius of settled sediment, and r_1 is the radius at top of liquid.

$$\varepsilon = \frac{V_l - \frac{m_s}{\rho_s}}{V_l}$$

where V_l is the volume of the liquid and m_s is the mass of solid particles.

From Equation 3 the minimum centrifuging time required to isolate the particles of interest was calculated for the three different centrifuges used. The first separation done was the separation of the silt from the clays. This was performed at 1000 rpm using a swinging-bucket IEC multi bench-top centrifuge (radius measured at ~ 8.5 cm, slurry height ~ 9 cm) for 194 s. This setting was used for all samples, regardless of actual slurry height or solids loading, and should guarantee that the supernatant contains only <2 μm particles. After this, the supernatant from all samples except the ore was centrifuged at 25000 rpm for 40 min using a Beckman™ ultracentrifuge with 45Ti fixed rotor to dewater the samples. The excess water was kept, as the water from middlings and tailings samples had a definite yellow color, indicating the presence of extremely fine particles or soluble organics. The three tailings samples were combined at this stage. Finally, the samples were centrifuged at 3500 rpm using the IEC multi bench top centrifuge for 26.5 min to separate the ultrafine clays (<0.2 μm) from the rest of the clays. The ore sample was not centrifuged to remove excess water, but was freeze-dried to concentrate the sample and to obtain some dry solids. Freeze drying was also performed on 60 mL aliquots of the other clay samples to obtain dry powder for further analysis.

Laser particle size analysis was conducted using a Mastersizer™ 2000 to confirm that the appropriate size distribution had been obtained.

2.1.5 X-ray diffraction

After sieving, sub-samples from each of the non-clay fractions were micronized using a McCrone micronizing mill loaded with corundum grinding balls and isopropyl alcohol. Approximately three grams of sample were taken for each sub-sample. In samples with less than three grams of material the entire sample was micronized. The micronized samples were dried in an oven at 65°C to remove the isopropyl alcohol. Sub samples from each of the freeze-dried clay solids were used without micronizing, due to their small particle size.

For run 2 samples, the micronized powders were inserted into a back-filled cavity mount (Burkhe et al., 1998) and analyzed with a Rigaku Rotoflex XRD with a rotating Co anode and horizontal goniometer. The divergence slit and scattering slits were set to 0.5°, the receiving slit was 0.3°, and the monochromater slit was 0.8°. The sampling rate varied from 0.25°/minute to 0.4°/minute, and the sampling step size varied between 0.01° and 0.02°.

For samples from runs 3–5, two different types of random powder mounted samples were prepared from the micronized samples. The first type was the same back-filled cavity mount used for the run 2 samples. A second type was tried after noting preferred orientation in some samples. This second sample preparation method involved passing the micronized sample through a small 400 μm sieve onto a horizontal X-ray slide (Omotoso, 2006). This process created loosely agglomerated spheres of the powdered samples, which reduced preferred orientation in the pattern. Figure 11 shows the steps in this process.

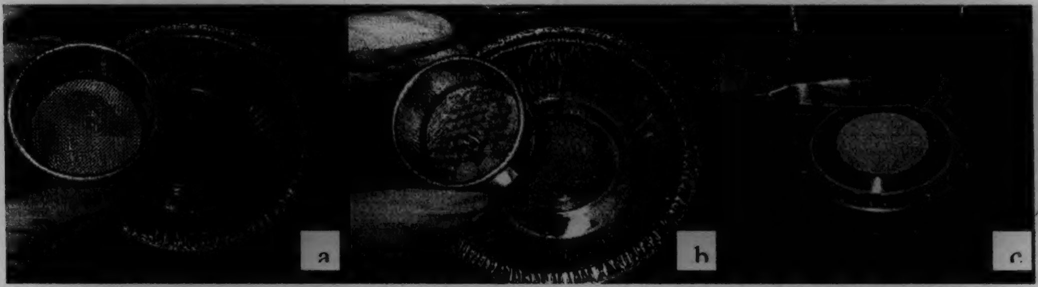

Figure 11: Sample preparation of XRD slides to minimize preferred orientation. a) XRD slide is placed into a small aluminum pan. b) Using a 400 µm sieve, the sample is sieve mixed, and micronized sample is deposited onto the XRD slide. c) A flat edge is used to scrape the excess powder off the slide and create a flat sample.

The sieved samples were analyzed using a Bruker D8 Advance θ–θ diffractometer with an incident beam parabolic mirror (Co K_α), a 25 mm sample diameter, and a VANTEC-1™ linear detector. A 0.2° exit slit was used to limit the incident beam size and resolution of the linear detector.

2.2 Quantitative analysis using the Rietveld procedure

Rietveld analysis on the run 2 samples was performed first using TOPAS-Academic™ (Coelho, 1994). A template file was made containing all the phases that had been identified during the qualitative analysis phase and others that have been previously identified using high resolution synchrotron powder diffraction data (Omotoso, 2006). This template also contained the fundamental parameters necessary for modeling the instrument contributions from a fundamental parameter approach using a full-axial model. The procedure generally followed was to use this template file to generate an initial solution by simultaneously refining the scale (i.e., relative amounts) of each phase, the crystallite size of each phase, the lattice parameters of quartz, and the background using a fifth order Chebyshev polynomial (Bruker AXS, 2003); (Mason and Handscomb, 2003). After the initial refinement, any phase that had refined to a weight-percent of zero was removed from the refinement. Next, the preferred orientation of quartz, and the lattice parameters of any phase present in amounts greater than 10 wt% were refined. When the clay minerals were present in quantities less than 10 wt%, their preferred orientations were refined at this stage as well. Finally, the crystallite sizes were evaluated for the major phases and reset if suspiciously high or low.

Rietveld analysis on the run 3–5 samples was done using AUTOQUAN™ (Agfa NDT). As before, all phases identified as either present or possibly present were included in the refinement. The instrument profile function for the Rigaku Rotoflex XRD was obtained through the fundamental parameters approach, while the profile for the Bruker AXS D8 was obtained by fitting a LaB_6 standard. A second-order background polynomial was selected and the refinement was started at 12° 2θ to eliminate the influence of beam spill at low angles. Sample displacement and zero error were refined for all samples. This was necessary to account for the zero error introduced by the linear detector combined with a parallel beam. The same settings were then applied to analyze the run 2 samples for consistency. AUTOQUAN™ automatically refines lattice parameters and crystallite size within pre-set restraints. AUTOQUAN™ also applies a spherical harmonics orientation, adjusting the harmonic order based on the quality of data and the quantity of the phase present.

Finally, TOPAS ™ (Bruker-AXS, 2003) was used to analyze the tailings and froth patterns from runs 3–5 that had been collected using the Bruker AXS D8. For this iteration of TOPAS ™ refinement, the instrument parameters were defined using a LaB_6 standard and the emission profile was set to include 3 Co K_α peaks and 1 Co K_β, as some secondary peaks were noted in the obtained patterns. To keep these results comparable with the AUTOQUAN ™ results, the refinement was started at 12° 2θ, sample displacement and zero error were refined, and a second order Chebyshev background polynomial was selected. Crystallite size refinement was allowed, but a minimum crystallite size of 50 nm was set for all phases, with the exception of the clay minerals, where the minimum was set to 25 nm.

Details on the clay mineral analysis can be found in the chapter on clay characterization (chapter 3).

2.2.1 Elemental analysis using X-ray fluorescence spectrometry

XRF samples were prepared using 0.6 g sub-samples of the freeze dried or micronized solids. The sample solids were first dried by heating them in quartz crucibles to 105°C for one hour to dry them. They were then ashed at 1000°C for four hours to burn off any organics, fully oxidize the elements, and decompose any carbonate minerals. Fused beads for XRF analysis were prepared from the ashed samples by combining ~ 0.2 g of sample with ~ 14 g of flux and ~ 0.01 g of lithium nitrate. Two different fluxes were used, as a 66% lithium metaborate-tetraborate mix worked best for the froth samples, while a 50%

lithium metaborate-tetraborate mix worked best for the tailings samples. The majority of the samples were then fused in a KATANAX™ fuser using a platinum crucible and mould. The rest of the samples were fused in "The Bee™ " electric fluxer by Claisse Scientifics.

Successfully fused beads (i.e., beads that did not crystallize or crack) were then analyzed three times in a Bruker S4 Explorer™ equipped with a wavelength dispersive spectrometer (WDS), and quantified using calibration curves generated from reference standards. The samples were then analyzed using a standardless routine to estimate the concentration of all the elements in the sample. The standardless routine provides an opportunity to quantify minor elements that may not present in the calibration standard. The approximate precision for the elements in these samples was around 0.1 wt%. The instrument could detect to lower levels but was not consistent in its detection; consequently, any elements detected at less than 0.1wt% were listed as "trace".

2.3 Results and discussion

2.3.1 Warm water extraction

The mass balance of bitumen, solids, and water around extraction is shown in Table 12. As shown in the table, the ore contains 8.5 wt% bitumen, corresponding to a mid grade ore. These values also correspond to an average 89% recovery of bitumen into the primary froth and an average 92% overall bitumen recovery, confirming that this ore sample is a good processing ore. The mass losses were due primarily to the evaporation of water (~ 84% of losses) as well as some losses on the walls of the extraction vessel. The balance of the mass loss can be explained as solids lost to the thimble during recovery of Dean-Stark-extracted solids. This was especially evident in the middlings samples, where the recovered weight was 38% lower than the weight reported by Maxxam (Table 13). That the fine solids were lost is evidenced by the fact that the discrepancy between the solids weight reported by Maxxam in the thimble and the delivered solids weight increases in direct proportion with the weight-percent of fines found in the sample.

Table 12: Mass balances of bitumen, solids, and water around extraction

		ASSAY				DISTRIBUTION			
	Wt% of total feed	**Bitumen**	**Solids**	**Water**	**Dean stark loss**	**Bitumen**	**Solids**	**Water**	**Dean stark loss**
Water	68.5%	0%	0%	100%	0%	0%	0%	99%	0%
Ore	31.5%	8.5%	89.1%	1.7%	0.7%	100%	100%	1%	100%
Total Feed	100.0%	2.7%	28.0%	69.1%	0.2%	100%	100%	100%	100%
Primary Froth	5.3%	44.6%	22.3%	32.3%	0.8%	88.8%	4.2%	2.5%	9.0%
Secondary Froth	0.6%	15.2%	26.4%	57.1%	1.3%	3.2%	0.5%	0.5%	1.6%
Middlings	65.7%	0.2%	9.8%	89.4%	0.6%	5.7%	22.9%	85.0%	82.5%
Tailings	27.0%	0.3%	74.6%	25.0%	0.1%	3.2%	72.0%	9.8%	6.9%
Sum of Streams	98.6%	2.7%	28.3%	68.5%	0.5%	101.0%	99.6%	97.7%	100.0%
Losses	1.9%	-1.4%	5.3%	83.7%	24.0%	-1.0%	0.4%	2.3%	100.0%

Table 13: Analysis of mass losses during sample preparation

	Ore	Primary Froth	Secondary Froth	Middlings	Tailings
Weight Reported by Maxxam (g)	445.8	57.9	8.0	313.4	952.3
Delivered Weight (g)	443.5	49.9	5.5	194.3	941.0
Weight after Homogenization (g)	441.4	49.8	5.5	193.8	940.7
Weight after Sieving (g)	423.6	49.3	5.4	192.3	932.7
Weight after Silt Separation (g)	437.0	50.1	5.3	203.4	934.7
Weight after Excess Water Removal (g)		48.9	5.2	150.4	935.3
weight after 0.2 µm separation (g)	438.9	49.0	N/A	185.3	935.5
Total Solid Losses (g)	6.	8.9	2.8	128.1	16.8
% Loss	2%	15%	35%	41%	2%
% loss from cleaning	0.5%	13.80%	31.50%	38.00%	1.20%

2.3.2 Particle size distribution of process solids

Figure 12 shows the particle size distribution of the samples. Since the middlings and tailings were derived from the overall tailings by sedimentation it is unsurprising that the middlings contains the majority of the finer particles which take longer to settle (as per Stokes law) while the tailings is dominated by coarse particles. The primary froth has more coarse material than would be expected based on Stokes law, indicating that the particles in the froth are floated due to the attraction to the bitumen.

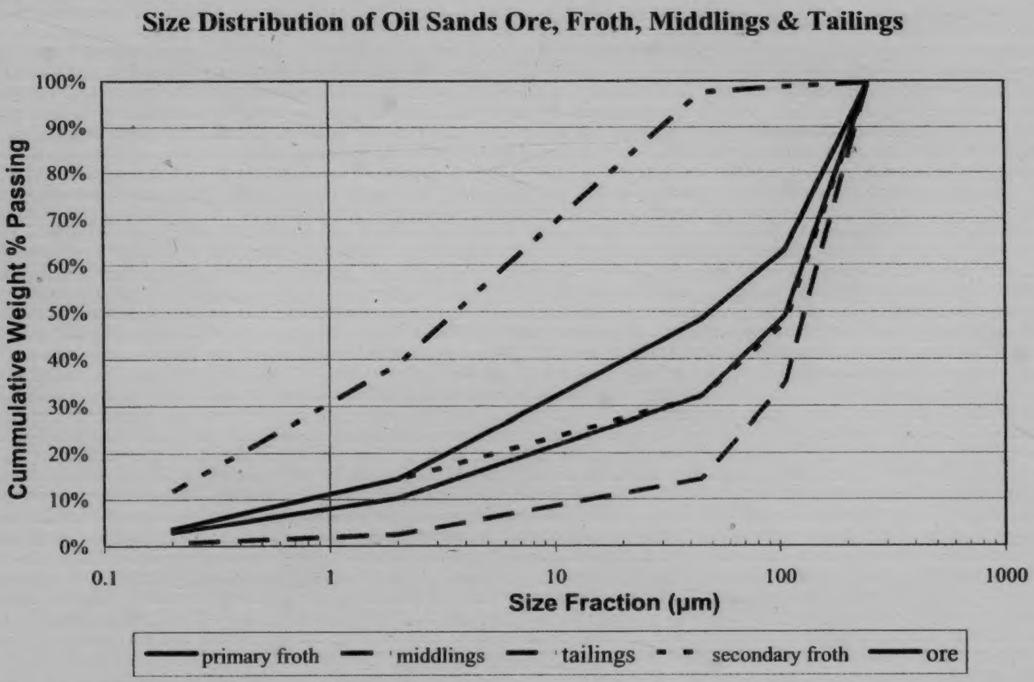

Figure 12 :Particle size distribution of process streams.

The primary froth solids are very distinctive in appearance. The >250 μm solids are black with very few other particles. The 106–250 μm samples are mostly black sand with some white sand. The 45–106 μm solids have black and white sand with a large quantity of reddish sand not seen elsewhere. Secondary froth solids appear much more like the tailings solids than like the primary froth solids, though the fines fraction seems more like the primary froth solids than the tailings – i.e., black/dark brown.

Table 13 shows the mass loss for each sample during the different stages of size separations. For all samples, except the ore, the majority of the sample loss occurred during Dean Stark extraction. The loss of ore solids during Dean Stark extraction was relatively minimal, possibly because the fine material stuck to the coarse material present in the thimble, rather than being lost into the thimble filter.

Table 14 shows the mass balance around extraction of the different particle sizes of solids. As shown the middlings comprise only 16% of the total solids, but 70% of the total clays and 73% of the total ultrafine clays. This means that the clay minerals present in the ore will have a much larger impact on the properties of the middlings stream than on the properties of any other stream.

Table 14: Distribution of sand, fines, clays and ultrafine clays around extraction

		ASSAY (wt%)				DISTRIBUTION (wt%)			
	Wt% of all streams	**>45 µm**	**<45 µm**	**<2 µm**	**<0.2 µm**	**>45 µm**	**<45 µm**	**<2 µm**	**<0.2 µm**
Primary Froth	4.2%	52%	48%	14%	4%	3%	7%	7%	6%
Secondary Froth	0.5%	68%	32%	14%	0%	0%	0%	1%	0%
Middlings	15.8%	2%	98%	39%	12%	1%	53%	70%	73%
Tailings	79.6%	86%	14%	2%	1%	96%	39%	22%	21%
Ore	100%	68%	32%	10%	3%	100%	100%	100%	100%
Sum of streams	100%	71%	29%	9%	3%	100%	100%	100%	100%

A break down of the particle-size distribution for the sand (> 45 µm) is shown in Table 15. As shown, the majority of the sand is in the 106–250 µm size range, which is ideal for most mineral processing techniques.

Table 15: Distribution of particle sizes in sand fractions around extraction

		ASSAY (wt%)			DISTRIBUTION (wt%)		
	Wt% of all streams	**>250 µm**	**106-250 µm**	**45-106 µm**	**>250 µm**	**106-250 µm**	**45-106 µm**
Primary Froth	4.2%	0%	37%	15%	3%	3%	4%
Secondary Froth	0.5%	0%	52%	16%	0%	0%	0%
Middlings	15.8%	0%	1%	1%	16%	0%	1%
Tailings	79.6%	0%	65%	21%	81%	96%	95%
Ore	100%	0%	50%	17%	100%	100%	100%
Sum of streams	100%	0%	53%	17%	100%	100%	100%

2.3.3 Element balances

The XRF results for all the streams assayed are shown in Appendix A (Tables A-1 to A-3); a complete mass balance of the 15 major elements detected is also shown in Appendix A (Tables A-4 to A-27).

Of the elements present in the oil sands the three most interesting for secondary uses are titanium, zircon, and iron. Furthermore, all three elements are preferentially enriched to the primary froth, with the primary froth accounting for 53% of the total titanium, 29% of the total iron, and 33% of the total zirconium (Table A-12). The enrichment is most pronounced for the titanium, especially in the sand fraction (> 45 µm) where a ten fold increase in titanium assay is noted between the ore and primary froth (Table A-9). This enrichment indicates that the titanium-containing minerals in the sand fraction are effectively collected by the bitumen. The enrichment of the zirconium and the iron, while substantial, are not as complete as the enrichment of the titanium minerals.

It is also interesting to note how the three minerals distribute among the different size fractions. Titanium and iron exhibit similar distributions, with the majority concentrated into the fines (2–45 μm) fraction of each stream. The fines account for 83% of the total iron (Tables A-15) and 74% of the total titanium (Table A-18). The two elements differ most in distribution within the clay size fraction, where only 20% of the total titanium is found in the clay size fraction (Table A-18) as compared with 44% of the total iron (Table A-15). Unlike the titanium and iron, the zirconium is primarily concentrated in the sand fraction (> 45 μm) of the oil sands, with only 30% contained in the fines fraction and less than 1% concentrated in the clay size fraction (Table A-19).

The combination of size and stream distributions indicates that the limiting factor for zirconium reclamation is likely the ability of the coarser zircon particles to float with the bitumen during the bitumen extraction. Titanium's effective flotation is apparently achieved in the primary separation vessel; however, a large portion of the titanium is concentrated in the fines, which are much more difficult to process. Furthermore, the iron enrichment in the fines means that any titanium recovered from the fines is more likely to be contaminated with iron than the titanium in the coarser streams.

Apart from titanium, zircon, and iron, there are other interesting elemental distributions that should be noted. Least surprising is the fact that the majority of the silicon is concentrated in the tailings and the sand fractions of the other streams. It is also not surprising that the main elements other than silicon found in clay minerals (aluminum, potassium, and magnesium) are concentrated in the fines stream. Calcium is also found concentrated in the fines fractions for all streams except the tailings, indicating that calcium in the tailings is likely present mostly in non-clay minerals. Aluminum and potassium are fairly evenly divided between the silt and the clay. Magnesium, conversely, is concentrated in the clay stream for all the streams other than the primary froth. Calcium is concentrated in the silt for all streams other than the middlings. The majority of the coarser magnesium is found in the primary froth, likely as siderite. In the clay-size fraction, the majority of the aluminum, silicon, and potassium are found in the middlings. The primary froth shows a slight depletion in potassium and aluminum relative to the other streams, and an enrichment of calcium. This combination of elements indicates that the primary froth is likely to be depleted in micaceous phases.

Among the minor elements, chlorine is found to be enriched in the primary froth clays as 42% of the total chlorine detected in this fraction (Table A-6). Manganese is also enriched in the froth, particularly in the silt fraction (2–45 μm). It should be noted that elements such as calcium, magnesium, potassium, and chlorine are sensitive to the water chemistry of the flood water used during extraction and retained during Dean Stark extraction. Since the water chemistry was not analyzed in this study, the mass balance of these soluble ions is not complete.

2.3.4 Mineral identification

Identification of the major phases (i.e., 30 wt% or greater) present in the XRD traces was a relatively straightforward task. In the majority of cases the only major phase present was quartz. With the minor phases, identification was not straightforward and generally had to be done manually, as JADE™ (the search-match software used in this study) had difficulty matching minor and trace phases which were present in quantities less than 20%. Manual identification consisted of concentrating on matching each of the observable peaks with one or more of the minerals identified by the literature survey undertaken earlier as possibly present. With this method, it was fairly straightforward to identify the presence of various mineral groupings (i.e., plagioclase feldspars, potassium feldspars, illitic clay minerals, kaolinitic clay minerals, and chloritic clay minerals). It was, however, more difficult to determine the exact mineral species present, particularly in the case of the feldspars, where overlap between species was very large and in all likelihood more than one of each type was present. In these cases, refinement concentrated on picking one or two minerals that seemed to best fit the pattern. Further difficulties existed with the identification of the titanium minerals because small quantities of rutile and anatase can be masked by the presence of the feldspars and clay minerals. For completeness, these minerals were included in the refinements when there was a possibility that their presence was masked by other phases.

The phases present in each sample were identified by using JADE ™ to assist in the comparison of the experimental patterns with patterns of minerals previously identified by other mineralogical assessments of the oil sands. If peaks remained unidentified after the original list of 90 minerals had been checked, the JADE ™ search/match program was used to generate other suggestions. Table 16 to Table 18 show the qualitative analysis for the >2 μm fractions of the froth, tailings, and middlings streams. The detected corundum was most likely from the alumina grinding balls used in the micronizing mill.

Table 16: Qualitative XRD analysis of run 2 samples

	Tailings				**Middlings**	**Primary Froth**		
	>250 µm	**106–250 µm**	**45–106 µm**	**2–45 µm**	**2–45 µm**	**106–250 µm**	**45–106 µm**	**2–45 µm**
Anatase						Y	Y	Y
Ankerite	?	?	?	?	?	?	?	?
Brookite						?		?
Chlorite				Y	Y	?		Y
Corundum	Y	Y	?	Y	?	?	Y	Y
Epidote				?				
Hematite						Y	?	?
Ilmenite						?	Y	Y
Kaolinite	?		Y	Y	Y	Y	Y	Y
Kutnohorite						?		?
Magnetite							?	?
K-Feldspar	?	Y	?	?	?	Y	?	
Illite/Muscovite	?		Y		Y	Y	Y	Y
Plagioclase					?	?		Y
Pyrite						?	Y	Y
Quartz	Y	Y	Y	Y	Y	Y	Y	Y
Rhodochrosite								?
Rutile		?	?			Y	Y	Y
Schorl						Y	Y	?
Siderite					Y	?	?	Y
Zircon						?	?	?

Table 17: Qualitative XRD analysis of run 3-5 tailings and middlings

	Tailings				Middlings	
	>250 µm	106–250 µm	45–106 µm	2–45 µm	>45 µm	2–45 µm
Anatase					?	?
Ankerite	?	?	?	?		
Chlorite					?	Y
Corundum	Y	Y	Y	?	Y	Y
Epidote		?	?	?		?
Kaolinite	Y		?	Y	Y	Y
Magnetite					?	
K-Feldspar	Y	Y	Y	Y	?	
Illite/Muscovite	Y		?	Y	Y	Y
Plagioclase	Y		Y	Y	?	?
Pyrite	Y					
Quartz	Y	Y	Y	Y	Y	Y
Rhodochrosite	Y				?	
Rutile				?	?	?
Schorl		?			?	
Siderite	Y				Y	?
Zircon					?	?

Table 18: Qualitative XRD analysis of run 3-5 Froth streams

	Primary Froth			Secondary Froth	
	>106 µm	45–106 µm	2–45 µm	>45 µm	2–45 µm
Anatase	?	Y	Y		Y
Ankerite			?		?
Brookite		?	?		
Chlorite			Y		Y
Corundum	Y	Y	Y	Y	Y
Epidote			?		
Hematite		?	?		
Illite/Muscovite	?	Y	Y	Y	Y
Ilmenite		Y	?		?
Kaolinite	?	Y	Y	?	Y
Kutnohorite		?			
Magnetite			?		?
K-Feldspar	Y	Y	Y	?	
Pyrite		Y	Y		?
Quartz	Y	Y	Y	Y	Y
Rhodochrosite			Y		Y
Rutile	Y	Y	Y	?	Y
Schorl		?	?		Y
Siderite		?	Y		?
Zircon		Y	?	?	?

2.3.5 Mineral quantification

Many different approaches to quantitative analysis were taken in the analysis of these samples. There did not seem to be a consistent approach that worked well for all samples. As such, the quantitative results are presented in two different ways. The first way is as an average of all the refinements obtained. The second way chooses the result that has a low refinement error (i.e. the weighted averages of the errors is small), and that best matches the XRF results. These results are found in Appendix A (Tables A-28 to A-32). The error in the refinements was the larger of either the error as calculated from the refinement software, or 15% of the value. 15% of the value was chosen because the maximum range in quartz results between different refinements on the same sample was just under 15%. For mineral balances the best values were used.

2.3.6 Mineral balances

The XRD results for all the streams assayed are shown in Appendix A (Tables A-28 to A-32), and a complete mass balance for the assayed minerals is also shown in Appendix A (Tables A-33 to A-64). The minerals can be considered in four broad categories: – clay minerals, other silicates, iron-containing minerals, and titanium-containing minerals.

2.3.6.1 Clay minerals

As expected, the majority (> 60%) (Table A-61) of the clay minerals detected are concentrated in the clay-size fraction of the different streams. The clay minerals not found in the clay size are generally found in the silt-size fraction, so that the vast majority of the clay minerals are in the fines. The only stream that had any appreciable quantity of clay minerals in the sand-size fraction was the tailings, where 14% of the total clay minerals detected were in the >45 μm fraction (Table A-61). This may be due to the large quantity of material in this size fraction, which makes complete clay dispersion and separation more difficult. It is no surprise, therefore, that the majority of the clay minerals (73%) partition, along with the majority of the clay size fraction, to the middlings stream, while only 7% of the total clay minerals partition to the primary froth.

Chlorite, kaolinite, and kaolinite-smectite make up the bulk of the clay minerals that partition to the primary froth, with the primary froth accounting for 10% of the total chlorite, 8% of the total kaolinite, and 8% of the total kaolinite-smectite. The primary froth accounts for only 4% of the total illite-smectite, while the middlings accounts for 75% of the total illite-smectite, indicating that the illite-smectite has a preference for the aqueous middlings stream (Table A-42).

2.3.6.2 Other silicates

The majority of the feldspar present in this ore is a potassium feldspar, primarily microcline; however, in the middlings the "best" refinement was obtained when a plagioclase feldspar is included in the refinement. For the purposes of the mineral balance discussion, the two feldspars are combined to give a total distribution of feldspars around extraction. Both quartz and feldspar are concentrated in the >45 μm fraction; this fraction accounting for 82% of the quartz (Table A-56) and 71% of the feldspars (Table A-63), with microcline being slightly finer than the quartz. It is, therefore, not surprising that the majority of both the microcline and quartz ended up in the tailings stream, as larger particles have more difficulty floating than smaller particles. Quartz showed no affinity for the primary froth, as all quartz present likely is the result of entrainment or association with other minerals that were attracted to the froth. The finer microcline showed a slight affinity for the primary froth, with 23% of the total <45 μm microcline reporting to the primary froth (Table A-38). Overall, it seems that the distribution of these minerals is dominated by the difficulty in suspending large hydrophilic particles.

2.3.6.3 Zircon

Zircon is strongly enriched in the primary froth, with 93% of the detected zircon partitioning to this stream. This is a significantly higher figure than predicted by elemental analysis. This is most likely due to the difficulty of detecting the small concentrations of zircon that remain in the other streams. As well, in contrast to the elemental results, most (63%) of the detected zircon was found in the silt fraction as opposed to the sand fraction (Table A-60). Once again, this is likely due to the detrimental effects of a large quantity of quartz on the detectability of zircon by Rietveld analysis.

2.3.6.4 Titanium-bearing minerals

As predicted by XRF results, the majority (76%) of the titanium minerals detected were in the <45 μm fraction. This trend was consistent for all the detected titanium-bearing minerals (rutile, anatase, brookite, and ilmenite). Ilmenite was the coarsest, with only 61% of the ilmenite found in the <45 μm fraction (Table A-49), and brookite was the finest, with 88% in the <45 μm fraction (Table A-45). Also, as predicted, the titanium minerals were strongly enriched in the primary froth, with 79% of the total titanium minerals detected reporting to the froth (Table A-62). Of the titanium-rich minerals, brookite and ilmenite were only detected in the froth streams. They were, however, present in quantities close to the lower detection limit. Rutile and anatase were detected in all streams if not in all size fractions of every stream. Of the detected anatase, 68% reported to the primary froth, compared with 74% of the rutile (Table A-42). This is expected, since rutile is known to have a higher contact angle with water than anatase does (Wu and Nancollas, 1998), indicating that it is less hydrophilic than the anatase. It is therefore reasonable to assume that the rutile will be more easily collected by the hydrophobic bitumen.

2.3.6.5 Iron bearing minerals

Like the titanium-bearing minerals, the iron-bearing minerals are concentrated in the <45 µm fraction (74%) and in the primary froth (56%) (Table A-64). Of the five iron–bearing minerals detected (ilmenite, lepidocrocite, schorl, siderite, and pyrite), all except schorl had the majority of their weight in the <45 µm fraction, whereas 57% of the schorl was >45 µm (Table A-58). In addition, all the minerals except siderite had more than 75% of their detected weight in the primary froth (Table A-42). Only 38% of the siderite was detected in the primary froth (Table A-42). This distribution is expected of pyrite, which is more hydrophobic than the other iron-bearing minerals detected (Wills, 1997). Ilmenite, on the other hand, is expected to be less hydrophobic than siderite. As such, it is interesting that ilmenite is strongly enriched in the froth, while the siderite is not as strongly enriched in the froth.

2.3.7 Comparisons between XRF and XRD results

The weight-percent silicon, aluminum, iron, potassium, and titanium expected were calculated from the detected mineral compositions and standard mineral formulas for the detected minerals. These results were then compared to the actual elemental assays for the elements as determined by XRF analysis. The results of the comparisons are shown in Appendix A (Table A-65 to Table A-73).

As shown, the silicon content was within the 15% error of the XRD results for all samples, except for the 2–45 μm fraction of the secondary froth and ore, and the 45–106 μm fraction of the primary froth. For the froth samples, the predicted value was higher than the actual value. Conversely, for the ore, the predicted value was lower than the actual value. The relatively close matches for all samples lend weight to the accuracy of the XRD results.

The aluminum values were higher than predicted for the primary froth clays but lower than predicted for the coarse fractions of everything except the middlings. This indicates that either there is less kaolinite than predicted in the primary froth (and hence less aluminum) or the illite that is present has less aluminum and potassium than was predicted from the standard formulas used. It may also indicate that the total amount of clay minerals in this stream is less than predicted, possibly due to the presence of iron-oxides that were not detected in the XRD, such as feroxyhite. Given the high quantity of iron detected, the latter seems likely. This result would suggest lower levels of aluminum and potassium levels than predicted by XRD. The low levels of aluminum predicted in the coarse fraction may indicate the presence of more feldspars than were detected. These high levels of feldspars seem likely, given the difficulty in modeling an appropriate feldspar in these fractions.

The iron content predicted from the XRD analysis was universally lower than the actual value of iron in the sample. This is likely due to the presence of the fine iron oxides detected in the TEM that were not detected in the XRD and possibly due to iron substitution present in the clay minerals and other minerals (such as in "leucoxene").

As with the iron content, the predicted titanium content was almost universally lower than the actual content of titanium, with the exception of some primary froth streams which accurately predicted the titanium content. This speaks to the difficulty in modeling the rutile present in the samples. Rutile was generally easy to identify, but was almost always poorly refined, irrespective of the Rietveld analysis software used. Also, for many of the other streams, the titanium content was lower than the detectability limit in the XRD, and as such, any mineral present was simply not in sufficient quantities to be quantifiable.

The predicted potassium contents followed similar trends to the aluminum content, where the predicted value was generally higher than the actual value for the clay size fractions and was lower than predicted for the coarse fractions. Again, this is likely due to either a difference in the structure of the illite/illite-smectite or the presence of fine iron oxides, which will generally reduce the total amount of clay minerals present in the clay fraction. In the coarse fraction, the low predicted value indicates that more potassium feldspars are likely to be present than were detected.

Overall, the agreement between the XRD and XRF results were acceptable. The discrepancies noted were generally due to the difficulty in assessing minor quantities of certain phases within the oil sands, because the level of spectral overlap present in the samples was too high.

2.4 Conclusions

The mass, element, and mineral balances around extraction reveal several interesting trends. As reported by other researchers, the titanium and zircon-bearing minerals are enriched in the primary froth, with 53% of the total titanium and 33% of the total zirconium reporting to this fraction (based on elemental analysis). The limiting factor for zirconium enrichment seems to be an incomplete affinity for the primary froth, likely due to the fact that zirconium is among the least hydrophobic minerals (Wills, 1997). The enrichment of the titanium is more complete, likely because most titanium minerals are more hydrophobic and smaller than the zircon bearing minerals. Iron is also enriched in the froth, but not as strongly as the zircon and titanium, because iron is a minor constituent of many of the silicate minerals detected. Of the iron-bearing minerals, all except for siderite were found to be enriched in the primary froth.

The mineral balance of the clay minerals showed that the non-charged, less asymmetric phases of kaolinite and chlorite preferentially reported to the primary froth. The charged clay and more asymmetric clay minerals of illite-smectite and illite, conversely, preferred the middlings stream. This distribution is important, because it indicates that the more highly active clay minerals, i.e., the ones that will have a negative impact on settling behaviour, tend to concentrate in the stream where settling behaviour is most important (the middlings).

3 Characterization of Oil Sands Clays

Clay mineral characterization is important for several reasons. First, although mixed layer clay minerals have been identified as a component of the oil sands, their structure is not well known. The structure of the mixed layer clay minerals can, in turn, be used by others to improve models of clay behaviour in thickeners, tailings ponds or in processing. Second, knowledge of where iron and other colour inducing chromophores are located will help with the development of bleaching techniques, so that the kaolinite found in the oil sands can be used in high-value applications such as paper making, concrete admixture or fine ceramics. Finally, exploring the relationship between particle thickness, charge distribution and the degree of mixed layering seen in XRD patterns will substantially add to the body of knowledge in clay science and may help address problems seen with other unusual clay mineral deposits such as the Birdwood kaolin in Australia (Zbik, 2006).

The characterization of the clay minerals can be separated into three parts: identification, quantification, and microstructural analysis. Identification uses X-ray diffraction (XRD) analysis after seven different pretreatments on oriented clay slides to identify the types of clay minerals present. Quantification uses Rietveld analysis of XRD patterns from ethylene glycol oriented clay slides and random powder mounts to determine the quantity of each mineral present. Microstructural analysis involves determining the fundamental particle thickness of the clay minerals in each stream and identifying charge distribution in the clay minerals. The particle thickness is determined in several different ways, including measurement of particles using high-resolution transmission electron microscopy (HRTEM) and calculation of the effect of particle thickness on peak broadening in XRD traces. Determining the charge distribution involves calculating the structural formula of specific clay minerals from elemental data, calculating the distribution of silicon and aluminum in the tetrahedral sheet, and calculating the distribution of other cations in the octahedral sheet and the interlayer.

3.1 Materials and methods

3.1.1 Separation of clay minerals and elemental analysis

The separation methods and elemental analysis methods used in this project are outlined in Chapter 2: Mass and Mineral balances.

3.1.2 X-ray diffraction analysis

In this project, X-ray analysis of the clay fraction of the oil sands was accomplished in two ways: the analysis of oriented-clay slides and the analysis of dried clays in a random powder mount. Oriented-clay slides were used to identify and quantify the relative amounts of the different clay minerals, while the random powder mount was used to identify and quantity the non-clay minerals present in the samples.

3.1.2.1 Random powder mounts

Freeze-dried solids from each fraction were analyzed by random powder XRD. The freeze-dried solids were passed through a 400 μm sieve onto a horizontal sample holder. The excess material was then removed by passing a straightedge over the surface of the sample holder. This method was found to reduce the preferred orientation in the samples (Omotoso, 2006).

3.1.2.2 Preparation of oriented clay slides

Three 20 mL aliquots from each sample were obtained. A small scoop of $CaCl_2$ was added to two aliquots from each sample, and a small scoop of KCl was added to the remaining aliquot. In each aliquot the salt was allowed to dissolve thoroughly, and the resultant mixture was filtered onto a 0.45 μm type HE millipore filter paper using a millipore filter set up. Once the clay had been filtered, two ~ 3 mL rinses of deionized water were allowed through the filter to wash away any excess chloride. The wet filter cake was then placed cake-side down on a zero-background quartz slide (for the calcium-saturated samples) or onto a small piece of glass slide (for the potassium-saturated samples) and allowed to dry in an oven until the filter paper was mostly dry but still pliable. The filter paper was then peeled off the filter cake, leaving the filter cake stuck to the slide. The oriented slides were then subject to the following pretreatments modified from Chichester et al. (1969).

3.1.2.3 Pretreatments

Calcium saturated – 54% relative humidity (RH)

The calcium-saturated samples were placed in a small desiccator containing a super-saturated solution of magnesium nitrate in deionized water and allowed to equilibrate for at least 24 h. This solution maintained the relative humidity of the desiccator at 54% RH. This pre-treatment was used to cause the smectitic and vermiculitic clay minerals to absorb two layers of water into their interlayer, thus expanding them to a (001) spacing of 1.5 nm.

Calcium saturated – ethylene glycol solvation

After testing, the calcium saturated 54% RH samples were placed in a small desiccator containing a Petri dish full of ethylene glycol. The desiccator was then placed in an oven at 65°C for at least 12 h. The desiccator was removed from the oven and allowed to sit at room temperature for at least 24 h. This pretreatment was used to cause the smectitic clay minerals to further expand to a (001) spacing of 1.7 nm to allow them to be differentiated from vermiculitic swelling clay minerals, which will have a (001) spacing of 1.5 nm under these conditions.

Calcium-saturated – glycerol solvation

The duplicate calcium-saturated 54% RH samples were placed in a small glass desiccator containing a Petri dish full of glycerol. The desiccator was then placed in an oven at 105°C for at least 4 h, removed, and allowed to cool to room temperature. This test was used to cause the octahedrally substituted smectites to expand to a (001) spacing of 1.7

nm while the vermiculites and tetrahedrally substituted smectites remained at a (001) spacing of 1.5 nm, thus allowing differentiation between beidellite-type smectites and montmorillonite-type smectites.

Potassium-saturated – 0% RH

The potassium-saturated samples were heated in an oven to 105°C for 12 h to drive off any water in the interlayer. The samples were then cooled and placed in a desiccator at 0% RH until they were tested. This test was used to collapse the (001) spacing for all swelling clay minerals down to 1.0 nm. This test allows the presence of chlorite and hydroxyl-interlayered vermiculites to be detected, as the chlorite (001) spacing will remain at 1.4 nm. This test also emphasizes the presence of kaolinite-smectite as the collapse to a (001) spacing of 1.0 nm for the smectitic component increases the spacing of the overall kaolinite-smectite, according to Méring's principle (Moore & Reynolds, 1997).

Potassium-saturated – 54% RH

After testing at 0% RH the potassium-saturated slides were placed in the desiccator, maintained at 54% RH, allowed to equilibrate for 24 h, and then re-measured. This test is used to differentiate vermiculitic intergrades and vermiculite from smectitic intergrades and smectite. Vermiculitic clay minerals will not rehydrate, whereas illitic clay minerals will rehydrate to have one water layer in their interlayer, giving them a (001) spacing of 1.2 nm.

Potassium saturated – 300°C

After the 54% RH test, the potassium saturated slides were placed in a furnace at 300°C for 6 h. The sample was then cooled and measured again. This sample is used to test for the presence of hydroxyl-interlayered vermiculites. If there are organics or small aluminum hydroxyl islands present in the sample, it may have a peak at 1.4 nm, which is possibly indicative of chlorite. If this peak disappears upon heating to 300°C, then the mineral was likely hydroxyl-interlayered vermiculite, as both organics and partial sheets break down at this temperature.

Potassium-saturated – 550°C

After the 300°C test the potassium saturated slide was placed in a furnace at 550°C for 5 h. The sample was then cooled and measured a further time. This test allows for the quantification of chlorite vs. kaolinite, as kaolinite decomposes at ~ 500°C, meaning any peaks remaining at 1.4 and 0.7 nm after this test will be from chlorite.

3.1.2.4 Preparation of clay quantitative standard

To check the accuracy of the clay quantification methods used, a standard sample was prepared from a mixture of source clay minerals. The source clay minerals used were ripidolite (CCa-2), smectite (Swy-2), kaolinite (KGa1-b), illite(70)-smectite (ISCz-2), and illite (R3M1). Each source clay mineral was homogenized using a mortar and pestle. The kaolinite and ripidolite samples were quite pure so no further purification was performed. The illite, smectite and illite-smectite samples were all sieved and centrifuged to obtain the <2 μm fraction and freeze dried to obtain dry powders. The pure clay powders were combined in a small vial and mixed for 10 minutes with a Retsch mixer mill. The mixture was then prepared into slides and analyzed along with the other samples.

3.1.2.5 X-ray diffraction data collection

All samples were run on a Bruker D8 Advance X-ray diffractometer, with an incident beam parabolic mirror (Co K_{α}), a 25-mm sample diameter, and a VANTEC-1™ linear detector. A 0.2 mm exit slit was used to limit the resolution. The oriented samples were run from 4° to 36° (2θ), while the powdered samples were run from 4° to 99.6°. All tests were run at ambient temperature and humidity. These conditions are contrary to standard procedure for clay slides, but the humidity of the sample chamber was not controllable. For the tests where humidity is a concern (K-sat samples and the Ca-sat 54% RH samples), the samples were removed from their humidity-controlled containers and run one at a time. Duplicate tests were also done on some samples after these had been exposed to the atmosphere for various lengths of time. The Ca-saturated samples showed no signs of dehydration, even after being exposed to the atmosphere for up to 72 h. Some signs of rehydration occurred in the K-sat samples within the first run, but subsequent runs showed no difference in degree of rehydration.

3.1.2.6 Quantification of clay minerals

Clay minerals in the oriented slides were quantified using NEWMOD™ modeling of the glycolated samples and TOPAS™. First, NEWMOD™ was used to simulate the mixed layering observed in the samples. The NEWMOD™ -generated profiles were then modeled with TOPAS™ to extract the pure diffraction profiles, using the fundamental parameters specified in the NEWMOD™ profiles. This approach is necessary, because NEWMOD™ is not equipped to model instrument functions from a parabolic mirror and the linear detector used to collect the diffraction data. Peak positions and areas obtained for the pure diffraction profiles were used for quantifying the clay minerals (including mixed layered), using the reference intensity ratio (RIR) method described in Equations 4 and 5 (Moore and Reynolds, 1997).

$$\mathrm{RIR}_i = I_{p,i}/I_{p,s} \qquad \textbf{Equation 5}$$

$$\mathrm{Wt\%}_i = 100 \times \left\{ \frac{I_i}{RIR_i} \middle/ \sum_{i=1}^{n} \left(\frac{I_i}{RIR_i} \right) \right\} \qquad \textbf{Equation 6}$$

$I_{p,i}$ is the single-line integrated intensity of the pure diffraction profile of the ith modelled phase (generated from NEWMOD™ and TOPAS™) and $I_{p,s}$ is the integrated intensity of the pure diffraction profile of a reference model phase, which is illite (002) in this study. The weight percentage of the ith phase is given in Equation 5, where I_i is the peak area of the ith phase (same line as in the reference model) in the unknown sample. An approximation of this technique is an assumption that the degree of preferred orientation is the same for all phases.

The non-clay minerals present in the sample were quantified using AUTOQUAN™, with smectite being used to model the swelling components of the illite-smectite and kaolinite-smectite.

3.1.2.6.1 NEWMOD™ modeling

NEWMOD™ models for the clay minerals identified as present in the oil sands, were generated to help quantify the minerals present. These clay minerals were illite (dioctahedral mica), kaolinite, chlorite, illite-smectite, and kaolinite-smectite. Since the exact amount of mixed layering was unknown for the mixed-layered clay minerals, the illite-smectite and kaolinite-smectite series were modeled in 5% increments of smectite from 5% smectite to 50% smectite. R0 ordering was used for all kaolinite-smectites, whereas the ordering series outlined by Moore & Reynolds (1997) was used for the illite-smectite (R30 for 5% smectite, R1 for 15%-40% smectite, and R0 for >40% smectite). Illite was modeled using a dioctahedral mica with 0.2 atoms of iron and 0.8 atoms of potassium per formula unit. The smectite portion of the mixed-layered clay minerals was modeled using dioctahedral smectite-two glycol layers with 0.2 atoms of iron per formula unit. Chlorite was modeled using tri-trioctahedral chlorite with 0.2 atoms of iron per formula unit in the silicate layer, 0.8 atoms of iron in the single hydroxide layer. The instrument parameters used were as shown in Table 19.

Table 19: Modelling parameters for NEWMOD™ models

Parameter	Value
Lambda	1.78896 (Co Kα_1)
Divergence Slit	0.5°
Goniometer Radius	200 mm
Soller Slit 1	6.6°
Soller Slit 2	2°
Sample Length	45 mm
Quartz Reference Intensity	30000
Sigmaster	12
Mustar	45
Exchange Capacity	0.36
D001A	9.98
D001B	9.98
Theta Comp Slit	Out
RNDPWD	No
Proportional N Parameter	Default (All Prop N = 1)
Crystallite size distribution	Prop(8) = 1 High N = 35 Low N = 7
Exchange Cation	Calcium
2 Theta Range	2°–36°
Increment	0.01
Lorentz Polarization Factor	31.1 (internally calculated for graphite monochromator with cobalt radiation)

3.1.2.6.2 TOPAS™ modelling of NEWMOD™ profiles

The peak positions and intensities for the NEWMOD™-generated profiles were obtained using TOPAS™. The instrument profile was modelled using the fundamental-parameters approach, with the instrument parameters input into NEWMOD™. A first-order Chebyshev polynomial was used to model the background for the profile. For the regions less than 18°, a 1/x dependence was also used to account for background diffraction from the air.

Peaks were modeled individually (i.e. no structure file was used) within various refinement windows. The initial refinement windows used were 5°–12°, 12°–18°, 18°–26°, and 26°–34°. The refinement windows were adjusted slightly in subsequent refinements, giving slightly different values of peak intensity and of error in peak intensity. The final peak intensity for each peak was calculated as the weighted average of the different peak intensities obtained.

3.1.2.6.3 TOPAS™ modelling of sample profiles

Like the TOPAS™ modelling of the NEWMOD™ profiles, the peaks in the clay samples were modelled individually within set refinement windows. The refinement windows were fixed to maximize consistency between samples. The refinement windows used were: 5°–12°, 12°–18°, 18°–26°, and 26°–34°. The instrument parameter file was obtained by using LaB_6 and adjusting the instrument profile until the peaks were well modeled. The instrument details were then further refined, using ripidolite to better model the instrumental behaviour at low angles. As with the NEWMOD™ profiles, a first order Chebyshev polynomial was used to model the background for the profile, and a 1/X dependence was added for the first two refinement windows.

Because illite-smectite was present along with discrete illite, three peaks were used to model the peak cluster at ~ 20° 2θ. The central peak (0.5nm) was restrained to a minimum crystallite size (Scherrer) of 17 nm (Lvol-IB[16] =10 nm), and the two other peaks corresponding to illite-smectite were constrained to have equal crystallite sizes. The minimum crystallite thickness restraint is based on the thickness of illite that would give a maximum of 80 m^2/g specific surface area. In the samples where chlorite was present, an additional peak was added at 21.8° 2θ. In addition, the peak position of the illite 002 peak was restrained to between 20.5° and 20.83°, the peak position for the first illite-smectite 002/003 peak was restrained to between 19.5° and 20.7°, and the peak position for the second illite-smectite 002/003 peak was restrained to between 20.8° and 21.5°.

---

[16] As defined in section 3.1.2.7.2

Further restraints were used on the illite-smectite 001/002 peak in samples containing chlorite. For these samples the peak position was restrained to between 7.8° and 10°.

3.1.2.6.4 Determination of degree of interstratification

The percentage smectite of the illite-smectite component of the oil sands was determined by comparing the position of the 001 illite-smectite peak after solvation with ethylene glycol, to the 001 illite-smectite peak position in a series of calculated ethylene-glycol patterns.

There are, however, several flaws inherent in this comparison technique. The first is that it cannot account for sample displacement. In an attempt to overcome this difficulty, the profiles were shifted so that non-clay peaks were aligned. For the <0.2 μm samples lepidocrocite was used for the alignment, and for the 0.2–2 μm peaks, quartz was used for alignment. This alignment was done visually using EVA's sample displacement correction tool. Even with the visual alignment, the refined peak position of the lepidocrocite and quartz varied slightly among samples and refinements. Consequently, a second calculation was done to adjust the observed peak positions to a fixed value for lepidocrocite and quartz after refinements were completed.

Another flaw of this technique is the sample composition made measurement awkward. The 0.2–2 μm samples contained very little illite/smectite and also contained chlorite. Both factors made it difficult to correctly ascertain that peak position of the 001/002 illite-smectite peak, meaning that many restraints on the refinement had to be used. With these restraints in place, the values were quite similar to that of the <0.2 μm samples.

A second method of determining the percentage smectite of the illite-smectite component is to look at the difference in the 001/002 illite-smectite and 002/003 illite/illite-smectite peak positions after ethylene glycol solvation (Δ2θ). This technique is much more accurate for pure illite-smectite samples, because it eliminates sample displacement errors. Because these samples contain significant quantities of discrete illite and/or chlorite, the position of the 002/003 illite-smectite peak is difficult to accurately ascertain. Therefore this method was not used.

Kaolinite-smectite determination is somewhat more straightforward, since there is only one method of determination: measuring Δ2θ between the 001 and 002 peaks. As with the illite-smectite, the presence of chlorite can have an adverse affect on the determination of this value.

Error calculations are shown in Appendix B.

3.1.2.7 Surface area determination

Surface area contributions for kaolinite, kaolinite-smectite, illite, and illite-smectite were calculated from crystallite sizes determined by XRD. Error calculations are shown in Appendix B.

3.1.2.7.1 Crystallite size determination

TOPAS^{TM} was used to profile the individual peaks of the ethylene-glycol-solvated clay slides. The crystallite size was measured for kaolinite-smectite (001), kaolinite (001), illite (002), illite-smectite (002), illite-smectite (003), kaolinite (002), and kaolinite-smectite (002) peaks. The crystallite size of the 002 and 003 peaks of illite-smectite were constrained to be equal. The peak position of the illite 002 peak was restrained to be between the peak positions of the illite-smectite 002 and 003 peaks. Since the values of the crystallite size measured for the (001) and (002) peaks for kaolinite and kaolinite smectite were very close, the average of the two values was used for calculations.

3.1.2.7.2 Definition of LVol-IB in TOPAS^{TM}

LVol-IB is an indirect measure of crystallite thickness determined, by comparing the integral breadth of a diffraction peak to the volume weighted mean "column heights" (LVol) using the Scherrer equation modified by Stokes & Wilson (1942) (Equation 6).

$$\beta_i = \lambda / \left(L_{vol} \cos\theta\right).$$ **Equation 7**

β is the experimental angular integral breadth of a Debye-Scherrer line, θ is the Bragg angle, and λ is the X-ray wavelength. LVol will be equivalent to the crystallite thickness for the (001) diffraction peaks, as is the case for the oriented clay slides used in this experiment.

3.1.2.7.3 Fundamental thickness determination

The fundamental crystallite thickness of the mixed layer clay minerals was determined from the measured crystallite size by the method of Drits et al. (1997), as follows:

$$T_F = \frac{100T_M}{(T_M - 1)S + 100} d_{001}$$ **Equation 8**

where T_M is the mean number of layers in the mixed layer crystals (Equation 8), S is the percentage of smectite layers in the mixed layer crystals, and d_{001} is the spacing of the layers of the non-swelling component.

$$T_M = \frac{100\tau + (d_{S001} - d_{001})S}{100d_{001} + (d_{S001} - d_{001})S}$$ **Equation 9**

where τ is the crystallite size measured in TOPAS™, d_{S001} is the d spacing of a fully expanded smectite layer (1.7 nm), and d_{001} is the d-spacing of the non-swelling layer (1.0 nm for illite, 0.712 nm for kaolinite).

The fundamental particle thickness for the non-mixed layer clay minerals was taken as the crystallite size measured in TOPAS$^{\text{TM}}$.

3.1.2.7.4 Mean crystallite area, volume, mass, and surface area

The mean crystallite area, volume, mass, and surface area were calculated from the fundamental thickness according to the method of Nadeau (1987)[17], as follows:

$$A = (iT_F)^{\frac{1}{h}}$$ **Equation 10**

where A is the mean crystallite area (nm^2), T_F is the fundamental thickness in nm, i is the intercept of the straight line correlation observed by Nadeau that links the logarithm of particle thickness to particle area, and h is the slope of the same line. For kaolinites (including kaolinite-smectite), h = 0.657 and i = 38.7. For illites and smectites, h = 0.571 and i = 127.9.

Mean particle volume (nm^3) $V = \frac{A^{h+1}}{i}$ **Equation 11**

Mean particle mass (g) $M = V\rho 10^{-21}$ **Equation 12**

In Equation 11, ρ is the bulk density of the clay particle in g/cm^3 (usually determined from a source clay or from a unit cell model).

The basal surface area S_b (m^2/g) is then given as:

$$S_B = \frac{2A10^{-18}}{M}$$ **Equation 13**

and the lateral surface area is given as

---

[17] The equations in this section are direct quotes from Nadeau (1987), the explanation is my own with paraphrases from Nadeau.

$$S_L = \frac{T_F P_{Hex} 10^{-18}}{M}$$ **Equation 14**

where P_{Hex} is the perimeter of a regular hexagon having the same area as the particle

$$P_{Hex} = 3.72A^{0.5}$$ **Equation 15**

The total surface area of a particle is simply the addition of the basal surface area and the lateral surface area.

3.1.2.7.5 Total stream surface area

The total surface area of the stream was determined by the weighted contributions of the kaolinite, kaolinite-smectite, illite, and illite-smectite surface areas, as per Omotoso et al, (2002).

3.1.2.7.6 Limitations of surface area analysis by XRD

There are several limitations to this method of determining surface area. First, because only about 0.2 g of material or less are used for an individual XRD sample, great care must be taken in sample preparation to ensure that the sample is representative. Second, there is the possibility for a significant amount of error associated with modelling the clay peaks using the refinement options in TOPAS™, as much of the refinement depends on judicious use of restraints. Third, the surface area calculations are based on linear fit models. These, in turn, are based on relatively limited TEM data, which may not be representative of the true surface-area-to-thickness ratios exhibited by the clay minerals in the oil sands. Lastly, the total surface area completely neglects the surface area contributions of non-clay minerals or clay minerals such as chlorite. Except for the fine iron oxides, this is justifiable, given that the specific surface areas of non-clay minerals and chlorite are much smaller than those of clay minerals used. Despite these limitations the calculated surface area correlates well with other measurements of surface area for these samples and does provide a reasonable explanation for the behaviour observed in these streams.

3.1.3 Methylene blue adsorption test

Methylene blue analysis (ASTM, 1992) was conducted on each clay fraction as another method of measuring the surface area of the clay size samples. The <0.2 μm samples were tested using aliquots of the <0.2 μm slurry obtained after centrifuge separation. The amount of solids in these samples was determined by thoroughly dispersing the sample, drying an aliquot of 10 mL, and weighing the amount of solids remaining after drying. Freeze-dried solids were used for the 0.2-2 μm. samples

The dried solids were dispersed into 50 mL of 0.015 M $NaHCO_3$, along with 2 mL of 10% w/w NaOH. The resultant mixture was stirred using a magnetic stir bar for at least 20 min, or until the sample was completely dispersed (i.e., absence of remaining sediment, streaming birefringence of clay minerals[18]). Stirring was combined with 10 minute intervals of sonication in an ultrasonic bath in the case of difficult-to-disperse samples. Once the samples were dispersed, 2 mL of 10% v/v H_2SO_4 was added, and the pH was measured to ensure it was below pH 3. The sample was then titrated in 1 mL intervals with a fresh solution of 0.006 N methylene blue. After each addition a transfer pipette was used to place one drop of the titrated mixture onto Whatman #4 qualitative filter paper. The droplet was examined for the presence of a blue halo, which would indicate the end of the titration. If no halo appeared, another 1 mL of methylene blue was added to the solution. When a light blue halo appeared around the drop, the sample was left to stir for 2 min and another drop was placed on the filter paper. The end point was reached when the halo was still present after the second drop. On each day of testing, a bentonite standard was also tested in this manner to verify that the concentration of methylene blue and the application of the technique were consistent.

---

[18] Streaming birefringence in clays is characterized by an opalescent sheen when the slurry is stirred.

A similar procedure to that used for the freeze dried specimens was used for the slurry specimens, except that concentrated $NaHCO_3$ was added to the slurry to bring the concentration of $NaHCO_3$in the slurry to 0.015 M. At the end point of titration, the volume of methylene blue added to the slurry was recorded and used to calculate both the methylene blue index (MBI) and the methylene blue surface area, according to the methods of Hang and Brindley (1970):

$$MBI\left(meq/100\,g\;solids\right)=\frac{\left(vol.MB\times normality\;of\;MB\right)}{weight\;solids,\,g}\times 100$$

Equation 16

$$SA\left({}^{m^2}\!\!/_{g}\right)=MBI\times SA_{MB}\times 0.0602\,{}^{m^2}\!\!/_{g}$$

Equation 17

where SA_{MB} is the surface area of a molecule of methylene blue (1.30 nm^2/molecule). Error calculations are shown in Appendix B.

3.1.4 TEM analysis

Two types of samples were used for TEM analysis: dispersed samples and oriented thin sections. The dispersed samples were prepared either by dispersing a drop of dilute clay slurry directly onto a lacy carbon-coated copper grid. Oriented thin sections were prepared by partially filling a microtome mould with Spurr's resin, curing it, and then dispersing about 1–2 mL of the desired sample onto the partially cured resin. The water in the slurry was allowed to evaporate, and the solids were allowed to settle onto the resin surface to form a layer oriented with the basal planes parallel to the mould surface. The mould was then filled with Spurr's resin and cured. The cured block was trimmed and pieces 50 nm in thickness were sliced using an Ultracut E™ microtome. The microtome slices were captured on a lacy carbon-coated copper grid. Samples were examined using two different microscopes: a JEOL 2010 and a JEOL 2200FS TEM/STEM, both operated at 200 kV. The JEOL 2010 was equipped with a NORAN UTW EDX spectrometers. The JEOL 2200 FS was equipped with an INCAEnergyTEM EDX spectrometer and a High Angle Annular Dark Field (HAADF) Scanning Transmission Electron Microscope (STEM) attachment.

3.1.5 Thermogravimetric analysis

Thermogravimetric analysis was conducted on the freeze-dried and oven-dried solids of all size fractions using a variety of experimental procedures.

The first set of TG tests was conducted on oven-dried samples from the middlings, following the procedure of Friesen et al. (2005). The sample was heated at 10°/minute under a nitrogen atmosphere until 1000°C. Then the atmosphere was switched to air and the sample was held at 1000°C for 20 minutes. This procedure is consistent with the standard methods for TG analysis on clays. The plots, however, were difficult to interpret accurately, as there was significant overlap between the presumed clay dehydroxylation mass loss peak and the peaks indicating decomposition of residual organics.

A second set of TG tests was conducted on the middlings fraction using a TG with evolved-gas-analysis capabilities. These experiments were run under nitrogen, but a small oxygen leak was present, meaning that some oxygen may have been present during the analysis. As with the first round of tests, the sample was heated at 10°C/minute under a nitrogen atmosphere until 1000°C. The amounts of carbon dioxide, carbon monoxide, water vapour, and "tars" (combination of various organic molecules) present in the sample chamber were monitored during the test.

In an attempt to improve the differentiation between the peaks, an experiment was conducted using a NETZSCH STA 509 PC TGA by Luxx. This instrument has the ability to conduct tests under either nitrogen or air, but cannot switch atmospheres partway through the test. It was decided that air should be used as the burn-off medium to ensure the complete oxidation of any residual organics. The temperature profile was also radically altered. In this experiment the samples from all clay fractions were heated at 10°C/min until 110°C, held for 20 min, heated at 10°C/min until 470°C, held for 20 min, heated at 10°C/min until 575°C, held for 20 min, heated at 10°C/min until 1000°C, held for 20 min, and finally cooled. Two problems were noted with the data from this set of experiments. First, the dehydroxylation of the pure kaolinite reference run under these conditions began prior to 470°C (something not readily apparent from the earlier tests). Consequently it was impossible to determine how much of the mass loss in the 420-470°C was attributable to dehydroxylation of clays and how much was due to the decomposition of organics. Second the amount of iron that could be oxidized was unknown, and hence, it was not clear if any weight loss was being offset by the weight gain of oxygen during the oxidation of iron. This weight gain could be up to 1.5 wt% for the primary froth, if all the iron present in the sample was oxidized from Fe^{2+} to Fe^{3+}.

The final set of experiments was conducted on all clay fractions using a NETZSCH STA 509 PC TGA by Luxx with a nitrogen atmosphere. This time the samples were heated at 10°C/min until 110°C, held for 15 min, then heated at 5°C/min until 420°C, held for 10 min, heated for 5°C/min until 575°C, held for 10 min, heated at 10°C/min until 1000°C, held for 10 min, and finally cooled.

3.2 Results

3.2.1 Particle size distribution

Particle size analysis of the clay size samples was performed using a Mastersizer 2000^{TM}. As shown by the particle size distribution (Figure 13), the centrifugation was successful at separating out particles less than 0.2 μm in size. The middlings stream had a few larger particles present, but overall the average particle size was in the expected range (Table 20).

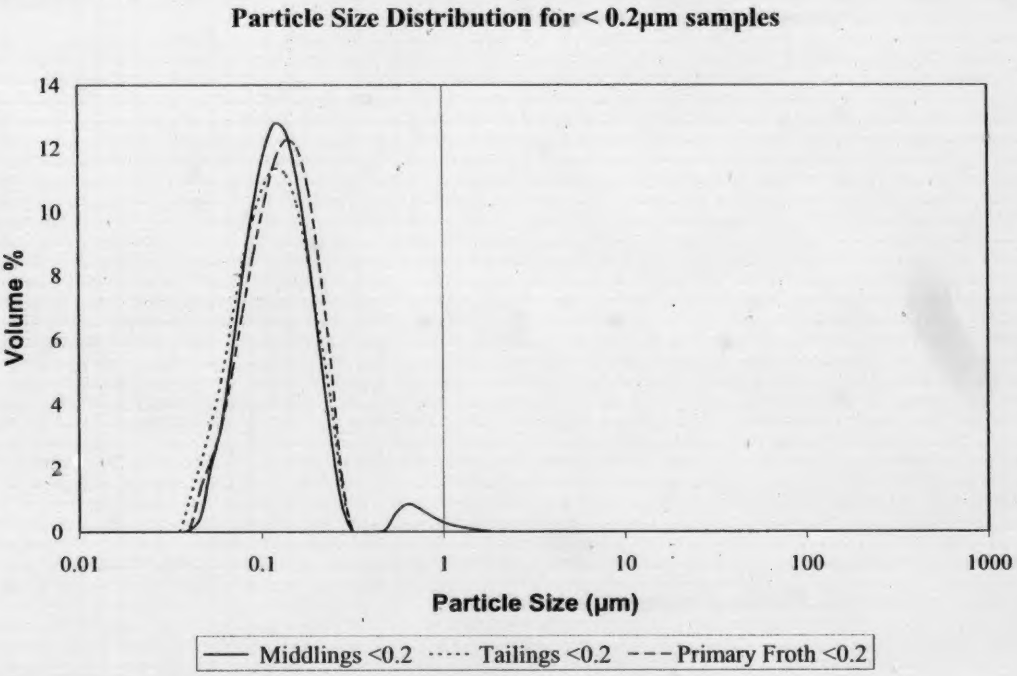

Figure 13: Particle size distribution for <0.2 µm.

Table 20: Particle size distribution numbers for d_{10}, d_{50}, and d_{90}[19]

	d_{10}	d_{50}	d_{90}
Primary Froth, <0.2	0.08	0.14	0.23
Middlings, <0.2	0.08	0.13	0.22
Tailings, <0.2	0.07	0.13	0.22
Secondary Froth, <2	0.11	1.93	12.58
Primary Froth, 0.2-2	0.08	0.29	3.35
Middlings, 0.2-2	0.08	0.14	1.16
Tailings, 0.2-2	0.13	3.70	17.86

---

[19] d_{10}, d_{50} and d_{90} represent the sizes at which 10%, 50% and 90% of the particles are smaller than the size given.

The distribution in particle size was much more varied for the 0.2–2 μm fractions, as shown in Figure 14. This may be due to the fact that the Mastersizer uses the equivalent projected spherical diameter as a measure of particle size. Therefore, for highly asymmetrical particles (such as clay minerals) undergoing Brownian motion, the projected spherical diameter is likely to be dominated by the largest dimension of the particle. This dimension, however, will not dominate as strongly for particle size by settling. Even with the large variation in sizes, the d_{50} for most streams, with the exception of the tailings stream, was under the 2 μm cut-off. Furthermore, the refractive index of kaolinite was used as the refractive index for all particles, which does not take into account differences in mineralogy or the presence of residual organics. These differences may cause a slight overestimate of the particle size meaning that all the samples were satisfactorily separated into the <0.2 μm and <2 μm streams.

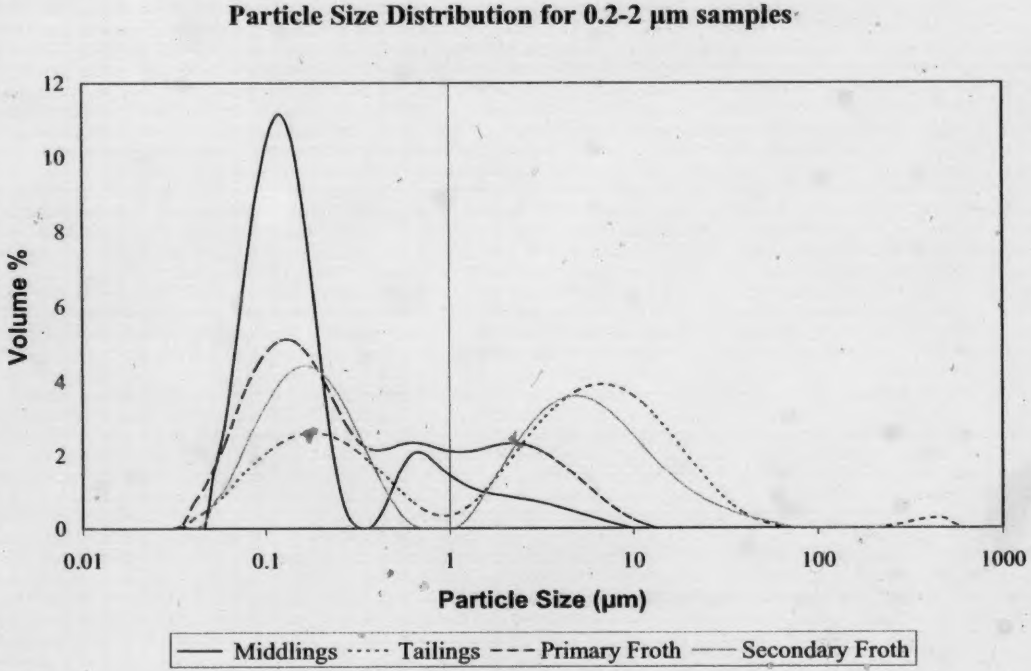

Figure 14: Particle size distribution for the 0.2–2 micron streams.

3.2.2 Clay mass balance

After centrifugation, the total amount of fines, clay, and ultrafine clays was calculated and compared for the different process streams, as shown in Table 21. Despite containing only 16% of the total solids weight, the middlings stream contained over 70% of the total clays.

Table 21: Mass balance of fines, clays, and ultrafine clays around extraction

		Assay				Distribution			
	wt%	>45 µm	<45 µm	<2 µm	<0.2 µm	>45 µm	<45 µm	<2 µm	<0.2 µm
Primary Froth	4.2%	51.5%	48.5%	14.4%	3.6%	3.0%	7.0%	6.9%	6.0%
Middlings	15.8%	2.4%	97.6%	38.8%	11.8%	0.5%	53.1%	70.1%	73.1%
Tailings	79.6%	85.6%	14.4%	2.4%	0.7%	96.0%	39.4%	22.3%	21.0%
Secondary Froth	0.5%	68.0%	32.0%	14.3%	0.0%	0.4%	0.5%	0.7%	0.0%
Ore (calculated)	100.0%	71.0%	29.0%	8.7%	2.5%	100.0%	100.0%	100.0%	100.0%
Ore (measured)	100.0%	67.8%	32.2%	10.2%	2.9%	100.0%	100.0%	100.0%	100.0%

3.2.3 Elements mass balance

Full elemental analysis results can be found in Appendix A. Table 22 shows the element balances for the most important elements in the ultrafine clays. As shown, the primary froth is strongly enriched with iron and titanium as compared to the other streams. The primary froth is also slightly enriched with magnesium, as compared to the other streams. This enrichment comes at the expense of the other elements in the froth. No enrichment or depletion was noted in the tailings. Titanium and iron were both depleted somewhat in the middlings.

Table 22: Element balance for ultrafine (<0.2 µm) clay fraction

ASSAY							
Stream	**Al_2O_3**	**Fe_2O_3**	**K_2O**	**MgO**	**SiO_2**	**TiO_2**	**Other**	**Weight(g)**
Primary Froth	28%	17%	3%	2%	47%	1%	4%	1.78
Middlings	32%	7%	3%	2%	53%	1%	3%	21.8
Tailings	31%	8%	3%	2%	51%	1%	5%	6.21
Ore	30%	5%	4%	2%	50%	1%	10%	11.6
Sum of Streams	32%	8%	3%	2%	52%	1%	4%	29.79
DISTRIBUTION								
Stream	**Al_2O_3**	**Fe_2O_3**	**K_2O**	**MgO**	**SiO_2**	**TiO_2**	**Other**	**Weight**
Primary Froth	5%	13%	5%	7%	5%	12%	6%	6%
Middlings	75%	65%	74%	71%	74%	66%	63%	73%
Tailings	20%	22%	21%	22%	21%	22%	31%	21%
Ore	100%	100%	100%	100%	100%	100%	100%	100%
Sum of Streams	100%	100%	100%	100%	100%	100%	100%	100%

As with the ultrafine clays, the overall clay size fraction also showed strong enrichment of iron and titanium to the froth (Table 23). Unlike the ultrafine clays, the tailings showed a slight enrichment in silicon and a corresponding depletion of aluminum in the overall clay fraction. The tailings also showed a slight depletion of titanium and iron.

Table 23: Element balance for clay size (<2 μm) fraction

ASSAY								
Stream	**Al_2O_3**	**Fe_2O_3**	**K_2O**	**MgO**	**SiO_2**	**TiO_2**	**Other**	**Weight(g)**
Primary Froth	27%	16%	3%	2%	45%	3%	6%	7.059
Secondary Froth	25%	13%	3%	4%	46%	4%	5%	0.757
Middlings	33%	6%	3%	1%	54%	1%	2%	71.94
Tailings	27%	6%	3%	1%	59%	1%	2%	22.849
Ore	31%	6%	4%	1%	52%	1%	4%	41.494
Sum of Streams	31%	6%	3%	1%	55%	1%	2%	102.605
DISTRIBUTION								
Stream	**Al_2O_3**	**Fe_2O_3**	**K_2O**	**MgO**	**SiO_2**	**TiO_2**	**Other**	**Weight**
Primary Froth	6%	17%	6%	7%	6%	16%	16%	7%
Secondary Froth	1%	2%	1%	2%	1%	3%	2%	1%
Middlings	74%	62%	72%	71%	70%	60%	59%	70%
Tailings	20%	19%	22%	20%	24%	21%	23%	22%
Ore	100%	100%	100%	100%	100%	100%	100%	100%
Sum of Streams	100%	100%	100%	100%	100%	100%	100%	100%

3.2.4 Identification of clay minerals

3.2.4.1 Mineral identification of 0.2–2μm samples & <2 μm secondary froth

No peaks were observed at d-spacings above 1.5 nm in any of the samples, indicating that no discrete smectite is present in detectable quantities. All samples in the 0.2—2 μm category exhibited the presence of a peak at ~ 1.4 nm, indicating the possibility of chlorite. This peak shifted to slightly lower angles on solvation with both ethylene glycol and glycerol for all samples. This is probably due to a small shift in sample geometry due to the physical presence of the solvating compound. A substantial shift towards higher angles (smaller d-spacings) upon heating was noticed in all samples, and the appearance of high-angle asymmetry was noticed in the middlings sample. This could indicate the presence of a small amount of hydroxyl-interlayered vermiculite.

All samples exhibited a peak at ~ 1.0 nm, which could indicate the presence of illite, vermiculite, or illite-smectite. This peak exhibited distinct low angle asymmetry in the calcium saturated 54% RH samples, indicating the presence of something besides pure illite. Solvation with ethylene glycol caused a sharpening of this peak with a corresponding flattening of the background between the 1.4 nm and the 1.0 nm peak. It is difficult, however, to estimate the degree of this response, as it does appear to be quite slight and is almost completely lost in the background of the 1.4 nm peak. This behaviour is indicative of illite-smectite or depotassified illite. The potassium-saturated samples, however, did not respond strongly to rehydration. Although this is characteristic of depotassified illite rather than illite-smectite, this is not a conclusive test, as only a slight swelling is anticipated upon rehydration, even for pure smectite. Also, the small number of smectite layers in the illite-smectite, along with the large amount of discrete illite, may have completely masked any response.

Glycerol solvation produced the same kind of sharpening of the 1.0 nm peak as the ethylene glycol solvation, although the background response was not as strong as the response with ethylene glycol. This suggests the presence of an illite-smectite with some octahedral and some tetrahedral charge in the smectite layers, as purely tetrahedrally charged smectite such as beideillite should exhibit the same solvation profile with glycerol as with the 54% RH, and purely octahedrally charged smectites should exhibit the same solvation with glycerol as with ethylene glycol (Chichester et al., 1969).

A strong peak at 0.7 nm was present in all samples before they were heated to 550 °C. This peak disappeared after heating. This indicates that the bulk of the peak is kaolinite and/or kaolinite-smectite. This peak had a very slight low-angle asymmetry for all test conditions other than the 550°C test. This asymmetry was most pronounced in the potassium-saturated samples. Sharpening of the peak was observed upon solvation with ethylene glycol and glycerol, though to a lesser extent. This asymmetry and response to ethylene glycol may be indicative of a randomly interstratified kaolinite-smectite.

The primary froth samples in this size fraction showed a large peak at 0.6 nm, which corresponds to lepidocrocite, an iron-oxide hydroxide. A small amount of lepidocrocite was also noted in the middlings and secondary froth, though none was apparent in the tailings stream.

3.2.4.2 Mineral identification of <0.2 μm samples

Unlike the 0.2–2 μm samples, no peak was observed in the <0.2 μm samples at 1.4 nm, indicating that no chlorite was present. The disappearance of the 0.7 nm peak after heating confirmed that no chlorite was present in the sample. As with the 0.2–2 μm samples, low-angle asymmetry was observed on the 0.7 nm peak, indicating the presence of kaolinite-smectite.

All samples exhibited very distinctive asymmetry of the 1.0 nm and a pronounced hump at around 1.2 nm upon solvation with ethylene glycol, indicating the presence of illite-smectite. Re-expansion of the 1.0 nm peak was observed in the potassium-saturated 54% RH sample for the middlings and tailings, but was not discernable for the ore or primary froth. As with the 0.2–2 μm samples, this could be because a large amount of discrete illite was masking the response of any illite-smectite present.

An intermediate response to solvation with glycerol was also noted in these samples, again indicating that the smectite layers of the illite-smectite have some octahedral charge and probably some tetrahedral charge. It is interesting to note that the response to glycerol for the primary froth was very different from the response of the middlings. The middlings sample exhibited low-angle asymmetry that was between the 54% RH sample and the ethylene glycol sample. The primary froth, on the other hand, showed a peak at 1.2 nm, as in the case of the ethylene glycol, but the intensity of this peak was much lower than for the ethylene glycol sample. This may indicate that two different illite-smectites are present in the primary froth.

All samples in this size fraction contained lepidocrocite.

3.2.4.3 Differences between process streams

As expected, the tailings samples exhibited the least amount of lepidocrocite and swelling behaviour for their size fraction. The primary froth exhibited the most lepidocrocite and had a different profile which was shifted to lower angles for the swelling component of the illite than the other samples. This may be due to a combination of four reasons: different ordering of the interstratified layers, a higher degree of interstratification, more iron present in the interstratified layers, and/or the presence of multiple types of illite-smectite.

3.2.5 Quantification of clay minerals

3.2.5.1 Determination of degree of interstratification

The percentage of smectite in illite-smectite was calculated from corrected peak positions according to:

$$\%S = 106(d_{001/002}) - 107.1 \qquad \textbf{Equation 18}$$

where $d_{001/002}$ is the d-spacing in nm of the 001/002 illite-smectite peak and $\%S$ is the degree of smectite mixed layering in the illite-smectite.

The percentage of smectite in kaolinite-smectite was calculated from the corrected peak positions according to:

$$\%S = 500(d_{002/003} - d_{001/002}) - 184.4 \qquad \textbf{Equation 19}$$

where $d_{002/003}$ is the d-spacing in nm of the 002/003 kaolinite-smectite peak, $d_{001/002}$ is the d-spacing in nm of the 001/002 kaolinite-smectite peak, and $\%S$ is the degree of smectite mixed-layering in the kaolinite-smectite. The results of the percentage of smectite layering determination for illite-smectite and kaolinite-smectite are shown in Table 24.

Table 24: Degree of interstratification (% smectite) for illite-smectite and kaolinite-smectite in oil sands streams

Size Fraction	Stream	% Smectite in Kaolinite-Smectite	% Smectite in Illite-Smectite
0.2-2 μm	Ore	9±4	17±8
	Primary Froth	7±5	27±11
	Middlings	7±4	13±9
	Tailings	6±4	12±8
<2 μm	Secondary Froth	7±5	12±7
	Quant Standard	1±5	31±5
<0.2 μm	Ore	18±4	28±6
	Primary Froth	15±4	27±6
	Middlings	18±4	28±6
	Tailings	17±4	28±6

Equations 17 and 18 are derived from a linear regression analysis of NEWMOD™ generated models of illite-smectite and kaolinite-smectite. The values in Table 24 seem a little higher than other values reported in the literature: ~ 18% smectite layers in the kaolinite-smectite were measured but ~ 10% smectite layers in kaolinite-smectite were reported in the literature (Omotoso et al., 2002). The value for the percentage of kaolinite-smectite in the mixture of standard clay minerals was similarly calculated as ~ 1% smectite, when, in fact, no mixed layering was present. Estimation of the degree of uncertainty in the measurements can be found in Appendix A.

3.2.5.2 Quantification of clay minerals

Table 25 shows the quantification results for the <0.2 μm and 0.2–2 μm samples given in Figure 15 and Figure 16. In general, the <0.2 μm streams have less kaolinite than the 0.2–

2 µm samples. The main difference between the clay minerals in the process streams is that the primary and secondary froth samples are substantially depleted in illite-smectite and enriched in kaolinite and chlorite compared with the samples in the other streams.

Table 25: Clay mineral composition of the clay size fractions (wt%)

Size Fraction	Stream	Chlorite (±2)	Kaolinite-Smectite (±2)	Kaolinite (±2)	Illite-Smectite (±5)	Illite (±5)
0.2-2 µm	Ore	7	13	25	29	26
	Primary Froth	10	11	41	11	27
	Middlings	7	10	31	24	29
	Tailings	7	8	34	25	26
< 2 µm	Secondary Froth	7	17	43	11	22
< 0.2 µm	Ore	-	25	15	47	14
	Primary Froth	-	25	19	42	14
	Middlings	-	21	13	53	12
	Tailings	-	19	15	54	13

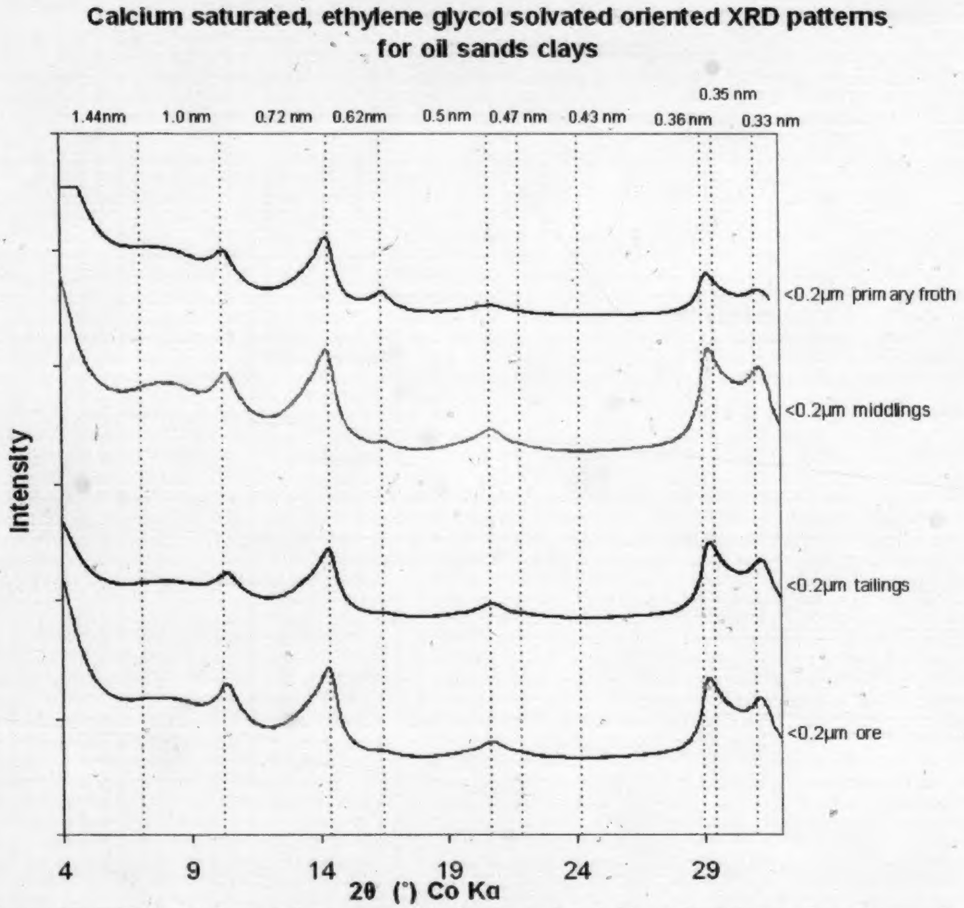

Figure 15: XRD trace for calcium saturated, ethylene glycol solvated <0.2 µm oil sands sample.

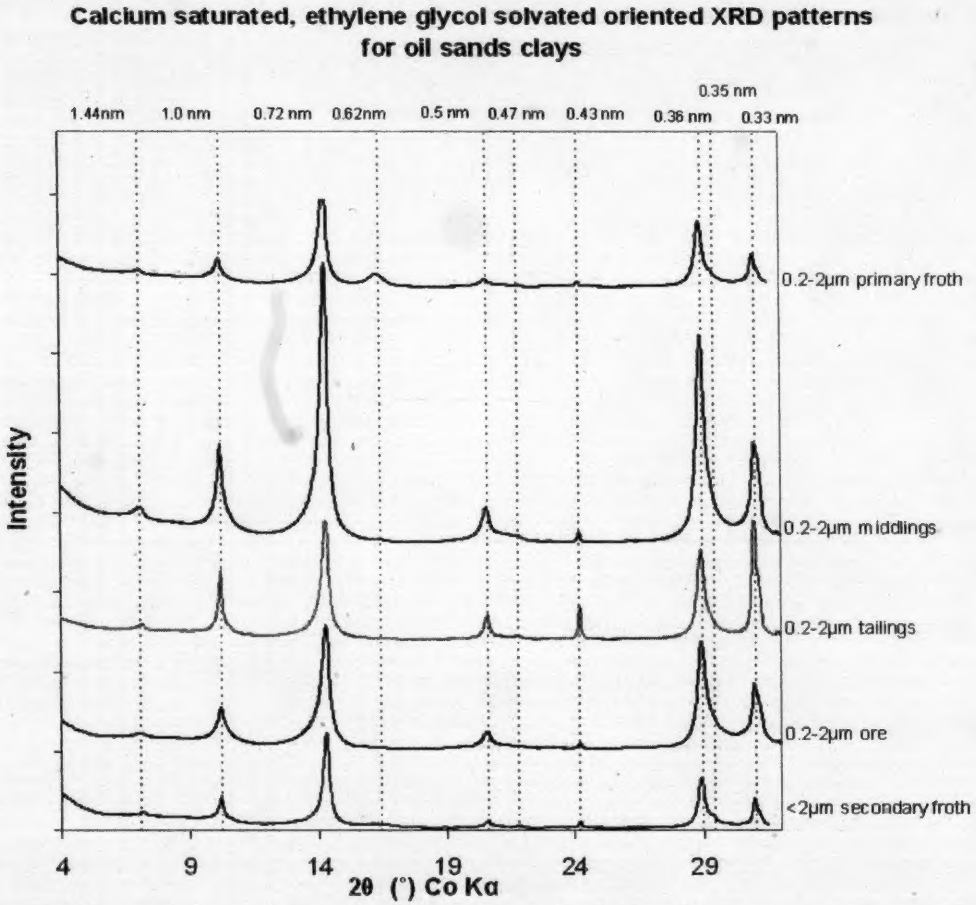

Figure 16: XRD trace for calcium saturated, ethylene glycol solvated 0.2–2 μm oil sands samples.

The distribution of non-clay minerals in each stream (as determined by AUTOQUAN^{TM}) is shown in Table 26. Although lepidocrocite appeared in the oriented clay slides for all the <0.2 μm samples, only the primary froth had enough lepidocrocite to be quantifiable using AUTOQUAN^{TM}. The 0.2–2 μm tailings stream was the only stream with a substantial amount of non-clay material present.

Table 26: Distribution of non-clay minerals in the clay fraction of the oil sands

Size Fraction	Stream	Anatase	Lepidocrocite	Pyrite	Quartz	Rutile	Siderite	Ankerite	% non-clay
0.2-2 μm	Ore	trace		trace	5±1	trace	1±0		6±2
	Primary Froth	1±1	2±0	trace	5±1	1±0	2±0		11±3
	Middlings	trace		trace	6±1	trace	1±0		9±2
	Tailings	1±0			28±4	trace	trace		30±4
<2 μm	Secondary Froth	2±0	1±0		7±1	1±0	trace	trace	11±2
<0.2 μm	Ore		1±0		1±0				2±1
	Primary Froth	1±0	1±0		1±0	trace			2±1
	Middlings		trace				trace	1±0	1±0
	Tailings				trace				0±0

3.2.5.2.1 Comparison with source clay quantitative standard

To check the accuracy of the quantification of the clay minerals in the oil sands samples, a mixture of five different source clay minerals was prepared (Section 3.1.2.4). This sample was then tested in the same manner as the oil sands samples and the weight fraction of each mineral calculated. Table 27 shows the composition created by mixing, as well as the composition calculated by XRD quantification. For kaolinite, chlorite and smectite the model results were close to the actual weight fractions of the minerals added to the mixture. The errors were quite high for the illite and illite-smectite, which may be partially due to the difficulties in modelling the overlapping 002 of illite and illite-smectite. The sum of illite and illite-smectite are close to the actual amounts of the phases.

Table 27: Quantitative clay standard analysis

	wt% added	wt% XRD
Kaolinite (Kga1-b)	43%	45%
I (70) - S (ISCZ-2)	16%	6%
Illite (R3M1)	26%	31%
Ripidolite (CCa-2)	5%	7%
Smectite (Swy-2)	11%	11%

3.2.6 Clay activity

3.2.6.1 Methylene blue analysis

The methylene blue titration of the <0.2 μm fractions produced similar results for all three streams, although the froth had a slightly lower methylene blue index (MBI) than the middlings or tailings (Table 28). For the 0.2–2 μm fraction, the primary froth had by far the highest MBI, perhaps indicating the presence of more clay minerals with either larger surface areas or with more charged sites, and, therefore, a larger cation exchange capacity/clay activity. The tailings had the lowest MBI, which was expected. The MBI of the ore sample was very similar to the <0.2 μm fraction for the middlings and tailings, which was also expected; the majority of the clay minerals should be in these fractions. The MBI for the 0.2–2 μm fraction of the ore sample was closest to that of the primary froth, and was quite different from that of the middlings and tailings. This difference may indicate that incomplete dispersion of ultrafine particles occurred in the ore and primary froth, resulting in agglomerated ultrafine particles remaining in the 0.2–2 μm fraction, and, therefore, a higher-than-expected surface area in the 0.2–2 μm fraction. Alternatively, the discrepancy in the MBI results could be due to residual organics and iron oxides present in the ore and primary froth samples. The MBI results for the 0.2–2 μm middlings fraction was somewhat lower than expected.

It should be noted that the methylene blue titration method, while an oil sands industry standard, is susceptible to significant errors. Sources of error include improper dispersion of the sample, operator error in identifying the end point, and interference effects from iron oxides and residual organics. A bentonite clay standard was used as a reference for end point determination to mitigate operator error. Sample dispersion was assumed to be complete once the sample exhibited streaming birefringence of the clay minerals and no sediment remained at the bottom of the beaker. The contributions from the iron oxides were theoretically eliminated by addition of acid to lower the pH of the sample below the isoelectric point of the iron oxides.

Table 28: Clay activity results

	< 0.2 µm fraction			**0.2–2 µm fraction**		
	MBI (meq/100g)	**Surface area calculated from MBI (m2/g)**	**Surface area calculated from XRD results (m2/g)**	**MBI (meq/100g)**	**Surface area calculated from MBI (m2/g)**	**Surface area calculated from XRD results (m2/g)**
Ore	37±2	287±9	309±29	20±1	154±5	116±24
Primary froth	31±5	240±34	275±28	22±3	176±18	67±21
Middlings	37±1	290±3	336±30	11±2	85±12	83±21
Tailings	38±2	297±15	319±30	9±1	69±2	51±14

3.2.6.2 Surface area estimation by XRD

The surface area measured by methylene blue analysis was close to that of the XRD-predicted values for the <0.2 µm fraction, but was off for the 0.2–2 µm fractions. This was especially true for the primary froth, where the XRD results predicted a much lower surface area than was measured in the methylene blue analysis. For the middlings, tailings, and ore, the discrepancy between the predicted values and the measured surface area could be due to the fact that only kaolinite, kaolinite-smectite, illite, and illite-smectite were considered to contribute to the surface area. These samples also contained chlorite, which would contribute slightly to the surface area. Furthermore, the swelling components are very difficult to model in the XRD as they form very broad peaks that are only slightly above the background. The XRD surface areas, consequently, would tend to underestimate the surface area of the sample. For the primary froth, the discrepancy is most likely due to the amount of fine iron oxides and iron oxide-hydroxides that have been observed in the froth fraction. These minerals are very difficult to quantify using XRD because their fine particle size makes causes them to show up as broad peaks which are easily lost in the background of the pattern. Their fine particle size, however, also means that they can contribute to the surface area measured by methylene blue analysis if not properly isolated.

The high activity measured in the <0.2 μm fractions (especially that of the middlings), combined with the fact that the majority of the <0.2 μm micron fraction ends up in the middlings, explains the slow settling of the fine tailings.

3.2.7 Thermogravimetric analysis

There were two main reasons for doing the TG analysis on the clay fractions of the oil sands: to determine the amount of residual organics present, and to help verify XRD results by determining the amount of kaolinite (and therefore the degree of weight loss due to clay dehydroxylation) in each sample. A summary of the TG results is shown in Table 29.

Table 29: TG results

			Water loss wt%		Organic loss wt%			Clay loss wt%			High temperature loss wt%		Total	
Atmosphere			N_2	Air	N_2	Air	Air	N_2	Air	Air	N_2	Air	N_2	Air
Temperature Range (in °C)			up to 115	up to 115	115-420	115-468	115-420	420-575	468-575	420-575	575-1000	575-1000		
Dean Stark	<0.2	Middlings	2.61	4.72	5.02	9.88	4.35	4.96	2.52	8.05	1.35	0.96	13.94	18.08
		ore	2.46	3.41	6.49	10.12	5.19	4.57	-1.03	3.90	2.40	0.01	15.92	12.50
		Primary Froth	1.19	4.88	6.82	16.86	10.35	5.42	1.73	8.24	6.68	1.42	20.10	24.88
		Tailings	2.72	4.93	4.87	10.81	5.04	5.22	2.01	7.78	2.39	1.02	15.19	18.78
	<2	ore		0.24		11.26	5.81		2.48	7.93		1.06		15.05
		secondary Froth		4.45		21.53	14.91		2.25	8.88		1.72		29.96
	0.2–2	Middlings	1.52	1.75	3.00		2.95	6.33		7.73	2.40	0.79	13.25	13.22
		ore	1.95	2.50	4.42		4.50	6.03		7.87	2.94	0.94	15.35	15.81
		Primary Froth	2.88	3.85	7.23	21.67	13.87	6.14	2.49	10.29	7.29	1.50	23.54	29.51
		Tailings	1.19	1.76	2.32	5.69	2.50	4.64	2.23	5.41	2.20	0.75	10.36	10.42
Source Clay	<2	Illite		0.16		0.16	0.07		-0.12	-0.03		-0.20		0.00
		Illite-Smectite		5.67		2.37	1.40		1.47	2.45		1.90		11.41
		Kaolinite	0.41	0.61	1.04	5.36	0.44	11.53	7.18	12.10	0.87	0.38	13.84	13.53
		Ripidolite		0.13		0.13	0.05		2.93	3.01		5.81		9.01

As shown, the 0.2 –2 µm fraction of the primary froth and the <2 µm fraction of the secondary froth exhibited the largest overall mass loss, followed by the <0.2 µm primary froth. The tailings stream exhibited the lowest loss. This trend was consistent, irrespective of TG procedure.

Carbon, hydrogen, sulphur, and nitrogen composition were determined using a Vario MICRO cube Elemental Analyzer, as shown in Table 30. A strong correlation (RSQ = 0.97) is observed between the percentage of carbon and the TG mass loss between 420–575°C, when the TG analysis is run under air. Good correlations were also observed between percentage of carbon and both total weight loss and organic loss under nitrogen. These results confirm that the stream with the most residual organics present after Dean Stark extraction is the 0.2–2 µm fraction of the primary froth. The remaining fractions were all found to have similarly low amounts of residual organics present.

Table 30: C, H, N, S determination

Size fraction	**Stream**	**wt% C**	**wt% H**	**wt% S**	**Wt% N**
< 0.2	Middlings	3.84	1.53	0.54	0.18
	Ore	4.60	1.51	0.78	0.20
	Primary Froth	8.67	2.19	0.91	0.36
	Tailings	4.42	1.64	0.50	0.22
0.2–2	Middlings	2.46	1.27	0.46	0.16
	Ore	4.67	1.46	0.74	0.21
	Primary Froth	12.65	1.94	1.07	0.40
	Tailings	2.15	1.12	0.41	0.15

All the clays exhibited similar amounts of weight loss in the clay stream, and, therefore, showed no correlation between percentage kaolinite as determined by XRD and the amount of dehydroxylation as determined by TGA.

3.2.8 Particle morphology by TEM

Dispersed samples of middlings and primary froth in both the 0.2–2 μm and <0.2 μm size fractions were examined in the both a JEOL 2022 FS and a JEOL 2010 TEM. The length and width of the clay particles in the micrographs obtained were then measured and compiled as shown in Table 31. Two interesting trends are observed based on these measurements. The first is that the middlings have a slightly higher average-length-to-width ratio than the primary froth, for both the 0.2–2 μm and <0.2 μm fractions. This is consistent with the XRD results which show that the middlings contain more illite and illite-smectite (i.e., lath like particles) and less kaolinite (i.e., pseudohexagonal particles) than the primary froth. The difference in average particle size measured in the primary froth and the middlings was also interesting. In the 0.2–2 μm fractions the middlings had particles that were substantially longer and wider than the primary froth particles of the same size fraction. On first glance, this appears to contradict the Mastersizer results, which showed that the middlings had a smaller particle size than the primary froth. However, the Mastersizer measures the equivalent projected spherical diameter as a measure of particle size, which means that for platy particles such as clay minerals, the particles may be counted as both very small particles when observed edge on, and as very large particles when observed on the basal surface. The middlings had a pronounced bimodal distribution of particle size, whereas the primary froth had a wider range. This could indicate that the primary froth samples had particles that were more uniform in size and thickness, resulting in a larger overall size relative to the middlings, as the middlings are composed of particles with high-surface-area-to-volume-ratios (thin, elongated structures). This hypothesis is consistent with the XRD crystallite measurements of the middlings, which showed the average crystallite size of the primary froth to be larger than that of the middlings (Table 32). In the <0.2 μm fraction, the middlings were smaller than the primary froth, which is consistent with the Mastersizer results. The morphology of the middlings noted here exemplifies why the rheological behaviour of the middlings is so undesirable from a tailings-management perspective, as increased aspect ratios and decreased particle sizes both increase the yield strength of a slurry of particles (Brenner, 1974) (Scales, 2008).

Table 31: Length and width measurement for dispersed particles in primary froth and middlings samples

Size fraction	Stream	Average length (L) (nm)	Average width (W) (nm)	Average of L/W ratio	# of Particles
< 0.2 μm	Middlings	182	113	1.75	184
	Primary Froth	375	244	1.67	887
0.2-2 μm	Middlings	889	529	1.82	515
	Primary Froth	515	303	1.74	166

Table 32: Crystallite size (thickness) measurements for different clay minerals as determined by XRD

Size Fraction	Stream	Chlorite (nm)	Kaolinite-smectite (nm)	Kaolinite (nm)	Illite-smectite (nm)	Illite (nm)	Average particle thickness (nm)
0.2-2 µm	Primary Froth	14	8	28	11	21	21
	Middlings	17	7	25	6	25	18
< 0.2 µm	Primary Froth		4	10	4	10	6
	Middlings		4	10	3	8	5

A final trend noted in the examination of the dispersed particles was the prevalence of fine iron oxides such as those displayed in Figure 17. These areas were prevalent in both the middlings and the primary froth, but were more common in the primary froth samples. The electron diffraction pattern in Figure 17was indexed to feroxyhite (hexagonal, a=0.293 nm, c=0.46 nm) and the EDX spectrum in Figure 18 shows mostly iron and oxygen. Feroxyhite was not detected in any of the XRD patterns, but the extremely fine nature of these particles could cause the broadened peaks to be lost in the background of the patterns.

100 nm
(001)
(002)
(100)
(012)

Figure 17: TEM bright field (BF) image of 0.2 to 2 µm middlings sample showing iron-rich particles. A SAD pattern from the circled region is shown in the inset (JEOL 2010)[20]

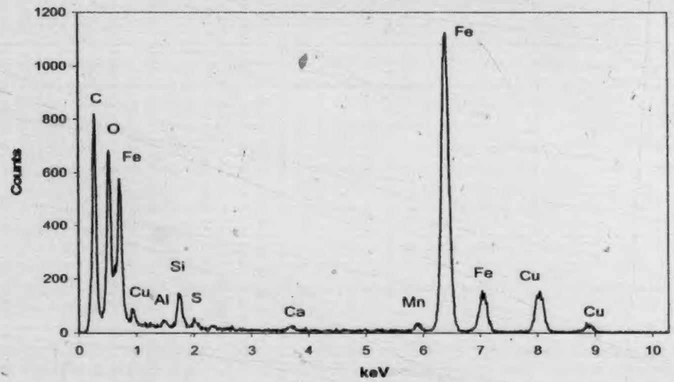

Figure 18: EDX spectrum from iron-rich particles circled in Figure 17 (JEOL 2010)[20].

---

[20] Published in Kaminsky et al. (2006) Clay Science 12, Supplement 2, 217-222

3.2.9 Fundamental particle thickness

Using a JEOL 2010 TEM, lattice fringe images of individual clay particles were identified from high-magnification images (400 000–1 000 000X). Particle thicknesses were estimated by two methods: first, by measuring the 001 spacing from the SAD patterns and then counting the fringes in the particle, or second, by directly measuring the thickness. In this set of images the primary type of clay particle observed in both the 0.2–2 μm and <0.2 μm middlings samples was illite. The results are summarized in Table 33. Some diffraction patterns exhibiting the characteristic 0.72 nm spacing of kaolinite were obtained, but no lattice fringes showed this spacing. This failure to obtain lattice fringe images of kaolinite, despite the prevalence of kaolinite in the sample, as shown by the XRD results, indicates that the TEM conditions used were causing kaolinite in the samples to decompose before they could be recorded. This sensitivity of kaolinite to the electron beam has been noted previously by other authors in the field (Ma and Eggleton, 1999). Attempts were made to record kaolinite lattice fringe images after sample cooling and by using a lower magnification and lower beam intensity, but these attempts were unsuccessful.

Table 33: Particle thickness measurements by XRD and HRTEM

Sample	Clay mineral type	Mean crystallite size (nm)	
		XRD (PVP-10)	HRTEM
< 0.2 μm	Kaolinite (002) & (003)	6.1±0.1	
	Illite (002) & (003)	4.4±0.1	4*
0.2–2 μm	Kaolinite (001), (002) & (003)	19.3± 0.5	
	Illite (001), (002) & (003)	18.9± 0.5	6**
	Chlorite (001), (002) & (003)	9 ± 1	-

*Mean of 15 crystallites ranging from 1.1 to 9.5 nm, measured at magnifications exceeding 400 000X.
** Mean of 39 crystallites ranging from 1.4 to 18 nm.

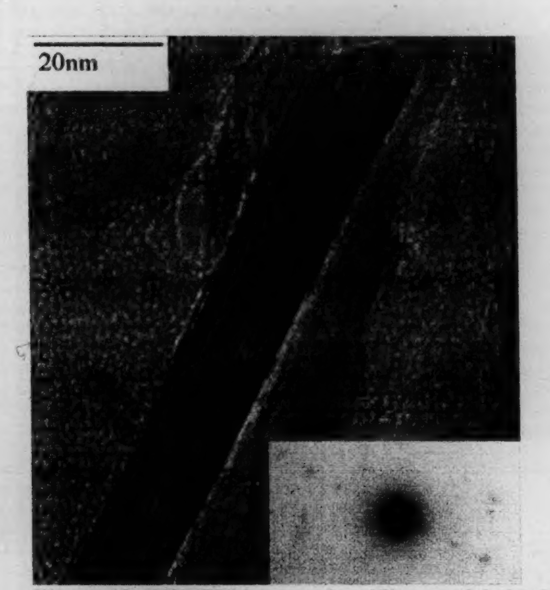

Figure 19: HRTEM image of an illite particle in the 0.2 to 2 µm middlings. A SAD pattern is included in the insert showing the 1nm d-spacing characteristic of illite (JEOL 2010).

Figure 19 depicts a typical particle from the 0.2-2 µm middlings. The frayed appearance of the edge of the particle is a fairly common occurrence. The fringe thickness at the wedge varies from 1.0 to 1.5 nm. It is possible that the layers at the frayed wedge are de-potassified, similar to the phenomenon reported for hydrous mica or degraded illite (Wallace et al., 2004). Distinct smectite layers were not observed in the lattice fringe images. Figure 20 shows some typical particles from the <0.2-µm fraction sample. All the particles observed are fundamental particles without mixed layering.

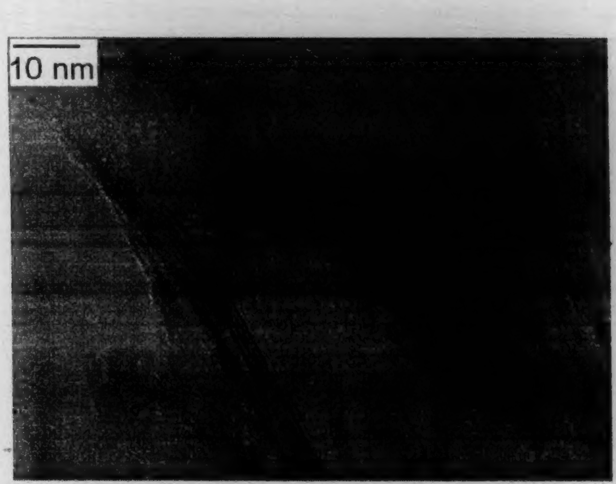

Figure 20: Image showing typical particles in <0.2-μm middlings sample (JEOL 2010) .

Table 33 also shows the results from the particle size measurements on the PVP-10 intercalated samples (Eberl et al., 1998). In the 0.2–2 μm fraction sample, chlorite 002 and 004 peaks overlap with kaolinite 001 and 002 peaks. To use these peaks for crystallite size determination, the chlorite peak positions and coherent scattering domains were constrained to the resolved 001 reflection, while kaolinite parameters were constrained to the resolved 003 reflection parameters. In both samples, the microstrain in illite and kaolinite was found to be negligible. The percent expandability (% S) (or percent smectite interlayer) was calculated from the PVP-10 sample's mean fundamental particle size and from NEWMOD™ analysis of the glycolated sample, using **Equation 20** as proposed by Srodon et al.(1992):

$$\%S = 100\% * d_{001}/N \qquad \textbf{Equation 20}$$

where N is the total number of interlayers and d is the basal spacing (nm). The results are given in Table 34. Given the uncertainty in measuring crystallite sizes from HRTEM images and XRD patterns, both measurements are essentially identical for the <0.2 μm fraction sample. There is a large variation between the illite crystallite thickness in the 0.2–2 μm fraction measured by XRD and TEM. Given that the smaller crystallites are in small concentrations in this fraction, it is most likely that the limited sensitivity of XRD prevented observation of the mixed layer components above the background and accurate modeling.

Table 34: Percent expandability of illite and kaolinite in the <0.2 μm middlings sample

Mineral	%S PVP-10	%S NEWMOD™	%S TEM
Kaolinite	12	11	Not determined
Illite	23	22	25

A second set of samples was prepared and examined in the JEOL 2010 TEM. For these images, all particle thicknesses were measured directly from the images and the d-spacings were determined by dividing the particle thickness by the number of fringes observed. As with the previous samples, no kaolinite lattice images were detected in these samples, due to the extreme sensitivity of the kaolinite to the electron beam. Of the particles that were observed, most had the characteristic 1.0 nm d-spacing of illite; however, there were others whose measured spacing was closer to 1.2 nm, possibly indicating the presence of smectite layers within a particle. Particles exhibiting inconsistent layer spacings, as shown in Figure 21 (Hooshiar, 2007), were further indications of this possibility. It is possible that both of these phenomena are due to an incorrect amount of defocus. However, the presence of well resolved layers, exhibiting 1.0 nm spacing close to the areas of inconsistency, suggests that it is due to mixed layering or depotassification of the illite rather than an experimental artefact. Many particles exhibiting the frayed edges demonstrated in Figure 19 were also observed in these samples.

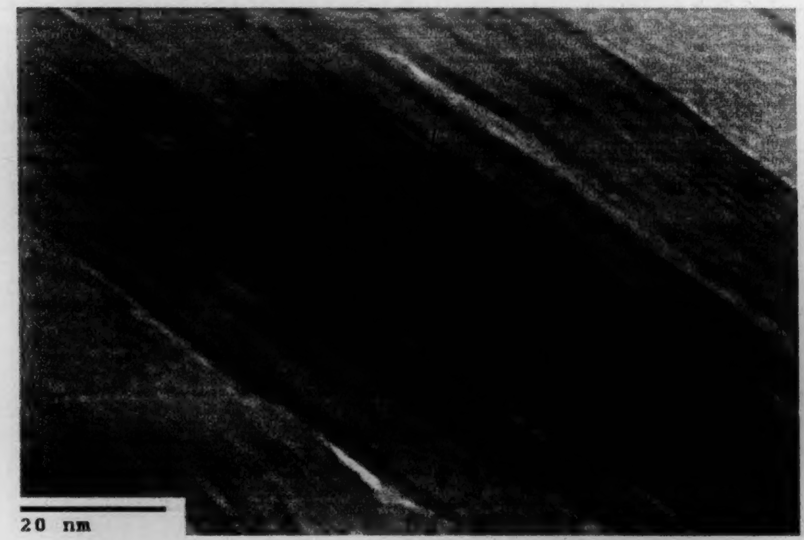

Figure 21: HRTEM image of 0.2-2 μm middlings sample showing regions with inconsistent layer spacings (JEOL 2010).

Table 35 depicts the summary of the measurements on the lattice fringe images obtained for the middlings and primary froth. As shown, the average number of layers observed per particle remained constant for both the primary froth samples and the <0.2 μm middlings at four layers per particle, a value consistent with the initial TEM results previously described. The 0.2–2 μm middlings sample had a slightly higher average of five layers per particle, which was a bit lower than prior results. It is interesting to note that the measured average d-spacing of the primary froth particles was higher than that of the middlings samples, possibly indicating that there are more smectite-like layers within the particles of the primary froth.

Table 35: Average particle thickness and d-spacings for particles observed in HRTEM

Stream	Size fraction	Average d-spacing	# of particles	Average thickness	Average # of layers
Middlings	<0.2 µm	1.00	26	3.41	4
	0.2-2 µm	1.07	23	5.05	5
	Total	1.04	49	4.18	4
Primary Froth	<0.2 µm	1.06	30	3.63	4
	0.2-2 µm	1.10	97	3.99	4
	Total	1.09	127	3.91	4

As well, differences were observed between the thickness distribution of the primary froth and middlings particles. As shown in Figure 22, the <0.2 µm primary froth appears to have a bimodal distribution with one average between three and four layers and the other at seven layers. Conversely, the <0.2 µm middlings sample exhibits a single peak at four layers, with a slight shoulder at around six layers. This difference in particle thickness distribution may explain the difference in sample response to ethylene glycol noted in the XRD results. The slightly lower average of the major peak (between three and four layers, as opposed to four layers) would indicate a larger degree of smectite character for some particles, and, hence, a larger degree of swelling with ethylene glycol. This larger swelling for some particles would, in turn, lead to the low angle asymmetry observed in the XRD profiles. It may also explain why the methylene blue absorption was higher in this fraction.

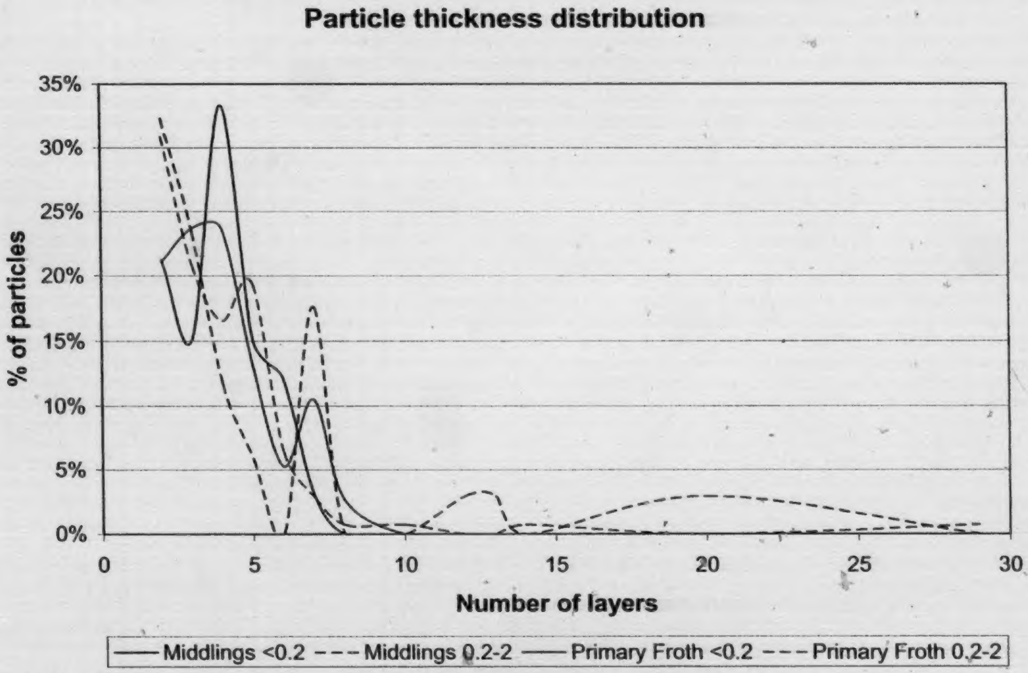

Figure 22: Thickness distribution of particles from HRTEM images. (JEOL 2010)

3.2.10 Charge distribution — TEM-EDX results

Initial EDX results were obtained in STEM mode using a JEOL 2200FS TEM. EDX analysis obtained on a dispersed sample of the pure, well characterized, clay illite RM30 revealed that these initial results were not reliable, as the silicon to aluminum ratio did not correlate with potassium content, and the potassium content was found to be significantly lower than the values for potassium content reported in the literature. Table 36 shows the results for all the particles analyzed by STEM-EDX. As shown, the majority of the particles contained some iron. In addition, more potassium was found in the ultrafine clay fraction than in the clay fraction. Further refinement of this data was performed by going through the data and selecting only those spectra from samples where there was clearly no overlap between particles. As shown in Table 37, the difference between primary froth and middlings particles is more significant, especially for the clay fraction, where 94% of the primary froth clay particles observed contained iron compared to only 53% of the middlings particles. This may indicate that the clay minerals in the primary froth are attracted to the froth due to their association with iron.

Table 36: Counts of particles containing iron and potassium (all STEM results)

	< 0.2 µm				0.2–2 µm			
	Middlings		Primary Froth		Middlings		Primary Froth	
	Count	%	Count	%	Count	%	Count	%
Contains Fe	35	66%	37	79%	39	66%	19	68%
Contains K	35	66%	30	64%	23	39%	8	29%
Contains Fe + K	30	57%	26	55%	20	34%	8	29%
Contains no Fe or K	13	25%	6	13%	17	29%	9	32%
Fe, no K	5	9%	11	23%	19	32%	11	39%
K, no Fe	5	9%	4	9%	3	5%	0	0%
Total number of particles	53	100%	47	100%	59	100%	28	100%

Table 37: Counts of particles containing iron and potassium (STEM results from pure clay areas)

	< 0.2 µm				0.2–2 µm			
	Middlings		Primary Froth		Middlings		Primary Froth	
	Count	%	Count	%	Count	%	Count	%
Contains Fe	8	89%	11	69%	9	53%	15	94%
Contains K	7	78%	10	63%	6	35%	7	44%
Contains Fe + K	3	33%	3	19%	2	12%	5	31%
Contains no Fe or K	1	11%	4	25%	9	53%	5	31%
Fe, no K	3	33%	6	38%	4	24%	6	38%
K, no Fe	2	22%	3	19%	2	12%	0	0%
Total number of particles	9	100%	16	100%	17	100%	16	100%

After the initial results obtained in STEM mode, some results were obtained in EM mode on the same microscope. These results showed that the potassium content was much closer to that reported in the literature for illite RM30. Therefore, these results were considered to be more accurate. Even fewer particles have been analyzed using this method, due to the difficulty of isolating the areas of interest in EM mode. Attempts at improving the dispersion of the clay particles were unsuccessful, resulting only in more isolated clusters of particles. The results are shown in Table 38, Table 39, and Table 40. These results are further broken down into four types of particles, according to the shape of the particle observed, i.e., kaolinite (pseudohexagonal, no potassium detected), illite (lath type with potassium), other (pseudohexagonal, with potassium), and uncategorized. These results are shown in Table 41. It is interesting to note that pseudohexagonal particles containing potassium (and iron) were detected in the primary froth, as pseudohexagonal particles are generally assumed to be kaolinite. Since these particles contain potassium and iron, they are potentially kaolinite-smectite.

Table 38: Counts of particles containing iron and potassium (all EM results) (JEOL 2022 FS)

	0.2–2 µm			
	Middlings		**Primary Froth**	
	Count	**Percentage**	**Count**	**Percentage**
Contains Fe	14	93%	17	100%
Contains K	14	93%	15	88%
Contains Fe + K	14	93%	15	88%
Contains no Fe or K	1	7%	0	0%
Fe, no K	0	0%	2	12%
K, no Fe	0	0%	0	0%
Total number of particles	15	100%	17	100%

Table 39: Counts of particles containing iron and potassium (EM results from pure clay areas) (JEOL 2022 FS)

	0.2–2 µm			
	Middlings		**Primary Froth**	
	Count	**%**	**Count**	**%**
Contains Fe	3	100%	12	100%
Contains K	3	100%	11	92%
Contains Fe + K	3	100%	11	92%
Contains no Fe or K	0	0%	0	0%
Fe, no K	0	0%	1	8%
K, no Fe	0	0%	0	0%
Total number of particles	3	100%	12	100%

Table 40: Average EDX results for 0.2–2 μm middlings and primary froth particles, as determined in EM mode (JEOL 2022 FS)

	Middlings		Primary Froth		Illite RM30	
Element	**Average of wt%**	**Count of wt%**	**Average of wt%**	**Count of wt%**	**Literature value**	**Experimental value**
Al	13.9%	3	17.5%	12	17.8%	17.3%
Ca	0.5%	2	0.2%	1	0%	0.0%
Cl			0.5%	5	0%	0.0%
Fe	2.2%	3	1.8%	12	1.0%	0.7%
K	2.0%	3	1.7%	11	8.3%	8.0%
Mg	1.1%	3	1.3%	6	1.0%	0.9%
Na			0.4%	2	0.1%	0.0%
O	53.0%	3	52.5%	12	46.4%	48.5%
S	0.3%	1	0.1%	1	0	0.4%
Si	26.9%	3	23.8%	12	24.3%	24.2%
SUM	100%	3	100%	12	99%	100%

Table 41: EM mode EDX results for 0.2–2 μm middlings and primary froth classified by type (JEOL 2022 FS)

Stream	**Middlings**		**Primary Froth**		
Classification	**illite**	**unclassified**	**Illite**	**Other**	**Unclassified**
Al	12.7%	16.3%	15.1%	21.4%	20.9%
Si	27.0%	26.8%	24.1%	23.1%	24.1%
K	2.4%	1.4%	2.2%	0.2%	1.6%
Fe	2.8%	1.1%	2.4%	0.9%	1.0%
Mg	1.3%	0.7%	1.2%	0.0%	1.7%
Ca	0.5%	0.6%	0.0%	0.2%	0.0%
Cl	0.0%	0.0%	0.7%	0.3%	0.0%
Na	0.0%	0.0%	0.5%	0.2%	0.0%
O	53.0%	53.2%	53.5%	53.5%	50.6%
S	0.3%	0.0%	0.0%	0.1%	0.0%
Ti	0.0%	0.0%	0.3%	0.0%	0.0%
Si/Al ratio	2.25	1.64	1.68	1.08	1.15
Count	2	1	7	2	3

From the EDX results, the structural formulae for the illite particles in the 0.2–2 μm primary froth (Table 42) and 0.2–2 μm middlings (Table 43) were calculated according to the method of Laird (1994). Assumptions made in this process included that: all detected elements were part of the structure, the anion charge was 22 (11 atoms of oxygen), the tetrahedral occupancy was 4 gram-equivalents, the octahedral occupancy was 2 gram equivalents, the iron had a charge of +2, and that residual iron could exchange in the interlayer to balance the charge on the molecule.

Based on the calculated formulae, the primary froth particles have a slightly higher charge than the middlings. Furthermore, the charge on the primary froth particles seems to be concentrated more in the tetrahedral layer, leading to a more localized charge. Conversely, the charge in the middlings seems to be concentrated in the octahedral layer. This distribution noted in the primary froth is consistent with clay that would interact easily with organic molecules having some polar (charged) functional groups and some non-polar sections (Moore & Reynolds, 1997). The polar sections would interact with the strong localized charges provided by the tetrahedral substitution, while the non-polar regions would interact with the pure siloxane surface of the unsubstituted portions of the clay. The charge distribution of the middlings, on the other hand, is consistent with a clay that would be surrounded easily by hydrated cations and attract a large amount of water to its surface.

Table 42: Layer charge calculations for 0.2–2 μm primary froth illite particles

Element	Wt%	Gram eq.	normalized gram eq.	Tet. Layer	Oct. layer	Interlayer	Tet. layer Charge	oct. layer charge	interlayer charge
Mg	1.20	0.10	0.20		0.20			0.40	
Al	15.10	1.68	2.29	0.47	1.82		1.40	5.47	
Si	24.10	3.43	3.51	3.51			14.04		
K	2.20	0.06	0.23			0.23			0.23
Fe	2.40	0.09	0.18		0.00	0.18		0.00	0.35
Ca		0.00	0.00			0.00			0.00
Ti	0.30	0.03	0.03	0.03			0.10		
Mn		0.00	0.00						
Na	0.04	0.00	0.01			0.01			0.01
sum gram equivalents		5.38	6.44			**Layer Charge**	**-0.47**	**-0.12**	**0.59**

Table 43: Layer charge calculations for 0.2–2 µm middlings illite particles

Element	Wt%	Gram eq.	normalized gram eq.	Tet. layer	Oct. layer	Interlayer	Tet. Layer Charge	oct layer charge	interlayer charge
Mg	1.3	0.11	0.21		0.21			0.42	
Al	12.7	1.41	1.87	0.19	1.68		0.57	5.03	
Si	27	3.84	3.81	3.81			15.24		
K	2.4	0.06	0.24			0.24			0.24
Fe	2.8	0.10	0.20		0.11	0.09		0.22	0.17
Ca	0.5	0.02	0.05			0.05			0.10
sum gram equivalents		5.55	6.38			Layer Charge	**-0.19**	**-0.32**	**0.51**

3.3 Discussion

The clay minerals found in the middlings were different from the clay minerals found in the froth. Firstly, the froth solids were enriched in chlorite and kaolinite and were depeleted in illite-smectite. Liendo (2005) found that kaolinite absorbed bitumen products more readily than montmorillonite or illite. This indicates that the enrichment of the kaolinite and chlorite to the froth solids is due to an affinity of these minerals for the bitumen rather than due to the rejection of the illite-smectite. The mechanism for this affinity remains unclear. Since the bitumen seems to have an affinity for these minerals, it is likely that ores containing large amounts of these minerals will have a larger amount of solids reporting to the froth and, hence, would cause more difficulty with down stream processes such as froth upgrading and coke production. Depending on the mechanism of kaolinite interaction with the bitumen, these minerals may also be problematitic in solvent extraction processes. If the kaolinite interaction is a relatively weak interaction between a neutral surface and a non-polar molecule, then solvent extraction may not be a concern. However, if the interaction is more complex then the kaolinite may still prefer the bitumen over the also hydrophobic solvent. Work by Ward & Brady (1998) suggests that the adsorption of organic acids on kaolinite occurs primarily on aluminum sites on exposed edges of the kaolinite. This is significant as it may explain why the clay minerals in the froth had a smaller basal surface area in TEM analysis than the middlings clay minerals. The smaller basal surface area would mean an increased number of edges and, therefore, an increased number of sites for the organics to adsorb on.

Apart from the preferential enrichment of kaolinite and chlorite to the froth, there are other ways in which the froth clay minerals are different from the middlings clays. The middlings clays exhibit a higher aspect ratio than the clays in the primary froth both in terms of their length to width ratio and in terms of the surface area to thickness ratio. The high aspect ratios cause slurries of these particles to have higher yield strengths and higher relative viscosities, making the slurry more resistant to flow. (Brenner, 1974) The increased resistance to flow means that settling of the particles is more difficult.

The illitic particles in the middlings also appeared to have a lower total charge than the illitic particles in the primary froth. Furthermore, the charge was more concentrated in the octahedral layer meaning that the effect of the charge would be more diffuse at the surface of the clay. The presence of this diffuse charge means that a similarly diffuse charge is required in the interlayer in order to balance the diffuse charge on the clay surface. In practice this means a hydrated cation is present where the layers of water surrounding the cation act to diffuse the charge present. Consequently, the charge distribution of the middlings is indicative of a clay that would trap more water than the clay in the primary froth. The tetrahedral charge on the primary froth, on the other hand, is indicative of a clay that is closer to pure illite where the charge can be balanced by a cation that is not heavily hydrated. The localized charge could also be balanced by negatively charged functional groups present in the bitumen. In fact, the presence of a few localized charges, combined with relatively large expanses of neutral surfaces, is ideal for the interaction with large organic molecules having polar and non-polar segments, as is the case with some of the organic molecules present in the bitumen.

The most interesting difference between the clay size fraction of the middlings and that of the froth is the amount of iron in the froth stream. Iron accounts for 15 wt% of the elements detected in the clay size fraction of the froth. Some of this iron appears to be present in the form of iron-oxide hydroxides which are not detected by the XRD. Furthermore, iron is found associated with many of the clay mineral particles in the TEM. The exact nature of the iron associated with the clay minerals is unknown. In some instances, it is clear that there are discrete dots on the surface of the clay minerals that are rich in iron; in other cases the clay surface appears to be completely uniform indicating that the iron is structural. Kessick (1979) reported the presence of tightly bound organic matter complexed with iron (III) on the surface of clay minerals in the oil sands. He believed that this complexed organic matter provided a critical link between the clay particles and the bitumen. This is particularly interesting in light of the large amounts of residual organics found in the primary froth clays. It is quite possible that the iron is playing some role in affiliating the clay surfaces with the organics – whether humic acids or residual bitumen.

Iron oxides are also known to play a role in the oxidation of organics by iron-reducing bacteria. Some of these bacteria have also been found to reduce structural iron found within kaolinite (Lee et al. 2002). Iron reducing bacteria are known to be present in oil sands tailings ponds (Penner, 2006). It is possible that some of the bacteria are present within the deposit and that they may use the clay surfaces as a support while reducing the iron oxides present in the oil sands.It is also possible that some of the residual organics present in the froth clay fraction are the remnants of bacteria and that this residual coating may be influencing the interaction of the bitumen with the clay.

3.4 Conclusions

- The primary froth stream is enriched in chlorite and kaolinite, and severely depleted in illite-smectite.
- The illite-smectite present in the froth, while apparently containing the same amount of smectite as the middlings, shows a more pronounced low angle asymmetry upon solvation with ethylene glycol.
- The thickness distribution of the particles observed in the primary froth reveals a bimodal distribution with one set of particles slightly thicker than the particles found in the middlings and one set of particles slightly thinner, which may explain the asymmetry in the XRD pattern observed upon solvation with ethylene glycol.
- The charge distribution of the primary froth indicates that a significant amount of iron may be associated with the interlayer of the illitic component, contributing to the asymmetry in the XRD pattern observed upon solvation with ethylene glycol.

- The middlings stream contains the most active particles. The middlings contain the largest concentration of illite–smectite in all streams. As well, the middlings clay minerals appear to have a larger basal surface area and a smaller thickness, on average, than the particles present in the other streams.
- The charge distribution of the middlings clays is consistent with a clay mineral that would capture a large quantity of water, whereas the charge distribution in the primary froth is consistent with a clay mineral that would strongly interact with organic molecules having some polar functional groups.

4 Characterization of the Coarse Solids in the Athabasca Oil Sands

4.1 Introduction

Coarse solids make up the majority of tailings waste produced by the extraction of bitumen from oil sands where in situ mining and the hot water extraction process are used. Moreover, the particle size of these solids indicates that they are relatively amenable to further processing or uses, such as in landfills, tailings dykes or concrete. Therefore, it is advantageous to characterize this fraction of the various waste streams to evaluate potential uses and liabilities.

This study attempts to assess the potential opportunities and liabilities presented in this waste by addressing the following:

- Mineral types
- Impact of coarse mineral distribution on extraction
- Distribution of valuable minerals in the process streams
- Association of impurities with valuable minerals
- Degree of valuable mineral liberation.

4.2 Materials and methods

The extraction and size separation procedures are outlined in Chapter 2- Mass and Mineral Balances.

4.2.1 Thermogravimetric analysis

Thermogravimetric (TG) analysis was conducted on micronized subsamples of all size fractions using a two of experimental procedures. The first set of TG tests were conducted at CANMET following the procedure of Friesen et al., (2005) whereby the sample was heated at 10°/min under a nitrogen atmosphere up to 1000°C, at which point the atmosphere was switched to air. The sample was then held at 1000°C for 20 min.

A second set of TG tests was conducted using a TG with evolved gas analysis capabilities. These experiments were run under nitrogen. However, a small oxygen leak was detected during the standard run used to test the equipment. Attempts to remove the leak reduced the leak to a sporadic occurrence but were unsuccessful at removing it completely. Since this was the only equipment with EG capabilities the samples were run anyway with the knowledge that some oxygen was possibly present during the analysis. As with the first round of tests, the sample was heated at 10°/min under a nitrogen atmosphere until 1000°C. The amount of carbon dioxide, carbon monoxide, water vapour, and "tars" (combination of various organic molecules) present in the sample chamber was monitored during the test.

4.2.2 Density separation

Density separation was performed using LST heavy liquid on the solids that remained after sub-samples had been taken for XRD & XRF analysis. LST is an aqueous solution of sodium heteropolytungstanate, containing between 70-80 wt% tungsten. The shipped density of LST is 2.85 g/cm^3. However, it can be adjusted to some extent via the addition or evaporation of water. The maximum density for LST is 2.95 g/cm^3 at 25°C and 3.6 g/cm^3 at higher temperatures (85°C) (Central Chemical Consulting, 2006). Since the density of quartz (the most prevalent light mineral in the oil sands) is 2.65 g/cm^3, any density greater than 2.7 g/cm^3 was deemed acceptable for concentrating the heavy minerals.

Separation involved placing approximately 75 mL of LST in a 100 mL beaker and then adding no more than 30 g of solids to the beaker. The solids were thoroughly mixed with the LST using a plastic stirring rod. After mixing, the beaker was covered with a layer of parafilm and the solids were allowed to separate. Minerals with a density greater than the LST sank, while the minerals with a density less than the LST rose to the surface. Separation was deemed to be complete when the LST separating the light and heavy minerals was clear of floating particles. At that point, the light minerals were scraped off the top of the LST with a plastic spoon and transferred onto a small filter, where the solids were then washed thoroughly with hot deionized water. If more sample was available, another 20 g of solids were added to the beaker containing the remaining LST and the heavy minerals from the first separation. The separation process was repeated until the amount of LST remaining in the beaker after separation was less than 40 mL. Once the LST amount dropped below 40 mL (due to evaporation and entrapment of LST in the separated particles), the LST and solids were carefully poured onto another filter. The heavy minerals were then rinsed out of the beaker and washed thoroughly with hot deionized water.

4.2.3 SEM analysis

Scanning Electron Microscope (SEM) analysis was performed on two sets of samples using a Hitachi S-2700 SEM equipped with a PGT (Princeton Gamma-Tech) IMIX digital imaging system and a PGT PRISM IG (intrinsic germanium) detector for energy dispersive X-ray (EDX) analysis and a GW Electronics System 47 four quadrant solid state backscattered electron detector. The first set was taken from solids after sieving. For these samples, a small quantity of the solids was mixed with epoxy and carbon black to create a 3.2 cm (1 ¼") mount that was then ground and polished flat. Images of the samples were taken in back-scattered mode at 50X magnification using a false colour table to improve contrast. Images were taken three fields of view apart, starting at the top left hand corner of the sample and proceeding in a standard raster style pattern until at least 15 fields of view were obtained. In each field of view, particles that exhibited a contrast other than that of quartz (typically a pale purple/pink colour) were analyzed with spot EDX for 10-30 seconds. Particles exhibiting very fine dispersion were examined and analyzed at higher magnification (no standard set). Figure 23 shows an example of a typical image from the >106 µm froth sample. After SEM analysis the images were analyzed with image analysis software for the total percentage area in each of three colour categories: purple/pink (primarily quartz, some clays), red (primarily feldspars), and yellow (heavy minerals). The EDX data was then examined to see if it was possible to separate titanium bearing, iron bearing, and zircon bearing minerals by contrast alone.

600 micrometers
+140 mesh Run 2 Froth (BSE image)

Figure 23: Typical false-colour image of >106 µm froth sample showing purple (quartz), red (feldspars), mottled yellow (inter grown quartz with heavy minerals), and yellow particles (heavy minerals) (Hitachi S-2700).

A second set of samples was made from the heavy mineral fraction of the three most successful separations (2–45 µm froth, >45 µm froth and >45 µm tailings). These samples were prepared as probe mounts. For these samples, a very small quantity was confined to a ~ 3 mm diameter circular area in the center of a 1.0 cm x 1.0 cm x 0.3 cm block. These samples were ground and polished and then carbon coated. The samples were analyzed in back scattered mode in the SEM. EDX analysis was performed on each particle in each field of view until enough images had been taken across the sample so that at least 150 particles were analyzed per sample. The EDX spectra were then quantified using the Quant™ program and a series of pre-loaded standards, thus providing quantitative EDX data on each particle. The approximate precision of the EDX results was between 0.1 and 0.5 wt%. Some X-ray maps were also taken of these samples to get an idea of the homogeneity of the distribution of iron in leucoxene-type particles.

4.2.4 XRD analysis

XRD analysis was performed on the coarse solids from the froth, middlings, and tailings as outlined in Chapter 2. The solids that were extracted via density separation (in both the coarse froth and tailings streams) were analyzed via XRD in the same manner. In addition, the heavy solids from the coarse froth were analyzed by Omotoso using synchrotron X-ray diffraction at APS 33BM using a wavelength of 0.617971 nm. Diffraction data was collected on a flat plate ~ 1 mm deep in $\theta - 2\theta$ mode, with a scintillation detector. The high resolution pattern was primarily used for phase identification.

4.2.4.1 Micro-XRD analysis

A single particle identified by SEM analysis as having a "leucoxene" composition ((Fe/(Fe+Ti)) = 0.3) was selected for micro-XRD. An XRD spectrum was collected from the selected particle that was embedded in an SEM probe mount. A D8 Discover XRD by Bruker equipped with a 0.1 mm collimator was used for this micro-XRD analysis.

4.2.5 TEM analysis

Two focused ion beam (FIB) sections of the identified "leucoxene" particle were made for TEM analysis by Fibics Inc.; the locations are shown in Figure 24. FIB sectioning uses a focused ion beam to cut away material around a protected area of interest. The area of interest can then be lifted out and thinned to electron transparency. A complete description of this process is available on the Fibics website (Fibics incorporated, 2008). Both sections were analyzed using several different microscopes, including: a JEOL 2010, a JEOL 2200FS, and a FEI Tecnai F20. All three microscopes were operated at 200 kV and were equipped with an EDX detector. The JEOL 2200FS and the FEI Tecnai F20 had scanning transmission electron microscope (STEM) mode capabilities.

Diffraction patterns were solved with the aid of a visual basic macro that calculated d-spacings and interplanar angles from lattice parameter information according the equations for triclinic systems. This program is found in Appendix C.

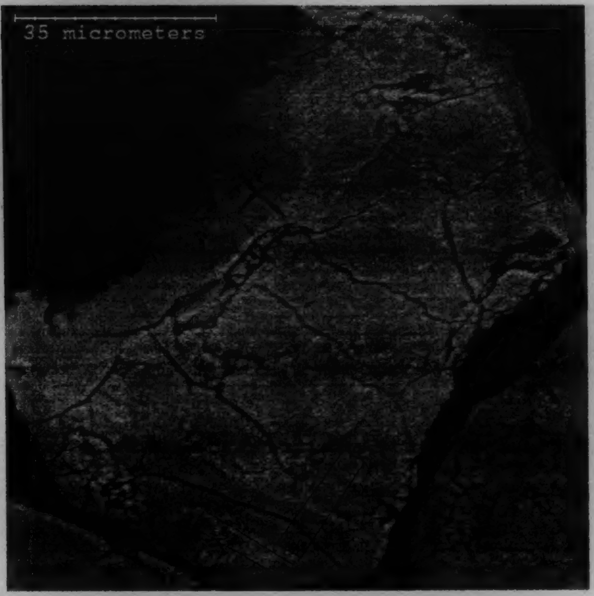

Figure 24: SEM image of "leucoxene" particle showing location of FIB sections.

4.3 Results and discussion

4.3.1 TG analysis

TG curves for the froth, middlings, and tailings samples were analyzed as shown in Figure 25 -Figure 27. The froth solids exhibited the largest mass losses of the various samples, with the 2-45 μm froth solids having a mass loss of 28%. The majority of the mass loss for the froth solids occurred in the 250-500°C temperature range. In this temperature range, hydrocarbons along with carbon monoxide, carbon dioxide, and water were all detected in the evolved gas, indicating that the mass loss was due to the decomposition of residual organics. A significant amount of mass loss also occurred in the 500-530°C range, during which carbon dioxide and water were detected in the evolved gas. This temperature range is consistent with the dehydroxylation of kaolinite but overlaps with the decomposition of the residual organics and the decomposition of siderite. Hence, it was not possible to conclusively determine the amount of mass loss correlating to each possible source. The tailings samples exhibited a similar mass loss profile as the froth samples, while possessing a significantly lower total mass loss (~2 wt% mass loss). In contrast, a greater percentage of the mass loss occurred in the 500-530 °C temperature range for the middlings samples. No carbon dioxide was detected in the evolved gas for the 500-530 °C temperature range, indicating that clay dehydroxylation was responsible for the weight loss in this range. For the 250-500 °C temperature range of the middlings, hydrocarbons, carbon monoxide, and carbon dioxide were detected indicating that residual organics were also present on these samples.

The above results indicate the presence of a significant amount of residual hydrocarbons remaining on the surface of the froth solids after Dean Stark treatment. The presence of these hydrocarbons is significant, as it may impact surface properties. As well, their presence may hamper any attempts to separate valuable minerals via surface sensitive methods such as grease tables or froth flotation.

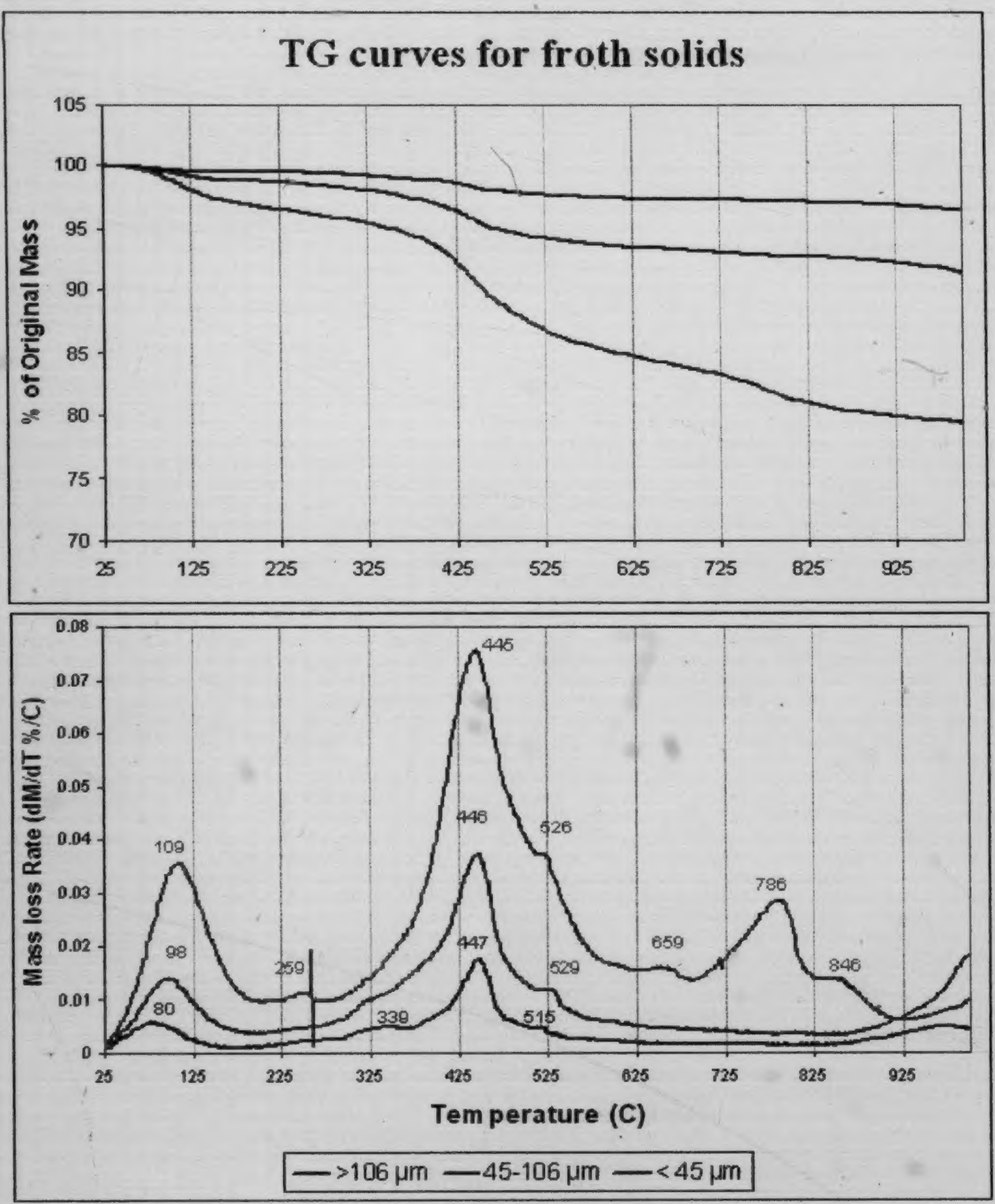

Figure 25: TG curves for froth solids. Temperaures at peak mass loss rate are shown on the figure.

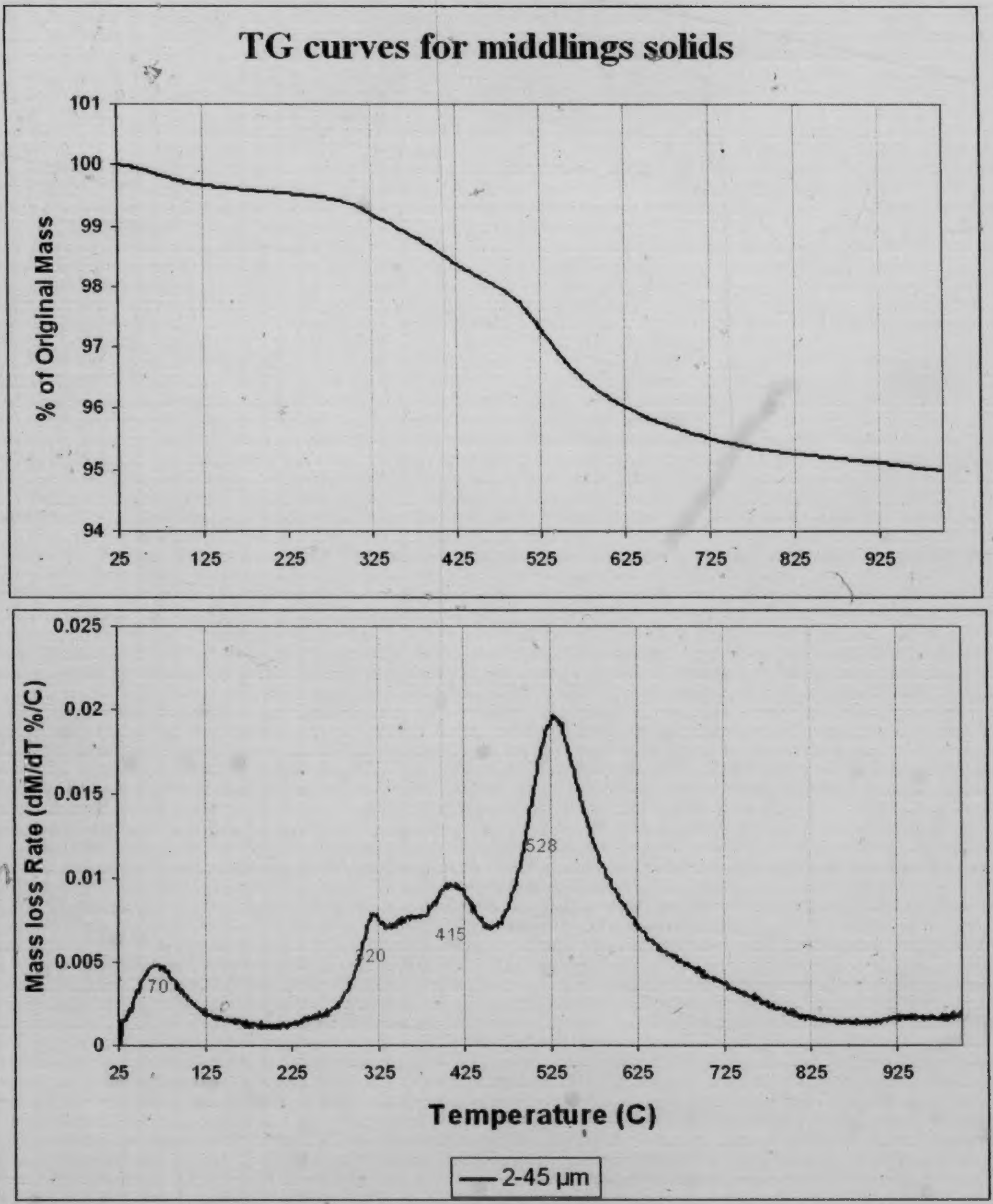

Figure 26: TG curves for middlings solids. Temperaures at peak mass loss rate are shown on the figure.

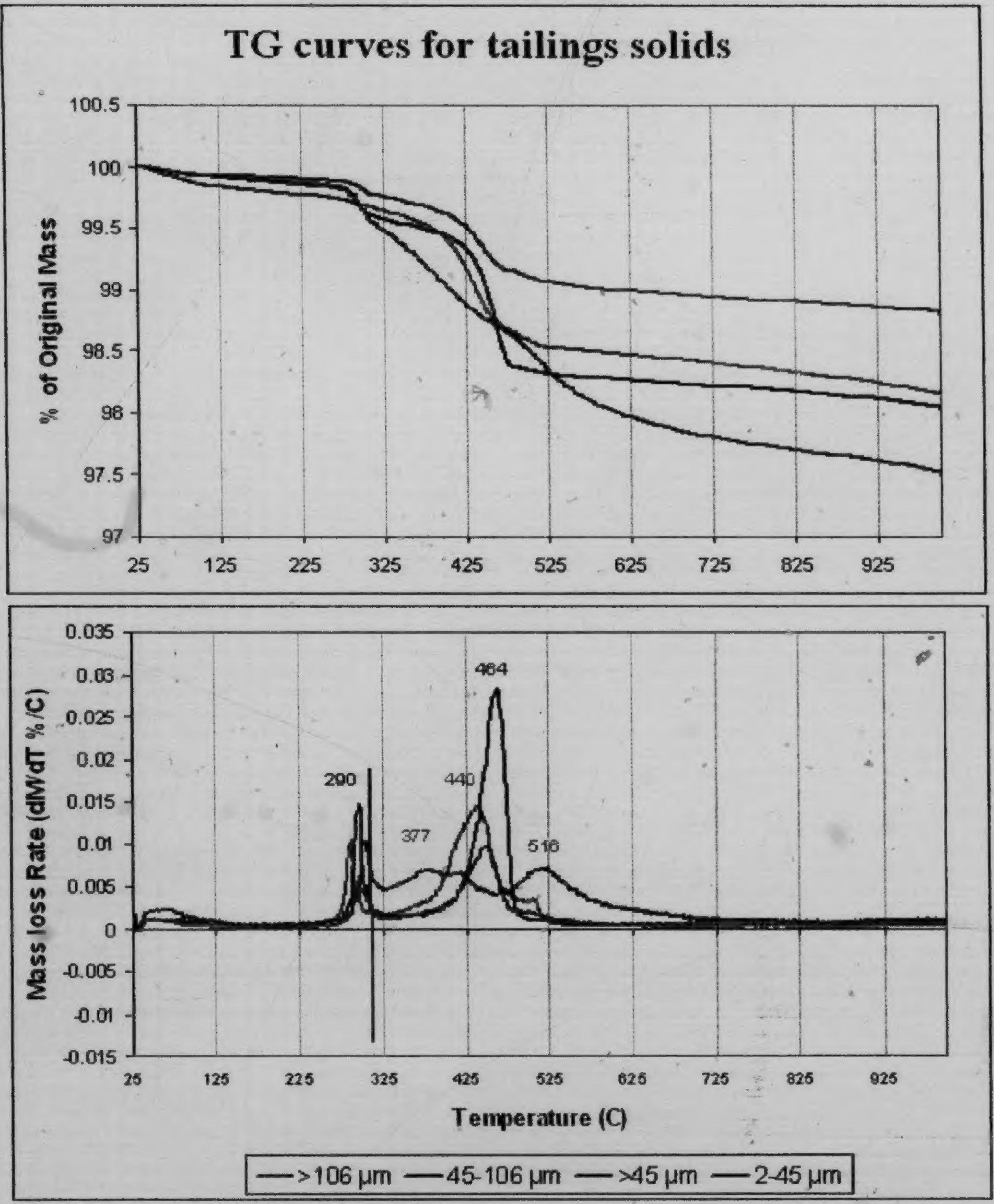

Figure 27: TG curves for tailings solids. Temperaures at peak mass loss rate are shown on the figure.

4.3.2 Analysis of the effectiveness of density separation

Table 44 shows the results of the density separations performed. Since there was not sufficient material recovered to analyze the heavies present in each size fraction, the >45 µm fractions were combined into a single sample for the primary froth and tailings. Separation of the <45 µm fraction in the middlings sample was not as effective, as there was a minute amount of heavy minerals and a large amount of clay minerals present. Consequently, this sample was not analyzed and no similar separation was attempted on the <45 µm tailings.

Table 44: LST separations of R3-5 solids

Sample	Total weight	# of sep.	LST density min.	LST density max.	Total weight of lights in weigh boat	Total weight of heavies in weigh boat	% Heavy minerals	% Loss
Middlings >45 µm	1.34	1	2.85	2.85	0.9043	0.014	1.04%	31.5%
Middlings 2-45 µm	20.042	1	2.85	2.85	19.085	0.775	3.87%	0.9%
Primary froth >106 µm	12.668	1	2.88	2.88	11.789	0.46	3.63%	3.3%
Primary froth 45-106 µm	4.662	1	2.85	2.85	3.517	1.066	22.87%	1.7%
Primary froth 2-45 µm	14.024	1	2.88	2.88	10.262	2.654	18.92%	7.9%
Tailings >106 µm	589.018	9	2.84	2.88	587.755	2.354	0.40%	-0.2%
Tailings 45-106 µm	177.53	4	2.81	2.87	176.144	0.897	0.51%	0.3%
Tailings >45 µm (combined heavies)	3.199	1	2.86	2.86	2.179	0.9804	30.65%	1.2%

In order to evaluate the success of the separations, small sub-samples of the solids were taken before and after density separation and pressed onto sticky carbon disks for evaluation with SEM/EDX. EDX spectra were taken from each sample at low magnification (50 X), giving an overall composition. The EDX spectra were quantified and then separated into "light" and "heavy" elements. Elements with an atomic number greater than or equal to 21 were considered heavy, and those with an atomic number less than 21 (i.e., up to calcium) were considered light. The total wt% of heavy elements before and after separation was compared. As shown in Table 45, the amount of heavy elements after separation was always significantly greater than the amount before separation. Nevertheless, a significant amount of light elements was still noted in the tailings samples after separation. Consequently, all the coarse (>45 μm) particles from the tailings were combined and separated once more to maximize the concentration of the heavy minerals of interest. The froth samples were also combined; however, separation was not repeated, as the concentration of heavy minerals was deemed sufficient.

Table 45: Overall EDX analysis of samples before and after LST separation (wt%)

	Primary Froth >106 μm		**Run 3-5 Primary Froth -140+325**		**R3-5 Tailings +140**		**R3-5 Tailings - 140+325**	
Element (wt%)	**Before**	**After**	**Before**	**After**	**Before**	**After**	**Before**	**After**
Al	1.9	7.1	12.0	6.1	1.3	4.0	2.1	5.4
Ca	0.5	0.6	2.2	0.8		0.5	0.1	0.7
Fe	1.9	20.7	9.5	24.6		13.6	0.8	17.5
K	0.6	0.4	2.2	0.3	1.0	1.1	1.3	2.3
Mg		1.3	1.1	1.5			0.1	0.4
Mn		0.7		1.1		1.2	0.0	0.4
P		1.2						
S	0.5	0.8	3.4	1.0			0.7	0.9
Si	92.8	20.0	56.7	13.2	97.7	72.8	95.3	64.1
Ti	1.9	47.3	9.9	40.9		6.9	0.7	8.7
Zr				10.6				
% Heavies	3.8	68.7	19.4	77.2	0.0	21.7	1.5	26.5

This analysis indicated that while the LST separation was successful at concentrating the heavy minerals, less heavy minerals were recovered than expected (under the assumption that all the heavy elements detected in the unseparated samples reported to the heavy fraction after separation). Table 46 depicts the percentage of the expected mass that was recovered in each fraction. As shown, the LST separation was very effective for the 45-106 µm froth sample; however, it was very ineffective for the 45-106 µm tailings sample. There are several reasons for this discrepancy. Firstly, the analytical method used (SEM-EDX) examined a very small portion of the overall sample, and, therefore, may not have been representative of the sample as a whole. Secondly, it is probable that some of the heavy elements were associated with non-heavy minerals (either as a small portion of their structure or as inclusions in a larger particle), thus reducing the amount of heavy solids expected. Both reasons were particularly true for the tailings sample (which showed the greatest discrepancy in actual recovery versus expected recovery), as there was a very large quantity of sample that required separation. As well, the presence of significant quantities of Fe-containing silicates and poorly liberated Ti bearing minerals (see SEM analysis) could have aided in the establishment of the discrepancy. Finally, the efficiency of the separation appears to be dependent on the amount of material separated in each pass of the heavy minerals with an increased amount of lights being trapped in the settling heavies for large feed passes.

Table 46: Evaluation of LST separation – SEM/EDX results

	Mass of unseparated sample (g)	Wt% heavy elements in unseparated sample	Mass of separated heavies (g)	Wt% heavy elements in separated heavies	Mass heavies expected (g)	% of expected mass actually recovered
Primary Froth >106 μm	12.668	3.8	0.46	68.7	0.7	66%
Primary Froth 45-106 μm	4.662	19.4	1.066	77.2	1.2	91%
Tailings >106 μm	589.018	0.0	2.354	21.71	0	
Tailings 45-106 μm	177.53	1.5	0.897	26.5	10.1	9%

Table 47: Evaluation of LST separation – XRF/XRD results

Sample	% heavies obtained	% heavies predicted - XRD
Middlings >45μm	1.0%	9%
Middlings 2-45μm	3.9%	2%
Primary Froth >106μm	3.6%	1%
Primary Froth 45-106μm	22.9%	18%
Primary Froth 2-45μm	18.9%	32%
Tailings >106 μm	0.4%	<1%
Tailings 45-106μm	0.5%	<1%

Separation efficiency was also determined using XRD analysis on the samples before separation. The percentage of heavy minerals detected by XRD (carbonates, sulphides, phosphates, tourmalines, iron oxides, titanium oxides, and zircon, all with SG >2.8) were added and compared with the weight fraction of heavy minerals obtained by density separation. Table 47 shows that, for the coarse primary froth samples and the 2–45μm middlings sample a greater amount of heavies were recovered than predicted from XRD data. This is explained by the presence of quartz and other non-heavy minerals found in the heavies fraction. This presence is due to either the entrapment of the light material in the LST or the poorly liberated nature of some particles. Less than the expected amount of heavies was recovered for the froth silt (2-45 μm). This is understandable as the extremely fine nature of the material tended to lead to poor settling characteristics, and therefore, the froth silt did not settle into distinctive layers during separation. Recovery in this fraction might be improved by using a centrifuge in conjunction with the LST.

4.3.3 Analysis of XRF results of coarse solids

The XRF data (Table 48 and Table 49) was consistent with the elemental composition of the different streams analyzed in the MDA study (Table 50) (Alberta Chamber of Resources, 1996). For instance, the "main tailings" stream in the MDA study contained approximately 0.1 wt% titanium and the tailings fractions of the samples contained ~ 0.1 wt% titanium. Since there is no equivalent to a secondary froth stream in the MDA study, the closest comparable stream is the primary froth with the Syncrude froth feed. These streams do not match as well as the tailings samples do. The Syncrude froth feed is reported to contain 5.5 wt% titanium, whereas the primary froth solids contain only 4 wt% titanium. This discrepancy may be due to the different hydrodynamics of the batch extraction unit versus the true primary separation vessel. The primary separation vessel is very tall which allows more time for entrained solids to drop out of the froth, whereas the time for the entrained particle to drop out of the froth is quite short in batch extraction. This could mean that fewer large particles end up in the froth solids in production than in the froth solids in batch extraction. The >106 μm fraction contains significantly less titanium than the other fractions, which could explain the reason for the observed differences.

It is also interesting to compare the zirconium contents obtained between these results and the MDA study. As shown in Table 50 zirconium was only quantified in the Suncor Beach sand. This stream contained a zirconium concentration of 1.34 wt% Zr (~1.8% ZrO_2) which is similar to the ZrO_2 concentrations detected in the primary froth of between 0.5wt% and 3.7wt% for the different coarse streams. The lack of detection of zircon in the other streams of the MDA study is not surprising as the zirconium in the tailings stream was found to be present in very small quantities near the detection limit of the XRF in this study. It is possible that either the assays used in the MDA study were not as sensitive or that the zirconium was over detected in this study. It should be noted that zircon particles were found in the tailings stream of this study, by SEM analysis in quantities consistent with the zirconium levels detected in the XRF. A zircon mass balance was performed in the MDA study resulting in ~89% of the zircon reporting to the Plant 5 froth. However, since zircon assays were not available for all the streams and the mass balance was based on the assumption of steady state conditions rather than a true mass balance of the ore, this assay was considered tentative.

Table 48 XRF analysis results from froth samples (wt%)

Stream	Primary Froth					Secondary Froth		
Size Fraction	<0.2 µm	0.2-2 µm	2-45 µm	45-106 µm	>106 µm	<2 µm	2-45 µm	>45 µm
Sample Weight	1.78	5.28	16.71	7.24	18.03	0.76	0.94	3.60
SiO_2 (±1.65)	44.0%	43.3%	51.1%	68.1%	90.9%	46.1%	43.0%	90.2%
Al_2O_3 (±1.15)	25.1%	25.6%	14.0%	7.5%	4.2%	22.6%	23.8%	4.9%
Fe_2O_3 (±0.36)	15.1%	14.5%	15.9%	5.2%	0.8%	13.1%	16.3%	0.9%
TiO_2 (±0.57)	1.0%	2.9%	11.0%	10.1%	1.4%	3.8%	9.5%	1.6%
K_2O (±0.05)	2.5%	2.5%	1.2%	0.7%	0.5%	2.5%	1.0%	0.6%
Cl (±0.1)	5.5%	4.6%	0.4%	0.4%	0.4%	2.1%	0.5%	0.3%
MgO (±0.15)	1.9%	1.3%	1.1%	0.6%	0.0%	3.5%	1.2%	0.0%
CaO (±0.02)	1.1%	1.7%	1.7%	0.5%	0.2%	1.6%	1.4%	0.2%
Cr_2O_3 (±0.02)	0.7%	0.7%	0.3%	0.2%	0.2%	1.7%	0.2%	0.2%
ZrO_2 (±0.36)	0.1%	0.1%	1.4%	3.7%	0.5%	0.0%	1.1%	0.4%
Na_2O (±0.04)	0.2%	0.1%	0.1%	0.2%	0.0%	0.0%	0.1%	0.2%
MnO (±0.03)	0.3%	0.5%	0.8%	0.2%	0.0%	0.6%	0.8%	0.0%
P_2O_5 (±0.06)	0.3%	0.4%	0.4%	0.3%	0.1%	0.5%	0.3%	0.1%
SO_3 (±0.03)	0.2%	1.1%	0.1%	0.1%	0.1%	0.3%	0.1%	0.1%
ZnO (±0.08)	0.1%	0.1%	0.2%	0.2%	0.1%	0.4%	0.2%	0.2%
CuO (±0.01)	0.1%	0.1%	0.2%	0.1%	0.1%	0.4%	0.2%	0.1%
Other	1.6%	0.3%	0.2%	1.9%	0.4%	0.9%	0.5%	0.0%
Trace (< 0.1%)	As_2O_3, SrO	CoO, Ho_2O_3, SrO	Dy_2O_3, SrO	As_2O_3, Au,Pt Dy_2O_3, Ho_2O_3,Pt, SrO, Y_2O_3	Er_2O_3, Ir, SrO	Er_2O_3, SrO	Dy_2O_3, Er_2O_3, SrO	

Table 49: XRF results for tailings samples

Stream	Middlings				Tailings					
Size Fraction	<0.2 µm	0.2-2 µm	2-45 µm	>45 µm	<0.2 µm	0.2-2 µm	2-45 µm	45-106 µm	106-250 µm	>250 µm
Sample Weight	21.83	50.12	108.87	4.46	6.26	16.59	111.42	192.46	604.58	4.18
SiO_2 (±1.65)	52.8%	55.1%	78.3%	56.1%	51.7%	61.7%	90.6%	94.0%	95.5%	77.3%
Al_2O_3 (±1.15)	32.3%	31.7%	14.9%	31.6%	30.0%	25.6%	5.3%	2.8%	2.6%	6.2%
Fe_2O_3 (±0.36)	6.7%	5.0%	2.1%	4.5%	7.6%	4.6%	0.6%	0.2%	0.1%	11.1%
TiO_2 (±0.57)	0.5%	1.2%	0.7%	1.0%	0.6%	1.2%	0.4%	0.2%	0.0%	0.2%
K_2O (±0.05)	3.2%	3.4%	2.2%	2.8%	3.1%	3.1%	1.2%	0.8%	0.5%	1.1%
Cl (±0.1)	0.4%	0.4%	0.4%	0.4%	0.7%	0.9%	0.5%	0.4%	0.4%	0.4%
MgO (±0.15)	1.8%	1.3%	0.0%	1.4%	1.7%	1.0%	0.0%	0.0%	0.0%	0.6%
CaO (±0.02)	0.8%	0.5%	0.2%	0.6%	0.9%	0.5%	0.1%	0.1%	0.1%	1.4%
Cr_2O_3 (±0.02)	0.2%	0.6%	0.2%	0.2%	0.7%	0.7%	0.2%	0.2%	0.2%	0.2%
ZrO_2 (±0.36)	0.0%	0.0%	0.0%	0.1%	0.0%	0.0%	0.0%	0.3%	0.1%	0.1%
Na_2O (±0.04)	0.5%	0.1%	0.1%	0.4%	0.1%	0.1%	0.2%	0.0%	0.0%	0.1%
MnO (±0.03)	0.2%	0.1%	0.1%	0.1%	0.1%	0.1%	0.0%	0.0%	0.0%	0.3%
P_2O_5 (±0.06)	0.1%	0.1%	0.0%	0.1%	0.1%	0.1%	0.1%	0.3%	0.1%	0.1%
SO_3 (±0.03)	0.1%	0.1%	0.1%	0.1%	0.4%	0.0%	0.1%	0.1%	0.1%	0.2%
ZnO (±0.08)	0.2%	0.1%	0.2%	0.2%	0.2%	0.2%	0.2%	0.1%	0.1%	0.2%
CuO (±0.01)	0.1%	0.1%	0.1%	0.2%	0.3%	0.2%	0.2%	0.1%	0.1%	0.1%
Other	0.1%	0.3%	0.4%	0.4%	1.8%	0.1%	0.3%	0.5%	0.1%	0.4%
Trace (< 0.1%)	CoO, SrO	Au, Pt, SrO	Pt, Sm_2O_3	SrO, Tb_4O_7	As_2O_3, CoO, SeO_2, SrO	Pt, SrO	Rh, SeO_2	SeO_2, Yb_2O_3	Pt	Ir, Pt, Tb_4O_7

Table 50: Chemical assays of selected Syncrude and Suncor samples, summarized from MDA study (Alberta Chamber of Resources, 1996)

	Syncrude Oil Sands Feed	Suncor Oil Sands Feed	Syncrude Main Tailings	Suncor Plant 1 Beach Sand	Syncrude Froth Feed
Si	46.16	41.74	47.46	34.02	25.05
Ca	0.08	0.1	0.04	0.24	0.81
Mn	0.02	0.01	0	0.09	0.21
S	0.08	0.05	0.05		0.68
Fe	0.68	0.54	0.29	4.2	7.17
Al	2.48	1.61	1.02	1.01	7.29
Mg	0.16	0	0.07	0.15	0.84
Na	0.94	0.12	0.98	0.07	0.4
K	1.17	0.71	0.82	0.29	1.3
Ti	0.26	0.22	0.08	5.51	5.5
TiO_2	0.43	0.37	0.13	9.18	9.18
Zr				1.34	

4.3.4 SEM analysis

4.3.4.1 Sub samples from sieved coarse solids

Four samples from the coarse sieved solids were examined in the SEM. These four samples were the >250 μm and 106-250 μm froth and tailings. No major difference in area fraction for each phase was observed among the three samples analyzed by phase fraction, as shown in Figure 28. In all fractions, the major phase was quartz, as expected from the XRD results. The relative amount of quartz and feldspar is fairly consistent among samples; the only difference being the amount of heavy minerals is considerably lower in the tailings (as expected). The >250 μm tailings sample was not included in this analysis, as it was the first sample examined and the contrast levels used and, therefore, the ability to differentiate between the contrast thresholds were not consistent with those used for the other samples. The analysis that was performed on the >250 μm tailings indicated that the vast majority (92.4%) of the area was probably quartz-based and the remaining area (7.6%) was most likely feldspars with an occasional heavier particle.

The most significant finding from the SEM analysis is the presence of "mottled" particles of finely disseminated quartz and iron-rich or titanium-rich minerals. These mottled particles were present in every sample examined, though they were far more common in the froth samples than in the tailings samples. Figure 29 shows an example of an iron-rich mottled particle. This particle shows iron, manganese and calcium in the EDX spectrum, indicating the iron-rich mineral is likely siderite, or possibly a mixture of siderite and calcite. Other mottled iron-rich samples have been found, where only iron appears in the EDX spectra. These particles could be siderite or one of many types of iron oxide compounds. Figure 30 shows an example of a titanium-rich mottled particle. The presence of these particles is significant, because it helps explain why silicon contamination is so prevalent in the rutile concentrates developed from the oil sands froth solids. The presence of mottled iron particles may also help explain the iron contamination found in the rutile concentrates. The presence of such closely interspersed silica may cause the magnetic susceptibility of the particle to be too low to separate out into a magnetic stream during magnetic separation and, hence, it will end up in the non-magnetic stream with the rutile, causing contamination.

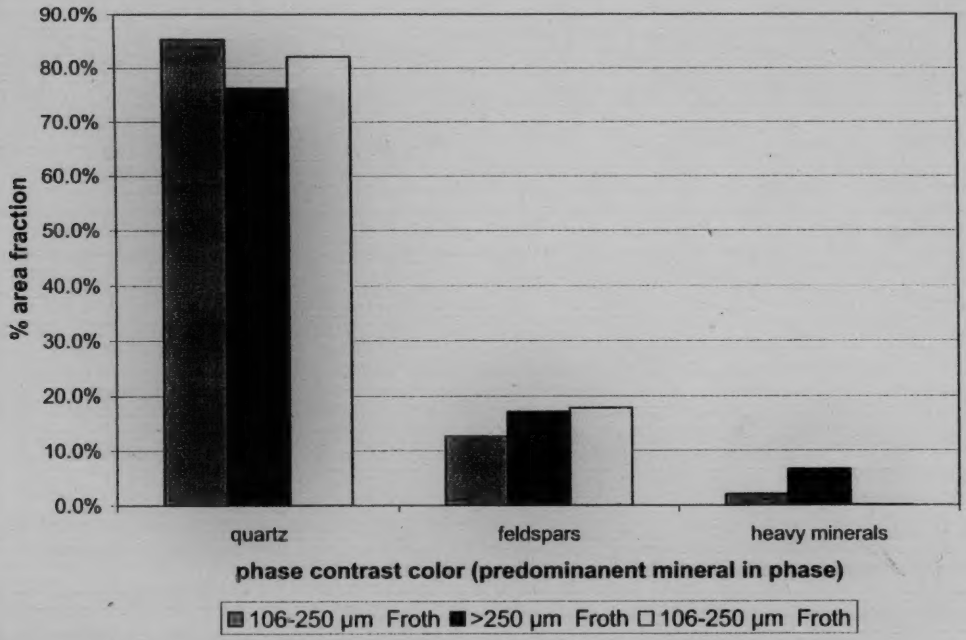

Figure 28: Area fraction by phase contrast in coarse fractions of froth solids and tailings.

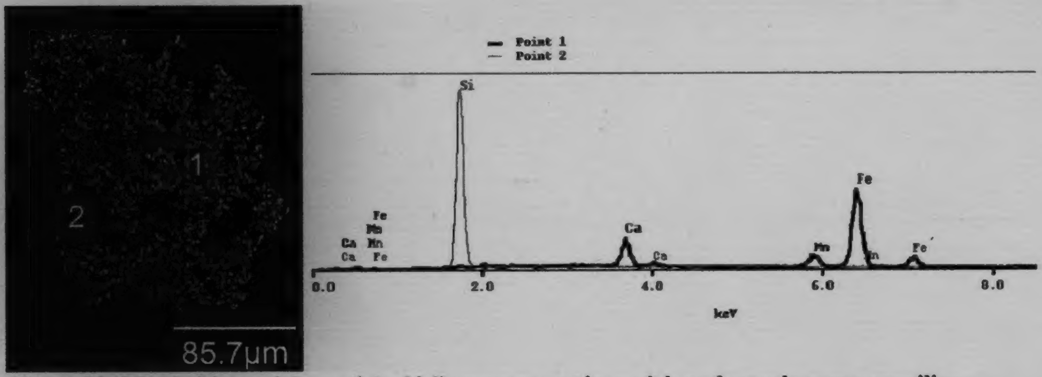

Figure 29: Mottled iron-rich particle. Yellow areas are iron-rich and purple areas are silica.

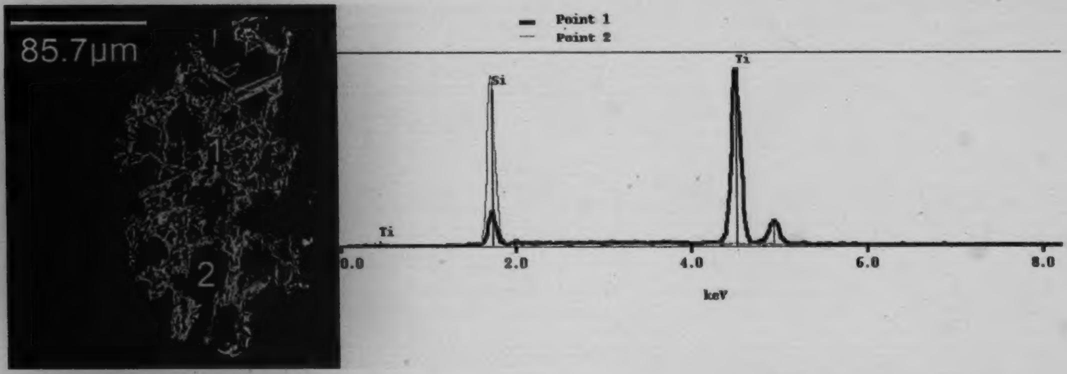

Figure 30: Mottled titanium-rich particle. Yellow areas are rich in titanium, purple areas are silica.

4.3.4.2 Sub-samples of heavy mineral fraction

4.3.4.2.1 Froth heavies

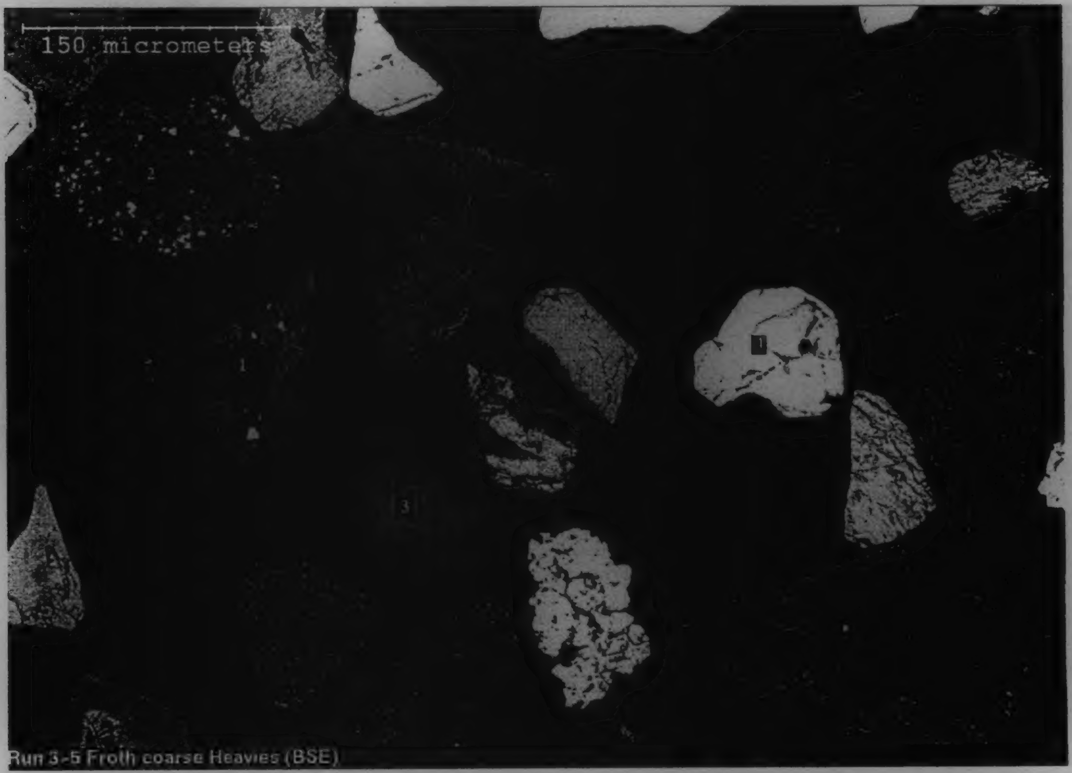
150 micrometers
1
2
3
Run 3-5 Froth coarse Heavies (BSE)

Figure 31: Typical backscattered SEM image from primary froth heavies.

Figure 31 shows a typical backscattered SEM image of the coarse heavy minerals in the froth tailings. As with the sieved coarse solids there is a significant number of grains where the heavy mineral particles (yellow & orange) are intergrown with silicate based material (purple) (particles labelled 1and 2). The intergrown grains are not limited to titanium oxides but also include iron sulphides, iron carbonates, iron-titanium oxides, and rare earth oxides. In addition to the finely intergrown particles, there are apparently well liberated particles that have variations in composition across the particle (particle 3) and pure, well liberated particles (particle 4).

Every particle in Figure 31 was analyzed by EDX spectroscopy to determine its composition (or composition of its components in the case of intergrown particles). The composition was then used to determine a mineral designation for each particle. Table 51 shows the classification scheme used. Each particle was also given a degree of liberation designation as shown in Table 52. All EDX data were analyzed on an oxygen-free basis due to the difficulty of accurately quantifying the oxygen detected.

Table 51: Criteria used for classification of particles by EDX

Mineral name	**Conditions for classification (based on light element free atomic %)**
Ilmenite	Ti+Fe >90, 0.45 <Fe/(Ti+Fe) <0.55
Leucoxene	Ti+Fe >90, Ti/(Ti+Fe) <0.9, 0.55 <Ti/(Ti+Fe) <0.9, 0.4 <Ti/(Ti+Fe) <0.45
Monazite	Contains rare earth elements and P
Pyrite	Fe+S >90, S/(Fe+S) >0.45
Quartz	Si >90
Rutile	Ti >85, Ti/(Ti+Fe) >0.9, Ti+Fe >90,
Siderite	Fe+Mn+Ca >90
Zircon	Zr+Si >90, 0.45 <Zr/(Zr+Si) <0.55
Other silicates	Al+Si >50

Table 52: Criteria used for classification of particle liberation

Liberation designation	Conditions for classification
Completely mixed	Particle made up of two or more finely intergrown phases that cannot be easily isolated by EDX.
Mottled	Particle made up of two or more intergrown phases that are easily discernable and isolated by EDX.
Slightly mottled	Particle appears to be a single uniform phase with a few inclusions of a second phase, typically on the edges of the particle.
Variegated	Particle appears uniform in secondary electron mode, but contains slight variations in coloring across the surface in back scattered electron mode indicating the presence of variations in composition.
Free	Particle appears uniform without indications of a second phase contained within the particle.

Table 53: Degree of liberation of various minerals in the froth heavies indicated by the percentage of particles in each class

	"Liberated"			Total liberated	Non-liberated		Total non-liberated
Mineral designation	**Free**	**Slightly mottled**	**Variegated**		**Mottled**	**Completely mixed**	
Rutile	0%	13%	31%	44%	34%	23%	56%
Ilmenite	0%	24%	47%	71%	24%	6%	29%
Leucoxene	3%	10%	71%	84%	13%	3%	16%
Monazite	38%	13%	0%	50%	25%	25%	50%
Pyrite	33%	17%	0%	50%	50%	0%	50%
Siderite	15%	0%	23%	38%	46%	15%	62%
Zircon	54%	38%	0%	92%	8%	0%	8%
Quartz	6%	0%	0%	6%	82%	12%	94%
Other silicates	44%	38%	8%	90%	5%	5%	10%
Unknown	25%	25%	25%	75%	25%	0%	25%
% of total particles counted	18%	19%	25%	63%	26%	11%	37%

Table 53 shows the degree of liberation of the various minerals identified in the froth heavies fraction. The zircon is well liberated in the froth heavies with only a few particles containing small inclusions of quartz or other silicates. On the other hand, the titanium minerals are generally not well liberated with a substantial number of these particles being classified as either mottled or completely mixed. Analysis of the heavy particles found in the oil sands extraction tailings shows that the mottled particles are even more prevalent in the tailings (Table 61). It is reasonable to assume, from the prevalence of the mottled particles in the tailings and the relatively small portion of the particle surface that is titanium-rich, that the particles could be easily removed from the froth by slightly changing the hydrodynamics of flotation. In fact, these particles would probably not report to the froth in a commercial froth flotation plant or would report in much smaller numbers. This is because the separation distance between froth and tailings is much larger in a commercial plant than in a batch extraction unit, leading to the elimination of the less hydrophobic minerals from the froth. This hypothesis is further supported by the fact that the MDA study (Alberta Chamber of Resources, (1996)), which looked at the liberation of the oil sands froth tailings heavies, indicated that the titanium minerals are generally well liberated.

Of greater significance is the number of titanium minerals classified as "variegated." These minerals would be classified as well liberated in a standard liberation analysis, because they contain no obvious second phase that would be detectable except in a high contrast back scattered electron image. X-ray maps of these particles from the SEM do not reveal a variation in composition (Figure 32), even though slight variations are noted in particle contrast (particle 1). In addition, an image at higher magnification reveals a fine surface structure (Figure 33), indicating that these particles are composed of very fine related phases that are closely intermixed (for instance mixed ilmenite and rutile to produce a "leucoxene" composition). This hypothesis is supported by the variation in iron within the iron-titanium oxide particles as determined by EDX analysis on the individual titanium bearing particles. Figure 34 shows that particles were found at virtually all Fe/(Fe+Ti) ratios from 0 to 0.55. If the particles were single phase, one would expect to see three bands of Fe/(Fe+Ti) ratios – those containing no iron, those with an Fe/(Fe+Ti) ratio of ~ 0.3 (pseudorutile), and those with an Fe/(Fe+Ti) ratio of about 0.5 (ilmenite).

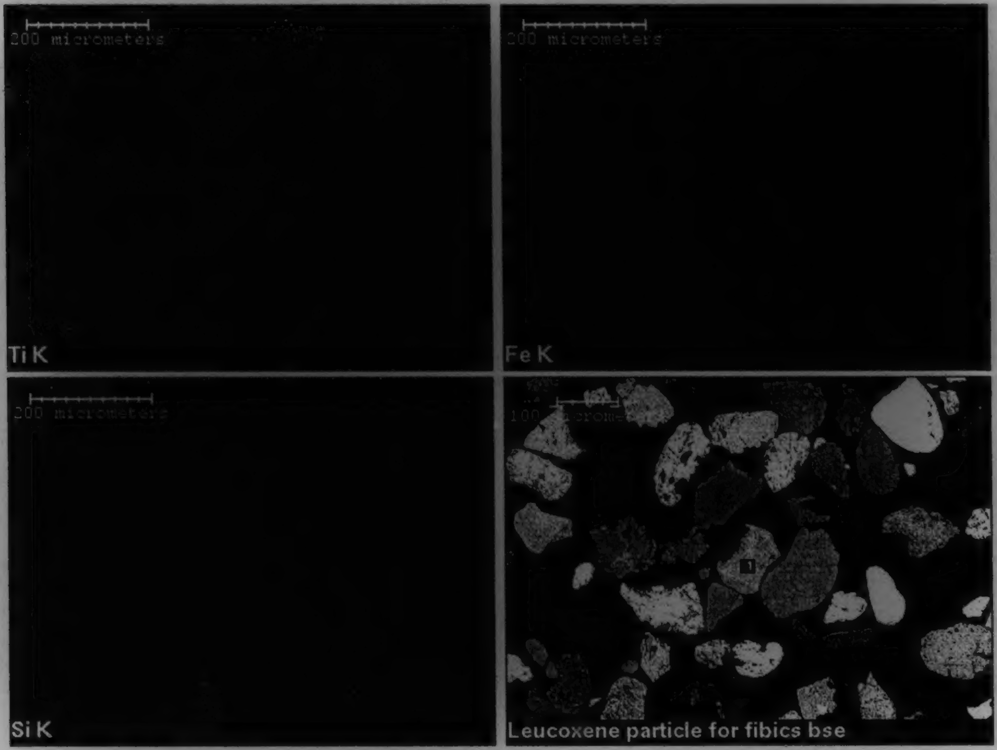
200 micrometers
Ti K
200 micrometers
Fe K
200 micrometers
Si K
100 micrometers
1
Leucoxene particle for fibics bse

Figure 32: Iron, silicon, and titanium X-ray maps of an area of froth heavies.

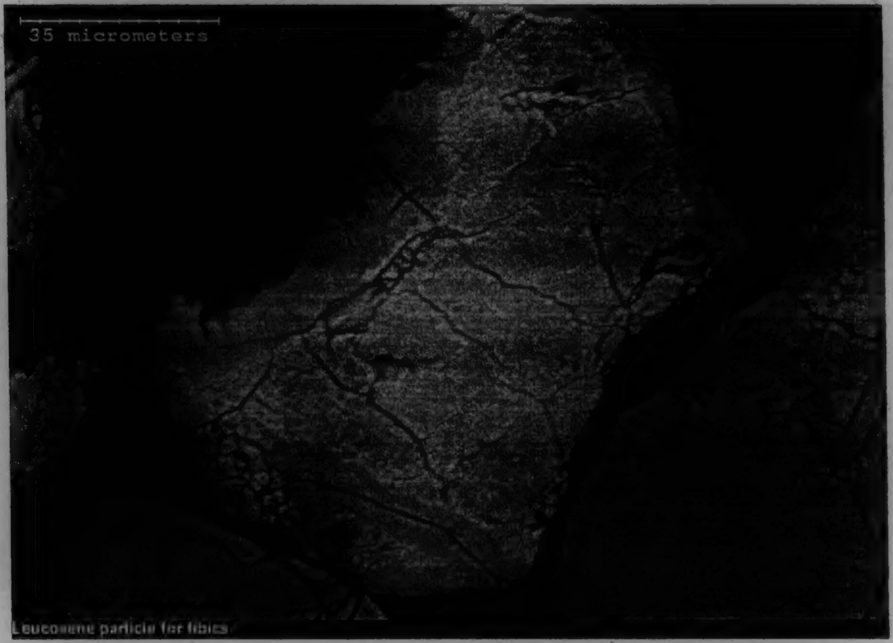

Figure 33: Higher magnification image of particle 1 in Figure 32 one showing contrast differences.

EDX analysis of particles considered to be liberated by traditional liberation analysis reveals that there is a significant number of particles that contain impurities such as manganese, iron, calcium, silicon, and aluminum. Over 92% of the “rutile” particles (as defined by SEM analysis, Table 51) observed contained extraneous elements. Similarly, none of the leucoxene or ilmenite particles were free of extraneous contaminants. Zircon, on the other hand, was relatively pure with two thirds of zircon particles containing only zirconium and silicon. Table 54 illustrates the level of contamination in well liberated particles of the valuable minerals (ilmenite, leucoxene, rutile, and zircon) as determined by SEM-EDX. It should be noted that “contamination” is used in this context to describe the presence of detected elements that are not part of the assumed mineral structure. In other words, a contaminant of rutile is anything other than titanium and oxygen. The use of the word contaminant does not indicate the origin of the extraneous elements, merely that they are extraneous and undesirable. Iron is the most frequently occurring contaminant in minerals where iron is not a fundamental constituent. The level of iron contamination was particularly significant in the "rutile" particles where iron was present in 85% of the particles at an average level of 3.65 at%. The presence of this iron is significant because it may mean that attempts at producing a high purity rutile concentrate may be unsuccessful.

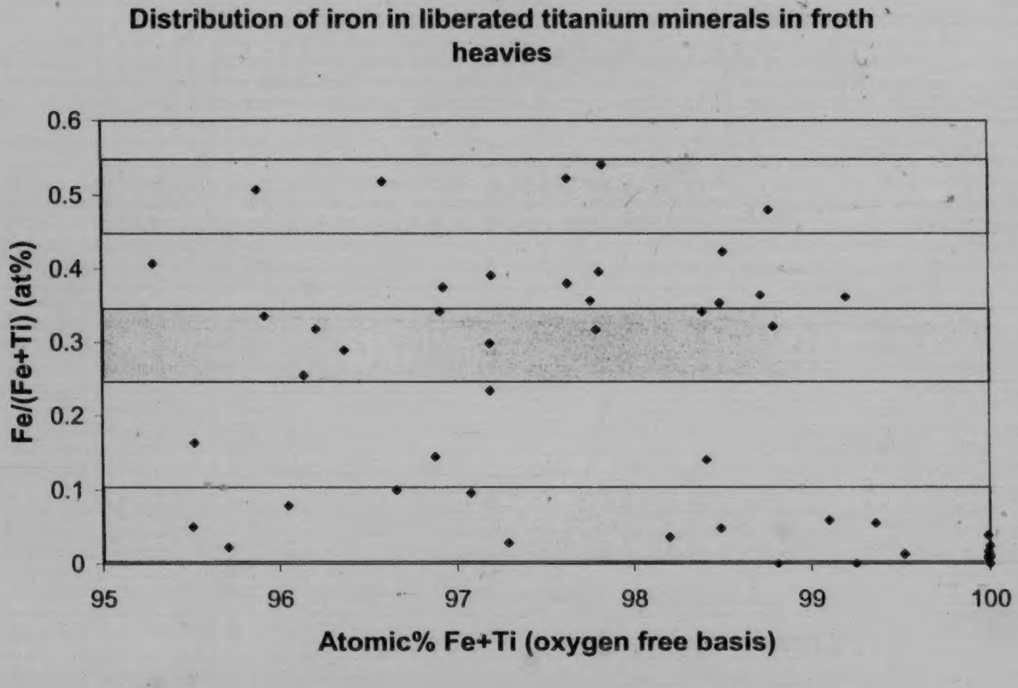

Figure 34: Distribution of iron in iron-titanium oxides, the grey area indicates the range of Fe/(Fe+Ti) ratios expected for rutile (<0.1), pseudorutile (0.25–0.35) and ilmenite (0.45–0.55).

Table 54: Contamination levels in liberated valuable minerals of heavy froth solids

Mineral Designation (n= number of particles)	Contaminant	% of particles containing contaminant	Contaminant level in particle (wt%)		
			Average	Max	Min
Ilmenite n=12	Al	25	2.4	3.8	1.3
	K	8	1.2	1.2	1.2
	Mg	25	3.1	3.5	2.2
	Mn	92	2.2	4.4	0.4
	Si	8	4.1	4.1	4.1
Leucoxene n=26	Al	54	0.7	1.1	0.2
	Ca	23	0.4	0.8	0.3
	Cr	4	0.5	0.5	0.5
	Mg	27	0.8	2.1	<0.1
	Mn	92	1.6	3.4	0.4
	Nb	4	2.5	2.5	2.5
	P	15	0.4	0.7	0.2
	Si	31	0.3	0.6	<0.1
Rutile n=27	Al	44	1.1	3.5	0.2
	Ca	7	0.7	1.1	0.2
	Fe	85	4.2	11.2	0.9
	Mg	4	0.6	0.6	0.6
	Mn	7	0.7	1.4	0
	Nb	7	4.2	6.2	2.31
	P	7	1.9	2.0	0.6
	Si	19	0.8	1.6	0.1
Zircon n=24	Al	13	0.4	1.0	<0.1
	Ca	4	2.4	2.6	2.4
	Fe	29	1.2	3.1	0.6
	Hf	4	5.5	5.5	5.5
	Mg	4	0.3	0.3	0.3

4.3.4.2.2 Comparison of heavy particles in the froth and tailings streams

Table 55 shows the percentage of counted particles that were in each mineral category for each particle stream. The total number of particles that contained titanium was relatively constant between the different streams (~ 44%); however, 62% of the titanium-containing minerals were poorly liberated in the tailings stream compared with only 12% of the minerals in the froth streams Another difference was that there were more titanium minerals that also contained iron in the froth streams as opposed to the tailings streams (21% of the particles in the >45 µm froth as opposed to 7% of the particles in the >45 µm tailings). Rutile (TiO_2) was the dominant titanium bearing mineral in all three streams and was also most likely to be poorly liberated.

Table 55: Particle breakdown in SEM/EDX analysis

Mineral Designation	2-45 µm Froth Heavies	>45 µm Primary Froth Heavies	>45 µm Tailings Heavies	Total
Ilmenite	4%	9%	1%	4%
Leucoxene	5%	12%	6%	7%
Monazite	1%	4%	0%	2%
Pyrite	11%	3%	5%	6%
Quartz	11%	9%	16%	12%
Rutile	30%	19%	10%	19%
Siderite	2%	4%	5%	4%
Zircon	7%	11%	3%	7%
Other silicates	18%	17%	11%	15%
Other titanium containing	5%	6%	27%	13%
Unknown	7%	7%	18%	11%
Total	169	180	200	549

Of the other minerals present, zircon was generally well liberated and concentrated in the froth; the few poorly liberated zircon particles were all in the tailings. Siderite was found primarily in the coarser >45 μm fractions, whereas pyrite was found primarily in the <45 μm fraction. This result is consistent with the XRD results. Interestingly, the pyrite present in the oil sands was found to be low in sulphur (Table 56). Since pyrite was detected in the XRD and is known to be a stoichiometric mineral with very little tolerance for variation away from stoichiometry this indicates that the sulphur content in these minerals was underestimated by the EDX detector, or that an additional iron bearing mineral was associated with these particles. Pyrrohotite (a non stoichiometric iron sulphide mineral) was not detected in the XRD analyses. Variations in composition among samples were also observed for the siderite particles which were iron-rich in the froth and calcium- and manganese-rich in the tailings, as shown in Table 57. It should be noted that siderite does not usually contain a great deal of calcium but has been found to contain up to 15 at% calcium (Deer et al, 1966, pp 487). The presence of manganese may explain the higher levels of calcium seen in these samples as rhodochrosite ($MnCO_3$) forms a solid solution series with both calcite and siderite (Blackburn & Dennen, 1988). Alternatively it is possible that some calcite is present intimately mixed with the siderite.

Table 56: Compositional variation in pyrite particles among samples

	2-45 μm Froth Heavies			**>45 μm Primary Froth Heavies**			**>45 μm Tailings Heavies**		
Element	**#**	**Range (At%)**	**Average (At %)**	**#**	**Range (At%)**	**Average (At %)**	**#**	**Range (At%)**	**Average (At %)**
Al	1	2-2	2	0	0-0	0	4	1-7	3
Fe	18	39-46	39	6	42-47	43	9	35-48	41
K	0	0-0	0	0	0-0	0	1	1-1	1
Mg	1	1-1	1	0	0-0	0	0	0-0	0
S	18	53-60	55	6	52-58	55	9	41-58	49
Si	2	1-4	2	0	0-0	0	4	1-15	5
Ti	10	1-1	1	2	0-4	2	2	0-1	1
W	0	0-0	0	0	0-0	0	1	1-1	1
# of particles	18			6			9		

Table 57: Compositional variation in siderite particles among samples

	2-45 µm Froth Heavies			>45 µm Primary Froth Heavies			>45 µm Tailings Heavies		
Element	**#**	**Range (At%)**	**Average (At %)**	**#**	**Range (At%)**	**Average (At %)**	**#**	**Range (At%)**	**Average (At %)**
Al	1	1-1	1	4	0-2	1	7	1-2	1
Ca	4	3-6	4	8	2-11	6	10	6-15	9
Cl	0	0-0	0	1	1-1	1	0	0-0	0
Fe	4	84-91	84	10	76-97	79	10	72-86	77
K	0	0-0	0	0	0-0	0	1	1-1	0
Mg	0	0-0	0	0	0-0	0	1	2-2	2
Mn	3	1-6	3	10	2-12	7	10	2-13	6
P	2	2-2	2	6	0-2	1	8	0-1	1
S	0	0-0	0	1	1-1	1	0	0-0	0
Si	2	1-5	3	7	1-6	2	8	1-3	2
Ti	4	1-2	2	5	0-2	1	9	0-1	1
W	0	0-0	0	1	1-1	1	0	0-0	0
# of particles	4			10			10		

Table 58 shows the compositional variation for rutile particles among samples. As shown, a few of the rutile particles detected in the froth contained a small quantity of sulphur. This may indicate the presence of residual organics bound to the particles, which is consistent with the TGA results. The amount of contamination of the "liberated" rutile particles is higher in the froth samples than in the tailings sample. Iron contamination of rutile particles in the tailings stream was 1.7% compared with 2.7% in the 2-45 µm froth and 3% in the >45 µm primary froth samples (Table 58) Similar variations were observed in the leucoxene particles (Table 59), where particles in the 2-45 µm froth contained only 28% iron on average compared with 31% iron in the tailings and 32% iron in the >45 µm froth. Calcium was present in small quantities in some of the rutile and leucoxene particles. It was difficult to determine exactly how many particles contained low amounts of calcium, as the detection limit for calcium in polished samples with the detector used is 0.3-0.5 wt%.

Table 58: Compositional variation in rutile particles among samples

	2-45 µm Froth Heavies			>45 µm Primary Froth Heavies			>45 µm Tailings Heavies		
Element	#	Range (At%)	Average (At %)	#	Range (At%)	Average (At %)	#	Range (At%)	Average (At %)
Al	18	1-6	2	26	0-6	2	14	1-4	2
Ca	0	0-0	0	5	0-1	1	2	0-1	1
Cr	0	0-0	0	1	0-0	0	0	0-0	0
Fe	26	1-7	2	41	1-10	3	19	0-5	2
K	1	1-1	1	1	1-1	1	2	0-0	0
Mg	1	1-1	1	2	0-1	1	0	0-0	0
Mn	0	0-0	0	3	0-1	1	1	0-0	0
Nb	1	3-3	3	4	0-3	1	0	0-0	0
P	6	2-3	2	4	1-3	2	3	1-2	1
S	1	1-1	1	2	0-3	2	0	0-0	0
Si	21	0-6	2	15	0-16	3	14	0-8	3
Ti	42	89-100	87	49	79-100	85	21	88-100	91
# of particles	42			49			21		

Table 59: Compositional variation in "leucoxene" particles among samples

	2-45 µm Froth Heavies			>45 µm Primary Froth Heavies			>45 µm Tailings Heavies		
Element	#	Range (At%)	Average (At %)	#	Range (At%)	Average (At %)	#	Range (At%)	Average (At %)
Al	2	1-2	1	17	0-2	1	5	1-4	2
Ca	0	0-0	0	8	0-1	0	1	0-0	0
Cl	1	3-3	3	0	0-0	0	0	0-0	0
Cr	0	0-0	0	1	0-0	0	0	0-0	0
Fe	8	11-34	26	29	10-42	29	11	23-37	30
Mg	0	0-0	0	7	0-4	2	0	0-0	0
Mn	5	1-2	1	27	0-4	1	11	0-3	1
Nb	0	0-0	0	1	1-1	1	1	1-1	1
P	0	0-0	0	4	0-1	1	2	1-1	1
Si	3	0-2	1	10	0-1	1	5	0-9	2
Ti	8	63-86	67	29	53-88	63	11	59-73	62
# of particles	8			29			11		

Table 60 illustrates the level of calcium, iron, silicon, and aluminum contamination in well liberated particles as determined by SEM-EDX. Iron is the most frequently occurring contaminant in all non-iron bearing minerals; however, the level of contamination is generally under 2%, with the exception of rutile where the average contamination is 2.5%. Aluminum and silicon are the next most common contaminants; again, like iron, they are generally present in quantities under 2%. However, for ilmenite, pyrite, and rutile, significantly more aluminum and silicon were detected. Calcium contamination was found in some particles, but nowhere near as frequently as the other elements. Calcium, when detected, was also generally present in much smaller quantities (<1 wt% for titanium bearing particles) than the other contaminants.

Table 60: Contamination by various elements in well liberated particles as determined by EDX

	% of Particles with contamination by element				**Average concentration of contaminating element (at %)**			
Element	**Ca**	**Fe**	**Si**	**Al**	**Ca**	**Fe**	**Si**	**Al**
Ilmenite	0	n/a	8	21			5.3	3.0
Leucoxene	15	n/a	33	46	0.5		1.5	1.4
Rutile	5	72	42	47	0.8	2.5	2.6	2.2
Pyrite	0	n/a	19	16			4.6	3.0
Siderite	n/a	n/a	68	45			2.2	1.3
Zircon	8	39	n/a	17	1.8	1.6		1.7
Quartz	3	33	n/a	49	1.2	1.2		1.6
K-Feldspar	0	50	n/a	n/a		0.7		
Plagioclase	n/a	67	n/a	n/a		0.8		

Table 61: Degree of liberation of potentially valuable minerals

	2-45 µm Froth Heavies	**>45 µm Primary Froth Heavies**	**>45 µm Tailings Heavies**	**% of liberated particles with no Fe, Si, Al or Ca contamination**
Ilmenite	100%	100%	100%	75%
Rutile	85%	77%	27%	17%
Leucoxene	100%	95%	85%	33%
Zircon	100%	95%	71%	47%
Pyrite	100%	100%	75%	56%
Siderite	67%	62%	33%	50%

SEM analysis was also used to roughly assess the degree of liberation of the valuable minerals. Table 61 shows the percentage of each valuable mineral, which was considered to be well liberated (as determined by number of particles of each type that were not associated with quartz or feldspar). As shown, rutile was much less liberated than the other valuable minerals, with 85% of rutile particles in the 2-45 µm froth heavies fraction being liberated, compared with 100% of the other valuable minerals. Furthermore, as shown in Table 61, only 17% of the supposedly liberated rutile particles detected were free of iron, aluminum, silicon or calcium contamination (i.e. none of these elements were detected in the EDX spectra <0.1wt%). This is significant, as it explains why the degree of contamination in the concentrate is so high despite the apparently excellent degree of liberation of the titanium bearing particles.

4.3.5 Analysis of heavy mineral fraction of froth solids by XRD and XRF

As shown in Table 62, the primary froth heavies contained approximately 33 wt% TiO_2 which is consistent with the SEM results where the expected TiO_2 concentration was predicted to be about 32% based on the number average of "rutile", "leucoxene" and "ilmenite" particles. The predicted ZrO_2 content from the SEM was also consistent with the ZrO_2 measured by the XRF (7 wt% vs. 8.5 wt%).

Table 62: XRF results from primary froth heavies

Compound	**Primary Froth Heavies >45 µm (wt%)**
SiO_2	22±2
Al_2O_3	14.7±0.9
Fe_2O_3	15.3±0.9
TiO_2	33±2
CaO	0.7±0
MgO	1.3±0
K_2O	0.2±0
ZrO_2	8.5±0
MnO	0.6±0
P_2O_5	0.7±0.3
Na_2O	0.5±0
SO_3	0.2±0.3
Cl	0.5±0
CuO	0.1±0
ZnO	0.2±0
Other (<0.1 wt%)	Cr_2O_3, Y_2O_3, GeO_2, Nb_2O_5, CeO_2, WO_3

Figure 35 shows an XRD trace of the heavy fraction of the primary froth along with the calculated pattern. The XRD analysis shows that the lattice parameter of siderite has shifted towards that of rhodocrosite. The XRD profile also shows that the siderite peak is quite broad but not entirely symmetrical. This indicates that the peak broadening is due to a range of composition rather than a small crystallite size. These results are consistent with the SEM results showing a large number of particles containing iron, manganese and calcium in a variety of compositions.

As shown by the XRD profile, all three main TiO_2 polymorphs are detected in the froth heavies, as is ilmenite. Neither pseudorutile nor pseudobrookite was detected. Similarly, none of the major iron oxides were detected. This is particularly interesting as these are the common alteration products of ilmenite and are generally mixed with rutile, anatase, or brookite in "leucoxene" particles. The lack of detection of these ilmenite alteration phases may indicate that these phases are extremely fine and so end up lost in the background of the other minerals.

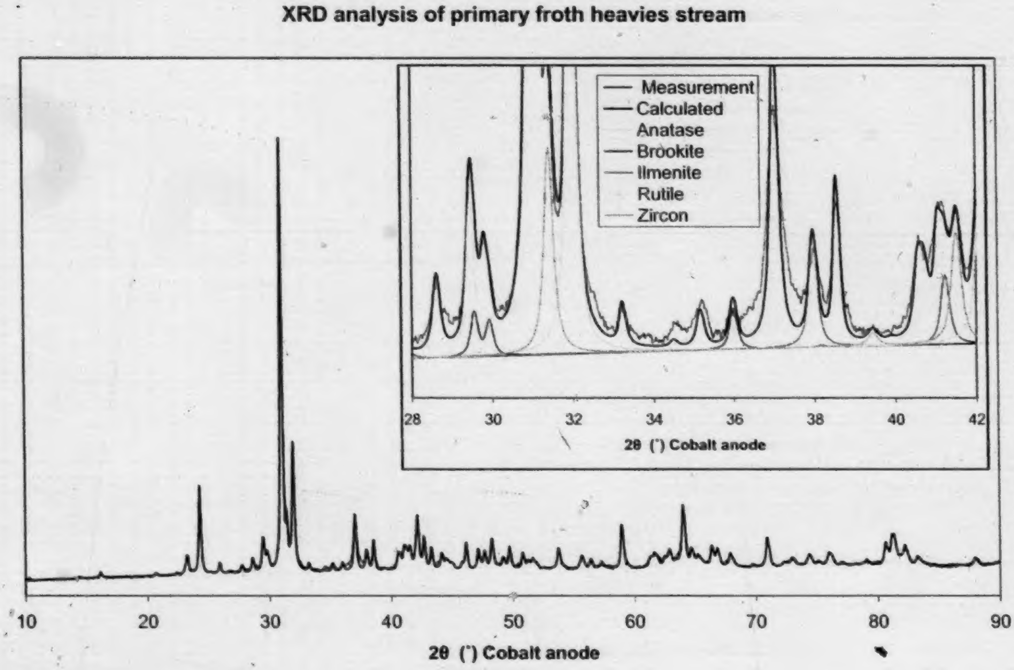

Figure 35: XRD traces of heavy fraction of primary froth.

Of further significance are the results of the quantification of the heavies fraction shown in Table 63. These results show that the total amount of titanium minerals detected is consistent with the XRF and SEM results (37% titanium bearing minerals overall corresponding to ~ 32 wt% TiO_2). The results are also consistent with the amount of ilmenite detected in the SEM (9% in SEM vs. 11% in XRD). If the "leucoxene" were explained as a mixture of ilmenite and TiO_2 polymorphs, we would expect to see more ilmenite and less TiO_2 polymorphs detected. This was not the case; however, as XRD appears to detect the leucoxene as simply one of the TiO_2 polymorphs. This discrepancy may account for the difficulty in obtaining the type of "pure" TiO_2 concentrate suggested by XRD analysis of the froth solids.

Table 63: Quantitative XRD results from primary froth heavies

Mineral	wt%
Rutile	16±4
Anatase	6±2
Brookite	4±4
Ilmenite	11±2
Zircon	9±2
Siderite	7±2
Pyrite	4±2
Feldspar	4±3
Schorl	25±5
Quartz	14±4

4.3.6 Micro-XRD analysis of "leucoxene" particle

The results of this analysis were of poor quality, but three peaks were revealed (Figure 36). These XRD peaks were at 0.325 nm, 0.247 nm, and 0.207 nm. The peaks correspond fairly closely with rutile <110>, <101>, and <210> respectively (0.325 nm, 0.249 nm and 0.205 nm). Furthermore, the <110> and <101> reflections are the most intense of the rutile reflections; thus they are the reflections most easily detected. The peaks did not match any of the most intense peaks for the other TiO_2 polymorphs or ilmenite or any other expected titanium mineral or iron oxide (e.g., pseudobrookite, pseudorutile, magnetite, hematite, or goethite).

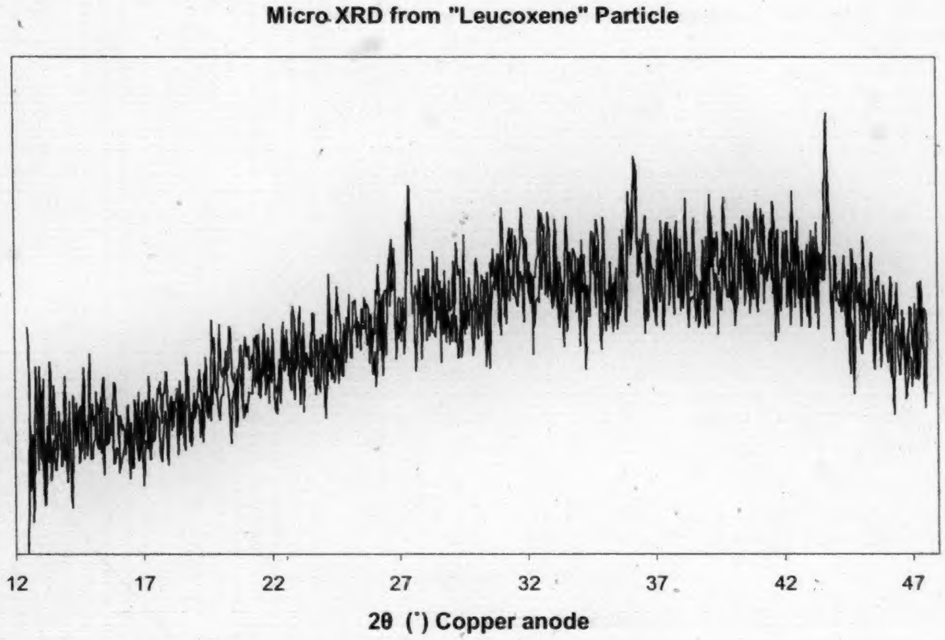

Figure 36: Micro-XRD pattern from "leucoxene" particle.

4.3.7 TEM analysis of "leucoxene" particle

To attempt to explain the discrepancy between the XRD and SEM results, FIB sections from the particle analyzed by micro-XRD were examined in TEM and STEM mode.

Initial analysis of the first FIB section was performed with a JEOL 2010 operated at 200 kV in TEM mode. This analysis was used to look for phase consistency across the sample by traversing the sample first in image mode and then in diffraction mode. Periodic EDX measurements were taken across the sample to check whether the iron content was consistent. As shown in Figure 37, the iron content was found to vary substantially across the sample.

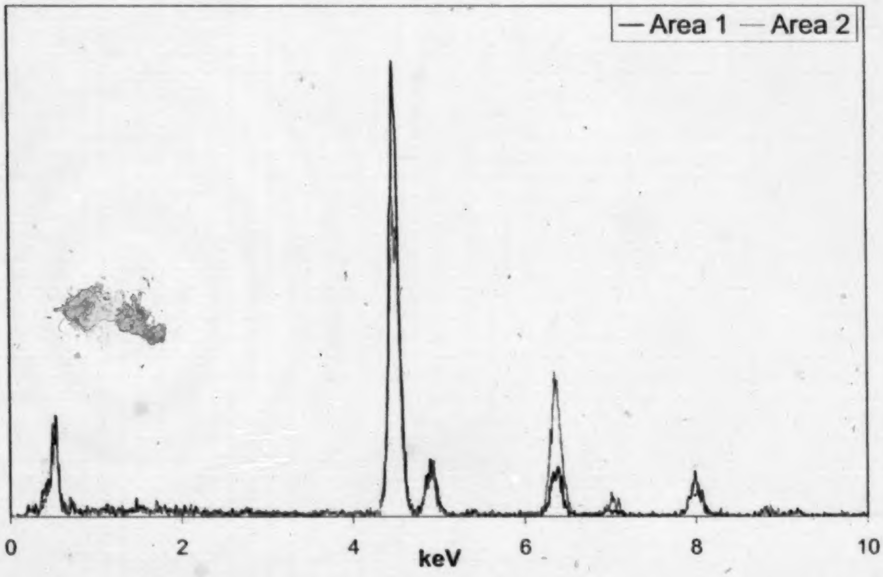

Figure 37: EDX spectra from taken from two regions in FIB Section 1. These regions correspond to Areas 1 and 2 labelled in Figure 39 (JEOL 2010).

Interestingly, despite the variation of iron content in the different regions, a single diffraction pattern appeared to be consistent throughout the entire sample (although the clarity of the pattern did vary somewhat over the sample). An example of this pattern is shown in Figure 38 (taken from the circled area in Figure 39). As shown, the pattern is actually comprised of three distinct patterns - two hematite patterns (patterns B and C) that are mirror images of one another and a rutile pattern (pattern A). The hematite patterns match zones [100] and [$\bar{1}$00] while the rutile pattern matches zone [010]. It should be noted that although the (003) reflection in hematite and the (100) reflection in rutile are allowed they are very faint (as shown in the simulated patterns) and so do not show up in these diffraction patterns. The absence of the (003) reflection in the hematite pattern confirms that the pattern is hematite and not ilmenite, which has a very similar structure but the (003) reflection is quite intense in ilmenite. The 180° misorientation between patterns B and C, and the existence of a common plane along the (006) spots, suggests that the two patterns are from a twinned hematite particle. This is consistent with the finding of Watari et al. of a twin axis along (006) reflections in hematite (1979) when it forms by dehydration from goethite. The same twin reflections were found in hematite platelets in metamorphic rutile by Banfield and Veblen (1991). Furthermore, they found these platelets parallel to the (100) and (010) planes of rutile. The hematite in FIB Section 1 appears to follow the same orientation relationship with rutile as shown by the overlapping rutile (200) and hematite (006) reflections in Figure 38.

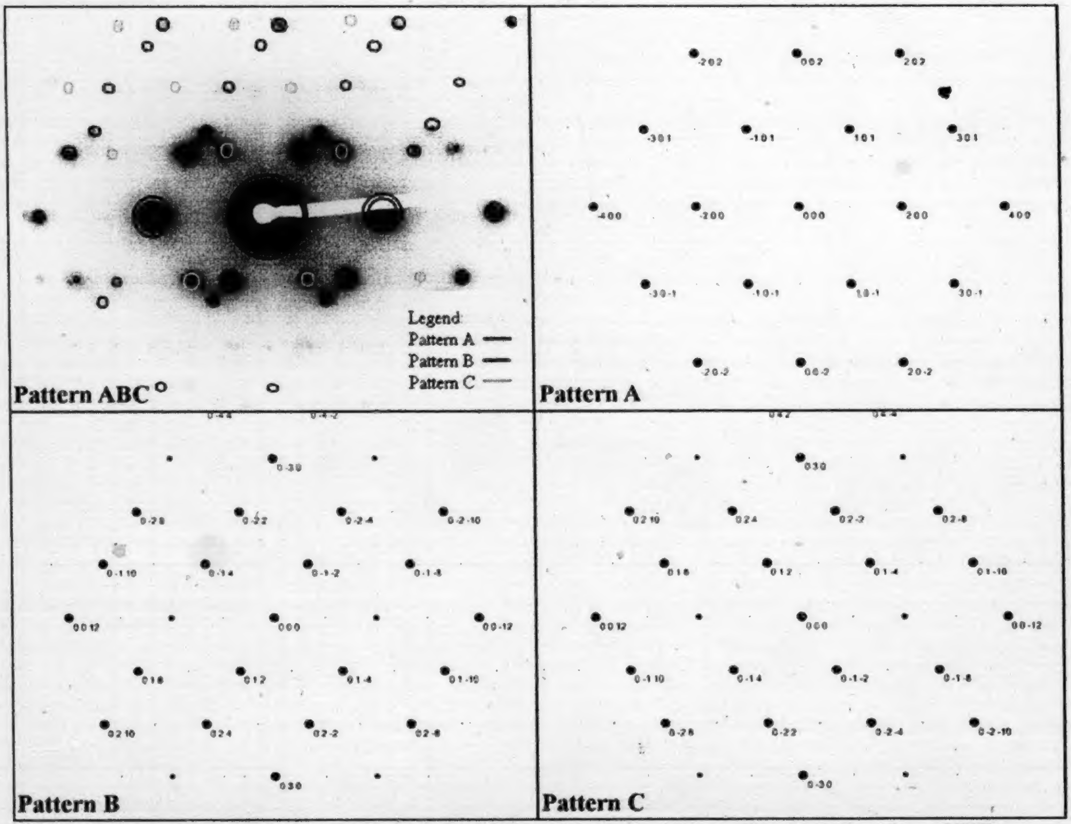
Legend
Pattern A
Pattern B
Pattern C
Pattern ABC
Pattern A
-202
002
202
-301
-101
101
301
-400
-200
000
200
400
-30-1
-10-1
10-1
30-1
-20-2
00-2
20-2
Pattern B
0-30
0-28
0-22
0-2-4
0-2-10
0-1 10
0-14
0-1-2
0-1-8
0012
000
00-12
018
012
01-4
01-10
0210
024
02-2
02-8
030
Pattern C
030
0210
024
02-2
02-8
018
012
01-4
01-10
0012
000
00-12
0-1 10
0-14
0-1-2
0-1-8
0-28
0-22
0-2-4
0-2-10
0-30

Figure 38: Pattern ABC is the typical matrix diffraction pattern from the circled region of FIB Section 1 shown in Figure 39, and is comprised of three overlapped patterns A, B and C. Pattern A is rutile $[0\bar{1}0]$, Pattern B is hematite $[100]$, and Pattern C is hematite $[\bar{1}00]$ (JEOL 2200 FS).

After this initial analysis, this first FIB section was examined with the FEI Tecnai F20 TEM operated at 200kV in STEM and TEM mode. The high angle annular dark field (HAADF) detector in STEM mode was used to help identify changes in composition across the sample, since STEM imaging provides a form of atomic number contrast.

Three distinct regions were observed in STEM mode, as shown in Figure 39.

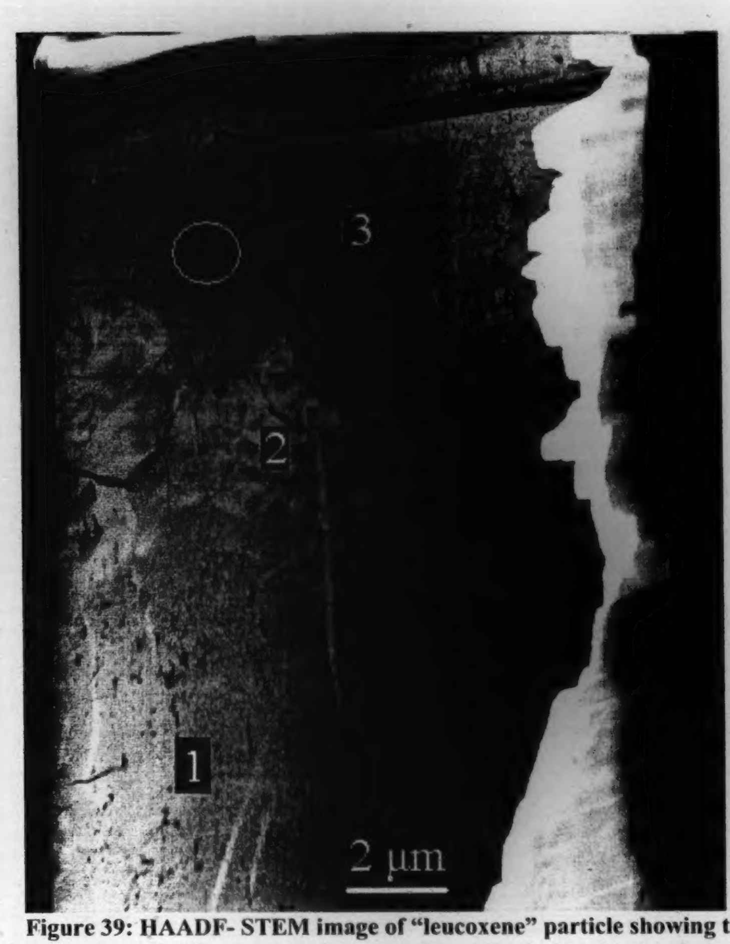

Figure 39: HAADF- STEM image of "leucoxene" particle showing three distinct regions. The dark spots shown in the micrograph are pores while the bright streaks are areas that were found to be rich in iron (FEI Tecnai F20).

Area 3 appeared to be quite porous but with a fairly uniform compositional contrast observed across the region at low magnification. Area 2 appeared to be much less porous but with white streaks visible throughout the region; small cracks were also visible running through this region. Area 1 contained porosity, white streaks, and cracks. Examination of the EDX data previously obtained in the JEOL 2010 revealed that Area 2 was enriched with iron, relative to Area 1, as shown in Figure 37.

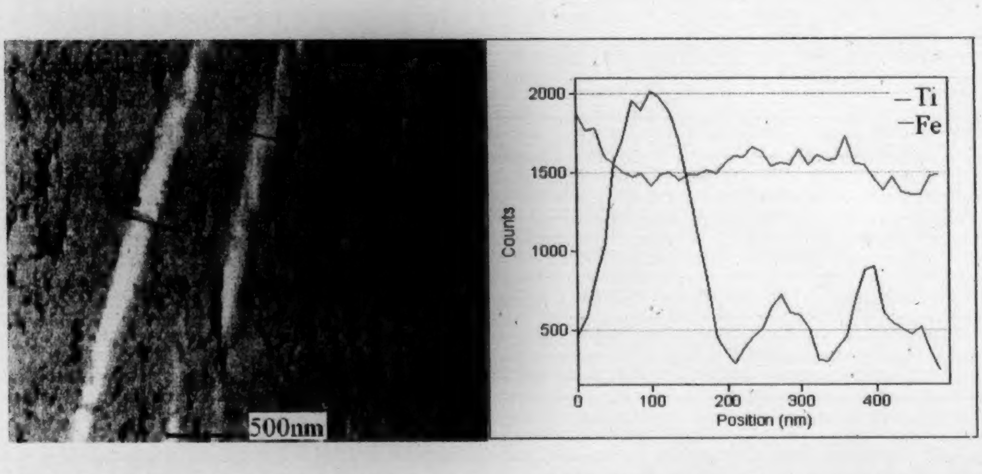

Figure 40: Close up HAADF STEM image of Area 1 from Figure 39 and an X-ray line scan of the streaked region (FEI Tecnai F20).

Investigation of the two largest streaks in Area 1 revealed that the streaks were enriched with iron as shown in Figure 40. A higher magnification TEM image of the area showed strong amplitude contrast at the streak, as well as in some patches slightly removed from the streak (Figure 41). Networks of tiny dark spots were also observed in this image, indicating the presence of small pores which appeared to coalesce into the larger pores visible in Figure 39.

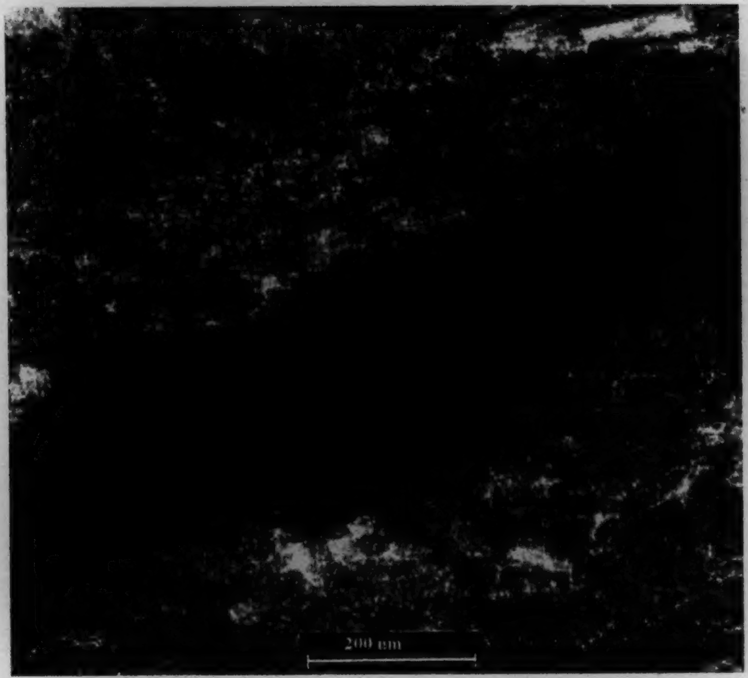

Figure 41: TEM bright field image of streaked region shown in Figure 40, the dark regions indicate areas of strong amplitude contrast due to either increase mass/thickness or due to a strongly diffracting region. The bright regions are areas where the electrons passed through the sample with very little energy loss – characteristic of small pores in the sample (FEI Tecnai F20).

After this initial analysis a more detailed look at the region containing more iron was performed. Figure 42 shows the boundary of Area 2 and Area 3 in Section 1, confirming that Area 3 is more porous than Area 2. Area 2 in this image has an almost rippled appearance and appeared quite dense although small cracks were apparent.

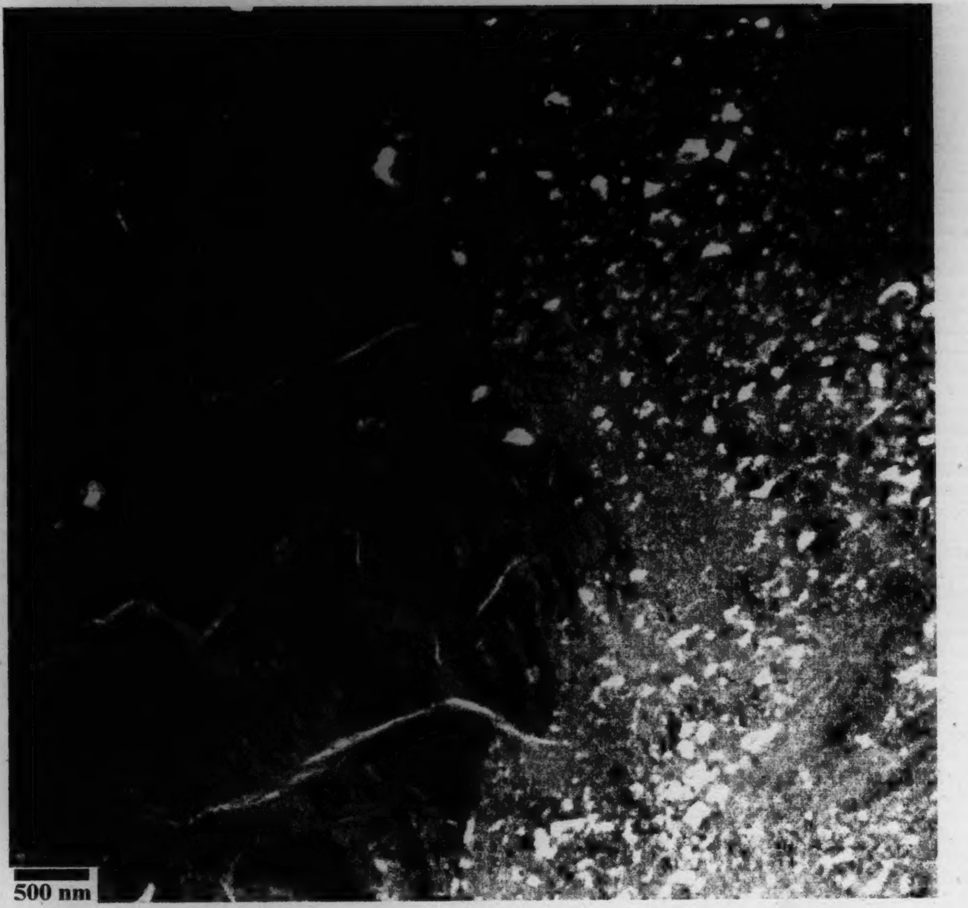

Figure 42: TEM bright field image showing border of Section 1 Area 2 (left) and Section 1 Area 3 (right) (JEOL 2010).

A higher magnification image in Figure 43 shows what appears to be two different areas. EDX analysis of these regions revealed that Area B contained more iron than Area A (Figure 44). No difference was found between the two areas in diffraction mode. The diffraction pattern from these two regions (Figure 45) was consistent with pseudobrookite of zone type <141>. Pseudobrookite is known to accommodate a fairly large variation in iron content (Bowles, 1988), so the variation of iron content observed is possible with this structure.

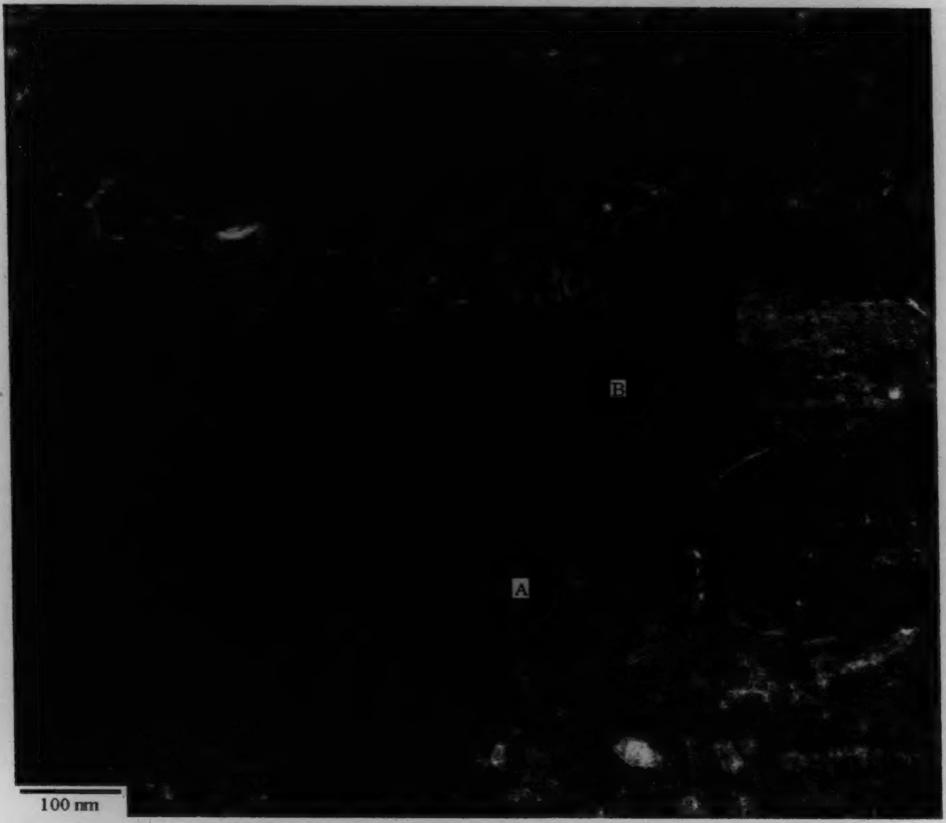

Figure 43: TEM bright field image of Section 1 Area 2 from Figure 39 showing two apparently different regions in the matrix, labelled A and B (JEOL 2010).

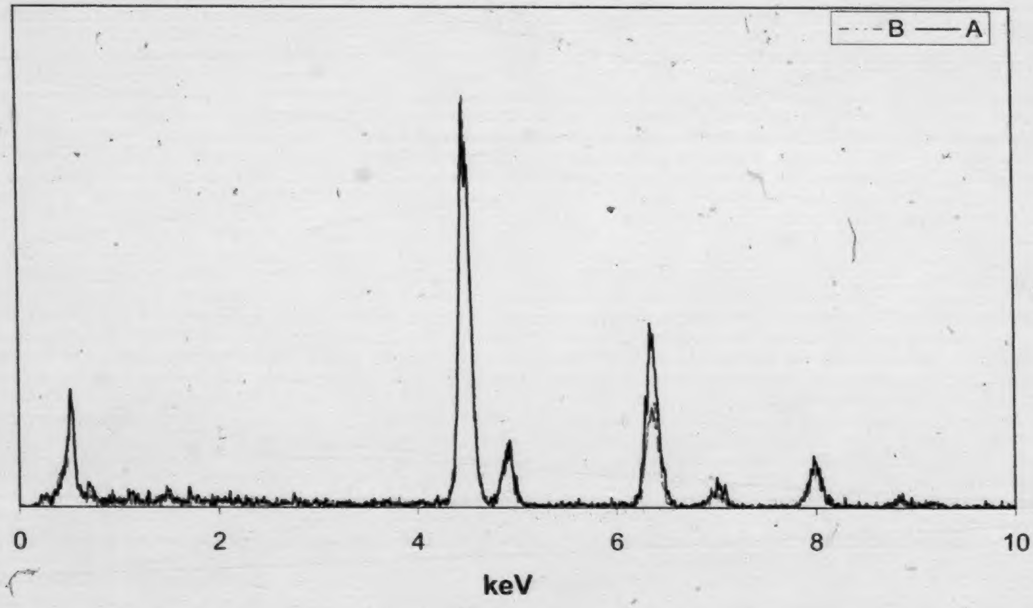

Figure 44: EDX spectra showing differences in composition between points A and B in Figure 43.

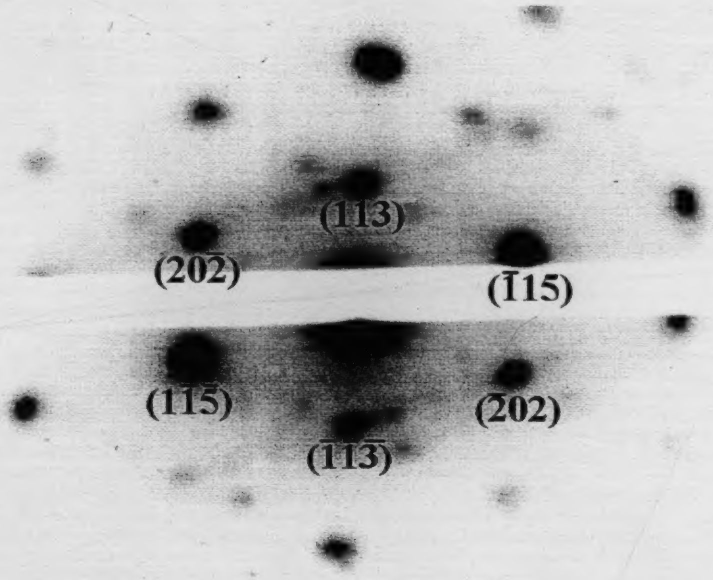

(113)
$(20\bar{2})$
$(\bar{1}15)$
$(11\bar{5})$
$(\bar{2}02)$
$(\bar{1}\bar{1}\bar{3})$

Figure 45: Diffraction pattern from region A in Figure 43, which is consistent with pseudobrookite zone type <141>.

Due to degradation of the first section making further analysis impossible, a second FIB section was obtained. This sample was obtained at right angles to the first sample and across the bottom of the "leucoxene" particle (Figure 24). Analysis of this second FIB section with the FEI Tecnai F20 and with the JEOL 2200 FS also revealed a heterogeneous mixture of regions. Section 2-Area 1 in Figure 46 was found to contain no iron, only titanium and oxygen (Figure 47). Diffraction patterns taken from three different zone axes within the region were found to be consistent with both brookite and anatase (Figure 48a-c). Anatase has been commonly found in surveys of oil sands minerals, whereas brookite has not (Kramers & Brown, 1975). Furthermore, anatase has been found as an alteration product of ilmenite in studies by Karkhanavala et al.(1959), so this region is likely anatase.

Surrounding the pure titanium oxide region (Section 2-Area 1) were smaller streaked areas containing a significant amount of iron (Section 2-Area 2). These streaks were very similar in appearance to the streaks observed in Section 1-Area 2. An electron diffraction pattern from this region reveals an overlap of pseudobrookite and Pattern C from Section 2-Area 1 (Figure 48d). As shown in Figure 48d, the anatase {013} reflections overlap with the {240} reflections of pseudobrookite indicating that the two sets of planes are parallel to each other. Gliszczynski (1944) noted the formation of oriented inclusions of anatase in pseudobrookite but no further details were given. The existence of this orientation relationship further indicates that the pure TiO_2 region was anatase.

When the sample was tilted off the anatase zone axes a faint ring pattern consistent with TiO was observed from the pure titanium oxide region. Dark field images taken from an area of the ring that did not overlap any other spots revealed the presence of small TiO inclusions within the anatase grain (Figure 49). TiO is a structure that can easily accommodate a wide range of defects, so it may have played a role in accommodating excess iron in the last stages of alteration of ilmenite to anatase.

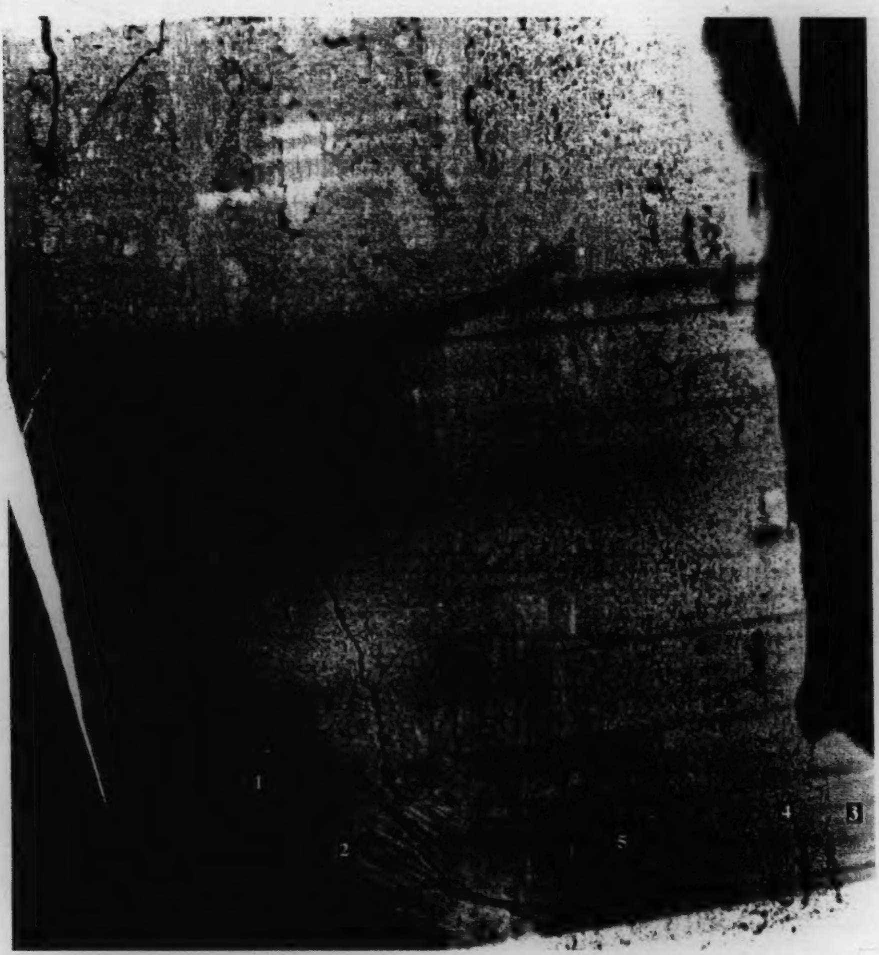

Figure 46: HAADF STEM image of FIB Section 2 from the "leucoxene" particle showing an inhomogeneous mixture of regions (FEI Technai F20).

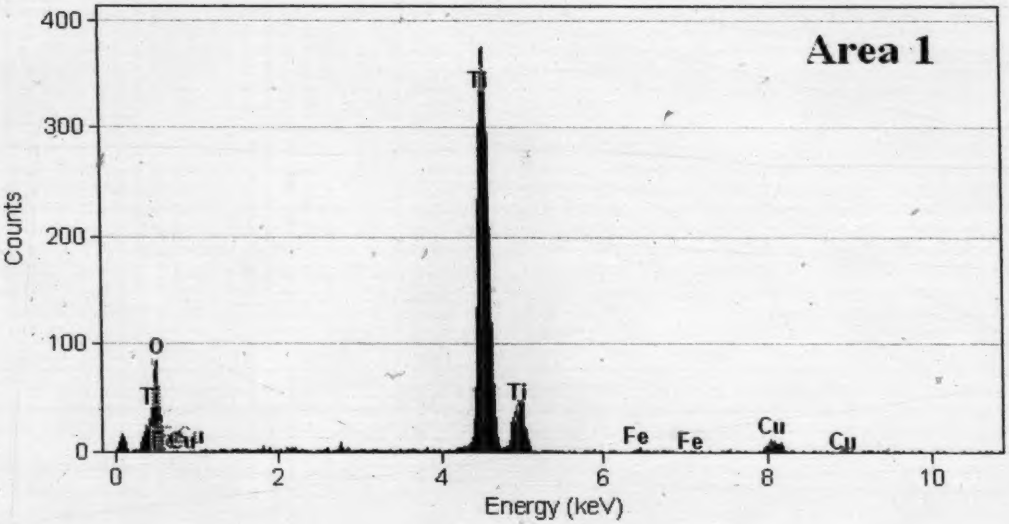

Figure 47: EDX spectra of Area 1 from FIB Section 2 (FEI Tecnai F20).

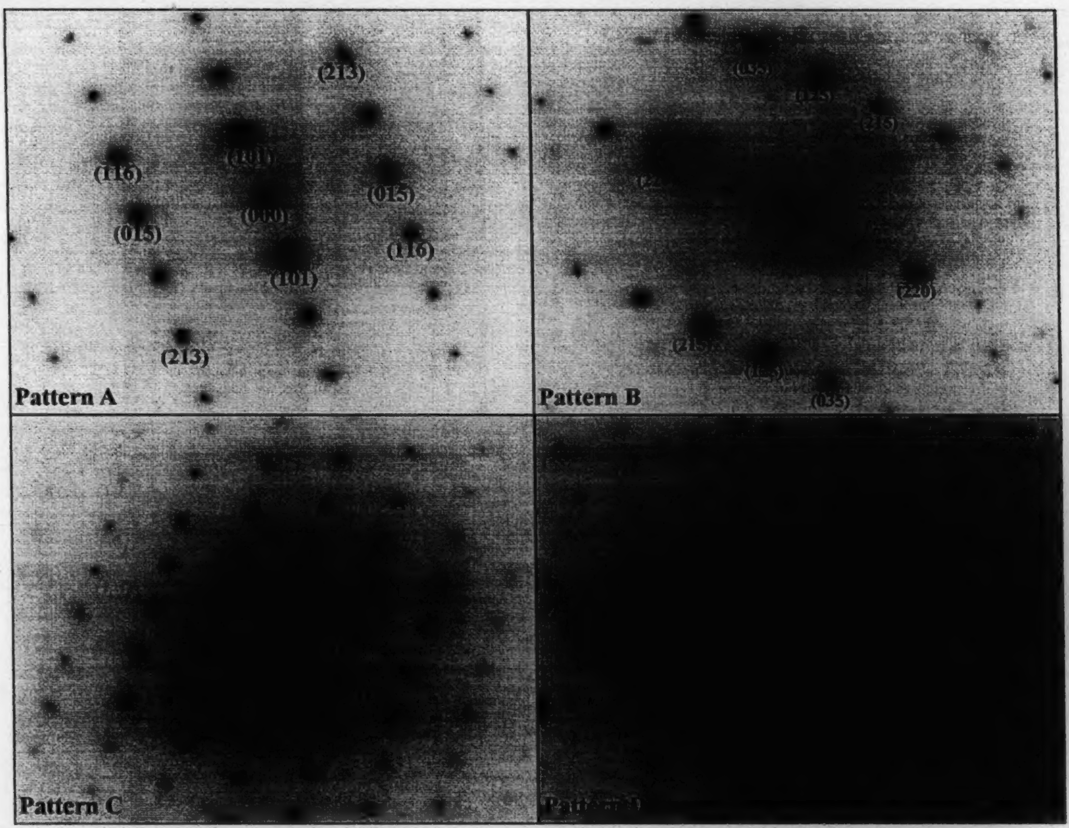
(213)
(101)
(116)
(015)
(015)
(116)
(101)
(213)
Pattern A
(215)
(220)
(215)
(035)
Pattern B
Pattern C

Figure 48: Diffraction patterns A, B, and C, were obtained from Area 1 in Figure 46 and correspond with either brookite or anatase (indexed as anatase). Pattern A is consistent with anatase zone type <553> or brookite zone type <103>. Pattern B is consistent with anatase zone type <151> or brookite zone type <156>. Pattern C is consistent with either anatase zone type <131> or brookite zone type <312>. Pattern D is from Area 2 in Figure 46 and shows an overlap with pattern C (blue dots) and pseudobrookite zone type <212> shown with red labels (FEI Tecnai F20).

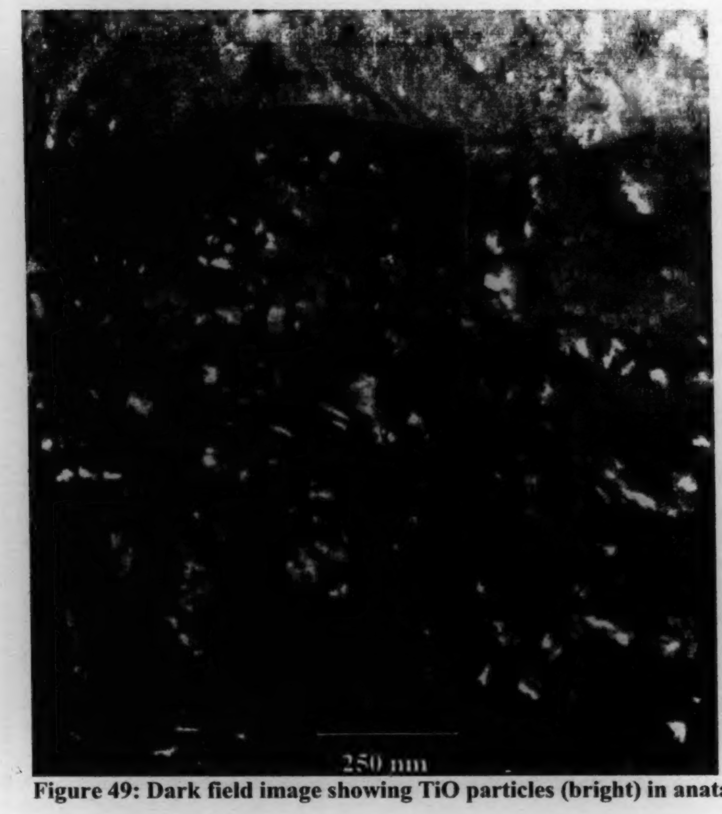

Figure 49: Dark field image showing TiO particles (bright) in anatase matrix (FEI Tecnai F20).

A second pure titanium oxide region was found on the edge of the sample (Section 2-Area 3 in Figure 46). Diffraction patterns from this area were consistent with rutile <103> and brookite <010> (Figure 50). Since rutile is the most common polymorph of TiO_2, this area is likely rutile and not brookite. Immediately next to the thin region of pure titanium oxide, the sample was porous and contained some iron, as shown in Figure 51. The morphology of this region is very similar to that of Section 1-Area 3.

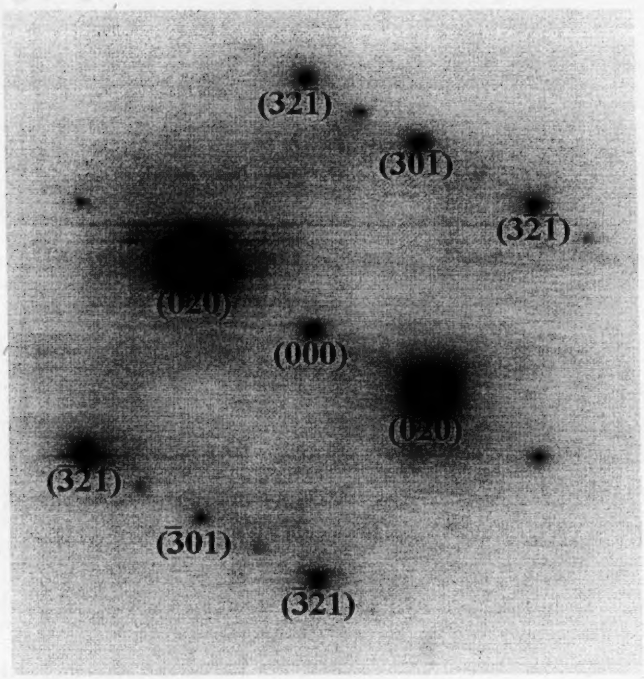
(321)
$(30\bar{1})$
$(32\bar{1})$
(020)
(000)
(020)
(321)
$(\bar{3}01)$
$(\bar{3}21)$

Figure 50: Diffraction pattern from FIB Section 2 Area 3, matching rutile [103] (JEOL 2010).

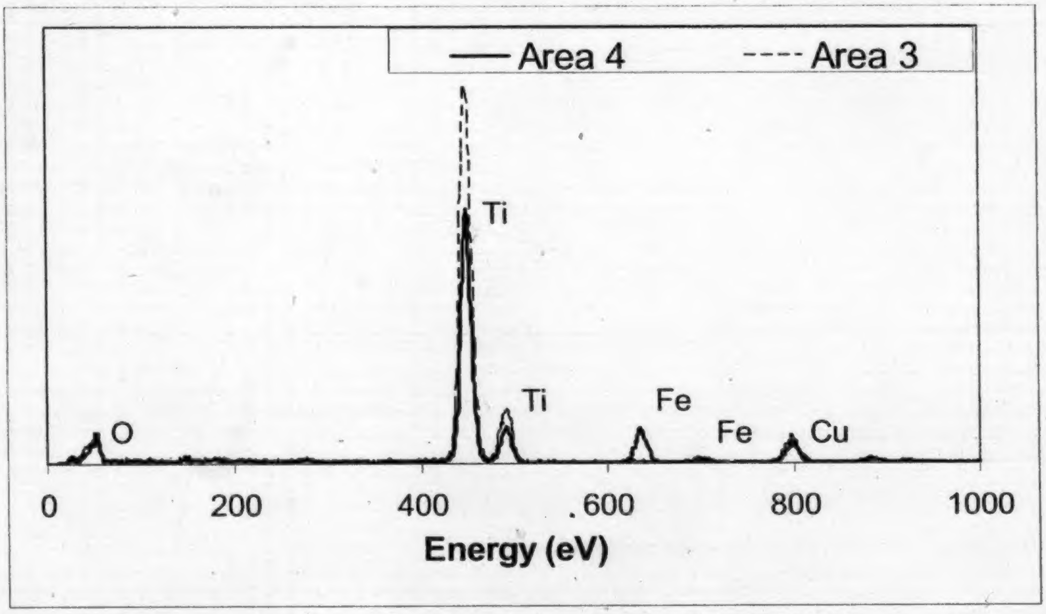

Figure 51: EDX spectra from Areas 3 and 4 as labelled on Figure 46 (JEOL 2010).

The diffraction pattern from this area is consistent with both rutile zone type <010> and pseudobrookite zone type <521> (Figure 52 – Pattern A), although it is more likely a rutile pattern since the area contains less iron than is typical for pseudobrookite and the pattern was also found in another region near the edge containing no iron. Extra spots were noted in this pattern (circled orange in Figure 52 – Pattern C) which may be due to the higher order Laue zone (HOLZ) spots from the rutile pattern, although this seems unlikely as the spots are not shifted in the manner predicted by HOLZ simulations. The sample was tilted with the aim of obtaining a second zone axis from the area. Interestingly as the sample was tilted (3° in X and 5° in Y), the main pattern remained but a complex pattern of extra spots emerged (Figure 52 – Pattern B). These spots were consistent with the same hematite [100] (green circles in pattern C, simulated as Pattern E)/ $[\bar{1}00]$ (red circles in pattern C, simulated as pattern F) twin pattern observed in FIB Section 1.

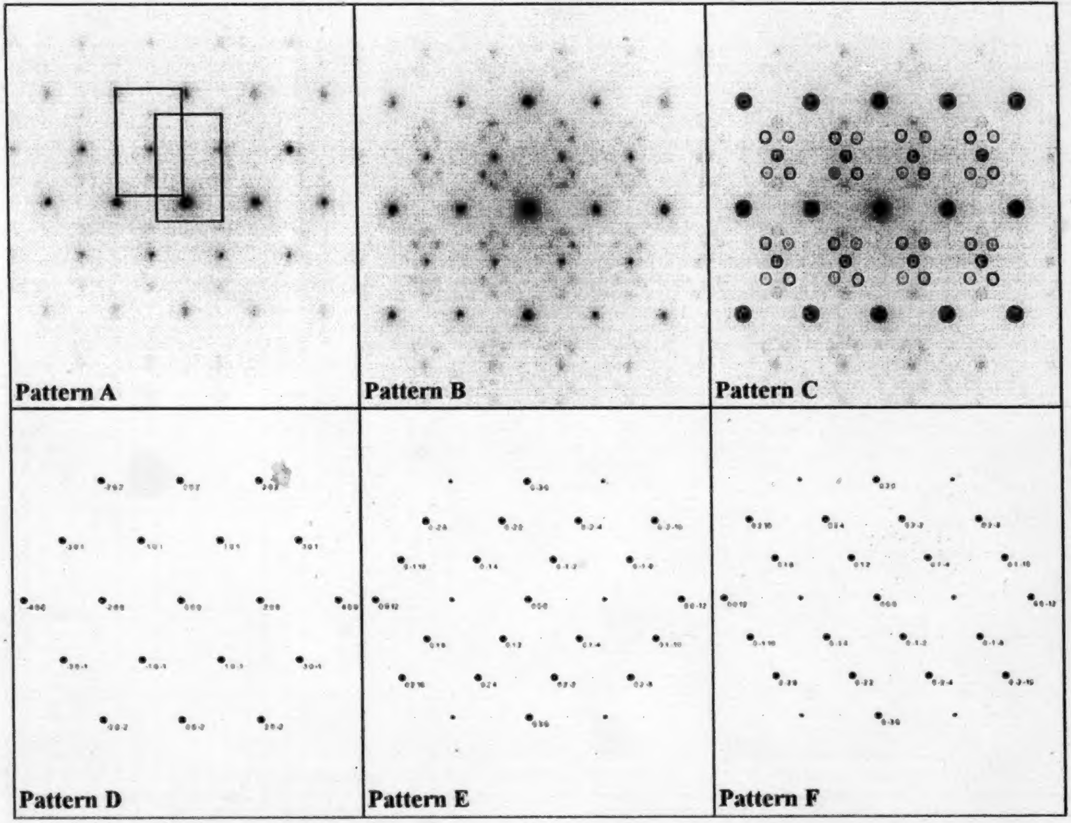

Figure 52: Diffraction patterns from FIB Section 2-Area 4 . Pattern A is from at zero tilt, showing a pattern consistent with rutile [0$\bar{1}$0], the boxes show how extra spots could be derived from a shift of the most intense spots of the main pattern. Pattern B shows the same area after tilting. Pattern C shows how the Pattern B is comprised of four overlayed patterns. Patterns D-F show the simulated diffraction patterns for rutile [0$\bar{1}$0] (D), hematite [100] (E) and hematite [$\bar{1}$00] (F) using Single Crystal™.

It is interesting to note that the porous regions are rutile and hematite, while the denser streaked regions are pseudobrookite. Pseudobrookite has been found along with rutile and hematite in altered ilmenite by Karkhanavala et al. (1959). It is possible that the microstructure shown here is common to such a reaction, but no description of the morphology or reaction pathway was given in this study. However, the porous structure of rutile with hematite platelets is consistent with the final stage of ilmenite alteration via pseudorutile as proposed by Grey & Reid (1975). This alteration sequence involves the electrochemical conversion of Fe^{2+} to Fe^{3+}, along with the diffusion of a third of the iron ions out of the ilmenite structure to form pseudorutile. The pseudorutile is then transformed to rutile + hematite by dissolution of the pseudorutile and reprecipitation of rutile + hematite. The hematite is leached out over time to leave pure rutile behind. The formation of pseudorutile produces a microstructure characterized by pores and microcracks (similar to those found in Fib Section 1, Areas 1 and 3 in Figure 39), due to the 6% volume reduction when ilmenite transforms to pseudorutile (Grey & Reid, 1975). No volume change in the formation of pseudobrookite from either ilmenite or pseudorutile has been commented on, but an examination of the unit cell volumes and densities for ilmenite, pseudorutile, and pseudobrookite would suggest that a volume increase would be expected for the formation of pseudobrookite from either pseudorutile or ilmenite. Such a volume increase may explain the rippled appearance of the pseudobrookite found in Section 1-Area 2 (Figure 42).

The question remains as to why there be some areas exhibiting the characteristic appearance of a pseudorutile alteration sequence along with pseudobrookite. One possible explanation is the presence of carbon in the form of a bitumen coating on the leucoxene particles. It is known that the basic mineralogy of the Athabasca deposit formed prior to the migration of the oil into the deposit (FTFC, 1995). Consequently, it is quite likely that the alteration of the ilmenite began prior to the migration of the oil into the deposit – especially since the formation of pseudorutile is associated with an aqueous environment. Once the oil was present in the deposit, it is natural to assume that this would have an effect on the alteration sequence. No studies of the alteration of ilmenite in the presence of bitumen exist; however, a fair amount of research has been done on the reduction of ilmenite with carbon. These studies may offer insight into the effect bitumen may have on ilmenite weathering. In particular, the study by Gupta et al. (1989) has shown that unaltered ilmenite produces rutile, unaltered ilmenite, and metallic iron when reduced with carbon at 1000°C, while altered ilmenite (containing some pseudorutile) produces pseudobrookite along with rutile and metallic iron. Gupta's study while obviously done under conditions very different from those in a geological environment, still indicates that the reduction of altered ilmenite proceeds differently from the reduction of pure ilmenite in the presence of carbon.

4.4 Conclusions

This study reveals several interesting characteristics of the coarse minerals present in both the tailings and froth streams.

4.4.1 Characteristic differences between heavy minerals in froth and tailings

Three clear differences between the heavy minerals contained in the froth and tailings streams were noted. Firstly, the heavy minerals ending up in the tailings stream are more likely to be poorly liberated than heavy minerals in the froth stream. Only 27% of TiO_2 particles in the tailings were considered liberated compared to 77% in the equivalent froth stream. Secondly, the iron present in the tailings fraction is more likely to be found in siderite, micas, or poorly liberated minerals, rather than in iron-bearing minerals such as ilmenite, leucoxene, or pyrite. Thirdly, the amount of iron contamination in liberated

TiO_2 particles in the tailings was lower (1.7%) than the amount of iron contamination in liberated TiO_2 particles in the froth (2.7% and 3%).

4.4.2 Degree of liberation of the valuable minerals

Past studies of the degree of liberation of the valuable minerals in the oil sands tailings have generally found both titanium bearing mineral and zircon particles to be well liberated. The MDA study (Alberta Chamber of Resources, 1996), for instance, found that the effective liberation in the Syncrude feed was 82% for rutile and 95% for zircon.

This study would seem to indicate that the above liberation values are fairly consistent. However, the degree of liberation determined optically does not give an accurate picture of the purity of the various minerals. For instance, even though 85% of the TiO_2 particles in the <45 μm froth were considered liberated, only 17% of the total liberated TiO_2 particles were free from contamination. This indicates that an optical degree of liberation is not a good predictor of concentrate purity. Of the titanium bearing minerals, ilmenite was the most liberated and the most pure with 75% of the ilmenite particles being well liberated and free of aluminum, silicon, and calcium contamination. TiO_2 is the least liberated and most contaminated, with only 7% of all TiO_2 particles both liberated and free of contamination.

As in the MDA study (Alberta Chamber of Resources, 1996), the zircon was found to be well liberated with 92% of zircon particles being liberated; however, only 44% of the zircon particles had no contamination. Even so, Fe is the only significant type of the contamination and 61% of the zircon particles were free of iron. Iron is problematic, as the presence of iron can cause discolouration of the concentrate, making it unsuitable for use in high end glazes and reducing its value.

4.4.3 Association of Fe with valuable minerals

Using SEM-EDX analysis, iron has been found associated with every mineral type present in the oil sands, with the exception of monazite. Additionally, it is the most frequently occurring type of contamination, with at least a third of all non-iron bearing particles containing some iron. This is particularly problematic for the TiO_2 particles.

Rutile is a far more valuable mineral than either ilmenite or leucoxene (Alberta Chamber of Resources, 1996); therefore, it is desirable to concentrate rutile on its own. To date, the rutile concentrates produced from oil sands tailings have contained far more silicon, aluminum, and iron than desired (Alberta Chamber of Resources, 1996). Understanding the reasons for the levels of these contaminants as well as the chemical form of the contaminants may help to improve the economics of the concentrates produced from the oil sands.

As shown in this study, the amount of TiO_2 detected by XRD was significantly higher than the percentage of particles corresponding to a rutile chemistry detected in the SEM. The TiO_2 polymorphs detected by XRD seemed to include all the non-ilmenite titanium bearing minerals detected in the SEM, including “leucoxene”. TEM analysis of these particles showed that the interior of the “leucoxene” particle examined appeared to be a very fine mixture of rutile and hematite, with rutile appearing as the dominant structure. Based on these results, it is not surprising that attempts to concentrate rutile have met with limited success, as the primarily rutile composition of the "leucoxene" particles decreases the particles' magnetic susceptibility. Therefore, depending the degree of magnetization used, these particles will report to the non-magnetic stream, along with the purer rutile particles. Furthermore, ultrafine hematite detected by TEM was not detected by XRD, so the amount was underestimated using quantitative techniques. The presence of multiple iron-containing minerals make determining the amount of "leucoxene" present (using XRF/XRD techniques) very difficult. Consequently, microprobe methods are likely the most accurate way of estimating the amount of leucoxene in a given sample of froth solids.

4.4.4 Association of silicon and aluminum with valuable minerals

Silicon and aluminum are the next most common contaminants, which like iron are found associated with every mineral type present in the oil sands with the exception of monazite. While there are slightly fewer particles contaminated with silicon and/or aluminum than iron, those that are contaminated are generally contaminated to a greater degree than the ones containing iron. Once again, the ubiquitous nature of the contamination suggests that the contamination is due to the presence of extremely fine clay particles that are associated with the larger particles. Again, this association is not discernible with the current methods of SEM analysis, but is quite plausible due to the extremely fine nature of clay minerals found in the oil sands.

4.4.5 Association of calcium with valuable minerals

The presence of greater than 0.1 wt% calcium in a titanium concentrate is cause for rejection of the concentrate (Oxenford, 2007). Consequently the deportment of calcium is a very serious question. The difficulty in assessing this question is that the detection limit for calcium with EDX in the SEM is between 0.3 and 0.5 wt%. In other words, calcium can only be detected in the SEM if it is already well beyond the acceptable limit for a concentrate. A further difficulty with this assessment is that the majority of other techniques that can detect calcium at the levels necessary are bulk techniques and, therefore, cannot be easily applied to individual particles.

From SEM analysis, it is clear that calcium is occasionally present in association with titanium bearing minerals in a concentration less than 1 wt%. The amount of calcium does not increase significantly with the degree of intergrowth or the presence of other minerals. Thus, there is no clear indication as to whether the calcium present is (or is not) due to an entirely bulk physical association.

The only minerals present in this oil sand sample that contain significant quantities of calcium are siderite and the rare earth containing particles (monazite). As well, calcium may be incorporated in smaller quantities in the feldspar and clay minerals. Thus, it is critical to control the amount of siderite that ends up reporting to the titanium concentrate, since monazite is only detected from EDX analysis of particles in the SEM and is present in very small quantities.

5 Conclusions and Future Work

5.1 Conclusions

While several mineralogical studies of oil sands ores, froths, and tailings have been conducted in the past, this is the first study to track the distribution of minerals throughout the entire warm water extraction process. As well, it is the first study to examine the distribution of minerals by size fraction. As such, there are several interesting conclusions about the distribution of minerals that fall into two areas of application: secondary resource potential and process management.

5.1.1 Secondary resource potential

As noted by other studies (Alberta Chamber of Resources, 1996), (Owen and Tipman, 1999), (Ityokumbol et al., 1987), (Majid and Sparks, 1999), titanium, zirconium, and iron were all concentrated in the froth. From the ore to the primary froth, zirconium showed fourfold enrichment, iron showed almost fivefold enrichment, and titanium showed tenfold enrichment. This indicates that 33% of the total zirconium, 29% of the total iron, and 53% of the total titanium were detected in the primary froth.

The zirconium in the froth was found exclusively as zircon and was quite well liberated, with 92% of its particles in the primary froth classified as either completely free or slightly variegated. Over 44% of the zircon particles were free from contamination of any kind. Furthermore, over 71% of the particles were free from iron — the major contaminant found to be associated with zircon. Hafnium, which is the other major contaminant of concern, was only found in 4% of the particles. No great differences were noted between the zircon found in the primary froth and the zircon found in the tailings. These results indicate that zircon should be relatively easy to concentrate from the froth solids and that producing a saleable concentrate should be relatively straightforward. Furthermore, the similarities between the zircon found in the froth and the zircon found in the tailings indicate that major difficulties arise in concentrating the zircon to the froth, as floating the large, relatively hydrophilic particles can prove problematic.

Titanium was found in various minerals, including anatase, brookite, rutile, ilmenite, and pseudobrookite. Anatase, brookite, rutile, and ilmenite were detected by XRD, while pseudobrookite was detected by TEM. The ilmenite in the froth solids was relatively well-liberated, with 71% of the ilmenite particles classified as liberated. However, the majority of these particles contained some form of contamination: 92% of the particles contained manganese, 25% of the particles contained aluminum, and 25% of the particles contained magnesium. The TiO_2 polymorphs were poorly liberated. Of the particles that were identified as TiO_2 in the SEM, only 7% of the particles were liberated and free of contamination. This percentage decreases when one considers the particles identified as "leucoxene" in the SEM, since TEM analysis shows that they are primarily TiO_2 polymorphs mixed with hematite. Consequently, the amount of recoverable pure TiO_2 in the oil sands is quite small, which explains the difficulty researchers have had in achieving a high grade TiO_2 concentrate free of silicon and iron contamination (Coward & Oxenford, 1997).

This study also highlighted the difficulty in using XRD to assess the value of the froth solids, as the pseudobrookite and hematite associated with the "leucoxene" particles were not detected in the XRD analysis. Consequently, the amount of pure TiO_2 indicated by XRD was significantly higher than the amount of recoverable, pure TiO_2.

Unlike the zircon particles that showed great similarities between the froth and tailings particles, there were substantial differences in the morphology noted between the froth and tailing titanium minerals. The titanium minerals from the tailings stream were more likely to be intergrown with quartz particles than those from the froth stream. This indicates that the majority of the liberated titanium was already recovered to the froth, and that the limiting factors on titanium recovery were the degrees of intergrowth and contamination. Furthermore, the titanium size distribution, which reveals that 74% of the titanium is located in the <45 μm stream, indicates that fine grinding or other techniques designed to improve the liberation of particles most likely will prove ineffective. Rather, the fine particle size suggests that slime management will be a major issue in titanium recovery, and that agglomeration techniques will need to be considered. The presence of residual organics, concentrated in the <45 μm stream of the primary froth, complicates this issue further.

5.1.2 Process management

The clay minerals are the areas of greatest concern from a process management perspective. This study found that the primary froth stream is enriched in chlorite and kaolinite, and severely depleted in illite-smectite. As well, it was discovered that the middlings are enriched in illite-smectite and contain clay minerals having more octahedral substitution and larger aspect ratios (which tend to have a higher cation exchange capacity and, hence, be more active). Differences also were noted between the charge and thickness distributions of the illitic clay minerals in the primary froth and middlings. The primary froth was found to contain illite with more tetrahedral substitution, whereas the middlings had more octahedral substitution. The thickness distribution of the particles observed in the primary froth revealed a bimodal distribution with one set of particles slightly thicker and one set of particles slightly thinner than the particles found in the middlings. This distribution indicates that ores rich in kaolinite and chlorite may prove problematic for solvent extraction and coking. It also indicates that ores rich in illite-smectite may prove problematic for tailings management and gelation during extraction.

5.2 Future Work

As with any study, this research has highlighted some areas where future research might be valuable.

5.2.1 Secondary resource potential

The research indicates that zircon recovery may be limited by flotation efficiency. This may be because zircon is usually considered a fairly hydrophilic mineral (Wills, 1997) meaning it is surprising that zircon has enriched to the froth as much as it has. As such, it would be interesting to investigate the mechanism of zircon recovery to the froth, and in doing so, examine new possibilities for process changes that could increase zircon recovery without hindering bitumen production. Even though it appears that flotation is not the limiting factor in recovering titanium from the oil sands, the study could also investigate titanium recovery to the froth. Such a study should pay particular attention to the role of tightly bound organics and their influence on the surface properties of the titanium-bearing and zirconium-bearing minerals.

Since iron is associated with the TiO_2 polymorphs on the micron scale, improving the purity of a TiO_2 concentrate will prove difficult using typical mineral processing techniques. However, it may be possible to achieve an acceptable purity level by separating the "leucoxene" particles from the purer TiO_2 polymorph particles via a magnetic separation, at the cost of a reduced yield. As such, it may be useful to investigate the magnetic susceptibility of the TiO_2 polymorphs as a function of iron content. Reduction of a "leucoxene" concentrate may also help to improve the separation of the particles containing hematite from those that are fully transformed to rutile, as the magnetic susceptibility of reduced "leucoxene" has been shown to be significantly higher than unreduced leucoxene or even pure hematite. (Karkhanavala et al., 1959). Such a study would allow the feasibility of magnetic separation to be evaluated on a scientific and economic basis.

Another area of future work would be to investigate the effects of the presence of bitumen on the weathering of ilmenite.

5.2.2 Process management

Several questions remain about the role of clay minerals in oil sands extraction, and therefore, many areas for future work exist. Of primary importance is the analysis of the charge distribution of the clay minerals in the primary froth and middlings. This should be continued by first collecting more TEM-EDX data on pure particles, and then by probing clay surfaces using both molecular probes and spectroscopic methods. Ideally, both of these tests would be conducted on particles that can be classified by mineral type – either by relying on particle morphology or by other means such as chemical composition or diffraction.

It also may be valuable to examine the relationship between iron, clay minerals, and bitumen. Infrared spectroscopy and Mossbauer spectroscopy could be used to analyze clay minerals before and after organic removal with hydrogen peroxide. The differences in iron concentration and location may better distinguish whether the iron is part of the clay mineral structure, or merely associated with the clay mineral surfaces.

Finally, it is important to compare clay mineral distributions after both solvent and warm water extraction. In doing so, it should be possible to determine how the kaolinite and chlorite clay minerals affect solvent extraction.

6 References

Agfa NDT Pantak Seifert GmbH_Co KG "AutoQuan 2.7.0" (Computer program)

Ahn, J. H., & Peacor, D. R. (1986). Transmission electron microscope data for rectorite: Implications for the origin and structure of fundamnetal particles. *Clays and Clay Minerals, 34(2)*, 180-186.

Alberta Chamber of Resources. (1996). *Mineral developments agreement co-products study* [Report], Alberta: Author.

Alberta Department of Energy. (2003). Alberta's Oil Sands. Retrieved January 11, 2005, from http://www.energy.gov.ab.ca/com/Sands/Introduction/Oil_Sands.htm.

Alberta Economic Development. (2004). Oil Sands Industry Update. Retrieved December 6, 2004, from http://www.alberta-canada.com/oandg/pdf/oilsands_mar2004.pdf.

ASTM (1992) *Standard Test Method for Methylene Blue Index of Clay* Designation C-837–81, reapproved 1992.

Bailey, S.W. (1980). Summary of recommendations of AIPEA nomenclature committee on clay minerals. *American Mineralogist, 65*, 17.

Banfield, J.F., & Veblen, D.R. (1991). The structure and origin of Fe-bearing platelets in metamorphic rutile. *American Mineralogist, 76,* 113–127.

Bayliss, P., & Levinson, A.A. (1976). Mineralogical review of the Alberta oil sand deposits (Lower Cretaceous, Mannville Group). *Bulletin of Canadian Petroleum Geology, 24* (2): 211–224.

Barber, M. (2004). *AST Dean Stark procedure: Determination of bitumen, water and solids.*Devon: Natural Resources Canada, Canada Energy Technology Centre, Advanced Separation Technologies Tailings & Environment.

Bichard, John A. (1987). *Oil sands composition and behaviour research.* Edmonton: Alberta Oil Sands Technology and Research Authority.

Blackburn, W.H. & Dennen, W.H. (1988). *Principles of mineralogy.* Dubuque : Wm. C. Brown Publishers, College Division.

Bowles, J.F. (1988). Definition and range of composition of naturally occurring minerals with the pseudobrookite structure. *American Mineralogist, 73* 1377–1383.

Bulmer, J.T. (ed) & Starr, J. (1979). *Syncrude analytical methods for oil sand and bitumen processing.* Edmonton Alberta: Syncrude Canada Limited.

Burkhe, V., Jenkins, R., & Smith, D. (Eds.). (1998). *A practical guide for the preparation of specimens for X-ray fluorescence and X-ray diffraction analysis*. New York: John Wiley and Sons.

Buseck, P. R., & Iijima, S. (1974). High resolution electron microscopy of silicates. *American Mineralogist, 59,* 1-21.

Brenner,H. (1974). Rheology of a dilute suspension of axisymmetric Brownian particles, *International Journal of Multiphase Flow, 1,* 195–341.

Bruker AXS Gmbh (2003). DiffracPlus Topas Version 2.1 (computer program). Karlsruhe, West Germany M88-E01066.

Callister, W. (2000). *Materials science and engineering: An introduction* (5th ed.). New York: John Wiley and Sons.

Camp, F.W. (1976a). Processing Athabasca tar sands: tailings disposal [Presentation at the 26th Canadian chemical engineering conference] Toronto, ON.

Camp, F.W. (1976b) The tar sands of Alberta, Canada, (3rd Ed.). Denver Colorado: Cameron Engineers Inc.

Central Chemical Consulting, (2006) LST heavy liquid, physical characteristics. Retrieved August 9, 2006, from the World Wide Web on from http://www.chem.com.au/products/lstheavyliquid/#physical.

Chachula, F. (2002). *Characterization and upgrading of a rutile concentrate produced from the oil sands tailings* [M.Sc. Thesis], Edmonton, AB: University of Alberta.

Chalaturnyk, R. J., Scott, J. D, & Ozum, B. (2002). Management of oil sands tailings. *Petroleum Science and Technology, 20*, 1025–1046.

Chichester, F.W., Youngberg, C.T., and M.E. Harward. (1969). "Clay Mineralogy of Soils Formed on Mazama Pumice, *Soil Science Society of America Proceedings, 33*, 115–120.

Ciu, Z., Liu, Q., Etsell, T.H., Oxenford, J., & Coward, J. (2003). Heavy minerals in the Athabasca oil sands tailings - potential and recovery processes. *Canadian Metallurgical Quarterly, 42* (4), 383–392

Cloutis, E.A., Gaffey, M. J., & Moslow, T.F. (1995). Characterization of minerals in oil sands by reflectance spectroscopy, *Fuel 74*(6) 874–879.

Coelho, A. (1994). TOPAS Academic (Computer software).

Cooper, T. H. & Regents of the University of Minnesota. (2005). Retrieved October 18, 2005, from http://www.soils.agri.umn.edu/academics/classes/soil2125/doc/s12chap1.htm.

Coward, J., & Oxenford, J. (1997). *Heavy mineral potential of Athabasca Oil Sands* [Presentation given at TiO2 –A view to 2000, Conference]. Vancouver, B.C.: Intertech conferences.

Cullity, B.D. (1978). *Elements of X-ray Diffraction* (second edition). Don Mills, Ontario: Addison-Wesley Publishing Company Inc.

Day, R. W. (2006). Soil mechanics. In, *Foundation engineering handbook: Design and construction with the 2006 international building code* (pp. 4.1). New York: McGraw-Hill.

Deer, W.A., Howie, R.A., & Zussman, J. (1966). *An introduction to the rock forming minerals* Harlow: Longman Group Limited.

Drits, Victor. Srodon, Jan., and D.D Eberl. (1997). XRD measurement of mean crystallite thickness of illite and illite-smectite: Reappraisal of the Kubler index and Scherrer equation. *Clays and Clay Minerals, 45* (3), 461–475.

Dudas, M. (1995). Soil Clay Mineralogy [Lecture notes]. Soils 415. Edmonton, AB: Department of Materials Engineering, Faculty of Engineering, University of Alberta.

Dudas, M.J. *Preliminary Characterization of Suncor, Syncrude and Oslo Sludges* Appendix B of Proskin, S.A. 1998. A geotechnical investigation of freeze–thaw dewatering of oil sands fine tailings. [Ph.D. Thesis, Department of Civil and Environmental Engineering] Edmonton AB: University of Alberta.

Dusseault, M.B. & Scafe, D. (1979). Mineralogical and engineering index properties of the basal McMurray formation clay shales. *Canadian Geotechnical Journal 16*(2), 285–294.

Dusseault, M. B., Scafe, D. W., & Scott, J. D. (1989). Oil sands mine waste management: Clay mineralogy, moisture transfer and disposal technology. *AOSTRA Journal of Research*, *5*, 303–320.

Eberl, Danny, Srodon, Jan, Lee, Mingchu, Nadeau, P.H., and Northrop, Roy N. (1987). "Sericite from the Silverton caldera, Colorado: Correlation amoung structure, composition, origin and particle thickness". *American Mineralogist, 72,* 914–934.

Eberl, D. D., Nuesch, R., Sucha, V., and Tsipursky, S. (1998). Measurement of fundamental illite particle thicknesses by XRD using PVP-10 intercalation. *Clays and Clay Minerals*, *46* (1), 89-97.

Fanning, Keramidas, & El-Desoky (1989). "Micas" in *Minerals in Soil Environments (2nd Edition)*. Madison, WI: Soil Science Society of America.

Fang, Hsai-Yang (1991). *Foundation Engineering Handbook.* Springer.

FTFC (Fine Tailings Fundamentals Consortium) (1995). Volume I, Clark hot water extraction fine tailings. In: *Advances in Oil Sands Tailings Research,* Alberta Department of Energy, Oil Sands and Research Division, Publisher.

Fibics Incorporated (2008) TEM sample preparation by FIB. Retrieved July 29, 2008 from the world wide web at http://www.fibics.com/SC_FIBTEM.html.

Friesen, W.I., Michaelian, K.H., Long, Y., and Dabros, T. (2005). Effect of solvent-to-bitumen ratio on the pyrolysisproperties of precipitated athabasca asphaltenes. *Energy Fuels*, *19*, 1109–1115.

Geankoplis, C. J.(1993). *Transport processes and unit operations*. Prentice-Hall, inc.

Gillot, F., Righi, D., & Elsass, F. (2000). Pedogenic smectites in podzol from central finland: An analytical electron microscopy study. *Clays and Clay Minerals, 48(6)*, 655-664.

Gliszczynski, S (1944). Explanation of intergrowths of pseudobrookite. *Neues Jahrbuch fuer Mineralogie, Geologie und Palaeontologie, Abhandlungen, Abteilung A: Mineralogie, Petrographie 79A,* 1-38.

Grey, I.E., & Reid, A.F. (1975). The structure of pseudorutile and its role in the natural alteration of ilmenite. *The American Mineralogist, 60,* 898–906.

Grim, R. E. (1968). Clay mineralogy (2nd ed.). New York: McGraw-Hill Book Company Inc.

Grim, R. E. (1962). *Applied Clay Mineralogy*. New York: McGraw-Hill Book Company Inc.

Guggenheim, S. Alietti, A., Bain, D.C., Drits, V.A., Formoso, M.L., Galan, E., Hudnall, W., Koster, H. M., Paquet, H., & Watanabe, T. (1997). Report of the association international pour L'etude des argiles (AIPEA) nomencalture committee for 1996. *Clays and Clay Minerals, 32,* 493-495.

Gupta, Suresh K., Rajakumar, V.,& Grieveson, Paul (1989). The influence of weathering on the reduction of ilmenite with carbon. *Metallurgical Transactions B: Process Metallurgy, 20B,*(5), 735–45.

Guthrie, George D. Jr, & Veblen, D. R. (1989). High resolution transmission electron microscopy of mixed-layer illite/smectite: Computer simulations. *Clays and Clay Minerals, 37(1)*, 1-11.

Hang, P. T., and Brindley, G. W. (1970). Methylene blue adsorption by clay minerals. determination of surface areas and cation exchange capacities. *Clays and Clay Minerals, 18*, 203–212.

Hepler, Loren (ed.) & Hsi, Chu (ed.) (1989). *AOSTRA technical handbook on oil sands, bitumens and heavy oils*. Edmonton: Alberta Oil Sands Technology and Research Authority.

Hill, R.J. & Howard, C. J. (1987). Quantitative phase analysis from neutron powder diffraction data using the Rietveld method. *Journal of Applied Crystallography 20*, 467–474.

Hooshiar, Ali (2007). [Personal communication (unpublished TEM micrographs)].

Ignasiak, T. M., Kotlyar, L., Longstaffe, F. J., Strausz, O. P., & Montgomerry, D. S. (1983) Separation and characterization of clay from athabasca asphaltene. *Fuel, 62*, 353–362.

Ignasiak, T.M., Zhang, Q., Kratochvil, C., Montgomery, D.S., & Strausz, O.P., (1985). Chemical and mineral characterization of the bitumen-free athabasca oil sands related to the bitumen concentration in sand tailings from the syncrude batch extraction test. AOSTRA Journal of Research, 2, 21–34.

Ityokumbol, M. T., Bulani, W., Kosaric, N. (1987). Economic and environmental benefits from froth flotation recovery of titanium, zirconium, iron and rare earth minerals from oilsand tailings. *Water Science and Technology, 19,* 323–331.

Johnston, C. (Speaker). (2008, May 12). Surface chemistry of clay minerals [Presentation]. CONRAD-Clay workshop. Calgary, AB.

Kaminsky, H.A.W., Etsell, T. H., Ivey, D.G., and Omotoso, O.E. (2006). Fundamental particle size of clay minerals in Athabasca oil sands tailings. *Clay Science 12* (supplement 2), 217–222

Karkhanavala, M.D., Momin, A.C. & Rege, S.G. (1959). An X-ray study of leucoxene from Quilon, India. *Economic Geology, 54,* 913–918.

Kasongo, T. (2006). *Role of fine clays and ionic species in bitumen extraction from oil sands ores using the hot water extraction process* [Ph. D. dissertation]. Edmonton, AB: University of Alberta.

Kasongo, T., Zhou, Z., Xu, Z., & Masliyah, J. (2000). Effect of clays and calcium ions on bitumen extraction from athabasca oil sands using flotation. *The Canadian Journal of Chemical Engineering, 78*, 674–680.

Kasperski, K. L. (1992). A review of properties and treatment of oil sands tailings. *AOSTRA Journal of Research, 8* (1), 11–53.

Kasperski, K. L. (2001). Review of research on aqueous extraction of bitumen from mined oil sands. [Division No. CWRC 01-17 (CF)]. Natural Resources Canada, CANMET-WRC.

Kessick, M.A., (1979). Structure and properties of oil sands and clay tailings *Journal of Canadian Petroleum Technology, 18* (1), 49–52.

Kim, J. W., Peacor, D. R., Tessier, D., & Elsass, F. (1995). A technique for maintaining texture and permanent expansion of smectite interlayers for TEM observations. *Clays and Clay Minerals, 43(1)*, 51-57.

Klimentidis, R., & Mackinnon, I. (1986). High resolution imagin of ordered mixed-layer clays. *Clays and Clay Minerals, 34*(2), 155-164.

Kotlyar, L.S., Sparks, B.D., & Kodama, H. (1984). Some chemical and mineralogical properties of fine solids derived from oil sands. *AOSTRA Journal of Research, 1,* 99–106.

Kotlyar, L.S., Sparks, B.D., & Kodama, H. (1985). Isolation of inorganic matter-humic complexes from athabasca oil sands. *AOSTRA Journal of Research, 2,* 103–111.

Kotlyar, L.S., Kodama, H., Sparks, B.D.,& Grattan-Bellew, P.E. (1987). Non-crystalline inorganic matter-humic complexes in athabasca oil sand and their relationship to bitumen recovery. *Applied Clay Science, 2,* 253–271.

Kotlyar, L. S., Kodama, H., & Ripmeester, J. A. (1990). Possible identification of poorly crystalline inorganic matter present in athabasca oil sands. *Applied Clay Science, 5,* 1–12.

Kotlyar, L.S., Deslandes, Y., Sparks, B.D., Kodama, H., & Schutte, R. (1993). Characterization of colloidal solids from athabasca fine tails. *Clay and Clay Minerals 41*(3) 341–345.

Kotlyar, L.S., Sparks, B.D., Woods, J., Capes, C.E., & Schutte, R. (1995) Bitwetted ultrafine solids and structure formation in oil sands fine tailings. *Fuel, 74,* 1146–1149.

Kramers, J.W. & Brown, R.A.A. (1975) Survey of heavy minerals in the athabasca oil sand deposit. [Presentation] Annual Meeting of CIM, October 26–29: Edmonton, AB.

Laird, David. (1994). Evaluation of the structural formula and alkylammonium methods of determining layer charge. In A.R. Mermut (Ed), *CMS Workshop lectures, volume 6, Layer Charge Characteristics of 2:1 silicate clay minerals*. Colorado, USA: Clay Minerals Society.

Langford, J. I. & Louër, D. (1996). Powder diffraction. *Reports on Progress in Physics, 59* (2), 131–234.

Lee, J. H., Peacor, D. R., Lewis, D. D., & Wintsch. (1984). Chlorite-Illite/muscovite interlayered and interstratified crystals: A TEM/STEM study. *Contributions in Mineralogy and Petrology, 88,* 372-385.

Lee, E.Y., Cho, K., & Ryu, H.W. (2002) Microbial refinement of kaolin by iron reducing bacteria. *Applied Clay Science, 22* 47-53.

Liendo, J. (2005). Fundamental Study on the Role of Fines in Upgrading [M.Sc. Thesis], Edmonton, AB: University of Alberta.

Lynd, L. E. & Lefond, S. J. (1983). Titanium Minerals in *Industrial Minerals and Rocks, 5th Ed.* Edited by Lefond, S.J. Society of Mining Engineers, of the American

Institute of Mining, Metallurgical and Petroleum Engineers, Inc. New York. 1303-1362.

Liu, J., Masliyah, J., & Xu, Z. (2004). Role of fine clays in bitumen extraction from oil sands. *American Institute of Chemical Engineers Journal, 50* (8), 1917–1927.

Ma, C. and Eggleton, R.A. (1999). Surface layer types of kaolinite: A high-resolution transmission electron microscope study. *Clays and Clay Minerals*, *47*, 2, 181–191.

MacKinnon, M.D. (1989). Development of the tailings pond at Syncrude's oil sands plant: 1978–1987. *AOSTRA Journal of Research*, *5* (2), 109–133.

Majid, A., & Sparks, B. D. (1999). Potential applications of oil sands industry wastes. *Journal of Canadian Petroleum Technology*, *38* (11), 29–33.

Masliyah, J., Zhou, Z., Xu, Z., Czarnecki, J., & Hamza, H. (2004). Understanding water-based bitumen extraction from athabasca oil sands. *The Canadian Journal of Chemical Engineering, 82*, 628–654.

Mason, J.C., & Handscomb, D. (2003). *Chebyshev polynomials.* CRC Press.

Mercier, P.H.J, Le Page, Y., Tu, Y., & Kotlyar, L.S. (2008) Powder X-ray diffraction determination of phyllosilicate mass and area versus particle thickness distributions for clays from the Athabasca oil sands. *Petroleum Science and Technology 26* (3) 307–321.

Mikula, R.J., Munoz, V.A., Wang, N., Bjornson, B., Cox, D., Moisan, B. & Wiwchar, K. (2003). Characterization of bitumen properties using microscopy and near infrared spectroscopy: *Processability of oxidized or degraded ores. Journal of Canadian Petroleum Technology, 42(8)*, 50-53.

Mitchell, J. K. (1976). *Fundamentals of soil behaviour* New York: John Wiley & Sons, Inc.

Moore, D. M. & Reynolds, J. R. C. (1997). *X-ray diffraction and the identification and analysis of clay minerals*. Oxford, UK: Oxford University Press.

Munoz, V. A., Kasperski, K. L., Omotoso, O. E., & Mikula, R. J. (2003). The use of microscopic bitumen froth morphology for the identification of problem oil sand ores. *Petroleum Science and Technology, 21* (9), 1509–1529.

Nadeau, P. H., Wilson, M. J., McHardy, W. J., & Tait, J. M. (1984). Interstratified clays as fundamental particles. *Science, 225*, 923–935.

Nadeau, P. H., Tait, J. M., McHardy, W. J., & Wilson, M. (1984b). Interstratified XRD characteristics of physical mixtures of elementary clay particles. *Clays and Clay Minerals, 19*, 67-76.

Nadeau, P. H. (1985). The physical dimensions of fundamental clay particles. *Clay Minerals, 20,* 499-514.

Nadeau, P.H. (1987). Relationships between the mean area, volume and thickness for dispersed particles of kaolinites and micaceous clays and their application to surface area and ion exchange properties. *Clay Minerals, 22*, 351–356.

National Energy Board. (2004). Canada's Oil Sands: opportunities and challenges to 2015 [Pamphlet]. Calgary, AB: Author.

Office of Solid Waste, U.S. Environmental Protection Agency. (1995). Titanium tetrachloride production by the chloride-ilmenite process. Retrieved April 18, 2007, from http://www.epa.gov/epaoswer/other/mining/minedock/tio2/tio2.pdf.

O'Keefe, M. A., Buseck, P. R., & Iijima, S. (1978). Computed crystal structure images for high resolution electron microscopy. *Nature, 274(27)*, 322-324.

Olson, C. G., Thompson, M. L, & Wilson, M. A. (2000). Phyllosilicates. In M. E. Sumner (Ed.), *Handbook of soil science* Boca Raton, FL: CRC Press LLC.

Omotoso, O. (2003). [Personal communication].

Omotoso, O. (2006). [Personal communication].

Omotoso, O., Mikula, R. J., & Stephens, P. W. (2002). Surface area of interstratified phyllosilicates in athabasca oil sands from synchrotron XRD. *Advances in X-ray Analysis*, *45*, 363–391.

Omotoso, O.E., & Mikula, Randy J. (2004). High surface areas caused by smectitic interstratification of kaolinite and illite in Athabasca oil sands. *Applied Clay Science, 25,* 37-47.

Omotoso, O., Mikula, R., Urquhart, S., Sulimma, H., & Stephens, P. (2006) Characterization of clays from poorly processing oil sands using synchrotron techniques. *Clay Science, 12, Supplement 2,*88–93.

Owen, M., and Tipman, R. (1999). Co-production of heavy minerals from oil sand tailings. *CIM Bulletin*, *92*, 65–73.

Oxenford, John (2007). [Personal communication].

Pauling, L. (1930). The structure of micas and related minerals. *Proceedings of the National Academy of Sciences of the United States of America 16*, 123-129.

Penner, T. J. (2006). Analysis of methanogenic microbial communities from oil sands processing tailings.[M.Sc. Thesis], Edmonton, AB: University of Alberta.

Radoslovich, E. W. (1959) Structural control of polymorphism in micas. *Nature, 183* 253.

Reitveld, H. M. (1969). A profile refinement method for nuclear and magnetic structures. *Journal Applied Crystallography, 2*, 65-71.

Rieder, M., Cavazzini, G., D'yakonov, Y. S., Frank-Kamenetskii, V., Gottardi, G., Guggenheim, S., Koval, P.,Muller, G., Neiva, A., Radoslovich, E., Robert, J., Sassi, F., Takeda, H., Weiss, Z., & Wones D. (1998). Nomenclature of the micas. *Clays and Clay Minerals, 46(5)*, 586-595.

Ripmeester, J.A.; Kotlyar, L.S.; Sparks, B.D. (1993) H NMR and the sol-gel transition in suspensions of colloidal clays. *Colloids and Surfaces A: Physicochemical and Engineering Aspects, 78*, 57–63.

Roberts, J.O.L., Yong, R.N., & Erskine, H.L. (1980) Surveys of some tar sand sludge ponds: results and interpretations. [Proceeding of the Applied Oilsands Geoscience Conference June 11-13, 1980] Edmonton, AB.

Sainz-Diaz, C. I., Hernández-Laguna, A., & Dove, M. T. (2001). Theoretical modeling of cis-vacant and trans-vacant configurations in the octahedral sheet of illites and smectites. *Physics and Chemistry of Minerals, 28*, 322–331.

Scales, P. (Speaker). (2008, May 1-2). Rheology of Clay Suspensions [Presentation]. CONRAD-Clay workshop, Calgary, AB.

Schroeder, P. (2008). Lecture notes for Clay Mineralogy. Retrieved May 11, 2008 from http://www.gly.uga.edu/schroeder/geol6550/CM06.html.

Scott, J.D., Dusseault, M.B., & Carrier III, W.D., (1985). Behaviour of the clay/bitumen/water sludge system from oil sands extraction plants. *Applied Clay Science, 1:* 207–218.

Smith, R., & Ng, S. (1993). In J. L. Liu (Ed.), *Towards a model for the prediction of fine tails volume* (pp. F3-1 – F3-33). Edmonton, AB: Environment Canada.

Srodon, J. (1980). Precise identification of illite/smectite interstratifications by X-ray powder diffraction. *Clays and Clay Minerals, 28(6)*, 401-411.

Srodon, J. (1999). Nature of mixed layer clays and mechanisms of their formation and alteration. *Annual Review of Earth and Planetary Sciences, 27,* 19–53.

Srodon, J., Elsass, F., McHardy, W.J., and Morgan, D.J. (1992). Chemistry of illite-smectite inferred from TEM measurements of fundamental particles. *Clay Minerals, 27*, 137–158.

Srodon, J. & Elsass, F. (1994). Effect of the shape of fundamental particles of XRD characteristics of illitic minerals. *European Journal of Minerals, 6*, 113-122.

Stokes, A.R., and A.J.C. Wilson. (1942). A method of calculating the integral breadths of Debye-Scherrer lines. *Proceedings of the Cambridge Philosophical Society, 38,* 313–322.

Sucha, V., Srodon, J., Elsass, F., & McHardy, W. J. (1996). Particle shape versus coherent scattering domain of illite/smectite: Evidence from HRTEM of dolna ves clays. *Clays and Clay Minerals, 44(5)* 665-671.

Tettenhorst, R. T., & Roberson, H. (1973). X-ray diffraction aspects of montmorillonites. *American Mineralogist, 58,* 73-80.

Thomas, E. (2004). E&ES213: Mineralogy Lecture March 22. Retrieved May 11, 2008, from http://ethomas.web.wesleyan.edu/ees123/sheet04.htm.

Titanium Corporation. (2007). Oil Sands Project. Retrieved February 8, 2008, from http://www.titaniumcorporation.com/s/OilSands.asp?ReportID=137458.

Tu, Y., O'Carroll, J. B., Kotlyar, L. S., Sparks, B. D., Ng, S., Chung, K. H., et al. (2005). Recovery of bitumen from oilsands: Gelation of ultra-fine clay in the primary separation vessel. *Fuel*, *84*, 653–660.

Vali, H., & Koster, H. M. (1986). Expanding behaviour, structural disorder, regular and random irregular interstratification of 2:1 layer-silicates studied by HRTEM. *Clay Minerals, 21*, 827-859.

Wallace, D., Tipman, R., Komishke, B., Wallwork, V., & Perkins, E. (2004). Fines/water interactions and consequences of the presence of degraded illite on oil sands extractability. *The Canadian Journal of Chemical Engineering, 82*, 667–677.

Ward, D. & Brady, P. (1998). Effect of Al and Organic Acids on the Surface Chemistry of Kaolinite. *Clays and Clay Minerals, 46,* 453-465.

Watari, F., Van Landuyt,J., Delavignette, P. & Amelinckx, S.(1979). Electron microscopic study of dehydration transformations I. Twin formation and mosaic structure in hematite derived from goethite. *Journal of Solid State Chemistry 29,* 137–150.

Western Oil Sands. (2002). Western Oil Sands annual report – 2002. Retrieved November 23 2004, from http://www.westernoilsands.com/pdf/2002annual.pdf.

Whitcomb & Associates. (2005). Prefeasibility study: Oils sands heavy minerals project. Retrieved March 30, 2007, from http://www.titaniumcorporation.com/s/Library.asp.

Wills, B. (1997). *Mineral processing technology* (6th ed.). London: Butterworth-Heinemann.

Wu, W., & Nancollas, G. H. (1998). Kinetics of heterogeneous nucleation of calcium phosphates on anatase and rutile surfaces. *Journal of Colloid and Interface Science, 199,* 206–211.

Yong, R.N & Sethi, A.J. (1978). Mineral particle interaction control of tar sand sludge stability. *The Journal of Canadian Petroleum Technology, 77*(4), 76-83.

Young, R.A. (ed) (1995) *The Reitveld method* Oxford University Press.

Zhao, S., Kotlyar, L. S., Sparks, B. D., Woods, J,, Gao, J., & Chung, K. (2001). Solids contents, properties and molecular structures of asphaltenes from different oilsands. *Fuel, 80,* 1907–1914.

Zbik, M. (2006). Micro-structural explanation for differences in gelation properties of kaolinites from Birdwood (S. Australia) and Georgia (U.S.A.).*Clay Science, 12 (Supplement 2),* 31–36.

Appendix A

Table A–1: XRF analysis results from froth samples

Stream	Primary Froth					Secondary Froth		
Size Fraction	<0.2 µm	0.2-2 µm	2-45 µm	45-106 µm	>106 µm	<2 µm	2-45 µm	>45 µm
Sample Weight (g)	1.78	5.28	16.71	7.24	18.03	0.76	0.94	3.60
SiO_2 (±1.65)	44.0%	43.3%	51.1%	68.1%	90.9%	46.1%	43.0%	90.2%
Al_2O_3 (±1.15)	25.1%	25.6%	14.0%	7.5%	4.2%	22.6%	23.8%	4.9%
Fe_2O_3 (±0.36)	15.1%	14.5%	15.9%	5.2%	0.8%	13.1%	16.3%	0.9%
TiO_2 (±0.57)	1.0%	2.9%	11.0%	10.1%	1.4%	3.8%	9.5%	1.6%
K_2O (±0.05)	2.5%	2.5%	1.2%	0.7%	0.5%	2.5%	1.0%	0.6%
Cl (±0.1)	5.5%	4.6%	0.4%	0.4%	0.4%	2.1%	0.5%	0.3%
MgO (±0.15)	1.9%	1.3%	1.1%	0.6%	0.0%	3.5%	1.2%	0.0%
CaO (±0.02)	1.1%	1.7%	1.7%	0.5%	0.2%	1.6%	1.4%	0.2%
Cr_2O_3 (±0.02)	0.7%	0.7%	0.3%	0.2%	0.2%	1.7%	0.2%	0.2%
ZrO_2 (±0.36)	0.1%	0.1%	1.4%	3.7%	0.5%	0.0%	1.1%	0.4%
Na_2O (±0.04)	0.2%	0.1%	0.1%	0.2%	0.0%	0.0%	0.1%	0.2%
MnO (±0.03)	0.3%	0.5%	0.8%	0.2%	0.0%	0.6%	0.8%	0.0%
P_2O_5 (±0.06)	0.3%	0.4%	0.4%	0.3%	0.1%	0.5%	0.3%	0.1%
SO_3 (±0.03)	0.2%	1.1%	0.1%	0.1%	0.1%	0.3%	0.1%	0.1%
ZnO (±0.08)	0.1%	0.1%	0.2%	0.2%	0.1%	0.4%	0.2%	0.2%
CuO (±0.01)	0.1%	0.1%	0.2%	0.1%	0.1%	0.4%	0.2%	0.1%
Other	1.6%	0.3%	0.2%	1.9%	0.4%	0.9%	0.5%	0.0%
Trace (< 0.1%)	As_2O_3, SrO	CoO, Ho_2O_3, SrO	Dy_2O_3, SrO	As_2O_3, Au,Pt Dy_2O_3, Ho_2O_3,Pt, SrO, Y_2O_3	Er_2O_3, Ir, SrO	Er_2O_3, SrO	Dy_2O_3, Er_2O_3, SrO	

Table A–2: XRF results for tailings samples

Stream	Middlings				Tailings					
Size Fraction	**<0.2 µm**	**0.2-2 µm**	**2-45 µm**	**>45 µm**	**<0.2 µm**	**0.2-2 µm**	**2-45 µm**	**45-106 µm**	**106-250 µm**	**>250 µm**
Sample Weight (g)	21.83	50.12	108.87	4.46	6.26	16.59	111.42	192.46	604.58	4.18
SiO_2 (±1.65)	52.8%	55.1%	78.3%	56.1%	51.7%	61.7%	90.6%	94.0%	95.5%	77.3%
Al_2O_3 (±1.15)	32.3%	31.7%	14.9%	31.6%	30.0%	25.6%	5.3%	2.8%	2.6%	6.2%
Fe_2O_3 (±0.36)	6.7%	5.0%	2.1%	4.5%	7.6%	4.6%	0.6%	0.2%	0.1%	11.1%
TiO_2 (±0.57)	0.5%	1.2%	0.7%	1.0%	0.6%	1.2%	0.4%	0.2%	0.0%	0.2%
K_2O (±0.05)	3.2%	3.4%	2.2%	2.8%	3.1%	3.1%	1.2%	0.8%	0.5%	1.1%
Cl (±0.1)	0.4%	0.4%	0.4%	0.4%	0.7%	0.9%	0.5%	0.4%	0.4%	0.4%
MgO (±0.15)	1.8%	1.3%	0.0%	1.4%	1.7%	1.0%	0.0%	0.0%	0.0%	0.6%
CaO (±0.02)	0.8%	0.5%	0.2%	0.6%	0.9%	0.5%	0.1%	0.1%	0.1%	1.4%
Cr_2O_3 (±0.02)	0.2%	0.6%	0.2%	0.2%	0.7%	0.7%	0.2%	0.2%	0.2%	0.2%
ZrO_2 (±0.36)	0.0%	0.0%	0.0%	0.1%	0.0%	0.0%	0.0%	0.3%	0.1%	0.1%
Na_2O (±0.04)	0.5%	0.1%	0.1%	0.4%	0.1%	0.1%	0.2%	0.0%	0.0%	0.1%
MnO (±0.03)	0.2%	0.1%	0.1%	0.1%	0.1%	0.1%	0.0%	0.0%	0.0%	0.3%
P_2O_5 (±0.06)	0.1%	0.1%	0.0%	0.1%	0.1%	0.1%	0.1%	0.3%	0.1%	0.1%
SO_3 (±0.03)	0.1%	0.1%	0.1%	0.1%	0.4%	0.0%	0.1%	0.1%	0.1%	0.2%
ZnO (±0.08)	0.2%	0.1%	0.2%	0.2%	0.2%	0.2%	0.2%	0.1%	0.1%	0.2%
CuO (±0.01)	0.1%	0.1%	0.1%	0.2%	0.3%	0.2%	0.2%	0.1%	0.1%	0.1%
Other	0.1%	0.3%	0.4%	0.4%	1.8%	0.1%	0.3%	0.5%	0.1%	0.4%
Trace (< 0.1%)	CoO, SrO	Au, Pt, SrO	Pt, Sm_2O_3	SrO, Tb_4O_7	As_2O_3, CoO, SeO_2, SrO	Pt, SrO	Rh, SeO_2	SeO_2, Yb_2O_3	Pt	Ir, Pt, Tb_4O_7

Table A–3: XRF results for ore samples

Size Fraction	<0.2 µm	0.2-2 µm	2-45 µm	45-106 µm	>106 µm
Sample Weight (g)	11.60	29.89	88.97	69.27	205.93
SiO_2 (±1.65)	52.9%	54.1%	67.3%	90.9%	93.1%
Al_2O_3 (±1.15)	30.1%	30.8%	20.6%	4.1%	2.3%
Fe_2O_3 (±0.36)	5.4%	6.0%	4.4%	0.6%	0.4%
TiO_2 (±0.57)	0.7%	1.4%	1.2%	0.7%	0.2%
K_2O (±0.05)	3.8%	3.5%	2.6%	0.8%	0.4%
Cl (±0.1)	0.5%	0.6%	0.6%	1.7%	1.7%
MgO (±0.15)	1.6%	1.4%	0.9%	0.0%	0.0%
CaO (±0.02)	0.6%	0.6%	0.5%	0.1%	0.1%
Cr_2O_3 (±0.02)	0.7%	0.7%	0.3%	0.5%	0.4%
ZrO_2 (±0.36)	0.0%	0.0%	0.1%	0.2%	0.6%
Na_2O (±0.04)	2.9%	0.1%	0.4%	0.1%	0.1%
MnO (±0.03)	0.1%	0.1%	0.1%	0.0%	0.0%
P_2O_5 (±0.06)	0.1%	0.2%	0.1%	0.0%	0.1%
SO_3 (±0.03)	0.4%	0.0%	0.2%	0.1%	0.1%
ZnO (±0.08)	0.2%	0.1%	0.1%	0.1%	0.2%
CuO (±0.01)	0.1%	0.1%	0.1%	0.1%	0.1%
Other	0.0%	0.2%	0.3%	0.1%	0.1%
Trace (< 0.1%)	SrO	Pt, SeO_2, SrO	Au, Pt, SeO_2, SrO	Pt	Pt

Table A–4: Element balance for <0.2 µm size fraction

<0.2 µm	ASSAY																
Stream	**Sample Weight**	**SiO_2**	**Al_2O_3**	**Fe_2O_3**	**K_2O**	**MgO**	**TiO_2**	**ZrO_2**	**CaO**	**Cl**	**Na_2O**	**Cr_2O_3**	**CuO**	**P_2O_5**	**MnO**	**CoO**	**ZnO**
Primary Froth	100.0%	44.0%	25.1%	15.1%	2.5%	1.9%	1.0%	0.1%	1.1%	5.5%	0.2%	0.7%	0.1%	0.3%	0.3%	0.0%	0.1%
Secondary Froth																	
Middlings	100.0%	52.8%	32.3%	6.7%	3.2%	1.8%	0.5%	0.0%	0.8%	0.4%	0.5%	0.2%	0.1%	0.1%	0.2%	0.0%	0.2%
Tailings	100.0%	51.7%	30.0%	7.6%	3.1%	1.7%	0.6%	0.0%	0.9%	0.7%	0.1%	0.7%	0.3%	0.1%	0.1%	0.1%	0.2%
Ore	100.0%	52.9%	30.1%	5.4%	3.8%	1.6%	0.7%	0.0%	0.6%	0.5%	2.9%	0.7%	0.1%	0.1%	0.1%	0.0%	0.2%
Sum of Streams	100.0%	52.1%	31.4%	7.4%	3.2%	1.8%	0.6%	0.0%	0.8%	0.8%	0.4%	0.3%	0.2%	0.1%	0.2%	0.0%	0.2%
<0.2 µm	**DISTRIBUTION**																
Stream	**Sample Weight**	**SiO_2**	**Al_2O_3**	**Fe_2O_3**	**K_2O**	**MgO**	**TiO_2**	**ZrO_2**	**CaO**	**Cl**	**Na_2O**	**Cr_2O_3**	**CuO**	**P_2O_5**	**MnO**	**CoO**	**ZnO**
Primary Froth	6%	5%	5%	12%	5%	6%	11%	100%	8%	43%	3%	13%	4%	14%	11%	0%	5%
Secondary Froth	0%	0%	0%	0%	0%	0%	0%	0%	0%	0%	0%	0%	0%	0%	0%	0%	0%
Middlings	73%	74%	75%	66%	74%	73%	68%	0%	70%	37%	90%	41%	62%	70%	72%	58%	74%
Tailings	21%	21%	20%	21%	21%	20%	22%	0%	22%	20%	6%	45%	35%	16%	17%	42%	21%
Ore	100%	100%	100%	100%	100%	100%	100%	100%	100%	100%	100%	100%	100%	100%	100%	100%	100%
Sum of Streams	100%	100%	100%	100%	100%	100%	100%	100%	100%	100%	100%	100%	100%	100%	100%	100%	100%

Table A–5: Element balance for 0.2-2 μm size fraction

0.2-2 μm	ASSAY																
Stream	**Sample Weight**	**SiO_2**	**Al_2O_3**	**Fe_2O_3**	**K_2O**	**MgO**	**TiO_2**	**ZrO_2**	**CaO**	**Cl**	**Na_2O**	**Cr_2O_3**	**CuO**	**P_2O_5**	**MnO**	**CoO**	**ZnO**
Primary Froth	100.0%	43.3%	25.6%	14.5%	2.5%	1.3%	2.9%	0.1%	1.7%	4.6%	0.1%	0.7%	0.1%	0.4%	0.5%	0.1%	0.1%
Secondary Froth																	
Middlings	100.0%	55.1%	31.7%	5.0%	3.4%	1.3%	1.2%	0.0%	0.5%	0.4%	0.1%	0.6%	0.1%	0.1%	0.1%	0.0%	0.1%
Tailings	100.0%	61.7%	25.6%	4.6%	3.1%	1.0%	1.2%	0.0%	0.5%	0.9%	0.1%	0.7%	0.2%	0.1%	0.1%	0.0%	0.2%
Ore	100.0%	54.1%	30.8%	6.0%	3.5%	1.4%	1.4%	0.0%	0.6%	0.6%	0.1%	0.7%	0.1%	0.2%	0.1%	0.0%	0.1%
Sum of Streams	100.0%	55.7%	29.8%	5.6%	3.3%	1.2%	1.3%	0.0%	0.6%	0.8%	0.1%	0.7%	0.1%	0.1%	0.1%	0.0%	0.1%
0.2-2 μm	**DISTRIBUTION**																
Stream	**Sample Weight**	**SiO_2**	**Al_2O_3**	**Fe_2O_3**	**K_2O**	**MgO**	**TiO_2**	**ZrO_2**	**CaO**	**Cl**	**Na_2O**	**Cr_2O_3**	**CuO**	**P_2O_5**	**MnO**	**CoO**	**ZnO**
Primary Froth	7%	6%	6%	19%	6%	8%	16%	100%	21%	43%	9%	8%	7%	23%	26%	100%	7%
Secondary Froth	0%	0%	0%	0%	0%	0%	0%	0%	0%	0%	0%	0%	0%	0%	0%	0%	0%
Middlings	70%	69%	74%	62%	73%	73%	62%	0%	61%	31%	75%	67%	58%	54%	60%	0%	60%
Tailings	23%	26%	20%	19%	22%	19%	21%	0%	18%	26%	16%	25%	35%	23%	14%	0%	33%
Ore	100%	100%	100%	100%	100%	100%	100%	#DIV/0!	100%	100%	100%	100%	100%	100%	100%	100%	100%
Sum of Streams	100%	100%	100%	100%	100%	100%	100%	100%	100%	100%	100%	100%	100%	100%	100%	100%	100%

Table A–6: Element balance for <2 μm size fraction

<2 μm	ASSAY																
Stream	**Sample Weight**	**SiO_2**	**Al_2O_3**	**Fe_2O_3**	**K_2O**	**MgO**	**TiO_2**	**ZrO_2**	**CaO**	**Cl**	**Na_2O**	**Cr_2O_3**	**CuO**	**P_2O_5**	**MnO**	**CoO**	**ZnO**
Primary Froth	100.0%	43.5%	25.5%	14.7%	2.5%	1.5%	2.4%	0.1%	1.6%	4.9%	0.1%	0.7%	0.1%	0.3%	0.5%	0.1%	0.1%
Secondary Froth	100.0%	46.1%	22.6%	13.1%	2.5%	3.5%	3.8%	0.0%	1.6%	2.1%	0.0%	1.7%	0.4%	0.5%	0.6%	0.0%	0.4%
Middlings	100.0%	54.4%	31.9%	5.5%	3.4%	1.4%	1.0%	0.0%	0.6%	0.4%	0.2%	0.5%	0.1%	0.1%	0.1%	0.0%	0.1%
Tailings	100.0%	59.0%	26.8%	5.4%	3.1%	1.2%	1.0%	0.0%	0.6%	0.8%	0.1%	0.7%	0.2%	0.1%	0.1%	0.0%	0.2%
Ore	100.0%	53.8%	30.6%	5.8%	3.6%	1.5%	1.2%	0.0%	0.6%	0.6%	0.9%	0.7%	0.1%	0.2%	0.1%	0.0%	0.1%
Sum of Streams	100.0%	54.6%	30.2%	6.2%	3.2%	1.4%	1.1%	0.0%	0.7%	0.8%	0.2%	0.6%	0.1%	0.1%	0.2%	0.0%	0.1%
<2 μm	**DISTRIBUTION**																
Stream	**Sample Weight**	**SiO_2**	**Al_2O_3**	**Fe_2O_3**	**K_2O**	**MgO**	**TiO_2**	**ZrO_2**	**CaO**	**Cl**	**Na_2O**	**Cr_2O_3**	**CuO**	**P_2O_5**	**MnO**	**CoO**	**ZnO**
Primary Froth	7%	5%	6%	16%	5%	7%	15%	100%	16%	42%	5%	9%	6%	19%	20%	24%	6%
Secondary Froth	1%	1%	1%	2%	1%	2%	3%	0%	2%	2%	0%	2%	2%	3%	3%	0%	2%
Middlings	70%	70%	74%	63%	73%	72%	62%	0%	63%	32%	84%	61%	58%	57%	62%	44%	64%
Tailings	22%	24%	20%	19%	21%	19%	21%	0%	19%	24%	10%	28%	34%	21%	15%	32%	27%
Ore	100%	100%	100%	100%	100%	100%	100%	100%	100%	100%	100%	100%	100%	100%	100%	100%	100%
Sum of Streams	100%	100%	100%	100%	100%	100%	100%	100%	100%	100%	100%	100%	100%	100%	100%	100%	100%

Table A–7: Element balance for 2-45 µm size fraction

2-45 µm	ASSAY																
Stream	**Sample Weight**	**SiO_2**	**Al_2O_3**	**Fe_2O_3**	**K_2O**	**MgO**	**TiO_2**	**ZrO_2**	**CaO**	**Cl**	**Na_2O**	**Cr_2O_3**	**CuO**	**P_2O_5**	**MnO**	**CoO**	**ZnO**
Primary Froth	100.0%	51.1%	14.0%	15.9%	1.2%	1.1%	11.0%	1.4%	1.7%	0.4%	0.1%	0.3%	0.2%	0.4%	0.8%	0.0%	0.2%
Secondary Froth	100.0%	43.0%	23.8%	16.3%	1.0%	1.2%	9.5%	1.1%	1.4%	0.5%	0.1%	0.2%	0.2%	0.3%	0.8%	0.0%	0.2%
Middlings	100.0%	78.3%	14.9%	2.1%	2.2%	0.0%	0.7%	0.0%	0.2%	0.4%	0.1%	0.2%	0.1%	0.0%	0.1%	0.0%	0.2%
Tailings	100.0%	91.2%	5.4%	0.6%	1.2%	0.0%	0.4%	0.3%	0.1%	0.3%	0.1%	0.2%	0.1%	0.0%	0.0%	0.0%	0.2%
Ore	100.0%	67.3%	20.6%	4.4%	2.6%	0.9%	1.2%	0.1%	0.5%	0.6%	0.4%	0.3%	0.1%	0.1%	0.1%	0.1%	0.1%
Sum of Streams	100.0%	82.3%	10.4%	2.4%	1.6%	0.1%	1.3%	0.2%	0.3%	0.3%	0.1%	0.2%	0.1%	0.0%	0.1%	0.0%	0.2%
2-45 µm	**DISTRIBUTION**																
Stream	**Sample Weight**	**SiO_2**	**Al_2O_3**	**Fe_2O_3**	**K_2O**	**MgO**	**TiO_2**	**ZrO_2**	**CaO**	**Cl**	**Na_2O**	**Cr_2O_3**	**CuO**	**P_2O_5**	**MnO**	**CoO**	**ZnO**
Primary Froth	7%	4%	9%	47%	5%	94%	59%	42%	42%	7%	7%	10%	9%	96%	54%	100%	7%
Secondary Froth	0%	0%	1%	3%	0%	6%	3%	2%	2%	1%	0%	0%	1%	4%	3%	100%	0%
Middlings	46%	44%	66%	40%	61%	0%	25%	0%	35%	57%	47%	46%	47%	0%	37%	100%	44%
Tailings	47%	52%	24%	11%	33%	0%	13%	56%	21%	35%	45%	43%	43%	0%	6%	100%	48%
Ore	100%	100%	100%	100%	100%	100%	100%	100%	100%	100%	100%	100%	100%	100%	100%	100%	100%
Sum of Streams	100%	100%	100%	100%	100%	100%	100%	100%	100%	100%	100%	100%	100%	100%	100%	100%	100%

Table A–8: Element balance for <45 µm size fraction

<45 µm	ASSAY																
Stream	**Sample Weight**	**SiO_2**	**Al_2O_3**	**Fe_2O_3**	**K_2O**	**MgO**	**TiO_2**	**ZrO_2**	**CaO**	**Cl**	**Na_2O**	**Cr_2O_3**	**CuO**	**P_2O_5**	**MnO**	**CoO**	**ZnO**
Primary Froth	100.0%	48.9%	17.4%	15.5%	1.6%	1.2%	8.5%	1.0%	1.7%	1.7%	0.1%	0.4%	0.2%	0.4%	0.7%	0.0%	0.2%
Secondary Froth	100.0%	44.4%	23.3%	14.8%	1.6%	2.2%	6.9%	0.6%	1.5%	1.2%	0.1%	0.9%	0.3%	0.4%	0.7%	0.0%	0.3%
Middlings	100.0%	68.8%	21.7%	3.4%	2.6%	0.6%	0.8%	0.0%	0.4%	0.4%	0.2%	0.3%	0.1%	0.0%	0.1%	0.0%	0.1%
Tailings	100.0%	85.8%	9.0%	1.4%	1.5%	0.2%	0.5%	0.2%	0.2%	0.4%	0.1%	0.3%	0.1%	0.0%	0.0%	0.0%	0.2%
Ore	100.0%	63.0%	23.8%	4.8%	2.9%	1.1%	1.2%	0.1%	0.5%	0.6%	0.5%	0.5%	0.1%	0.2%	0.1%	0.1%	0.1%
Sum of Streams	100.0%	74.0%	16.4%	3.5%	2.1%	0.5%	1.2%	0.2%	0.4%	0.5%	0.1%	0.3%	0.1%	0.1%	0.1%	0.0%	0.2%
<45 µm	DISTRIBUTION																
Stream	**Sample Weight**	**SiO_2**	**Al_2O_3**	**Fe_2O_3**	**K_2O**	**MgO**	**TiO_2**	**ZrO_2**	**CaO**	**Cl**	**Na_2O**	**Cr_2O_3**	**CuO**	**P_2O_5**	**MnO**	**CoO**	**ZnO**
Primary Froth	7%	5%	7%	31%	5%	17%	48%	43%	29%	25%	7%	9%	8%	47%	41%	24%	7%
Secondary Froth	0%	0%	1%	2%	0%	2%	3%	2%	2%	1%	0%	2%	1%	3%	3%	0%	1%
Middlings	53%	49%	70%	52%	67%	64%	35%	0%	49%	45%	61%	55%	50%	36%	47%	44%	49%
Tailings	39%	46%	22%	15%	28%	17%	15%	55%	20%	30%	32%	34%	40%	13%	10%	32%	43%
Ore	100%	100%	100%	100%	100%	100%	100%	100%	100%	100%	100%	100%	100%	100%	100%	100%	100%
Sum of Streams	100%	100%	100%	100%	100%	100%	100%	100%	100%	100%	100%	100%	100%	100%	100%	100%	100%

Table A–9: Element balance for >45 µm size fraction

>45 µm	ASSAY																
Stream	**Sample Weight**	**SiO_2**	**Al_2O_3**	**Fe_2O_3**	**K_2O**	**MgO**	**TiO_2**	**ZrO_2**	**CaO**	**Cl**	**Na_2O**	**Cr_2O_3**	**CuO**	**P_2O_5**	**MnO**	**CoO**	**ZnO**
Primary Froth	100.0%	84.3%	5.2%	2.1%	0.6%	0.2%	3.9%	1.4%	0.3%	0.4%	0.1%	0.2%	0.1%	0.1%	0.1%	0.0%	0.1%
Secondary Froth	100.0%	90.2%	4.9%	0.9%	0.6%	0.0%	1.6%	0.4%	0.2%	0.3%	0.2%	0.2%	0.1%	0.1%	0.0%	0.0%	0.2%
Middlings	100.0%	56.1%	31.6%	4.5%	2.8%	1.4%	1.0%	0.1%	0.6%	0.4%	0.4%	0.2%	0.2%	0.1%	0.1%	0.0%	0.2%
Tailings	100.0%	95.0%	2.7%	0.2%	0.5%	0.0%	0.0%	0.1%	0.1%	0.4%	0.0%	0.2%	0.1%	0.1%	0.0%	0.0%	0.1%
Ore	100.0%	92.6%	2.8%	0.4%	0.5%	0.0%	0.3%	0.5%	0.1%	1.7%	0.1%	0.4%	0.1%	0.1%	0.0%	0.0%	0.2%
Sum of Streams	100.0%	94.5%	2.9%	0.3%	0.5%	0.0%	0.2%	0.2%	0.1%	0.4%	0.0%	0.2%	0.1%	0.1%	0.0%	0.0%	0.1%
>45 µm	**DISTRIBUTION**																
Stream	**Sample Weight**	**SiO_2**	**Al_2O_3**	**Fe_2O_3**	**K_2O**	**MgO**	**TiO_2**	**ZrO_2**	**CaO**	**Cl**	**Na_2O**	**Cr_2O_3**	**CuO**	**P_2O_5**	**MnO**	**CoO**	**ZnO**
Primary Froth	3%	3%	5%	21%	3%	34%	68%	28%	9%	3%	33%	3%	3%	3%	30%	100%	4%
Secondary Froth	0%	0%	1%	1%	0%	0%	4%	1%	1%	0%	15%	0%	0%	0%	2%	100%	1%
Middlings	1%	0%	6%	8%	3%	47%	3%	0%	3%	0%	44%	1%	1%	1%	6%	100%	1%
Tailings	96%	97%	88%	69%	93%	19%	25%	71%	88%	96%	8%	96%	95%	96%	62%	100%	95%
Ore	100%	100%	100%	100%	100%	100%	100%	100%	100%	100%	100%	100%	100%	100%	100%	100%	100%
Sum of Streams	100%	100%	100%	100%	100%	100%	100%	100%	100%	100%	100%	100%	100%	100%	100%	100%	100%

Table A–10: Element balance for 45-106 µm size fraction

45-106 µm	ASSAY																
Stream	**Sample Weight**	**SiO_2**	**Al_2O_3**	**Fe_2O_3**	**K_2O**	**MgO**	**TiO_2**	**ZrO_2**	**CaO**	**Cl**	**Na_2O**	**Cr_2O_3**	**CuO**	**P_2O_5**	**MnO**	**CoO**	**ZnO**
Primary Froth	100.0%	68.1%	7.5%	5.2%	0.7%	0.6%	10.1%	3.7%	0.5%	0.4%	0.2%	0.2%	0.1%	0.3%	0.2%	0.0%	0.2%
Secondary Froth																	
Middlings																	
Tailings	100.0%	94.0%	2.8%	0.2%	0.8%	0.0%	0.2%	0.3%	0.1%	0.4%	0.0%	0.2%	0.1%	0.3%	0.0%	0.0%	0.1%
Ore	100.0%	90.9%	4.1%	0.6%	0.8%	0.0%	0.7%	0.2%	0.1%	1.7%	0.1%	0.5%	0.1%	0.0%	0.0%	0.0%	0.1%
Sum of Streams	100.0%	93.1%	3.0%	0.4%	0.8%	0.0%	0.5%	0.4%	0.1%	0.4%	0.0%	0.2%	0.1%	0.3%	0.0%	0.0%	0.1%
45-106 µm	**DISTRIBUTION**																
Stream	**Sample Weight**	**SiO_2**	**Al_2O_3**	**Fe_2O_3**	**K_2O**	**MgO**	**TiO_2**	**ZrO_2**	**CaO**	**Cl**	**Na_2O**	**Cr_2O_3**	**CuO**	**P_2O_5**	**MnO**	**CoO**	**ZnO**
Primary Froth	4%	3%	9%	48%	3%	100%	67%	36%	15%	3%	100%	4%	4%	5%	49%	100%	5%
Secondary Froth																	
Middlings																	
Tailings	96%	97%	91%	52%	97%	0%	33%	64%	85%	97%	0%	96%	96%	95%	51%	100%	95%
Ore	100%	100%	100%	100%	100%	100%	100%	100%	100%	100%	100%	100%	100%	100%	100%	100%	100%
Sum of Streams	100%	100%	100%	100%	100%	100%	100%	100%	100%	100%	100%	100%	100%	100%	100%	100%	100%

Table A–11: Element balance for >106 µm size fraction

>106 µm	ASSAY																
Stream	**Sample Weight**	**SiO_2**	**Al_2O_3**	**Fe_2O_3**	**K_2O**	**MgO**	**TiO_2**	**ZrO_2**	**CaO**	**Cl**	**Na_2O**	**Cr_2O_3**	**CuO**	**P_2O_5**	**MnO**	**CoO**	**ZnO**
Primary Froth	100.0%	90.9%	4.2%	0.8%	0.5%	0.0%	1.4%	0.5%	0.2%	0.4%	0.0%	0.2%	0.1%	0.1%	0.0%	0.0%	0.1%
Secondary Froth																	
Middlings																	
Tailings	100.0%	95.4%	2.6%	0.2%	0.5%	0.0%	0.0%	0.1%	0.1%	0.4%	0.0%	0.2%	0.1%	0.1%	0.0%	0.0%	0.1%
Ore	100.0%	93.1%	2.3%	0.4%	0.4%	0.0%	0.2%	0.6%	0.1%	1.7%	0.1%	0.4%	0.1%	0.1%	0.0%	0.0%	0.2%
Sum of Streams	100.0%	95.2%	2.7%	0.2%	0.5%	0.0%	0.0%	0.1%	0.1%	0.4%	0.0%	0.2%	0.1%	0.1%	0.0%	0.0%	0.1%
>106 µm	**DISTRIBUTION**																
Stream	**Sample Weight**	**SiO_2**	**Al_2O_3**	**Fe_2O_3**	**K_2O**	**MgO**	**TiO_2**	**ZrO_2**	**CaO**	**Cl**	**Na_2O**	**Cr_2O_3**	**CuO**	**P_2O_5**	**MnO**	**CoO**	**ZnO**
Primary Froth	3%	3%	5%	10%	3%	0%	97%	17%	7%	3%	0%	3%	3%	2%	18%	100%	3%
Secondary Froth																	
Middlings																	
Tailings	97%	97%	95%	90%	97%	100%	3%	83%	93%	97%	100%	97%	97%	98%	82%	100%	97%
Ore	100%	100%	100%	100%	100%	100%	100%	100%	100%	100%	100%	100%	100%	100%	100%	100%	100%
Sum of Streams	100%	100%	100%	100%	100%	100%	100%	100%	100%	100%	100%	100%	100%	100%	100%	100%	100%

Table A–12: Total element balance around extraction

TOTAL	**ASSAY**																
Stream	**Sample Weight**	**SiO_2**	**Al_2O_3**	**Fe_2O_3**	**K_2O**	**MgO**	**TiO_2**	**ZrO_2**	**CaO**	**Cl**	**Na_2O**	**Cr_2O_3**	**CuO**	**P_2O_5**	**MnO**	**CoO**	**ZnO**
Primary Froth	100.0%	66.9%	11.2%	8.7%	1.1%	0.7%	6.2%	1.2%	1.0%	1.0%	0.1%	0.3%	0.1%	0.3%	0.4%	0.0%	0.1%
Secondary Froth	100.0%	75.3%	10.9%	5.4%	1.0%	0.7%	3.3%	0.5%	0.6%	0.6%	0.1%	0.4%	0.2%	0.2%	0.2%	0.0%	0.2%
Middlings	100.0%	68.5%	21.9%	3.5%	2.7%	0.6%	0.8%	0.0%	0.4%	0.4%	0.2%	0.3%	0.1%	0.0%	0.1%	0.0%	0.1%
Tailings	100.0%	93.7%	3.6%	0.4%	0.7%	0.0%	0.1%	0.1%	0.1%	0.4%	0.0%	0.2%	0.1%	0.1%	0.0%	0.0%	0.1%
Ore	100.0%	83.0%	9.5%	1.8%	1.3%	0.3%	0.6%	0.3%	0.3%	1.4%	0.2%	0.4%	0.1%	0.1%	0.0%	0.0%	0.1%
Sum of Streams	100.0%	88.5%	6.8%	1.2%	1.0%	0.1%	0.5%	0.2%	0.2%	0.5%	0.0%	0.2%	0.1%	0.1%	0.0%	0.0%	0.1%
TOTAL	**DISTRIBUTION**																
Stream	**Sample Weight**	**SiO_2**	**Al_2O_3**	**Fe_2O_3**	**K_2O**	**MgO**	**TiO_2**	**ZrO_2**	**CaO**	**Cl**	**Na_2O**	**Cr_2O_3**	**CuO**	**P_2O_5**	**MnO**	**CoO**	**ZnO**
Primary Froth	4%	3%	7%	29%	5%	19%	53%	33%	21%	10%	9%	6%	5%	9%	39%	24%	5%
Secondary Froth	0%	0%	1%	2%	0%	2%	3%	1%	1%	1%	1%	1%	1%	1%	3%	0%	1%
Middlings	16%	12%	51%	44%	42%	62%	26%	0%	31%	14%	60%	23%	18%	5%	40%	43%	17%
Tailings	80%	84%	42%	25%	54%	17%	18%	67%	48%	76%	31%	70%	77%	84%	18%	33%	78%
Ore	100%	100%	100%	100%	100%	100%	100%	100%	100%	100%	100%	100%	100%	100%	100%	100%	100%
Sum of Streams	100%	100%	100%	100%	100%	100%	100%	100%	100%	100%	100%	100%	100%	100%	100%	100%	100%

Table A–13: Silicon balance around extraction

SiO_2	ASSAY										
Stream	**<0.2 µm**	**0.2-2 µm**	**<2 µm**	**2-45 µm**	**<45 µm**	**>45 µm**	**45-106 µm**	**>106 µm**	**106-250 µm**	**>250 µm**	**Total**
Primary Froth	44.0%	43.3%	43.5%	51.1%	48.9%	84.3%	68.1%	90.9%			66.9%
Secondary Froth			46.1%	43.0%	44.4%	90.2%					75.3%
Middlings	52.8%	55.1%	54.4%	78.3%	68.8%	56.1%					68.5%
Tailings	51.7%	61.7%	59.0%	91.2%	85.8%	95.0%	94.0%	95.4%	95.5%	77.3%	93.7%
Ore	52.9%	54.1%	53.8%	67.3%	63.0%	92.6%	90.9%	93.1%			83.0%
Sum of Streams	52.1%	55.7%	54.6%	82.3%	74.0%	94.5%	93.1%	95.2%	95.5%	77.3%	88.5%
SiO_2	**DISTRIBUTION**										
Stream	**<0.2 µm**	**0.2-2 µm**	**<2 µm**	**2-45 µm**	**<45 µm**	**>45 µm**	**45-106 µm**	**>106 µm**	**106-250 µm**	**>250 µm**	**Total**
Primary Froth	2%	7%	9%	26%	35%	65%	15%	50%	0%	0%	100%
Secondary Froth	0%	0%	9%	10%	19%	81%	0%	0%	0%	0%	100%
Middlings	9%	22%	31%	67%	98%	2%	0%	0%	0%	0%	100%
Tailings	0%	1%	2%	12%	13%	87%	21%	66%	66%	0%	100%
Ore	2%	5%	7%	18%	24%	76%	19%	57%	0%	0%	100%
Sum of Streams	1%	4%	5%	19%	24%	76%	18%	57%	55%	0%	100%

Table A–14: Aluminum balance around extraction

Al_2O_3	ASSAY										
Stream	**<0.2 µm**	**0.2-2 µm**	**<2 µm**	**2-45 µm**	**<45 µm**	**>45 µm**	**45-106 µm**	**>106 µm**	**106-250 µm**	**>250 µm**	**Total**
Primary Froth	25.1%	25.6%	25.5%	14.0%	17.4%	5.2%	7.5%	4.2%			11.2%
Secondary Froth			22.6%	23.8%	23.3%	4.9%					10.9%
Middlings	32.3%	31.7%	31.9%	14.9%	21.7%	31.6%					21.9%
Tailings	30.0%	25.6%	26.8%	5.4%	9.0%	2.7%	2.8%	2.6%	2.6%	6.2%	3.6%
Ore	30.1%	30.8%	30.6%	20.6%	23.8%	2.8%	4.1%	2.3%			9.5%
Sum of Streams	31.4%	29.8%	30.2%	10.4%	16.4%	2.9%	3.0%	2.7%	2.6%	6.2%	6.8%
Al_2O_3	**DISTRIBUTION**										
Stream	**<0.2 µm**	**0.2-2 µm**	**<2 µm**	**2-45 µm**	**<45 µm**	**>45 µm**	**45-106 µm**	**>106 µm**	**106-250 µm**	**>250 µm**	**Total**
Primary Froth	8%	25%	33%	43%	75%	24%	10%	14%	0%	0%	100%
Secondary Froth	0%	0%	30%	39%	69%	31%	0%	0%	0%	0%	100%
Middlings	17%	39%	57%	40%	97%	3%	0%	0%	0%	0%	100%
Tailings	6%	13%	18%	18%	36%	63%	16%	47%	46%	1%	100%
Ore	9%	24%	33%	47%	80%	20%	7%	12%	0%	0%	100%
Sum of Streams	12%	27%	39%	31%	70%	30%	8%	21%	20%	0%	100%

Table A–15: Iron balance around extraction

Fe_2O_3	ASSAY										
Stream	**<0.2 µm**	**0.2-2 µm**	**<2 µm**	**2-45 µm**	**<45 µm**	**>45 µm**	**45-106 µm**	**>106 µm**	**106-250 µm**	**>250 µm**	**Total**
Primary Froth	15.1%	14.5%	14.7%	15.9%	15.5%	2.1%	5.2%	0.8%			8.7%
Secondary Froth			13.1%	16.3%	14.8%	0.9%					5.4%
Middlings	6.7%	5.0%	5.5%	2.1%	3.4%	4.5%					3.5%
Tailings	7.6%	4.6%	5.4%	0.6%	1.4%	0.2%	0.2%	0.2%	0.1%	11.1%	0.4%
Ore	5.4%	6.0%	5.8%	4.4%	4.8%	0.4%	0.6%	0.4%			1.8%
Sum of Streams	7.4%	5.6%	6.2%	2.4%	3.5%	0.3%	0.4%	0.2%	0.1%	11.1%	1.2%
Fe_2O_3	DISTRIBUTION										
Stream	**<0.2 µm**	**0.2-2 µm**	**<2 µm**	**2-45 µm**	**<45 µm**	**>45 µm**	**45-106 µm**	**>106 µm**	**106-250 µm**	**>250 µm**	**Total**
Primary Froth	6%	18%	24%	63%	87%	12%	9%	3%	0%	0%	100%
Secondary Froth	0%	0%	34%	53%	88%	11%	0%	0%	0%	0%	100%
Middlings	23%	39%	62%	35%	97%	3%	0%	0%	0%	0%	100%
Tailings	13%	21%	34%	17%	51%	47%	11%	36%	23%	13%	100%
Ore	8%	24%	32%	52%	84%	15%	5%	10%	0%	0%	100%
Sum of Streams	15%	28%	44%	39%	83%	17%	5%	10%	6%	3%	100%

Table A–16: Potassium balance around extraction

K_2O	ASSAY										
Stream	**<0.2 µm**	**0.2-2 µm**	**<2 µm**	**2-45 µm**	**<45 µm**	**>45 µm**	**45-106 µm**	**>106 µm**	**106-250 µm**	**>250 µm**	**Total**
Primary Froth	2.5%	2.5%	2.5%	1.2%	1.6%	0.6%	0.7%	0.5%			1.1%
Secondary Froth			2.5%	1.0%	1.6%	0.6%					1.0%
Middlings	3.2%	3.4%	3.4%	2.2%	2.6%	2.8%					2.7%
Tailings	3.1%	3.1%	3.1%	1.2%	1.5%	0.5%	0.8%	0.5%	0.5%	1.1%	0.7%
Ore	3.8%	3.5%	3.6%	2.6%	2.9%	0.5%	0.8%	0.4%			1.3%
Sum of Streams	3.2%	3.3%	3.2%	1.6%	2.1%	0.5%	0.8%	0.5%	0.5%	1.1%	1.0%
K_2O	**DISTRIBUTION**										
Stream	**<0.2 µm**	**0.2-2 µm**	**<2 µm**	**2-45 µm**	**<45 µm**	**>45 µm**	**45-106 µm**	**>106 µm**	**106-250 µm**	**>250 µm**	**Total**
Primary Froth	8%	25%	33%	38%	71%	28%	10%	19%	0%	0%	100%
Secondary Froth	0%	0%	37%	18%	55%	44%	0%	0%	0%	0%	100%
Middlings	14%	35%	49%	48%	98%	3%	0%	0%	0%	0%	100%
Tailings	3%	8%	11%	20%	32%	67%	23%	44%	44%	1%	100%
Ore	8%	20%	28%	44%	72%	28%	11%	17%	0%	0%	100%
Sum of Streams	8%	20%	28%	33%	61%	39%	13%	25%	23%	0%	100%

Table A–17: Magnesium balance around extraction

MgO	ASSAY										
Stream	**<0.2 μm**	**0.2-2 μm**	**<2 μm**	**2-45 μm**	**<45 μm**	**>45 μm**	**45-106 μm**	**>106 μm**	**106-250 μm**	**>250 μm**	**Total**
Primary Froth	1.9%	1.3%	1.5%	1.1%	1.2%	0.2%	0.6%	0.0%			0.7%
Secondary Froth			3.5%	1.2%	2.2%	0.0%					0.7%
Middlings	1.8%	1.3%	1.4%	0.0%	0.6%	1.4%					0.6%
Tailings	1.7%	1.0%	1.2%	0.0%	0.2%	0.0%	0.0%	0.0%	0.0%	0.6%	0.0%
Ore	1.6%	1.4%	1.5%	0.9%	1.1%	0.0%	0.0%	0.0%			0.3%
Sum of Streams	1.8%	1.2%	1.4%	0.1%	0.5%	0.0%	0.0%	0.0%	0.0%	0.6%	0.1%
MgO	**DISTRIBUTION**										
Stream	**<0.2 μm**	**0.2-2 μm**	**<2 μm**	**2-45 μm**	**<45 μm**	**>45 μm**	**45-106 μm**	**>106 μm**	**106-250 μm**	**>250 μm**	**Total**
Primary Froth	10%	21%	32%	54%	85%	13%	13%	0%	0%	0%	100%
Secondary Froth	0%	0%	69%	28%	97%	0%	0%	0%	0%	0%	100%
Middlings	35%	59%	95%	0%	95%	6%	0%	0%	0%	0%	100%
Tailings	35%	54%	89%	0%	89%	8%	0%	8%	0%	8%	100%
Ore	14%	30%	44%	56%	100%	0%	0%	0%	0%	0%	100%
Sum of Streams	30%	50%	82%	11%	93%	7%	3%	1%	0%	1%	100%

Table A–18: Titanium balance around extraction

TiO_2	ASSAY									
Stream	**<0.2 µm**	**0.2-2 µm**	**<2 µm**	**2-45 µm**	**<45 µm**	**>45 µm**	**45-106 µm**	**>106 µm**	**106-250 µm**	**>250 µm**	**Total**
Primary Froth	1.0%	2.9%	2.4%	11.0%	8.5%	3.9%	10.1%	1.4%			6.2%
Secondary Froth			3.8%	9.5%	6.9%	1.6%					3.3%
Middlings	0.5%	1.2%	1.0%	0.7%	0.8%	1.0%					0.8%
Tailings	0.6%	1.2%	1.0%	0.4%	0.5%	0.0%	0.2%	0.0%	0.0%	0.2%	0.1%
Ore	0.7%	1.4%	1.2%	1.2%	1.2%	0.3%	0.7%	0.2%			0.6%
Sum of Streams	0.6%	1.3%	1.1%	1.3%	1.2%	0.2%	0.5%	0.0%	0.0%	0.2%	0.5%
TiO_2	**DISTRIBUTION**										
Stream	**<0.2 µm**	**0.2-2 µm**	**<2 µm**	**2-45 µm**	**<45 µm**	**>45 µm**	**45-106 µm**	**>106 µm**	**106-250 µm**	**>250 µm**	**Total**
Primary Froth	1%	5%	6%	61%	67%	33%	24%	9%	0%	0%	100%
Secondary Froth	0%	0%	16%	51%	68%	32%	0%	0%	0%	0%	100%
Middlings	8%	38%	46%	51%	97%	3%	0%	0%	0%	0%	100%
Tailings	4%	19%	22%	39%	61%	36%	35%	1%	0%	1%	100%
Ore	3%	17%	20%	45%	65%	35%	19%	16%	0%	0%	100%
Sum of Streams	3%	16%	20%	55%	74%	26%	19%	5%	0%	0%	100%

Table A–19: Zirconium balance around extraction

ZrO_2	ASSAY										
Stream	**<0.2 µm**	**0.2-2 µm**	**<2 µm**	**2-45 µm**	**<45 µm**	**>45 µm**	**45-106 µm**	**>106 µm**	**106-250 µm**	**>250 µm**	**Total**
Primary Froth	0.1%	0.1%	0.1%	1.4%	1.0%	1.4%	3.7%	0.5%			1.2%
Secondary Froth			0.0%	1.1%	0.6%	0.4%					0.5%
Middlings	0.0%	0.0%	0.0%	0.0%	0.0%	0.1%					0.0%
Tailings	0.0%	0.0%	0.0%	0.3%	0.2%	0.1%	0.3%	0.1%	0.1%	0.1%	0.1%
Ore	0.0%	0.0%	0.0%	0.1%	0.1%	0.5%	0.2%	0.6%			0.3%
Sum of Streams	0.0%	0.0%	0.0%	0.2%	0.2%	0.2%	0.4%	0.1%	0.1%	0.1%	0.2%
ZrO_2	DISTRIBUTION										
Stream	**<0.2 µm**	**0.2-2 µm**	**<2 µm**	**2-45 µm**	**<45 µm**	**>45 µm**	**45-106 µm**	**>106 µm**	**106-250 µm**	**>250 µm**	**Total**
Primary Froth	0%	1%	1%	39%	40%	59%	45%	14%	0%	0%	100%
Secondary Froth	0%	0%	0%	40%	40%	61%	0%	0%	0%	0%	100%
Middlings	0%	0%	0%	0%	0%	102%	0%	0%	0%	0%	100%
Tailings	0%	0%	0%	25%	25%	73%	40%	34%	33%	0%	100%
Ore	0%	0%	0%	9%	9%	91%	8%	83%	0%	0%	100%
Sum of Streams	0%	0%	0%	30%	30%	70%	41%	27%	22%	0%	100%

Table A–20: Calcium balance around extraction

CaO	ASSAY										
Stream	**<0.2 µm**	**0.2-2 µm**	**<2 µm**	**2-45 µm**	**<45 µm**	**>45 µm**	**45-106 µm**	**>106 µm**	**106-250 µm**	**>250 µm**	**Total**
Primary Froth	1.1%	1.7%	1.6%	1.7%	1.7%	0.3%	0.5%	0.2%			1.0%
Secondary Froth			1.6%	1.4%	1.5%	0.2%					0.6%
Middlings	0.8%	0.5%	0.6%	0.2%	0.4%	0.6%					0.4%
Tailings	0.9%	0.5%	0.6%	0.1%	0.2%	0.1%	0.1%	0.1%	0.1%	1.4%	0.1%
Ore	0.6%	0.6%	0.6%	0.5%	0.5%	0.1%	0.1%	0.1%			0.3%
Sum of Streams	0.8%	0.6%	0.7%	0.3%	0.4%	0.1%	0.1%	0.1%	0.1%	1.4%	0.2%
CaO	**DISTRIBUTION**										
Stream	**<0.2 µm**	**0.2-2 µm**	**<2 µm**	**2-45 µm**	**<45 µm**	**>45 µm**	**45-106 µm**	**>106 µm**	**106-250 µm**	**>250 µm**	**Total**
Primary Froth	4%	19%	23%	60%	82%	17%	8%	9%	0%	0%	100%
Secondary Froth	0%	0%	36%	40%	76%	23%	0%	0%	0%	0%	100%
Middlings	24%	38%	62%	34%	96%	4%	0%	0%	0%	0%	100%
Tailings	5%	7%	12%	13%	25%	74%	20%	54%	49%	5%	100%
Ore	7%	17%	24%	42%	66%	34%	8%	26%	0%	0%	100%
Sum of Streams	11%	19%	30%	29%	59%	41%	11%	28%	23%	3%	100%

Table A–21: Chlorine balance around extraction

Cl	**ASSAY**										
Stream	**<0.2 µm**	**0.2-2 µm**	**<2 µm**	**2-45 µm**	**<45 µm**	**>45 µm**	**45-106 µm**	**>106 µm**	**106-250 µm**	**>250 µm**	**Total**
Primary Froth	5.5%	4.6%	4.9%	0.4%	1.7%	0.4%	0.4%	0.4%			1.0%
Secondary Froth			2.1%	0.5%	1.2%	0.3%					0.6%
Middlings	0.4%	0.4%	0.4%	0.4%	0.4%	0.4%					0.4%
Tailings	0.7%	0.9%	0.8%	0.3%	0.4%	0.4%	0.4%	0.4%	0.4%	0.4%	0.4%
Ore	0.5%	0.6%	0.6%	0.6%	0.6%	1.7%	1.7%	1.7%			1.4%
Sum of Streams	0.8%	0.8%	0.8%	0.3%	0.5%	0.4%	0.4%	0.4%	0.4%	0.4%	0.5%
Cl	**DISTRIBUTION**										
Stream	**<0.2 µm**	**0.2-2 µm**	**<2 µm**	**2-45 µm**	**<45 µm**	**>45 µm**	**45-106 µm**	**>106 µm**	**106-250 µm**	**>250 µm**	**Total**
Primary Froth	19%	48%	67%	12%	79%	20%	5%	15%	0%	0%	100%
Secondary Froth	0%	0%	47%	13%	60%	37%	0%	0%	0%	0%	100%
Middlings	11%	23%	35%	63%	98%	2%	0%	0%	0%	0%	100%
Tailings	1%	4%	5%	7%	12%	88%	21%	68%	67%	0%	100%
Ore	1%	3%	4%	10%	15%	85%	21%	65%	0%	0%	100%
Sum of Streams	4%	11%	15%	16%	31%	69%	16%	52%	51%	0%	100%

Table A–22: Sodium balance around extraction

Na_2O	ASSAY									
Stream	**<0.2 µm**	**0.2-2 µm**	**<2 µm**	**2-45 µm**	**<45 µm**	**>45 µm**	**45-106 µm**	**>106 µm**	**106-250 µm**	**>250 µm**	**Total**
Primary Froth	0.2%	0.1%	0.1%	0.1%	0.1%	0.1%	0.2%	0.0%			0.1%
Secondary Froth			0.0%	0.1%	0.1%	0.2%					0.1%
Middlings	0.5%	0.1%	0.2%	0.1%	0.2%	0.4%					0.2%
Tailings	0.1%	0.1%	0.1%	0.1%	0.1%	0.0%	0.0%	0.0%	0.0%	0.1%	0.0%
Ore	2.9%	0.1%	0.9%	0.4%	0.5%	0.1%	0.1%	0.1%			0.2%
Sum of Streams	0.4%	0.1%	0.2%	0.1%	0.1%	0.0%	0.0%	0.0%	0.0%	0.1%	0.0%
Na_2O	DISTRIBUTION										
Stream	**<0.2 µm**	**0.2-2 µm**	**<2 µm**	**2-45 µm**	**<45 µm**	**>45 µm**	**45-106 µm**	**>106 µm**	**106-250 µm**	**>250 µm**	**Total**
Primary Froth	8%	14%	22%	48%	70%	28%	28%	0%	0%	0%	100%
Secondary Froth	0%	0%	0%	20%	20%	81%	0%	0%	0%	0%	100%
Middlings	33%	18%	50%	44%	95%	5%	0%	0%	0%	0%	100%
Tailings	4%	7%	12%	82%	94%	2%	0%	2%	0%	2%	100%
Ore	34%	3%	37%	34%	71%	29%	4%	25%	0%	0%	100%
Sum of Streams	22%	14%	36%	57%	93%	7%	2%	1%	0%	1%	100%

Table A–23: Chromium balance around extraction

Cr_2O_3	ASSAY										
Stream	**<0.2 µm**	**0.2-2 µm**	**<2 µm**	**2-45 µm**	**<45 µm**	**>45 µm**	**45-106 µm**	**>106 µm**	**106-250 µm**	**>250 µm**	**Total**
Primary Froth	0.7%	0.7%	0.7%	0.3%	0.4%	0.2%	0.2%	0.2%			0.3%
Secondary Froth			1.7%	0.2%	0.9%	0.2%					0.4%
Middlings	0.2%	0.6%	0.5%	0.2%	0.3%	0.2%					0.3%
Tailings	0.7%	0.7%	0.7%	0.2%	0.3%	0.2%	0.2%	0.2%	0.2%	0.2%	0.2%
Ore	0.7%	0.7%	0.7%	0.3%	0.5%	0.4%	0.5%	0.4%			0.4%
Sum of Streams	0.3%	0.7%	0.6%	0.2%	0.3%	0.2%	0.2%	0.2%	0.2%	0.2%	0.2%
Cr_2O_3	**DISTRIBUTION**										
Stream	**<0.2 µm**	**0.2-2 µm**	**<2 µm**	**2-45 µm**	**<45 µm**	**>45 µm**	**45-106 µm**	**>106 µm**	**106-250 µm**	**>250 µm**	**Total**
Primary Froth	9%	28%	37%	32%	69%	31%	10%	21%	0%	0%	100%
Secondary Froth	0%	0%	61%	9%	69%	28%	0%	0%	0%	0%	100%
Middlings	7%	57%	64%	34%	98%	1%	0%	0%	0%	0%	100%
Tailings	3%	7%	10%	11%	20%	79%	19%	61%	61%	0%	100%
Ore	4%	12%	16%	17%	33%	67%	20%	47%	0%	0%	100%
Sum of Streams	4%	20%	24%	18%	42%	58%	14%	44%	43%	0%	100%

Table A–24: Copper balance around extraction

CuO	ASSAY										
Stream	**<0.2 µm**	**0.2-2 µm**	**<2 µm**	**2-45 µm**	**<45 µm**	**>45 µm**	**45-106 µm**	**>106 µm**	**106-250 µm**	**>250 µm**	**Total**
Primary Froth	0.1%	0.1%	0.1%	0.2%	0.2%	0.1%	0.1%	0.1%			0.1%
Secondary Froth			0.4%	0.2%	0.3%	0.1%					0.2%
Middlings	0.1%	0.1%	0.1%	0.1%	0.1%	0.2%					0.1%
Tailings	0.3%	0.2%	0.2%	0.1%	0.1%	0.1%	0.1%	0.1%	0.1%	0.1%	0.1%
Ore	0.1%	0.1%	0.1%	0.1%	0.1%	0.1%	0.1%	0.1%			0.1%
Sum of Streams	0.2%	0.1%	0.1%	0.1%	0.1%	0.1%	0.1%	0.1%	0.1%	0.1%	0.1%
CuO	**DISTRIBUTION**										
Stream	**<0.2 µm**	**0.2-2 µm**	**<2 µm**	**2-45 µm**	**<45 µm**	**>45 µm**	**45-106 µm**	**>106 µm**	**106-250 µm**	**>250 µm**	**Total**
Primary Froth	3%	10%	12%	43%	55%	45%	12%	32%	0%	0%	100%
Secondary Froth	0%	0%	34%	21%	55%	44%	0%	0%	0%	0%	100%
Middlings	12%	24%	36%	61%	97%	3%	0%	0%	0%	0%	100%
Tailings	2%	3%	5%	13%	18%	82%	21%	60%	60%	0%	100%
Ore	3%	9%	12%	26%	38%	62%	16%	46%	0%	0%	100%
Sum of Streams	4%	7%	11%	23%	34%	66%	17%	48%	46%	0%	100%

Table A–25: Phosphorous balance around extraction

P_2O_5	ASSAY										
Stream	**<0.2 µm**	**0.2-2 µm**	**<2 µm**	**2-45 µm**	**<45 µm**	**>45 µm**	**45-106 µm**	**>106 µm**	**106-250 µm**	**>250 µm**	**Total**
Primary Froth	0.3%	0.4%	0.3%	0.4%	0.4%	0.1%	0.3%	0.1%			0.3%
Secondary Froth			0.5%	0.3%	0.4%	0.1%					0.2%
Middlings	0.1%	0.1%	0.1%	0.0%	0.0%	0.1%					0.0%
Tailings	0.1%	0.1%	0.1%	0.0%	0.0%	0.1%	0.3%	0.1%	0.1%	0.1%	0.1%
Ore	0.1%	0.2%	0.2%	0.1%	0.2%	0.1%	0.0%	0.1%			0.1%
Sum of Streams	0.1%	0.1%	0.1%	0.0%	0.1%	0.1%	0.3%	0.1%	0.1%	0.1%	0.1%
P_2O_5	**DISTRIBUTION**										
Stream	**<0.2 µm**	**0.2-2 µm**	**<2 µm**	**2-45 µm**	**<45 µm**	**>45 µm**	**45-106 µm**	**>106 µm**	**106-250 µm**	**>250 µm**	**Total**
Primary Froth	4%	15%	19%	52%	71%	28%	17%	11%	0%	0%	100%
Secondary Froth	0%	0%	31%	26%	57%	43%	0%	0%	0%	0%	100%
Middlings	35%	57%	92%	0%	92%	8%	0%	0%	0%	0%	100%
Tailings	1%	2%	2%	0%	2%	98%	40%	58%	57%	0%	100%
Ore	3%	17%	20%	31%	51%	49%	0%	49%	0%	0%	100%
Sum of Streams	3%	6%	9%	5%	14%	86%	35%	50%	48%	0%	100%

Table A–26: Manganese balance around extraction

MnO	**ASSAY**										
Stream	**<0.2 µm**	**0.2-2 µm**	**<2 µm**	**2-45 µm**	**<45 µm**	**>45 µm**	**45-106 µm**	**>106 µm**	**106-250 µm**	**>250 µm**	**Total**
Primary Froth	0.3%	0.5%	0.5%	0.8%	0.7%	0.1%	0.2%	0.0%			0.4%
Secondary Froth			0.6%	0.8%	0.7%	0.0%					0.2%
Middlings	0.2%	0.1%	0.1%	0.1%	0.1%	0.1%					0.1%
Tailings	0.1%	0.1%	0.1%	0.0%	0.0%	0.0%	0.0%	0.0%	0.0%	0.3%	0.0%
Ore	0.1%	0.1%	0.1%	0.1%	0.1%	0.0%	0.0%	0.0%			0.0%
Sum of Streams	0.2%	0.1%	0.2%	0.1%	0.1%	0.0%	0.0%	0.0%	0.0%	0.3%	0.0%
MnO	**DISTRIBUTION**										
Stream	**<0.2 µm**	**0.2-2 µm**	**<2 µm**	**2-45 µm**	**<45 µm**	**>45 µm**	**45-106 µm**	**>106 µm**	**106-250 µm**	**>250 µm**	**Total**
Primary Froth	3%	14%	17%	70%	87%	12%	9%	4%	0%	0%	100%
Secondary Froth	0%	0%	35%	54%	89%	10%	0%	0%	0%	0%	100%
Middlings	19%	32%	51%	47%	98%	2%	0%	0%	0%	0%	100%
Tailings	10%	16%	26%	18%	44%	53%	20%	34%	19%	15%	100%
Ore	4%	18%	22%	67%	89%	11%	6%	5%	0%	0%	100%
Sum of Streams	10%	22%	33%	51%	84%	16%	7%	8%	3%	3%	100%

Table A–27: Zinc balance around extraction

ZnO	ASSAY										
Stream	**<0.2 µm**	**0.2-2 µm**	**<2 µm**	**2-45 µm**	**<45 µm**	**>45 µm**	**45-106 µm**	**>106 µm**	**106-250 µm**	**>250 µm**	**Total**
Primary Froth	0.1%	0.1%	0.1%	0.2%	0.2%	0.1%	0.2%	0.1%			0.1%
Secondary Froth			0.4%	0.2%	0.3%	0.2%					0.2%
Middlings	0.2%	0.1%	0.1%	0.2%	0.1%	0.2%					0.1%
Tailings	0.2%	0.2%	0.2%	0.2%	0.2%	0.1%	0.1%	0.1%	0.1%	0.2%	0.1%
Ore	0.2%	0.1%	0.1%	0.1%	0.1%	0.2%	0.1%	0.2%			0.1%
Sum of Streams	0.2%	0.1%	0.1%	0.2%	0.2%	0.1%	0.1%	0.1%	0.1%	0.2%	0.1%
ZnO	**DISTRIBUTION**										
Stream	**<0.2 µm**	**0.2-2 µm**	**<2 µm**	**2-45 µm**	**<45 µm**	**>45 µm**	**45-106 µm**	**>106 µm**	**106-250 µm**	**>250 µm**	**Total**
Primary Froth	3%	8%	12%	39%	50%	50%	18%	32%	0%	0%	100%
Secondary Froth	0%	0%	25%	13%	38%	61%	0%	0%	0%	0%	100%
Middlings	13%	18%	31%	66%	97%	3%	0%	0%	0%	0%	100%
Tailings	1%	2%	3%	16%	19%	81%	20%	60%	60%	1%	100%
Ore	3%	6%	9%	17%	26%	74%	9%	64%	0%	0%	100%
Sum of Streams	3%	5%	8%	26%	34%	66%	17%	48%	46%	1%	100%

Table A–28: XRD results that best match XRF results for ore and froth samples

	Ore			Primary Froth			Secondary Froth	
	>106 µm	45-106 µm	2-45 µm	>106 µm	45-106 µm	2-45 µm	>45 µm	2-45 µm
Quartz	99±15	95±15	43±7	97±15	71±11	40±6	94±15	34±6
Microcline	1±1	1±1	6±2	1±1	4±1	8±2	2±1	3±1
Plagioclase		trace	1±1		1±1	trace		
Siderite			2±1		2±1	8±2	trace	11±1
Chlorite			3±2			2±1		2±1
Kaolinite		2±1	30±5		2±1	13±2	trace	31±5
Muscovite		1±1	13±2		2±1	7±2	1±1	5±1
Pyrite					1±1	3±1	trace	1±1
Anatase			1±1	trace	2±1	4±1	trace	4±1
Brookite					1±1	3±1	trace	1±1
Ilmenite				trace	3±1	2±1	trace	1±1
Rutile			trace	trace	4±1	4±1	1±1	3±1
Schorl				1±1	4±1	3±1	1±1	2±1
Zircon					4±1	3±1	trace	2±1

Table A–29: XRD results that best match XRF results for middlings and tailings samples

	Middlings		Tailings			
	>45 µm	2-45 µm	>250 µm	250-106 µm	45-106 µm	2-45 µm
Anatase	2±1	Trace				
Chlorite IIb-2	6±2	3±1				
Pyrite		Trace	2±1			
Quartz	23±4	58±9	73±11	98±15	93±14	88±14
Rutile	1±1	Trace				trace
Schorl	4±1			trace		
Siderite	1±1	1±1	13±2			
Zircon	1±1		trace			
Feldspar		2±1	2±1		1±1	1±1
Illite	15±3	16±3	3±1		1±1	5±1
Kaolinite	47±8	20±3	2±1		1±1	2±1
K-Feldspar			5±1	2±1	4±1	4±1

Table A–30: XRD results based on the average of all refined data for non-clay size fractions of ore and froth samples

	Ore			Primary Froth			Secondary Froth	
Phase Name	>106 µm	45-106 µm	2-45 µm	>106 µm	45-106 µm	2-45 µm	>45 µm	2-45 µm
Anatase			1±1	trace	1±1	4±1	trace	4±1
Ankerite		trace	1±1					1±1
Brookite	trace		trace		1±1	2±1	trace	1±1
Chlorite			3±2			3±2		4±2
Corundum	1±1	1±1	1±1	2±1	3±1	3±1	2±1	10±2
Ilmenite			trace	trace	3±1	1±1	trace	1±1
Magnetite						1±1		1±1
Orthoclase				2±1	2±1			
Pyrite	trace		trace	trace	1±1	2±1	trace	1±1
Quartz	97±15	91±14	42±7	90±14	65±10	39±6	90±14	31±5
Rhodochrosite			1±1			5±1		6±1
Rutile	trace	trace	trace	trace	4±1	4±1	1±1	3±1
Schorl	trace	trace	1±2	1±1	3±1	3±1	1±1	3±1
Siderite	trace	trace	2±1	trace	1±1	8±3	trace	9±2
Zircon	trace	trace	trace		4±1	2±1	trace	2±1
Illite		1±1	16±5	1±1	3±2	6±3	1±1	6±2
Microcline	1±1	2±1	5±2	2±1	3±2	4±3	2±1	3±2
Kaolinite	trace	3±2	25±6	trace	5±6	11±4	1±1	13±10
Plagioclase	trace	trace	1±2	trace	1±1	1±1		1±1
Sanidine						1±1	1±1	

Table A–31: XRD results based on the average of all refined data for non-clay size fractions of middlings and tailings samples

	Middlings		Tailings			
Phase Name	>45 µm	2-45 µm	>250 µm	250-106 µm	45-106 µm	2-45 µm
Anatase	2±1	1±1				
Ankerite		Trace	trace	trace	trace	trace
Chlorite IIb-2	9±4	3±2				1±1
Corundum	6±1	2±1	2±1	2±2	1±1	1±1
Orthoclase					1±1	
Pyrite			2±1			
Quartz	22±4	59±9	79±12	95±14	86±13	85±13
Rhodochrosite						
Rutile	1±1	Trace	trace	trace	trace	trace
Schorl	4±1					
Siderite	1±1	1±1	7±3	1±1		
Zircon	1±1		trace			
Illite	16±4	13±2	2±1		1±1	4±2
Microcline	9±1	4±2	4±1	2±1	3±1	4±2
Kaolinite	28±12	13±4	1±1		6±8	4±3
Plagioclase		2±2	1±1		2±4	1±1
Sanidine		2±1			1±1	

Table A–32: XRD results for clay fractions of oil sands streams

	0.2-2 µm				<0.2 µm				<2 µm
	Middlings	**Ore**	**Primary Froth**	**Tailings**	**Middlings**	**Ore**	**Primary Froth**	**Tailings**	**Secondary Froth**
Chlorite	6±2	6±2	9±2	5±2					6±2
Kaolinite-Smectite	9±2	12±2	10±2	5±2	21±2	24±2	25±2	19±2	15±2
Kaolinite	28±2	23±2	37±2	24±2	13±2	14±2	19±2	15±2	38±2
Illite-Smectite	22±5	27±5	10±5	18±5	53±5	46±5	41±5	54±5	9±5
Illite	26±5	24±5	24±5	18±5	12±5	14±5	14±5	13±5	20±5
Anatase	trace	1±1	trace	1±0	2±0		1±0		
Lepidocrocite		2±0			1±0	1±0	1±0	trace	
Pyrite	trace	Trace	trace						
Quartz	5±1	5±1	6±1	28±4	7±1	1±0	1±0		trace
Rutile	trace	1±0	trace	trace	1±0		trace		
siderite	1±0	2±0	1±0	trace	trace			trace	
Ankerite					trace			1±0	
% non-clay	6±2	11±3	9±2	30±4	11±2	2±1	2±1	1±0	0±0

Table A–33: Abbreviations used in mineral balance tables

Mineral Name	Abbreviation
Anatase	Anat.
Ankerite	Ank.
Brookite	Brook.
Chlorite	C.
Illite	Ill.
Illite-Smectite	I-S
Ilmenite	Ilm.
Kaolinite	K.
Kaolinite-Smectite	K-S
Lepidocrocite	Lep.
Microcline	Mic.
Plagioclase Oligoclase	Plag.
Pyrite	Pyr.
Quartz	Q
Rutile	Rut.
Schorl	Sch.
Siderite	Sid.
Zircon	Zr.

Table A–34: Mineral balance around extraction for <0.2 µm size fraction

<0.2 µm	ASSAY																		
Stream	**Anat.**	**Ank.**	**Brook.**	**C.**	**Ill.**	**I-S**	**Ilm.**	**K.**	**K-S**	**Lep.**	**Mic.**	**Plag.**	**Pyr.**	**Q**	**Rut.**	**Sch.**	**Sid.**	**Zr.**	**Total Stream**
Primary Froth	0.8%	0.0%	0.0%	0.0%	13.6%	40.8%	0.0%	18.7%	24.6%	0.8%	0.0%	0.0%	0.0%	0.5%	0.1%	0.0%	0.0%	0.0%	100.0%
Secondary Froth																			
Middlings	0.0%	0.9%	0.0%	0.0%	12.1%	52.6%	0.0%	13.3%	20.9%	0.1%	0.0%	0.0%	0.0%	0.0%	0.0%	0.0%	0.1%	0.0%	100.0%
Tailings	0.0%	0.0%	0.0%	0.0%	12.7%	53.6%	0.0%	14.9%	18.7%	0.0%	0.0%	0.0%	0.0%	0.2%	0.0%	0.0%	0.0%	0.0%	100.0%
Sum of streams	0.0%	0.6%	0.0%	0.0%	12.3%	52.1%	0.0%	14.0%	20.7%	0.1%	0.0%	0.0%	0.0%	0.1%	0.0%	0.0%	0.1%	0.0%	100.0%
Ore	0.0%	0.0%	0.0%	0.0%	13.6%	46.0%	0.0%	14.2%	24.3%	0.7%	0.0%	0.0%	0.0%	1.2%	0.0%	0.0%	0.0%	0.0%	100.0%
<0.2 µm	**DISTRIBUTION**																		
Stream	**Anat.**	**Ank.**	**Brook.**	**C.**	**Ill.**	**I-S**	**Ilm.**	**K.**	**K-S**	**Lep.**	**Mic.**	**Plag.**	**Pyr.**	**Q**	**Rut.**	**Sch.**	**Sid.**	**Zr.**	**Total Stream**
Primary Froth	100%	0%			7%	5%		8%	7%	33%				39%	100%		0%		6%
Secondary Froth	0%	0%			0%	0%		0%	0%	0%				0%	0%		0%		0%
Middlings	0%	100%			72%	74%		70%	74%	67%				0%	0%		100%		73%
Tailings	0%	0%			22%	22%		22%	19%	0%				61%	0%		0%		21%
Sum of streams	100%	100%			100%	100%		100%	100%	100%				100%	100%		100%		100%
Ore	100%	100%	100%	100%	100%	100%	100%	100%	100%	100%	100%	100%	100%	100%	100%	100%	100%	100%	100%

Table A–35: Mineral balance around extraction for 0.2-2 µm size fraction

0.2-2 µm	ASSAY																		
Stream	**Anat.**	**Ank.**	**Brook.**	**C.**	**Ill.**	**I-S**	**Ilm.**	**K.**	**K-S**	**Lep.**	**Mic.**	**Plag.**	**Pyr.**	**Q**	**Rut.**	**Sch.**	**Sid.**	**Zr.**	**Total Stream**
Primary Froth	1.3%	0.0%	0.0%	8.5%	24.3%	9.8%	0.0%	36.5%	9.7%	2.2%	0.0%	0.0%	0.2%	5.0%	0.6%	0.0%	1.9%	0.0%	100.0%
Secondary Froth																			
Middlings	0.3%	0.0%	0.0%	6.0%	26.4%	21.5%	0.0%	28.4%	9.0%	0.0%	0.0%	0.0%	0.1%	6.4%	0.3%	0.0%	1.5%	0.0%	100.0%
Tailings	0.6%	0.0%	0.0%	4.7%	18.3%	17.8%	0.0%	24.3%	5.5%	0.0%	0.0%	0.0%	0.0%	28.2%	0.4%	0.0%	0.3%	0.0%	100.0%
Sum of streams	0.5%	0.0%	0.0%	5.9%	24.4%	19.8%	0.0%	28.0%	8.3%	0.2%	0.0%	0.0%	0.1%	11.3%	0.4%	0.0%	1.2%	0.0%	100.0%
Ore	0.5%	0.0%	0.0%	6.4%	24.5%	27.4%	0.0%	23.4%	12.0%	0.0%	0.0%	0.0%	0.2%	4.6%	0.2%	0.0%	0.9%	0.0%	100.0%
0.2-2 µm	**DISTRIBUTION**																		
Stream	**Anat.**	**Ank.**	**Brook.**	**C.**	**Ill.**	**I-S**	**Ilm.**	**K.**	**K-S**	**Lep.**	**Mic.**	**Plag.**	**Pyr.**	**Q**	**Rut.**	**Sch.**	**Sid.**	**Zr.**	**Total Stream**
Primary Froth	20%			11%	7%	4%		10%	9%	100%			17%	3%	13%		11%		7%
Secondary Froth	0%			0%	0%	0%		0%	0%	0%			0%	0%	0%		0%		0%
Middlings	49%			71%	75%	76%		71%	76%	0%			83%	39%	63%		84%		70%
Tailings	31%			19%	17%	21%		20%	15%	0%			0%	57%	25%		5%		23%
Sum of streams	100%			100%	100%	100%		100%	100%	100%			100%	100%	100%		100%		100%
Ore	100%	100%	100%	100%	100%	100%	100%	100%	100%	100%	100%	100%	100%	100%	100%	100%	100%	100%	100%

Table A–36: Mineral balance around extraction for <2 µm size fraction

<2 µm	ASSAY																		
Stream	**Anat.**	**Ank.**	**Brook.**	**C.**	**Ill.**	**I-S**	**Ilm.**	**K.**	**K-S**	**Lep.**	**Mic.**	**Plag.**	**Pyr.**	**Q**	**Rut.**	**Sch.**	**Sid.**	**Zr.**	**Total Stream**
Primary Froth	1.2%	0.0%	0.0%	6.4%	21.6%	17.6%	0.0%	32.1%	13.4%	1.8%	0.0%	0.0%	0.1%	3.8%	0.5%	0.0%	1.4%	0.0%	100.0%
Secondary Froth	1.6%	0.2%	0.0%	6.0%	19.6%	9.4%	0.0%	38.2%	15.4%	1.3%	0.0%	0.0%	0.0%	7.0%	0.9%	0.0%	0.4%	0.0%	100.0%
Middlings	0.2%	0.3%	0.0%	4.2%	22.1%	30.9%	0.0%	23.8%	12.6%	0.0%	0.0%	0.0%	0.1%	4.5%	0.2%	0.0%	1.1%	0.0%	100.0%
Tailings	0.5%	0.0%	0.0%	3.4%	16.7%	27.6%	0.0%	21.7%	9.1%	0.0%	0.0%	0.0%	0.0%	20.5%	0.3%	0.0%	0.2%	0.0%	100.0%
Sum of streams	0.4%	0.2%	0.0%	4.2%	20.8%	29.1%	0.0%	24.0%	11.9%	0.2%	0.0%	0.0%	0.1%	8.0%	0.3%	0.0%	0.9%	0.0%	100.0%
Ore	0.3%	0.0%	0.0%	4.6%	21.4%	32.6%	0.0%	20.8%	15.4%	0.2%	0.0%	0.0%	0.1%	3.6%	0.2%	0.0%	0.6%	0.0%	100.0%
<2 µm	DISTRIBUTION																		
Stream	**Anat.**	**Ank.**	**Brook.**	**C.**	**Ill.**	**I-S**	**Ilm.**	**K.**	**K-S**	**Lep.**	**Mic.**	**Plag.**	**Pyr.**	**Q**	**Rut.**	**Sch.**	**Sid.**	**Zr.**	**Total Stream**
Primary Froth	23%	0%		11%	7%	4%		9%	8%	77%			17%	3%	13%		11%		7%
Secondary Froth	3%	1%		1%	1%	0%		1%	1%	6%			0%	1%	2%		0%		1%
Middlings	46%	99%		70%	74%	75%		70%	74%	17%			83%	39%	61%		84%		70%
Tailings	28%	0%		18%	18%	21%		20%	17%	0%			0%	57%	24%		5%		22%
Sum of streams	100%	100%		100%	100%	100%		100%	100%	100%			100%	100%	100%		100%		100%
Ore	100%	100%	100%	100%	100%	100%	100%	100%	100%	100%	100%	100%	100%	100%	100%	100%	100%	100%	100%

Table A–37: Mineral balance around extraction for 2-45 µm size fraction

2-45 µm	ASSAY																		
Stream	Anat.	Ank.	Brook.	C.	Ill.	I-S	Ilm.	K.	K-S	Lep.	Mic.	Plag.	Pyr.	Q	Rut.	Sch.	Sid.	Zr.	Total Stream
Primary Froth	4.0%	0.0%	3.0%	2.0%	7.0%	0.0%	2.0%	13.0%	0.0%	0.0%	8.0%	0.0%	3.0%	40.0%	4.0%	3.0%	8.0%	3.0%	100.0%
Secondary Froth	4.0%	0.0%	1.0%	2.0%	5.0%	0.0%	1.0%	31.0%	0.0%	0.0%	3.0%	0.0%	1.0%	34.0%	3.0%	2.0%	11.0%	2.0%	100.0%
Middlings	0.0%	0.0%	0.0%	3.0%	16.0%	0.0%	0.0%	20.0%	0.0%	0.0%	0.0%	2.0%	0.0%	58.0%	0.0%	0.0%	1.0%	0.0%	100.0%
Tailings	0.0%	0.0%	0.0%	0.0%	5.0%	0.0%	0.0%	2.0%	0.0%	0.0%	4.0%	1.0%	0.0%	88.0%	0.0%	0.0%	0.0%	0.0%	100.0%
Sum of streams	0.3%	0.0%	0.2%	1.5%	10.2%	0.0%	0.1%	11.1%	0.0%	0.0%	2.4%	1.4%	0.2%	70.7%	0.3%	0.2%	1.1%	0.2%	100.0%
Ore	1.0%	0.0%	0.0%	3.0%	13.1%	0.0%	0.0%	30.3%	0.0%	0.0%	6.1%	1.0%	0.0%	43.4%	0.0%	0.0%	2.0%	0.0%	100.0%
2-45 µm	DISTRIBUTION																		
Stream	Anat.	Ank.	Brook.	C.	Ill.	I-S	Ilm.	K.	K-S	Lep.	Mic.	Plag.	Pyr.	Q	Rut.	Sch.	Sid.	Zr.	Total Stream
Primary Froth	95%		98%	9%	5%		97%	8%			23%	0%	98%	4%	96%	96%	53%	96%	7%
Secondary Froth	5%		2%	1%	0%		3%	1%			0%	0%	2%	0%	4%	4%	4%	4%	0%
Middlings	0%		0%	90%	72%		0%	82%			0%	66%	0%	38%	0%	0%	43%	0%	46%
Tailings	0%		0%	0%	23%		0%	8%			77%	34%	0%	58%	0%	0%	0%	0%	47%
Sum of streams	100%		100%	100%	100%		100%	100%			100%	100%	100%	100%	100%	100%	100%	100%	100%
Ore	100%	100%	100%	100%	100%	100%	100%	100%	100%	100%	100%	100%	100%	100%	100%	100%	100%	100%	100%

Table A–38: Mineral balance around extraction for <45 µm size fraction

<45 µm	ASSAY																		
Stream	Anat.	Ank.	Brook.	C.	Ill.	I-S	Ilm.	K.	K-S	Lep.	Mic.	Plag.	Pyr.	Q	Rut.	Sch.	Sid.	Zr.	Total Stream
Primary Froth	3.2%	0.0%	2.1%	3.3%	11.3%	5.2%	1.4%	18.7%	4.0%	0.5%	5.6%	0.0%	2.1%	29.3%	3.0%	2.1%	6.1%	2.1%	100.0%
Secondary Froth	2.9%	0.1%	0.6%	3.8%	11.5%	4.2%	0.6%	34.2%	6.9%	0.6%	1.7%	0.0%	0.6%	22.0%	2.1%	1.1%	6.3%	1.1%	100.0%
Middlings	0.1%	0.1%	0.0%	3.5%	18.4%	12.3%	0.0%	21.5%	5.0%	0.0%	0.0%	1.2%	0.0%	36.7%	0.1%	0.0%	1.0%	0.0%	100.0%
Tailings	0.1%	0.0%	0.0%	0.6%	7.0%	4.7%	0.0%	5.3%	1.5%	0.0%	3.3%	0.8%	0.0%	76.5%	0.0%	0.0%	0.0%	0.0%	100.0%
Sum of streams	0.3%	0.1%	0.1%	2.3%	13.4%	8.8%	0.1%	15.0%	3.6%	0.0%	1.7%	1.0%	0.2%	51.8%	0.3%	0.2%	1.0%	0.2%	100.0%
Ore	0.8%	0.0%	0.0%	3.5%	15.8%	10.4%	0.0%	27.3%	4.9%	0.1%	4.1%	0.7%	0.0%	30.7%	0.1%	0.0%	1.6%	0.0%	100.0%
<45 µm	DISTRIBUTION																		
Stream	Anat.	Ank.	Brook.	C.	Ill.	I-S	Ilm.	K.	K-S	Lep.	Mic.	Plag.	Pyr.	Q	Rut.	Sch.	Sid.	Zr.	Total Stream
Primary Froth	70%	0%	98%	10%	6%	4%	97%	9%	8%	77%	23%	0%	90%	4%	73%	96%	42%	96%	7%
Secondary Froth	5%	1%	2%	1%	0%	0%	3%	1%	1%	6%	0%	0%	2%	0%	4%	4%	3%	4%	0%
Middlings	16%	99%	0%	79%	73%	75%	0%	76%	74%	17%	0%	66%	8%	38%	17%	0%	54%	0%	53%
Tailings	10%	0%	0%	10%	21%	21%	0%	14%	17%	0%	77%	34%	0%	58%	7%	0%	1%	0%	39%
Sum of streams	100%	100%	100%	100%	100%	100%	100%	100%	100%	100%	100%	100%	100%	100%	100%	100%	100%	100%	100%
Ore	100%	100%	100%	100%	100%	100%	100%	100%	100%	100%	100%	100%	100%	100%	100%	100%	100%	100%	100%

Table A–39: Mineral balance around extraction for >45 µm size fraction

>45 µm	ASSAY																		
Stream	**Anat.**	**Ank.**	**Brook.**	**C.**	**Ill.**	**I-S**	**Ilm.**	**K.**	**K-S**	**Lep.**	**Mic.**	**Plag.**	**Pyr.**	**Q**	**Rut.**	**Sch.**	**Sid.**	**Zr.**	**Total Stream**
Primary Froth	0.6%	0.0%	0.3%	0.0%	0.6%	0.0%	0.9%	0.6%	0.0%	0.0%	1.9%	0.3%	0.3%	89.9%	1.2%	1.9%	0.6%	1.2%	100.0%
Secondary Froth	0.0%	0.0%	0.0%	0.0%	1.0%	0.0%	0.0%	0.0%	0.0%	0.0%	2.0%	0.0%	0.0%	94.9%	1.0%	1.0%	0.0%	0.0%	100.0%
Middlings	2.0%	0.0%	0.0%	6.0%	15.0%	0.0%	0.0%	47.0%	0.0%	0.0%	0.0%	0.0%	0.0%	23.0%	1.0%	4.0%	1.0%	1.0%	100.0%
Tailings	0.0%	0.0%	0.0%	0.0%	0.3%	0.0%	0.0%	0.3%	0.0%	0.0%	2.5%	0.3%	0.0%	96.7%	0.0%	0.0%	0.1%	0.0%	100.0%
Sum of streams	0.0%	0.0%	0.0%	0.0%	0.3%	0.0%	0.0%	0.5%	0.0%	0.0%	2.5%	0.2%	0.0%	96.1%	0.0%	0.1%	0.1%	0.0%	100.0%
Ore	0.0%	0.0%	0.0%	0.0%	0.3%	0.0%	0.0%	0.5%	0.0%	0.0%	1.0%	0.0%	0.0%	98.2%	0.0%	0.0%	0.0%	0.0%	100.0%
>45 µm	DISTRIBUTION																		
Stream	**Anat.**	**Ank.**	**Brook.**	**C.**	**Ill.**	**I-S**	**Ilm.**	**K.**	**K-S**	**Lep.**	**Mic.**	**Plag.**	**Pyr.**	**Q**	**Rut.**	**Sch.**	**Sid.**	**Zr.**	**Total Stream**
Primary Froth	62%		100%	0%	5%		100%	3%			2%	3%	46%	3%	78%	69%	20%	87%	3%
Secondary Froth	0%		0%	0%	1%		0%	0%			0%	0%	0%	0%	10%	5%	0%	0%	0%
Middlings	38%		0%	100%	23%		0%	49%			0%	0%	0%	0%	12%	26%	6%	13%	1%
Tailings	0%		0%	0%	71%		0%	47%			97%	97%	54%	97%	0%	0%	74%	0%	96%
Sum of streams	100%		100%	100%	100%		100%	100%			100%	100%	100%	100%	100%	100%	100%	100%	100%
Ore	100%	100%	100%	100%	100%	100%	100%	100%	100%	100%	100%	100%	100%	100%	100%	100%	100%	100%	100%

Table A-40: Mineral balance around extraction for 45-106 µm size fraction

45-106 µm	ASSAY																		
Stream	Anat.	Ank.	Brook.	C.	Ill.	I-S	Ilm.	K.	K-S	Lep.	Mic.	Plag.	Pyr.	Q	Rut.	Sch.	Sid.	Zr.	Total Stream
Primary Froth	2.0%	0.0%	1.0%	0.0%	2.0%	0.0%	3.0%	2.0%	0.0%	0.0%	4.0%	1.0%	1.0%	70.3%	4.0%	4.0%	2.0%	4.0%	100.0%
Secondary Froth																			
Middlings																			
Tailings	0.0%	0.0%	0.0%	0.0%	1.0%	0.0%	0.0%	1.0%	0.0%	0.0%	4.0%	1.0%	0.0%	93.0%	0.0%	0.0%	0.0%	0.0%	100.0%
Sum of streams	0.1%	0.0%	0.0%	0.0%	1.0%	0.0%	0.1%	1.0%	0.0%	0.0%	4.0%	1.0%	0.0%	92.2%	0.1%	0.1%	0.1%	0.1%	100.0%
Ore	0.0%	0.0%	0.0%	0.0%	1.0%	0.0%	0.0%	2.0%	0.0%	0.0%	1.0%	0.0%	0.0%	96.0%	0.0%	0.0%	0.0%	0.0%	100.0%
45-106 µm	DISTRIBUTION																		
Stream	Anat.	Ank.	Brook.	C.	Ill.	I-S	Ilm.	K.	K-S	Lep.	Mic.	Plag.	Pyr.	Q	Rut.	Sch.	Sid.	Zr.	Total Stream
Primary Froth	100%		100%		7%		100%	7%			4%	4%	100%	3%	100%	100%	100%	100%	4%
Secondary Froth	0%		0%		0%		0%	0%			0%	0%	0%	0%	0%	0%	0%	0%	0%
Middlings	0%		0%		0%		0%	0%			0%	0%	0%	0%	0%	0%	0%	0%	0%
Tailings	0%		0%		93%		0%	93%			96%	96%	0%	97%	0%	0%	0%	0%	96%
Sum of streams	100%		100%		100%		100%	100%			100%	100%	100%	100%	100%	100%	100%	100%	100%
Ore	100%	100%	100%	100%	100%	100%	100%	100%	100%	100%	100%	100%	100%	100%	100%	100%	100%	100%	100%

Table A–41: Mineral balance around extraction for >106 µm size fraction

>106 µm	ASSAY																		
Stream	**Anat.**	**Ank.**	**Brook.**	**C.**	**Ill.**	**I-S**	**Ilm.**	**K.**	**K-S**	**Lep.**	**Mic.**	**Plag.**	**Pyr.**	**Q**	**Rut.**	**Sch.**	**Sid.**	**Zr.**	**Total Stream**
Primary Froth	0.0%	0.0%	0.0%	0.0%	0.0%	0.0%	0.0%	0.0%	0.0%	0.0%	1.0%	0.0%	0.0%	98.0%	0.0%	1.0%	0.0%	0.0%	100.0%
Secondary Froth																			
Middlings																			
Tailings	0.0%	0.0%	0.0%	0.0%	0.0%	0.0%	0.0%	0.0%	0.0%	0.0%	2.0%	0.0%	0.0%	97.8%	0.0%	0.0%	0.1%	0.0%	100.0%
Sum of streams	0.0%	0.0%	0.0%	0.0%	0.0%	0.0%	0.0%	0.0%	0.0%	0.0%	2.0%	0.0%	0.0%	97.8%	0.0%	0.0%	0.1%	0.0%	100.0%
Ore	0.0%	0.0%	0.0%	0.0%	0.0%	0.0%	0.0%	0.0%	0.0%	0.0%	1.0%	0.0%	0.0%	99.0%	0.0%	0.0%	0.0%	0.0%	100.0%
>106 µm	DISTRIBUTION																		
Stream	**Anat.**	**Ank.**	**Brook.**	**C.**	**Ill.**	**I-S**	**Ilm.**	**K.**	**K-S**	**Lep.**	**Mic.**	**Plag.**	**Pyr.**	**Q**	**Rut.**	**Sch.**	**Sid.**	**Zr.**	**Total Stream**
Primary Froth					0%			0%			1%	0%	0%	3%		100%	0%		3%
Secondary Froth					0%			0%			0%	0%	0%	0%		0%	0%		0%
Middlings					0%			0%			0%	0%	0%	0%		0%	0%		0%
Tailings					100%			100%			99%	100%	100%	97%		0%	100%		97%
Sum of streams					100%			100%			100%	100%	100%	100%		100%	100%		100%
Ore	100%	100%	100%	100%	100%	100%	100%	100%	100%	100%	100%	100%	100%	100%	100%	100%	100%	100%	100%

Table A–42: Mineral balance around extraction for sum of all size fractions

TOTAL	ASSAY																		
Stream	**Anat.**	**Ank.**	**Brook**	**C.**	**Ill.**	**I-S**	**Ilm.**	**K.**	**K-S**	**Lep.**	**Mic.**	**Plag.**	**Pyr.**	**Q**	**Rut.**	**Sch.**	**Sid.**	**Zr.**	**Total Stream**
Primary Froth	1.8%	0.0%	1.2%	1.6%	5.8%	2.5%	1.1%	9.4%	1.9%	0.3%	3.7%	0.1%	1.2%	60.5%	2.0%	2.0%	3.2%	1.6%	100.0%
Secondary Froth	0.9%	0.0%	0.2%	1.2%	4.4%	1.4%	0.2%	11.0%	2.2%	0.2%	1.9%	0.0%	0.2%	71.4%	1.3%	1.0%	2.0%	0.4%	100.0%
Middlings	0.1%	0.1%	0.0%	3.5%	18.3%	12.0%	0.0%	22.1%	4.9%	0.0%	0.0%	1.2%	0.0%	36.4%	0.1%	0.1%	1.0%	0.0%	100.0%
Tailings	0.0%	0.0%	0.0%	0.1%	1.2%	0.7%	0.0%	1.0%	0.2%	0.0%	2.6%	0.3%	0.0%	93.8%	0.0%	0.0%	0.1%	0.0%	100.0%
Sum of streams	0.1%	0.0%	0.0%	0.7%	4.1%	2.5%	0.0%	4.7%	1.0%	0.0%	2.2%	0.5%	0.1%	83.2%	0.1%	0.1%	0.4%	0.1%	100.0%
Ore	0.3%	0.0%	0.0%	1.1%	5.2%	3.3%	0.0%	9.1%	1.6%	0.0%	2.0%	0.2%	0.0%	76.6%	0.0%	0.0%	0.5%	0.0%	100.0%
TOTAL	**DISTRIBUTION**																		
Stream	**Anat.**	**Ank.**	**Brook.**	**C.**	**Ill.**	**I-S**	**Ilm.**	**K.**	**K-S**	**Lep.**	**Mic.**	**Plag.**	**Pyr.**	**Q**	**Rut.**	**Sch.**	**Sid.**	**Zr.**	**Total Stream**
Primary Froth	68%	0%	98%	10%	6%	4%	98%	8%	8%	77%	7%	1%	81%	3%	74%	81%	38%	93%	4%
Secondary Froth	4%	1%	2%	1%	0%	0%	2%	1%	1%	6%	0%	0%	1%	0%	5%	5%	3%	2%	0%
Middlings	20%	99%	0%	80%	70%	75%	0%	74%	74%	17%	0%	41%	6%	7%	16%	15%	45%	5%	16%
Tailings	8%	0%	0%	10%	24%	21%	0%	17%	17%	0%	93%	58%	12%	90%	5%	0%	14%	0%	80%
Sum of streams	100%	100%	100%	100%	100%	100%	100%	100%	100%	100%	100%	100%	100%	100%	100%	100%	100%	100%	100%
Ore	100%	100%	100%	100%	100%	100%	100%	100%	100%	100%	100%	100%	100%	100%	100%	100%	100%	100%	100%

Table A–43: Anatase balance around extraction

Anatase	ASSAY									
Stream	<0.2 µm	0.2-2 µm	<2 µm	2-45 µm	<45 µm	>45 µm	45-106 µm	>106 µm	106-250 µm	>250 µm	Total
Primary Froth	0.8%	1.3%	1.2%	4.0%	3.2%	0.6%	2.0%	0.0%			1.8%
Secondary Froth			1.6%	4.0%	2.9%	0.0%					0.9%
Middlings	0.0%	0.3%	0.2%	0.0%	0.1%	2.0%					0.1%
Tailings	0.0%	0.6%	0.5%	0.0%	0.1%	0.0%	0.0%	0.0%	0.0%	0.0%	0.0%
Sum of streams	0.0%	0.5%	0.4%	0.3%	0.3%	0.0%	0.1%	0.0%	0.0%	0.0%	0.1%
Ore	0.0%	0.5%	0.3%	1.0%	0.8%	0.0%	0.0%	0.0%			0.3%
Anatase	DISTRIBUTION										
Stream	<0.2 µm	0.2-2 µm	<2 µm	2-45 µm	<45 µm	>45 µm	45-106 µm	>106 µm	106-250 µm	>250 µm	Total
Primary Froth	2%	8%	9%	74%	84%	16%	16%	0%	0%	0%	100%
Secondary Froth	0%	0%	24%	76%	100%	0%	0%	0%	0%	0%	100%
Middlings	0%	66%	66%	0%	66%	34%	0%	0%	0%	0%	100%
Tailings	0%	100%	100%	0%	100%	0%	0%	0%	0%	0%	100%
Sum of streams	1%	26%	28%	54%	82%	18%	11%	0%	0%	0%	100%
Ore	0%	13%	13%	87%	100%	0%	0%	0%	0%	0%	100%

Table A–44: Ankerite balance around extraction

Ankerite	**ASSAY**										
Stream	**<0.2 µm**	**0.2-2 µm**	**<2 µm**	**2-45 µm**	**<45 µm**	**>45 µm**	**45-106 µm**	**>106 µm**	**106-250 µm**	**>250 µm**	**Total**
Primary Froth	0.0%	0.0%	0.0%	0.0%	0.0%	0.0%	0.0%	0.0%			0.0%
Secondary Froth			0.2%	0.0%	0.1%	0.0%					0.0%
Middlings	0.9%	0.0%	0.3%	0.0%	0.1%	0.0%					0.1%
Tailings	0.0%	0.0%	0.0%	0.0%	0.0%	0.0%	0.0%	0.0%	0.0%	0.0%	0.0%
Sum of streams	0.6%	0.0%	0.2%	0.0%	0.1%	0.0%	0.0%	0.0%	0.0%	0.0%	0.0%
Ore	0.0%	0.0%	0.0%	0.0%	0.0%	0.0%	0.0%	0.0%			0.0%
Ankerite	**DISTRIBUTION**										
Stream	**<0.2 µm**	**0.2-2 µm**	**<2 µm**	**2-45 µm**	**<45 µm**	**>45 µm**	**45-106 µm**	**>106 µm**	**106-250 µm**	**>250 µm**	**Total**
Primary Froth											
Secondary Froth	0%	0%	100%	0%	100%	0%	0%	0%	0%	0%	100%
Middlings	100%	0%	100%	0%	100%	0%	0%	0%	0%	0%	100%
Tailings											
Sum of streams	99%	0%	100%	0%	100%	0%	0%	0%	0%	0%	100%
Ore											

Table A–45: Brookite balance around extraction

Brookite	**ASSAY**										
Stream	**<0.2 µm**	**0.2-2 µm**	**<2 µm**	**2-45 µm**	**<45 µm**	**>45 µm**	**45-106 µm**	**>106 µm**	**106-250 µm**	**>250 µm**	**Total**
Primary Froth	0.0%	0.0%	0.0%	3.0%	2.1%	0.3%	1.0%	0.0%			1.2%
Secondary Froth			0.0%	1.0%	0.6%	0.0%					0.2%
Middlings	0.0%	0.0%	0.0%	0.0%	0.0%	0.0%					0.0%
Tailings	0.0%	0.0%	0.0%	0.0%	0.0%	0.0%	0.0%	0.0%	0.0%	0.0%	0.0%
Sum of streams	0.0%	0.0%	0.0%	0.2%	0.1%	0.0%	0.0%	0.0%	0.0%	0.0%	0.0%
Ore	0.0%	0.0%	0.0%	0.0%	0.0%	0.0%	0.0%	0.0%			0.0%
Brookite	**DISTRIBUTION**										
Stream	**<0.2 µm**	**0.2-2 µm**	**<2 µm**	**2-45 µm**	**<45 µm**	**>45 µm**	**45-106 µm**	**>106 µm**	**106-250 µm**	**>250 µm**	**Total**
Primary Froth	0%	0%	0%	87%	87%	13%	13%	0%	0%	0%	100%
Secondary Froth	0%	0%	0%	100%	100%	0%	0%	0%	0%	0%	100%
Middlings											
Tailings											
Sum of streams	0%	0%	0%	88%	88%	12%	12%	0%	0%	0%	100%
Ore											

Table A–46: Chlorite balance around extraction

Chlorite	ASSAY										
Stream	**<0.2 µm**	**0.2-2 µm**	**<2 µm**	**2-45 µm**	**<45 µm**	**>45 µm**	**45-106 µm**	**>106 µm**	**106-250 µm**	**>250 µm**	**Total**
Primary Froth	0.0%	8.5%	6.4%	2.0%	3.3%	0.0%	0.0%	0.0%			1.6%
Secondary Froth			6.0%	2.0%	3.8%	0.0%					1.2%
Middlings	0.0%	6.0%	4.2%	3.0%	3.5%	6.0%					3.5%
Tailings	0.0%	4.7%	3.4%	0.0%	0.6%	0.0%	0.0%	0.0%	0.0%	0.0%	0.1%
Sum of streams	0.0%	5.9%	4.2%	1.5%	2.3%	0.0%	0.0%	0.0%	0.0%	0.0%	0.7%
Ore	0.0%	6.4%	4.6%	3.0%	3.5%	0.0%	0.0%	0.0%			1.1%
Chlorite	**DISTRIBUTION**										
Stream	**<0.2 µm**	**0.2-2 µm**	**<2 µm**	**2-45 µm**	**<45 µm**	**>45 µm**	**45-106 µm**	**>106 µm**	**106-250 µm**	**>250 µm**	**Total**
Primary Froth	0%	57%	57%	43%	100%	0%	0%	0%	0%	0%	100%
Secondary Froth	0%	0%	71%	29%	100%	0%	0%	0%	0%	0%	100%
Middlings	0%	46%	46%	50%	96%	4%	0%	0%	0%	0%	100%
Tailings	0%	100%	100%	0%	100%	0%	0%	0%	0%	0%	100%
Sum of streams	0%	52%	52%	44%	97%	3%	0%	0%	0%	0%	100%
Ore	0%	42%	42%	58%	100%	0%	0%	0%	0%	0%	100%

Table A–47: Illite balance around extraction

Illite	**ASSAY**										
Stream	**<0.2 µm**	**0.2-2 µm**	**<2 µm**	**2-45 µm**	**<45 µm**	**>45 µm**	**45-106 µm**	**>106 µm**	**106-250 µm**	**>250 µm**	**Total**
Primary Froth	13.6%	24.3%	21.6%	7.0%	11.3%	0.6%	2.0%	0.0%			5.8%
Secondary Froth			19.6%	5.0%	11.5%	1.0%					4.4%
Middlings	12.1%	26.4%	22.1%	16.0%	18.4%	15.0%					18.3%
Tailings	12.7%	18.3%	16.7%	5.0%	7.0%	0.3%	1.0%	0.0%	0.0%	3.0%	1.2%
Sum of streams	12.3%	24.4%	20.8%	10.2%	13.4%	0.3%	1.0%	0.0%	0.0%	3.0%	4.1%
Ore	13.6%	24.5%	21.4%	13.1%	15.8%	0.3%	1.0%	0.0%			5.2%
Illite	**DISTRIBUTION**										
Stream	**<0.2 µm**	**0.2-2 µm**	**<2 µm**	**2-45 µm**	**<45 µm**	**>45 µm**	**45-106 µm**	**>106 µm**	**106-250 µm**	**>250 µm**	**Total**
Primary Froth	9%	45%	54%	41%	95%	5%	5%	0%	0%	0%	100%
Secondary Froth	0%	0%	64%	20%	84%	16%	0%	0%	0%	0%	100%
Middlings	8%	39%	47%	51%	98%	2%	0%	0%	0%	0%	100%
Tailings	7%	26%	33%	49%	82%	18%	17%	1%	0%	1%	100%
Sum of streams	8%	36%	44%	50%	94%	6%	4%	0%	0%	0%	100%
Ore	7%	35%	42%	55%	97%	3%	3%	0%	0%	0%	100%

Table A–48: Illite-Smectite balance around extraction

Illite-Smectite	**ASSAY**										
Stream	**<0.2 µm**	**0.2-2 µm**	**<2 µm**	**2-45 µm**	**<45 µm**	**>45 µm**	**45-106 µm**	**>106 µm**	**106-250 µm**	**>250 µm**	**Total**
Primary Froth	40.8%	9.8%	17.6%	0.0%	5.2%	0.0%	0.0%	0.0%			2.5%
Secondary Froth			9.4%	0.0%	4.2%	0.0%					1.4%
Middlings	52.6%	21.5%	30.9%	0.0%	12.3%	0.0%					12.0%
Tailings	53.6%	17.8%	27.6%	0.0%	4.7%	0.0%	0.0%	0.0%	0.0%	0.0%	0.7%
Sum of streams	52.1%	19.8%	29.1%	0.0%	8.8%	0.0%	0.0%	0.0%	0.0%	0.0%	2.5%
Ore	46.0%	27.4%	32.6%	0.0%	10.4%	0.0%	0.0%	0.0%			3.3%
Illite-Smectite	**DISTRIBUTION**										
Stream	**<0.2 µm**	**0.2-2 µm**	**<2 µm**	**2-45 µm**	**<45 µm**	**>45 µm**	**45-106 µm**	**>106 µm**	**106-250 µm**	**>250 µm**	**Total**
Primary Froth	58%	42%	100%	0%	100%	0%	0%	0%	0%	0%	100%
Secondary Froth	0%	0%	100%	0%	100%	0%	0%	0%	0%	0%	100%
Middlings	52%	48%	100%	0%	100%	0%	0%	0%	0%	0%	100%
Tailings	53%	47%	100%	0%	100%	0%	0%	0%	0%	0%	100%
Sum of streams	52%	48%	100%	0%	100%	0%	0%	0%	0%	0%	100%
Ore	39%	61%	100%	0%	100%	0%	0%	0%	0%	0%	100%

Table A–49: Ilmenite balance around extraction

Ilmenite	ASSAY										
Stream	**<0.2 µm**	**0.2-2 µm**	**<2 µm**	**2-45 µm**	**<45 µm**	**>45 µm**	**45-106 µm**	**>106 µm**	**106-250 µm**	**>250 µm**	**Total**
Primary Froth	0.0%	0.0%	0.0%	2.0%	1.4%	0.9%	3.0%	0.0%			1.1%
Secondary Froth			0.0%	1.0%	0.6%	0.0%					0.2%
Middlings	0.0%	0.0%	0.0%	0.0%	0.0%	0.0%					0.0%
Tailings	0.0%	0.0%	0.0%	0.0%	0.0%	0.0%	0.0%	0.0%	0.0%	0.0%	0.0%
Sum of streams	0.0%	0.0%	0.0%	0.1%	0.1%	0.0%	0.1%	0.0%	0.0%	0.0%	0.0%
Ore	0.0%	0.0%	0.0%	0.0%	0.0%	0.0%	0.0%	0.0%			0.0%
Ilmenite	**DISTRIBUTION**										
Stream	**<0.2 µm**	**0.2-2 µm**	**<2 µm**	**2-45 µm**	**<45 µm**	**>45 µm**	**45-106 µm**	**>106 µm**	**106-250 µm**	**>250 µm**	**Total**
Primary Froth	0%	0%	0%	61%	61%	39%	39%	0%	0%	0%	100%
Secondary Froth	0%	0%	0%	100%	100%	0%	0%	0%	0%	0%	100%
Middlings											
Tailings											
Sum of streams	0%	0%	0%	61%	61%	39%	39%	0%	0%	0%	100%
Ore											

Table A–50: Kaolinite balance around extraction

Kaolinite	ASSAY										
Stream	**<0.2 µm**	**0.2-2 µm**	**<2 µm**	**2-45 µm**	**<45 µm**	**>45 µm**	**45-106 µm**	**>106 µm**	**106-250 µm**	**>250 µm**	**Total**
Primary Froth	18.7%	36.5%	32.1%	13.0%	18.7%	0.6%	2.0%	0.0%			9.4%
Secondary Froth			38.2%	31.0%	34.2%	0.0%					11.0%
Middlings	13.3%	28.4%	23.8%	20.0%	21.5%	47.0%					22.1%
Tailings	14.9%	24.3%	21.7%	2.0%	5.3%	0.3%	1.0%	0.0%	0.0%	2.0%	1.0%
Sum of streams	14.0%	28.0%	24.0%	11.1%	15.0%	0.5%	1.0%	0.0%	0.0%	2.0%	4.7%
Ore	14.2%	23.4%	20.8%	30.3%	27.3%	0.5%	2.0%	0.0%			9.1%
Kaolinite	**DISTRIBUTION**										
Stream	**<0.2 µm**	**0.2-2 µm**	**<2 µm**	**2-45 µm**	**<45 µm**	**>45 µm**	**45-106 µm**	**>106 µm**	**106-250 µm**	**>250 µm**	**Total**
Primary Froth	7%	42%	49%	47%	97%	3%	3%	0%	0%	0%	100%
Secondary Froth	0%	0%	50%	50%	100%	0%	0%	0%	0%	0%	100%
Middlings	7%	35%	42%	53%	95%	5%	0%	0%	0%	0%	100%
Tailings	10%	44%	54%	24%	78%	22%	21%	1%	0%	1%	100%
Sum of streams	8%	36%	45%	48%	92%	8%	4%	0%	0%	0%	100%
Ore	4%	19%	24%	73%	96%	4%	4%	0%	0%	0%	100%

Table A–51: Kaolinite-smectite balance around extraction

Kaolinite-Smectite	**ASSAY**										
Stream	*<0.2 µm*	*0.2-2 µm*	*<2 µm*	*2-45 µm*	*<45 µm*	*>45 µm*	*45-106 µm*	*>106 µm*	*106-250 µm*	*>250 µm*	*Total*
Primary Froth	24.6%	9.7%	13.4%	0.0%	4.0%	0.0%	0.0%	0.0%			1.9%
Secondary Froth			15.4%	0.0%	6.9%	0.0%					2.2%
Middlings	20.9%	9.0%	12.6%	0.0%	5.0%	0.0%					4.9%
Tailings	18.7%	5.5%	9.1%	0.0%	1.5%	0.0%	0.0%	0.0%	0.0%	0.0%	0.2%
Sum of streams	20.7%	8.3%	11.9%	0.0%	3.6%	0.0%	0.0%	0.0%	0.0%	0.0%	1.0%
Ore	24.3%	12.0%	15.4%	0.0%	4.9%	0.0%	0.0%	0.0%			1.6%
Kaolinite-Smectite	**DISTRIBUTION**										
Stream	**<0.2 µm**	**0.2-2 µm**	**<2 µm**	**2-45 µm**	**<45 µm**	**>45 µm**	**45-106 µm**	**>106 µm**	**106-250 µm**	**>250 µm**	**Total**
Primary Froth	46%	54%	100%	0%	100%	0%	0%	0%	0%	0%	100%
Secondary Froth	0%	0%	100%	0%	100%	0%	0%	0%	0%	0%	100%
Middlings	50%	50%	100%	0%	100%	0%	0%	0%	0%	0%	100%
Tailings	56%	44%	100%	0%	100%	0%	0%	0%	0%	0%	100%
Sum of streams	50%	49%	100%	0%	100%	0%	0%	0%	0%	0%	100%
Ore	44%	56%	100%	0%	100%	0%	0%	0%	0%	0%	100%

Table A–52: Lepidocrocite balance around extraction

Lepidocrocite	**ASSAY**										
Stream	**<0.2 µm**	**0.2-2 µm**	**<2 µm**	**2-45 µm**	**<45 µm**	**>45 µm**	**45-106 µm**	**>106 µm**	**106-250 µm**	**>250 µm**	**Total**
Primary Froth	0.8%	2.2%	1.8%	0.0%	0.5%	0.0%	0.0%	0.0%			0.3%
Secondary Froth			1.3%	0.0%	0.6%	0.0%					0.2%
Middlings	0.1%	0.0%	0.0%	0.0%	0.0%	0.0%					0.0%
Tailings	0.0%	0.0%	0.0%	0.0%	0.0%	0.0%	0.0%	0.0%	0.0%	0.0%	0.0%
Sum of streams	0.1%	0.2%	0.2%	0.0%	0.0%	0.0%	0.0%	0.0%	0.0%	0.0%	0.0%
Ore	0.7%	0.0%	0.2%	0.0%	0.1%	0.0%	0.0%	0.0%			0.0%
Lepidocrocite	**DISTRIBUTION**										
Stream	**<0.2 µm**	**0.2-2 µm**	**<2 µm**	**2-45 µm**	**<45 µm**	**>45 µm**	**45-106 µm**	**>106 µm**	**106-250 µm**	**>250 µm**	**Total**
Primary Froth	11%	89%	100%	0%	100%	0%	0%	0%	0%	0%	100%
Secondary Froth	0%	0%	100%	0%	100%	0%	0%	0%	0%	0%	100%
Middlings	100%	0%	100%	0%	100%	0%	0%	0%	0%	0%	100%
Tailings											
Sum of streams	25%	68%	100%	0%	100%	0%	0%	0%	0%	0%	100%
Ore	100%	0%	100%	0%	100%	0%	0%	0%	0%	0%	100%

Table A–53 Microcline balance around extraction

Microcline	**ASSAY**										
Stream	**<0.2 µm**	**0.2-2 µm**	**<2 µm**	**2-45 µm**	**<45 µm**	**>45 µm**	**45-106 µm**	**>106 µm**	**106-250 µm**	**>250 µm**	**Total**
Primary Froth	0.0%	0.0%	0.0%	8.0%	5.6%	1.9%	4.0%	1.0%			3.7%
Secondary Froth			0.0%	3.0%	1.7%	2.0%					1.9%
Middlings	0.0%	0.0%	0.0%	0.0%	0.0%	0.0%					0.0%
Tailings	0.0%	0.0%	0.0%	4.0%	3.3%	2.5%	4.0%	2.0%	2.0%	5.0%	2.6%
Sum of streams	0.0%	0.0%	0.0%	2.4%	1.7%	2.5%	4.0%	2.0%	2.0%	5.0%	2.2%
Ore	0.0%	0.0%	0.0%	6.1%	4.1%	1.0%	1.0%	1.0%			2.0%
Microcline	**DISTRIBUTION**										
Stream	**<0.2 µm**	**0.2-2 µm**	**<2 µm**	**2-45 µm**	**<45 µm**	**>45 µm**	**45-106 µm**	**>106 µm**	**106-250 µm**	**>250 µm**	**Total**
Primary Froth	0%	0%	0%	74%	74%	26%	16%	10%	0%	0%	100%
Secondary Froth	0%	0%	0%	28%	28%	72%	0%	0%	0%	0%	100%
Middlings											
Tailings	0%	0%	0%	18%	18%	82%	31%	50%	49%	1%	100%
Sum of streams	0%	0%	0%	22%	22%	78%	30%	47%	46%	1%	100%
Ore	0%	0%	0%	66%	66%	34%	9%	25%	0%	0%	100%

Table A–54: Plagioclase Oligoclase balance around extraction

Plagioclase Oligoclase	ASSAY										
Stream	**<0.2 µm**	**0.2-2 µm**	**<2 µm**	**2-45 µm**	**<45 µm**	**>45 µm**	**45-106 µm**	**>106 µm**	**106-250 µm**	**>250 µm**	**Total**
Primary Froth	0.0%	0.0%	0.0%	0.0%	0.0%	0.3%	1.0%	0.0%			0.1%
Secondary Froth			0.0%	0.0%	0.0%	0.0%					0.0%
Middlings	0.0%	0.0%	0.0%	2.0%	1.2%	0.0%					1.2%
Tailings	0.0%	0.0%	0.0%	1.0%	0.8%	0.3%	1.0%	0.0%	0.0%	2.0%	0.3%
Sum of streams	0.0%	0.0%	0.0%	1.4%	1.0%	0.2%	1.0%	0.0%	0.0%	2.0%	0.5%
Ore	0.0%	0.0%	0.0%	1.0%	0.7%	0.0%	0.0%	0.0%			0.2%
Plagioclase Oligoclase	**DISTRIBUTION**										
Stream	**<0.2 µm**	**0.2-2 µm**	**<2 µm**	**2-45 µm**	**<45 µm**	**>45 µm**	**45-106 µm**	**>106 µm**	**106-250 µm**	**>250 µm**	**Total**
Primary Froth	0%	0%	0%	0%	0%	100%	100%	0%	0%	0%	100%
Secondary Froth											
Middlings	0%	0%	0%	100%	100%	0%	0%	0%	0%	0%	100%
Tailings	0%	0%	0%	36%	36%	64%	62%	3%	0%	3%	100%
Sum of streams	0%	0%	0%	61%	61%	39%	37%	2%	0%	2%	100%
Ore	0%	0%	0%	100%	100%	0%	0%	0%	0%	0%	100%

Table A–55: Pyrite balance around extraction

Pyrite	**ASSAY**										
Stream	**<0.2 µm**	**0.2-2 µm**	**<2 µm**	**2-45 µm**	**<45 µm**	**>45 µm**	**45-106 µm**	**>106 µm**	**106-250 µm**	**>250 µm**	**Total**
Primary Froth	0.0%	0.2%	0.1%	3.0%	2.1%	0.3%	1.0%	0.0%			1.2%
Secondary Froth			0.0%	1.0%	0.6%	0.0%					0.2%
Middlings	0.0%	0.1%	0.1%	0.0%	0.0%	0.0%					0.0%
Tailings	0.0%	0.0%	0.0%	0.0%	0.0%	0.0%	0.0%	0.0%	0.0%	2.0%	0.0%
Sum of streams	0.0%	0.1%	0.1%	0.2%	0.2%	0.0%	0.0%	0.0%	0.0%	2.0%	0.1%
Ore	0.0%	0.2%	0.1%	0.0%	0.0%	0.0%	0.0%	0.0%			0.0%
Pyrite	**DISTRIBUTION**										
Stream	**<0.2 µm**	**0.2-2 µm**	**<2 µm**	**2-45 µm**	**<45 µm**	**>45 µm**	**45-106 µm**	**>106 µm**	**106-250 µm**	**>250 µm**	**Total**
Primary Froth	0%	2%	2%	86%	88%	12%	12%	0%	0%	0%	100%
Secondary Froth	0%	0%	0%	100%	100%	0%	0%	0%	0%	0%	100%
Middlings	0%	100%	100%	0%	100%	0%	0%	0%	0%	0%	100%
Tailings	0%	0%	0%	0%	0%	100%	0%	100%	0%	100%	100%
Sum of streams	0%	8%	8%	71%	78%	22%	10%	12%	0%	12%	100%
Ore	0%	100%	100%	0%	100%	0%	0%	0%	0%	0%	100%

Table A–56: Quartz balance around extraction

Quartz	**ASSAY**										
Stream	**<0.2 µm**	**0.2-2 µm**	**<2 µm**	**2-45 µm**	**<45 µm**	**>45 µm**	**45-106 µm**	**>106 µm**	**106-250 µm**	**>250 µm**	**Total**
Primary Froth	0.5%	5.0%	3.8%	40.0%	29.3%	89.9%	70.3%	98.0%			60.5%
Secondary Froth			7.0%	34.0%	22.0%	94.9%					71.4%
Middlings	0.0%	6.4%	4.5%	58.0%	36.7%	23.0%					36.4%
Tailings	0.2%	28.2%	20.5%	88.0%	76.5%	96.7%	93.0%	97.8%	98.0%	73.0%	93.8%
Sum of streams	0.1%	11.3%	8.0%	70.7%	51.8%	96.1%	92.2%	97.8%	98.0%	73.0%	83.2%
Ore	1.2%	4.6%	3.6%	43.4%	30.7%	98.2%	96.0%	99.0%			76.6%
Quartz	**DISTRIBUTION**										
Stream	**<0.2 µm**	**0.2-2 µm**	**<2 µm**	**2-45 µm**	**<45 µm**	**>45 µm**	**45-106 µm**	**>106 µm**	**106-250 µm**	**>250 µm**	**Total**
Primary Froth	0%	1%	1%	23%	24%	76%	17%	59%	0%	0%	100%
Secondary Froth	0%	0%	1%	8%	10%	90%	0%	0%	0%	0%	100%
Middlings	0%	5%	5%	94%	98%	2%	0%	0%	0%	0%	100%
Tailings	0%	1%	1%	11%	12%	88%	20%	68%	68%	0%	100%
Sum of streams	0%	1%	1%	17%	18%	82%	19%	63%	61%	0%	100%
Ore	0%	0%	0%	12%	13%	87%	21%	66%	0%	0%	100%

Table A–57: Rutile balance around extraction

Rutile	**ASSAY**										
Stream	**<0.2 µm**	**0.2-2 µm**	**<2 µm**	**2-45 µm**	**<45 µm**	**>45 µm**	**45-106 µm**	**>106 µm**	**106-250 µm**	**>250 µm**	**Total**
Primary Froth	0.1%	0.6%	0.5%	4.0%	3.0%	1.2%	4.0%	0.0%			2.0%
Secondary Froth			0.9%	3.0%	2.1%	1.0%					1.3%
Middlings	0.0%	0.3%	0.2%	0.0%	0.1%	1.0%					0.1%
Tailings	0.0%	0.4%	0.3%	0.0%	0.0%	0.0%	0.0%	0.0%	0.0%	0.0%	0.0%
Sum of streams	0.0%	0.4%	0.3%	0.3%	0.3%	0.0%	0.1%	0.0%	0.0%	0.0%	0.1%
Ore	0.0%	0.2%	0.2%	0.0%	0.1%	0.0%	0.0%	0.0%			0.0%
Rutile	**DISTRIBUTION**										
Stream	**<0.2 µm**	**0.2-2 µm**	**<2 µm**	**2-45 µm**	**<45 µm**	**>45 µm**	**45-106 µm**	**>106 µm**	**106-250 µm**	**>250 µm**	**Total**
Primary Froth	0%	3%	4%	67%	71%	29%	29%	0%	0%	0%	100%
Secondary Froth	0%	0%	9%	40%	49%	51%	0%	0%	0%	0%	100%
Middlings	0%	79%	79%	0%	79%	21%	0%	0%	0%	0%	100%
Tailings	0%	100%	100%	0%	100%	0%	0%	0%	0%	0%	100%
Sum of streams	0%	20%	20%	52%	72%	28%	22%	0%	0%	0%	100%
Ore	0%	100%	100%	0%	100%	0%	0%	0%	0%	0%	100%

Table A–58: Schorl balance around extraction

Schorl	**ASSAY**										
Stream	**<0.2 µm**	**0.2-2 µm**	**<2 µm**	**2-45 µm**	**<45 µm**	**>45 µm**	**45-106 µm**	**>106 µm**	**106-250 µm**	**>250 µm**	**Total**
Primary Froth	0.0%	0.0%	0.0%	3.0%	2.1%	1.9%	4.0%	1.0%			2.0%
Secondary Froth			0.0%	2.0%	1.1%	1.0%					1.0%
Middlings	0.0%	0.0%	0.0%	0.0%	0.0%	4.0%					0.1%
Tailings	0.0%	0.0%	0.0%	0.0%	0.0%	0.0%	0.0%	0.0%	0.0%	0.0%	0.0%
Sum of streams	0.0%	0.0%	0.0%	0.2%	0.2%	0.1%	0.1%	0.0%	0.0%	0.0%	0.1%
Ore	0.0%	0.0%	0.0%	0.0%	0.0%	0.0%	0.0%	0.0%			0.0%
Schorl	**DISTRIBUTION**										
Stream	**<0.2 µm**	**0.2-2 µm**	**<2 µm**	**2-45 µm**	**<45 µm**	**>45 µm**	**45-106 µm**	**>106 µm**	**106-250 µm**	**>250 µm**	**Total**
Primary Froth	0%	0%	0%	52%	52%	48%	30%	19%	0%	0%	100%
Secondary Froth	0%	0%	0%	34%	34%	66%	0%	0%	0%	0%	100%
Middlings	0%	0%	0%	0%	0%	100%	0%	0%	0%	0%	100%
Tailings											
Sum of streams	0%	0%	0%	43%	43%	57%	24%	15%	0%	0%	100%
Ore											

Table A–59: Siderite balance around extraction

Siderite	**ASSAY**										
Stream	**<0.2 µm**	**0.2-2 µm**	**<2 µm**	**2-45 µm**	**<45 µm**	**>45 µm**	**45-106 µm**	**>106 µm**	**106-250 µm**	**>250 µm**	**Total**
Primary Froth	0.0%	1.9%	1.4%	8.0%	6.1%	0.6%	2.0%	0.0%			3.2%
Secondary Froth			0.4%	11.0%	6.3%	0.0%					2.0%
Middlings	0.1%	1.5%	1.1%	1.0%	1.0%	1.0%					1.0%
Tailings	0.0%	0.3%	0.2%	0.0%	0.0%	0.1%	0.0%	0.1%	0.0%	13.0%	0.1%
Sum of streams	0.1%	1.2%	0.9%	1.1%	1.0%	0.1%	0.1%	0.1%	0.0%	13.0%	0.4%
Ore	0.0%	0.9%	0.6%	2.0%	1.6%	0.0%	0.0%	0.0%			0.5%
Siderite	**DISTRIBUTION**										
Stream	**<0.2 µm**	**0.2-2 µm**	**<2 µm**	**2-45 µm**	**<45 µm**	**>45 µm**	**45-106 µm**	**>106 µm**	**106-250 µm**	**>250 µm**	**Total**
Primary Froth	0%	6%	6%	84%	91%	9%	9%	0%	0%	0%	100%
Secondary Froth	0%	0%	3%	97%	100%	0%	0%	0%	0%	0%	100%
Middlings	1%	39%	40%	57%	98%	2%	0%	0%	0%	0%	100%
Tailings	0%	7%	7%	0%	7%	93%	0%	93%	0%	93%	100%
Sum of streams	0%	21%	22%	61%	82%	18%	3%	13%	0%	13%	100%
Ore	0%	12%	12%	88%	100%	0%	0%	0%	0%	0%	100%

Table A–60: Zircon balance around extraction

Zircon	**ASSAY**									
Stream	**<0.2 µm**	**0.2-2 µm**	**<2 µm**	**2-45 µm**	**<45 µm**	**>45 µm**	**45-106 µm**	**>106 µm**	**106-250 µm**	**>250 µm**	**Total**
Primary Froth	0.0%	0.0%	0.0%	3.0%	2.1%	1.2%	4.0%	0.0%			1.6%
Secondary Froth			0.0%	2.0%	1.1%	0.0%					0.4%
Middlings	0.0%	0.0%	0.0%	0.0%	0.0%	1.0%					0.0%
Tailings	0.0%	0.0%	0.0%	0.0%	0.0%	0.0%	0.0%	0.0%	0.0%	0.0%	0.0%
Sum of streams	0.0%	0.0%	0.0%	0.2%	0.2%	0.0%	0.1%	0.0%	0.0%	0.0%	0.1%
Ore	0.0%	0.0%	0.0%	0.0%	0.0%	0.0%	0.0%	0.0%			0.0%
Zircon	**DISTRIBUTION**										
Stream	**<0.2 µm**	**0.2-2 µm**	**<2 µm**	**2-45 µm**	**<45 µm**	**>45 µm**	**45-106 µm**	**>106 µm**	**106-250 µm**	**>250 µm**	**Total**
Primary Froth	0%	0%	0%	63%	63%	37%	37%	0%	0%	0%	100%
Secondary Froth	0%	0%	0%	100%	100%	0%	0%	0%	0%	0%	100%
Middlings	0%	0%	0%	0%	0%	100%	0%	0%	0%	0%	100%
Tailings											
Sum of streams	0%	0%	0%	61%	61%	39%	34%	0%	0%	0%	100%
Ore											

Table A–61: Total clay balance around extraction

Total Clay	ASSAY										
Stream	**<0.2 µm**	**0.2-2 µm**	**<2 µm**	**2-45 µm**	**<45 µm**	**>45 µm**	**45-106 µm**	**>106 µm**	**106-250 µm**	**>250 µm**	**Total**
Primary Froth	97.7%	88.8%	91.0%	22.0%	42.5%	1.2%	4.0%	0.0%			21.2%
Secondary Froth			88.6%	38.0%	60.6%	1.0%					20.2%
Middlings	98.9%	91.3%	93.6%	39.0%	60.7%	68.0%					60.9%
Tailings	99.8%	70.5%	78.5%	7.0%	19.2%	0.5%	2.0%	0.0%	0.0%	5.0%	3.2%
Sum of streams	99.0%	86.3%	90.0%	22.8%	43.1%	0.9%	2.1%	0.0%	0.0%	5.0%	13.1%
Ore	98.1%	93.8%	95.0%	46.5%	62.0%	0.8%	3.0%	0.0%			20.4%
Total Clay	**DISTRIBUTION**										
Stream	**<0.2 µm**	**0.2-2 µm**	**<2 µm**	**2-45 µm**	**<45 µm**	**>45 µm**	**45-106 µm**	**>106 µm**	**106-250 µm**	**>250 µm**	**Total**
Primary Froth	17%	45%	62%	35%	97%	3%	3%	0%	0%	0%	100%
Secondary Froth	0%	0%	63%	34%	97%	3%	0%	0%	0%	0%	100%
Middlings	19%	41%	60%	38%	97%	3%	0%	0%	0%	0%	100%
Tailings	21%	39%	60%	26%	86%	14%	13%	1%	0%	1%	100%
Sum of streams	19%	40%	60%	35%	95%	5%	3%	0%	0%	0%	100%
Ore	14%	34%	48%	50%	97%	3%	3%	0%	0%	0%	100%

Table A–62: Total titanium mineral balance around extraction

Total Titanium	**ASSAY**										
Stream	**<0.2 µm**	**0.2-2 µm**	**<2 µm**	**2-45 µm**	**<45 µm**	**>45 µm**	**45-106 µm**	**>106 µm**	**106-250 µm**	**>250 µm**	**Total**
Primary Froth	1.0%	2.0%	1.7%	13.0%	9.7%	2.9%	9.9%	0.0%			6.2%
Secondary Froth			2.5%	9.0%	6.1%	1.0%					2.6%
Middlings	0.0%	0.7%	0.5%	0.0%	0.2%	3.0%					0.3%
Tailings	0.0%	1.0%	0.7%	0.0%	0.1%	0.0%	0.0%	0.0%	0.0%	0.0%	0.0%
Sum of streams	0.1%	0.8%	0.6%	0.9%	0.9%	0.1%	0.4%	0.0%	0.0%	0.0%	0.3%
Ore	0.0%	0.7%	0.5%	1.0%	0.8%	0.0%	0.0%	0.0%			0.3%
Total Titanium	**DISTRIBUTION**										
Stream	**<0.2 µm**	**0.2-2 µm**	**<2 µm**	**2-45 µm**	**<45 µm**	**>45 µm**	**45-106 µm**	**>106 µm**	**106-250 µm**	**>250 µm**	**Total**
Primary Froth	1%	3%	4%	72%	76%	24%	24%	0%	0%	0%	79%
Secondary Froth	0%	0%	13%	61%	74%	26%	0%	0%	0%	0%	4%
Middlings	0%	72%	72%	0%	72%	28%	0%	0%	0%	0%	12%
Tailings	0%	100%	100%	0%	100%	0%	0%	0%	0%	0%	4%
Sum of streams	0%	16%	17%	59%	76%	24%	19%	0%	0%	0%	100%
Ore	0%	19%	19%	81%	100%	0%	0%	0%	0%	0%	100%

Table A–63: Total feldspar balance around extraction

Total Feldspar	ASSAY										
Stream	**<0.2 µm**	**0.2-2 µm**	**<2 µm**	**2-45 µm**	**<45 µm**	**>45 µm**	**45-106 µm**	**>106 µm**	**106-250 µm**	**>250 µm**	**Total**
Primary Froth	0.0%	0.0%	0.0%	8.0%	5.6%	2.2%	5.0%	1.0%			3.8%
Secondary Froth			0.0%	3.0%	1.7%	2.0%					1.9%
Middlings	0.0%	0.0%	0.0%	2.0%	1.2%	0.0%					1.2%
Tailings	0.0%	0.0%	0.0%	5.0%	4.1%	2.7%	5.0%	2.0%	2.0%	7.0%	2.9%
Sum of streams	0.0%	0.0%	0.0%	3.8%	2.7%	2.7%	5.0%	2.0%	2.0%	7.0%	2.7%
Ore	0.0%	0.0%	0.0%	7.1%	4.8%	1.0%	1.0%	1.0%			2.2%
Total Feldspar	**DISTRIBUTION**										
Stream	**<0.2 µm**	**0.2-2 µm**	**<2 µm**	**2-45 µm**	**<45 µm**	**>45 µm**	**45-106 µm**	**>106 µm**	**106-250 µm**	**>250 µm**	**Total**
Primary Froth	0%	0%	0%	71%	71%	29%	19%	10%	0%	0%	6%
Secondary Froth	0%	0%	0%	28%	28%	72%	0%	0%	0%	0%	0%
Middlings	0%	0%	0%	100%	100%	0%	0%	0%	0%	0%	7%
Tailings	0%	0%	0%	20%	20%	80%	35%	45%	44%	1%	87%
Sum of streams	0%	0%	0%	29%	29%	71%	31%	40%	38%	1%	100%
Ore	0%	0%	0%	69%	69%	31%	8%	23%	0%	0%	100%

Table A–64: Total iron bearing mineral balance around extraction

Total Iron bearing	**ASSAY**										
Stream	**<0.2 µm**	**0.2-2 µm**	**<2 µm**	**2-45 µm**	**<45 µm**	**>45 µm**	**45-106 µm**	**>106 µm**	**106-250 µm**	**>250 µm**	**Total**
Primary Froth	0.8%	4.3%	3.4%	16.0%	12.3%	3.6%	9.9%	1.0%			7.8%
Secondary Froth			1.8%	15.0%	9.1%	1.0%					3.6%
Middlings	0.2%	1.6%	1.2%	1.0%	1.1%	5.0%					1.2%
Tailings	0.0%	0.3%	0.2%	0.0%	0.0%	0.1%	0.0%	0.1%	0.0%	15.0%	0.1%
Sum of streams	0.2%	1.5%	1.1%	1.6%	1.5%	0.2%	0.4%	0.1%	0.0%	15.0%	0.6%
Ore	0.7%	1.0%	0.9%	2.0%	1.7%	0.0%	0.0%	0.0%			0.5%
Total Iron bearing	**DISTRIBUTION**										
Stream	**<0.2 µm**	**0.2-2 µm**	**<2 µm**	**2-45 µm**	**<45 µm**	**>45 µm**	**45-106 µm**	**>106 µm**	**106-250 µm**	**>250 µm**	**Total**
Primary Froth	0%	6%	6%	70%	76%	24%	19%	5%	0%	0%	56%
Secondary Froth	0%	0%	7%	74%	81%	19%	0%	0%	0%	0%	3%
Middlings	2%	37%	39%	51%	90%	10%	0%	0%	0%	0%	31%
Tailings	0%	6%	6%	0%	6%	94%	0%	94%	0%	94%	10%
Sum of streams	1%	15%	17%	57%	74%	26%	11%	12%	0%	9%	100%
Ore	4%	14%	18%	82%	100%	0%	0%	0%	0%	0%	100%

Table A–65: Comparisons of elemental compositions from XRF and XRD for the <0.2 µm size fraction

<0.2 µm	**XRF**					
Stream	**SiO_2**	**Al_2O_3**	**Fe_2O_3**	**K_2O**	**MgO**	**TiO_2**
Primary Froth	44%	25%	15%	3%	2%	1%
Secondary Froth						
Middlings	53%	32%	7%	3%	2%	1%
Tailings	52%	30%	8%	3%	2%	1%
Sum of Streams	52%	31%	7%	3%	2%	1%
Ore	53%	30%	5%	4%	2%	1%
XRD						
Stream	**SiO_2**	**Al_2O_3**	**Fe_2O_3**	**K_2O**	**MgO**	**TiO_2**
Primary Froth	47%	35%	1%	5%	1%	1%
Secondary Froth						
Middlings	47%	35%	1%	6%	1%	0%
Tailings	48%	35%	1%	6%	1%	0%
Sum of streams	48%	35%	1%	6%	1%	0%
Ore	48%	35%	1%	5%	1%	0%

Table A–66: Comparisons of elemental compositions from XRF and XRD for the 0.2-2 µm size fraction

0.2-2 µm	**XRF**					
Stream	**SiO_2**	**Al_2O_3**	**Fe_2O_3**	**K_2O**	**MgO**	**TiO_2**
Primary Froth	43%	26%	15%	2%	1%	3%
Secondary Froth						
Middlings	55%	32%	5%	3%	1%	1%
Tailings	62%	26%	5%	3%	1%	1%
Sum of Streams	56%	30%	6%	3%	1%	1%
Ore	54%	31%	6%	4%	1%	1%
XRD						
Stream	**SiO_2**	**Al_2O_3**	**Fe_2O_3**	**K_2O**	**MgO**	**TiO_2**
Primary Froth	45%	34%	6%	3%	2%	2%
Secondary Froth						
Middlings	48%	34%	3%	4%	2%	1%
Tailings	60%	26%	2%	3%	1%	1%
Sum of streams	51%	32%	3%	4%	2%	1%
Ore	47%	35%	3%	5%	2%	1%

Table A–67: Comparisons of elemental compositions from XRF and XRD for the <2 µm size fraction

<2 µm	XRF					
Stream	**SiO_2**	**Al_2O_3**	**Fe_2O_3**	**K_2O**	**MgO**	**TiO_2**
Primary Froth	43%	25%	15%	2%	1%	2%
Secondary Froth	46%	23%	13%	2%	4%	4%
Middlings	54%	32%	6%	3%	1%	1%
Tailings	59%	27%	5%	3%	1%	1%
Sum of Streams	55%	30%	6%	3%	1%	1%
Ore	54%	31%	6%	4%	1%	1%
XRD						
Stream	**SiO_2**	**Al_2O_3**	**Fe_2O_3**	**K_2O**	**MgO**	**TiO_2**
Primary Froth	45%	34%	5%	4%	2%	2%
Secondary Froth	47%	34%	3%	3%	2%	2%
Middlings	48%	34%	2%	5%	1%	1%
Tailings	57%	29%	1%	4%	1%	1%
Sum of streams	50%	33%	2%	5%	1%	1%
Ore	48%	35%	2%	5%	2%	1%

Table A–68: Comparisons of elemental compositions from XRF and XRD for the 2-45 µm size fraction

2-45 µm	**XRF**					
Stream	**SiO_2**	**Al_2O_3**	**Fe_2O_3**	**K_2O**	**MgO**	**TiO_2**
Primary Froth	51%	14%	16%	1%	1%	11%
Secondary Froth	43%	24%	16%	1%	1%	9%
Middlings	78%	15%	2%	2%	0%	1%
Tailings	91%	5%	1%	1%	0%	0%
Sum of Streams	82%	10%	2%	2%	0%	1%
Ore	67%	21%	4%	3%	1%	1%
XRD						
Stream	**SiO_2**	**Al_2O_3**	**Fe_2O_3**	**K_2O**	**MgO**	**TiO_2**
Primary Froth	57%	11%	10%	2%	0%	12%
Secondary Froth	55%	16%	10%	1%	0%	9%
Middlings	77%	16%	2%	1%	1%	0%
Tailings	95%	4%	0%	1%	0%	0%
Sum of streams	84%	10%	1%	1%	0%	1%
Ore	68%	19%	2%	2%	1%	1%

Table A–69: Comparisons of elemental compositions from XRF and XRD for the <45 µm size fraction

<45 µm	XRF					
Stream	**SiO_2**	**Al_2O_3**	**Fe_2O_3**	**K_2O**	**MgO**	**TiO_2**
Primary Froth	49%	17%	16%	2%	1%	8%
Secondary Froth	44%	23%	15%	2%	2%	7%
Middlings	69%	22%	3%	3%	1%	1%
Tailings	86%	9%	1%	1%	0%	0%
Sum of Streams	74%	16%	4%	2%	0%	1%
Ore	63%	24%	5%	3%	1%	1%
XRD						
Stream	**SiO_2**	**Al_2O_3**	**Fe_2O_3**	**K_2O**	**MgO**	**TiO_2**
Primary Froth	54%	18%	8%	2%	1%	9%
Secondary Froth	51%	24%	7%	2%	1%	6%
Middlings	65%	23%	2%	3%	1%	0%
Tailings	88%	8%	0%	2%	0%	0%
Sum of streams	73%	17%	2%	2%	1%	1%
Ore	62%	24%	2%	3%	1%	1%

Table A–70: Comparisons of elemental compositions from XRF and XRD for the >45 µm size fraction

>45 µm	XRF					
Stream	**SiO_2**	**Al_2O_3**	**Fe_2O_3**	**K_2O**	**MgO**	**TiO_2**
Primary Froth	84%	5%	2%	1%	0%	4%
Secondary Froth	90%	5%	1%	1%	0%	2%
Middlings	56%	32%	5%	3%	1%	1%
Tailings	95%	3%	0%	1%	0%	0%
Sum of Streams	94%	3%	0%	1%	0%	0%
Ore	93%	3%	0%	1%	0%	0%
XRD						
Stream	**SiO_2**	**Al_2O_3**	**Fe_2O_3**	**K_2O**	**MgO**	**TiO_2**
Primary Froth	92%	1%	1%	0%	0%	2%
Secondary Froth	96%	1%	0%	0%	0%	1%
Middlings	55%	28%	3%	1%	1%	3%
Tailings	99%	1%	0%	0%	0%	0%
Sum of streams	98%	1%	0%	0%	0%	0%
Ore	99%	0%	0%	0%	0%	0%

Table A–71: Comparisons of elemental compositions from XRF and XRD for the 45-106 μm size fraction

45-106 μm	XRF					
Stream	**SiO_2**	**Al_2O_3**	**Fe_2O_3**	**K_2O**	**MgO**	**TiO_2**
Primary Froth	68%	8%	5%	1%	1%	10%
Secondary Froth						
Middlings						
Tailings	94%	3%	0%	1%	0%	0%
Sum of Streams	93%	3%	0%	1%	0%	1%
Ore	91%	4%	1%	1%	0%	1%
XRD						
Stream	**SiO_2**	**Al_2O_3**	**Fe_2O_3**	**K_2O**	**MgO**	**TiO_2**
Primary Froth	79%	4%	5%	1%	0%	9%
Secondary Froth						
Middlings						
Tailings	97%	2%	0%	1%	0%	0%
Sum of streams	97%	2%	0%	1%	0%	0%
Ore	97%	1%	0%	0%	0%	0%

Table A–72: Comparisons of elemental compositions from XRF and XRD for the >106 μm size fraction

>106 μm	**XRF**					
Stream	**SiO_2**	**Al_2O_3**	**Fe_2O_3**	**K_2O**	**MgO**	**TiO_2**
Primary Froth	91%	4%	1%	1%	0%	1%
Secondary Froth						
Middlings						
Tailings	95%	3%	0%	0%	0%	0%
Sum of Streams	95%	3%	0%	0%	0%	0%
Ore	93%	2%	0%	0%	0%	0%
XRD						
Stream	**SiO_2**	**Al_2O_3**	**Fe_2O_3**	**K_2O**	**MgO**	**TiO_2**
Primary Froth	98%	0%	0%	0%	0%	0%
Secondary Froth						
Middlings						
Tailings	99%	0%	0%	0%	0%	0%
Sum of streams	99%	0%	0%	0%	0%	0%
Ore	100%	0%	0%	0%	0%	0%

Table A–73: Comparisons of elemental compositions from XRF and XRD around extraction

Sum	XRF					
Stream	**SiO_2**	**Al_2O_3**	**Fe_2O_3**	**K_2O**	**MgO**	**TiO_2**
Primary Froth	67%	11%	9%	1%	1%	6%
Secondary Froth	75%	11%	5%	1%	1%	3%
Middlings	69%	22%	3%	3%	1%	1%
Tailings	94%	4%	0%	1%	0%	0%
Sum of Streams	89%	7%	1%	1%	0%	0%
Ore	83%	10%	2%	1%	0%	1%
XRD						
Stream	**SiO_2**	**Al_2O_3**	**Fe_2O_3**	**K_2O**	**MgO**	**TiO_2**
Primary Froth	74%	9%	5%	1%	0%	6%
Secondary Froth	82%	8%	2%	1%	0%	3%
Middlings	65%	23%	2%	3%	1%	0%
Tailings	97%	2%	0%	1%	0%	0%
Sum of streams	91%	5%	1%	1%	0%	0%
Ore	87%	8%	1%	1%	0%	0%

Appendix B

General Notes on Uncertainty analysis

In the following calculations the symbol δ indicates the actual uncertainty in a number not the relative uncertainty of the number.

Uncertainty in Methylene Blue Analysis

The methylene blue index is given by:

$$MBI = \frac{E \times V}{W} \times 100$$

Where E is the concentration of the methylene blue, V is the volume of methylene blue added to the sample and W is the weight of the sample.

Following the method for propagating uncertainties outlined in "An Introduction to Error Analysis" by John R. Taylor[21], the uncertainty in the methylene blue index can be simplified as:

$$\frac{\delta MBI}{MBI} = \sqrt{\left|\frac{\delta E}{E}\right|^2 + \left|\frac{\delta V}{V}\right|^2 + \left|\frac{\delta W}{W}\right|^2}$$

---

[21] Taylor, J. R. (1982). An introduction to error analysis. Mill Valley California: University Science Books.

According to the ASTM method C-837 (1992), the precision/uncertainty in methylene blue index is 0.25 meq/100g. However, this method assumes the use of 2 g of clay and a Methylene blue concentration of 0.01N. In the CANMET procedure used in this study, the standard method is to use between 0.2-2 grams of clay and a Methylene blue concentration of 0.06N. The increase in MB concentration decreases the precision of the experiment, as the increase in concentration means that the volume required to attain a given MBI will be lower while the uncertainty in the volume remains the same (1mL). Further increase in uncertainty arises when the mass of the sample decreases as that will also decrease the volume required.

Since the values uncertainty in the concentration and the uncertainty in the weight are very small relative to the uncertainty in the volume, they can be neglected from the equation leaving:

$$\frac{\delta MBI}{MBI} \approx \left|\frac{\delta V}{V}\right|$$

Similarly, since the methylene blue surface area is given by Hang and Brindley 1970[22] as: $SA_{MB} = MBI \times 130 \times 0.0602$, the relative uncertainty in the surface area is also the relative uncertainty in the volume.

---

[22] Hang, P. T., and Brindley, G. W (1970). Methylene Blue Adsorption by Clay Minerals. Determination of Surface Areas and Cation exchange capacities. Clays and Clay Minerals 18, 203-212

Uncertainty in Modelled values – peak area, peak position, crystallite size

Topas calculated an error for each parameter output. These errors were assumed to be the error for each refinement.

Uncertainty in % Smectite calculations

There were two components of error in % smectite: firstly, there was the error in calculated peak position for the sample, and secondly, there were the systemic errors in the calculations used to determine the correlation between % smectite and peak position.

The % smectite in either kaolinite-smectite or illite-smectite was given by a linear equation of the form $S = MX + B$, where X was either a peak position or a difference in peak positions. The error in S could therefore be given by:

$$\delta S = \sqrt{(X\delta M)^2 + (M\delta X)^2 + (\delta B)^2}$$

The errors in M and B were calculated using excel's LINEST function which was used to calculate the values of M and B. The error in X is given as the error in peak position as calculated from Topas academic, or if X was a difference in peak positions the error in X was given as the sum of the errors in peak position.

Uncertainty in Quantification

Quantification depends on peak areas and the reference intensity factors as follows:

$$\%X_i = \frac{\dfrac{PeakAreaX_i}{MIFX_i}}{\sum \dfrac{PeakAreaX_i}{MIFX_i}}$$

therefore:

$$\delta\%X_i = \sqrt{\sum\left(\frac{\delta\%X}{PeakArea}\delta PeakArea\right)^2 + \left(\frac{\delta\%X}{MIF}\delta MIF\right)^2}$$

Uncertainty in XRD Surface area calculations

The XRD surface area calculations were dependent on three measured quantities – the crystallite size of each mineral, the % smectite in each mixed layered minerals, and the quantity of each mineral. Unfortunately, none of these errors were insignificant, so a full uncertainty calculation was warranted. There were also the systemic uncertainties in the correlations provided by Nadeau, which were assumed to be negligible.

The total surface area of the material is given by:

$$SA = \sum\left(x_i\left(SB_i + SL_i\right)\right)$$

where x_i is the measure wt% of the i^{th} clay phase, SB_i is the calculated basal surface area for the i^{th} phase and SL_i is the calculated lateral surface area for the i^{th} phase.

Consequently the total uncertainty will be:

$$\delta SA = \sqrt{\sum\left(\left(\delta x_i\left(SB_i + SL_i\right)\right)^2 + \left(x_i \delta SB_i\right)^2 + \left(x_i \delta SL\right)^2\right)}$$

Neglecting the systematic uncertainties in the correlations provided by Nadeau and the errors in density for the different clay minerals, the errors in the lateral and basal surface area were found to depend solely on the errors in fundamental thickness as shown:

$$S_B = \frac{2\times10^3}{\rho T_F} \rightarrow \delta S_B = \frac{-2\times10^3}{\rho 3T_F^2}\delta T_F$$

$$S_L = \frac{3.72\times10^3}{\rho\left(iT_F\right)^{\frac{0..5}{h}}} \rightarrow \delta S_L = \frac{3.72\times10^3}{\rho\left(iT_F\right)^{\frac{1..5}{h}}}\frac{0.5}{h} i\delta T_F$$

For non-swelling clays, fundamental thickness was assumed to be equivalent to the measured crystallite size, and so the error in surface area was dependent solely on measured crystallite size for non-swelling clays. For swelling clays, the fundamental thickness was calculated from the measured thickness and the measured % smectite as follows:

$$T_F = \frac{d_{001}\left(100\tau + \left(d_{S001} - d_{001}\right)S\right)}{\tau S + 100d_{001} + \left(d_{S001} - 2d_{001}\right)S}$$

Where τ is the LVol- IB crystallite size measured in topas academic, d_{S001} is the d spacing of a fully expanded smectite layer (1.7nm), and d_{001} is the d-spacing of the non-swelling layer (1.0nm for illite, 0.712 nm for kaolinite).

Since both τ and *S* are measured values with errors, the error in fundamental thickness for swelling clays can be given by:

$$\delta T_F = \sqrt{\left(\frac{\delta}{\delta\tau}T_F\delta\tau\right)^2 + \left(\frac{\delta}{\delta S}T_F\delta S\right)^2}$$

where

$$\frac{\delta T_F}{\delta\tau} = \frac{100d_{001}\left(\tau S + 100d_{001} + \left(d_{S001} - 2d_{001}\right)S\right) - d_{001}S\left(100\tau + \left(d_{S001} - d_{001}\right)S\right)}{\left(\tau S + 100d_{001} + \left(d_{S001} - 2d_{001}\right)S\right)^2}$$

$$\frac{\delta T_F}{\delta S} = \frac{\left(d_{S001} - d_{001}\right)d_{001}\left(\tau S + 100d_{001} + \left(d_{S001} - 2d_{001}\right)S\right) - d_{001}\left(\tau + \left(d_{S001} - 2d_{001}\right)\right)\left(100\tau + \left(d_{S001} - d_{001}\right)S\right)}{\left(\tau S + 100d_{001} + \left(d_{S001} - 2d_{001}\right)S\right)^2}$$

Uncertainty in TEM Particle size and % Smectite calculations

The error in the TEM particle size measurements was assumed to be the standard deviation of the measurements of each sample.

The % smectite is given as:

$\%S = 100 \times \frac{d_{001}}{T}$ where T is the measured particle thickness and d_{001} is the d-spacing in nm of the 001 reflection for the particle. Therefore, the error in % smectite is simply

$$\%S = \left| 100 \times \frac{-d_{001}}{T^2} \times \delta T \right|$$

Combining data

The data from multiple refinement solutions were combined according to the method of weighted averages using the calculated errors as the weighting factor as follows:

$$w = \left(\frac{1}{\delta X} \right)^2$$

$$\overline{X}_w = \frac{\sum_i X_i w_i}{\sum w_i}$$

$$\delta \overline{X}_w = \left(\sum_i w_i \right)^{-0.5}$$

Where w is the weighting factor, δX is the error in the value X.

Appendix C- Visual basic modules used for solving diffraction patterns

The following five modules were written to help automate the process of solving diffraction patterns. The multiple pattern solver is based on fortran code by Narayan (1986). This code was modified to run through multiple possible phases and multiple diffraction patterns. The code uses the mineral data shown in Table C- 74 (input from an excel worksheet) and calculates d-spacings and interplanar angles for hkl indices between -9,-9,-9, and 999. The code then compares the input measured values of d-spacings and interplanar angle form the diffraction patterns with the calculated values and checks if they match within the tolerance level given (typically 10% of d-spacing and 2° in interplanar angle). When all four input d-spacing and angle combinations have been matched to a set of planes, the zone axes for that solution is calculated and the solution is output to another excel worksheet. The subsequent modules (TitaniumSGcheck, Planecheck, plotcheck, and ZAtype) can then be run to refine the solution. After all the modules are run the useful solutions can be simulated using an electron diffraction simulation program such as Web e-maps or single crystal.

Table C- 74: Mineral phases tested and their structural information

Mineral	a (nm)	b (nm)	c (nm)	α (°)	β (°)	γ (°)	Volume (nm^{3}x10^{-3})	Spacegroup #
anatase	0.379	0.379	0.951	90	90	90	136.3	141
brookite	0.918	0.545	0.515	90	90	90	257.4	61
ferro pseudobrookite	0.375	0.981	1.007	90	90	90	370.2	63
goethite	0.462	0.995	0.302	90	90	90	120.6	62
hematite	0.503	0.503	1.373	90	90	120	347.7	167
ilmenite	0.509	0.509	1.409	90	90	120	316.8	148

lepidocrocite	0.387	1.251	0.306	90	90	90	148.1	63
magnetite	0.840	0.840	0.840	90	90	90	514.6	227
pseudobrookite	0.980	0.998	0.373	90	90	90	364.7	63
pseudorutile	1.438	1.438	0.462	90	90	120	828.0	182
rutile	0.459	0.459	0.296	90	90	90	62.4	136
siderite	0.469	0.469	1.539	90	90	120	338.9	167
wustite	0.431	0.431	0.431	90	90	90	80.2	225

Multiple Pattern Solver

```
Option Explicit
Sub MultiplePatternSolve()

Application.ScreenUpdating = False
'This program is based on the code developed by C. Narayan JOURNAL OF ELECTRON MICROSCOPY
TECHNIQUE 3:151-158 (1986)
'The point of this program is to index diffraction patterns
'This program uses a vector consistency check to reduce the possible combinations

'December 2007
'Updated to check the three radial d-spacings and 1 vector addition d-spacing.

'==================DECLARATION OF VARIABLES============
'Define lattice parameters

Dim a As Single
Dim b As Single
Dim c As Single
Dim alpha As Single
Dim beta As Single
Dim gamma As Single

'define measured data
Dim d1 As Single
Dim d2 As Single
Dim d3 As Single
Dim d4 As Single
Dim angle12 As Single
Dim angle13 As Single
Dim angle23 As Single
Dim angle14 As Single
Dim angle24 As Single


'Other user defined inputs
Dim DErr As Single 'tolerence in d spacing (as a percentage)
Dim AngleErr As Single 'tolerance in angle (absolute value in degrees)
Dim minerals As Integer 'number of minerals to be tested
Dim patterns As Integer 'number of patterns to be tested
Dim SG As Integer 'SG number of mineral
Dim DiffPatternName As String
Dim stream As String 'sampling stream that sample comes from
Dim size As String 'size fraction of sample
Dim treatment As String 'pretreatment for sample
Dim MinName As String

'miller indices
Dim h As Integer '
Dim k As Integer
Dim l As Integer
Dim h3 As Integer
Dim k3 As Integer
Dim l3 As Integer


'loop counters/variables
Dim g As Integer 'counts number of minerals to be tested
Dim i As Integer 'cycles h
Dim j As Integer 'cycles k
Dim m As Integer 'cycles l
Dim i1 As Integer 'counts number of dspacing matches for d1
Dim i2 As Integer 'counts number of d spacing matches for d2
Dim i3 As Integer
Dim i4 As Integer
Dim t1 As Integer
Dim t3 As Integer
Dim t4 As Integer
Dim x As Integer
Dim t2 As Integer
Dim v As Integer
Dim w As Integer
Dim diff As Integer 'counts number of diffraction patterns to be tested


' calculation components
Dim s11 As Double
Dim s22 As Double
Dim s33 As Double
Dim s12 As Double
Dim s13 As Double
Dim s23 As Double
Dim vol As Double 'calculated volume of each crystal structure
Dim P As Double
Dim astar As Double
Dim bstar As Double
Dim cstar As Double
Dim bdotc As Double
Dim adotc As Double
Dim adotb As Double
Dim w11 As Double
Dim w22 As Double
Dim dstar As Double
Dim spacing As Double
Dim x11 As Double
Dim x22 As Double
Dim x33 As Double
Dim x44 As Double
Dim z1 As Double
Dim theta As Double
Dim z2 As Double
Dim theta2 As Double
Dim z3 As Double
Dim theta3 As Double
Dim z4 As Double
Dim theta4 As Double

'other internal variables
```

```
Dim dhkl As Double
Dim hkl1(10000, 3) As Integer
Dim dhkl1(10000) As Double
Dim hkl2(10000, 3) As Integer
Dim dhkl2(10000) As Double
Dim hkl3(10000, 3) As Integer
Dim dhkl3(10000) As Double
Dim hkl4(10000, 3) As Integer
Dim dhkl4(10000) As Double
Dim hkl5(10000, 3) As Integer
Dim dhkl5(10000) As Double
Dim combo1(15000, 12) As Integer
Dim dcomb1(15000, 9) As Double
Dim ZA1(15000, 3) As Integer

'Obtain number of minerals, patterns the tolerances
DErr = Sheets("sheet1").Cells(17, 2)
AngleErr = Sheets("sheet1").Cells(17, 3)
minerals = Sheets("sheet1").Cells(17, 4)
patterns = Sheets("sheet1").Cells(17, 5)

For diff = 1 To patterns 'for 1 - diff for

    'Obtain pattern info
    DiffPatternName = Sheets("Sheet1").Cells(19 + diff, 1)
    stream = Sheets("Sheet1").Cells(19 + diff, 2)
    size = Sheets("Sheet1").Cells(19 + diff, 3)
    treatment = Sheets("Sheet1").Cells(19 + diff, 4)
    d1 = Sheets("Sheet1").Cells(19 + diff, 5)
    d2 = Sheets("Sheet1").Cells(19 + diff, 6)
    d3 = Sheets("Sheet1").Cells(19 + diff, 7)
    d4 = Sheets("Sheet1").Cells(19 + diff, 8)
    angle12 = Sheets("Sheet1").Cells(19 + diff, 9)
    angle13 = Sheets("Sheet1").Cells(19 + diff, 10)
    angle23 = Sheets("Sheet1").Cells(19 + diff, 11)
    angle14 = Sheets("Sheet1").Cells(19 + diff, 12)
    angle24 = Sheets("Sheet1").Cells(19 + diff, 13)

    For g = 1 To minerals 'for 2 start mineral loop

'======================Obtain Mineral data ====================

        MinName = Sheets("Sheet1").Cells(2, 1 + g)
        SG = Sheets("Sheet1").Cells(14, 1 + g)

        'structural information
        a = Sheets("Sheet1").Cells(3, 1 + g)
        b = Sheets("Sheet1").Cells(4, 1 + g)
        c = Sheets("Sheet1").Cells(5, 1 + g)
        alpha = Sheets("Sheet1").Cells(9, 1 + g)
        beta = Sheets("Sheet1").Cells(10, 1 + g)
        gamma = Sheets("Sheet1").Cells(11, 1 + g)

        'Structural calculations
        s11 = (b * c * Sin(alpha)) ^ 2
        s22 = (a * c * Sin(beta)) ^ 2
    s33 = (a * b * Sin(gamma)) ^ 2
    s12 = (Cos(alpha) * Cos(beta) - Cos(gamma)) * a * b * c ^ 2
    s23 = (Cos(gamma) * Cos(beta) - Cos(alpha)) * b * c * a ^ 2
    s13 = (Cos(alpha) * Cos(gamma) - Cos(beta)) * a * c * b ^ 2
    vol = a * b * c * Sqr(1 - (Cos(alpha)) ^ 2 - (Cos(beta)) ^ 2 - (Cos(gamma)) ^ 2 + 2 * Cos(alpha) *
Cos(beta) * Cos(gamma))
    Sheets("Sheet1").Cells(12, 1 + g) = vol
    P = (1 - (Cos(alpha)) ^ 2 - (Cos(beta)) ^ 2 - (Cos(gamma)) ^ 2 + 2 * Cos(alpha) * Cos(beta) *
Cos(gamma))
    astar = (Sin(alpha) / a) ^ 2 * (1 / P)
    bstar = (Sin(beta) / b) ^ 2 * (1 / P)
    cstar = (Sin(gamma) / c) ^ 2 * (1 / P)
    bdotc = 1 / (b * c * P) * (Cos(beta) * Cos(gamma) - Cos(alpha))
    adotc = (Cos(gamma) * Cos(alpha) - Cos(beta)) / (a * c * P)
    adotb = (Cos(beta) * Cos(alpha) - Cos(gamma)) / (a * b * P)


    i3 = 0
    i2 = 0
    i1 = 0
'================finding d1, d2 and d3 possibilities ===================
    For i = -9 To 9 'for 3 i loop
      For j = -9 To 9 'for 4 j loop
        For m = -9 To 9 'for 5 k loop

        h = i
        k = j
        l = m

        If h = 0 And k = 0 And l = 0 Then 'if 1
        Else
            w11 = h ^ 2 * astar + k ^ 2 * bstar + l ^ 2 * cstar
            w22 = 2 * h * k * adotb + 2 * k * l * bdotc + 2 * h * l * adotc
            dstar = w11 + w22

            'calculation of d
            spacing = 1 / Sqr(dstar)

              If spacing >= (d1 * (1 - DErr)) And spacing <= (d1 * (1 + DErr)) Then
                i1 = i1 + 1
                hkl1(i1, 1) = h
                hkl1(i1, 2) = k
                hkl1(i1, 3) = l
                dhkl1(i1) = spacing
'                 Sheets("sheet4").Cells(1 + i1, 1) = MinName
'                 Sheets("sheet4").Cells(1 + i1, 2) = h
'                 Sheets("sheet4").Cells(1 + i1, 3) = k
'                 Sheets("sheet4").Cells(1 + i1, 4) = l
              End If 'end if 2

              If spacing >= (d2 * (1 - DErr)) And spacing <= (d2 * (1 + DErr)) Then
                i2 = i2 + 1
                hkl2(i2, 1) = h
                hkl2(i2, 2) = k
                hkl2(i2, 3) = l
                dhkl2(i2) = spacing
```

```
'               Sheets("sheet4").Cells(1 + i2, 5) = MinName
'                Sheets("sheet4").Cells(1 + i2, 6) = h
'                Sheets("sheet4").Cells(1 + i2, 7) = k
'                Sheets("sheet4").Cells(1 + i2, 8) = l
              End If 'end if 3

              If spacing >= (d3 * (1 - DErr)) And spacing <= (d3 * (1 + DErr)) Then
                i3 = i3 + 1
                hkl3(i3, 1) = h
                hkl3(i3, 2) = k
                hkl3(i3, 3) = l
                dhkl3(i3) = spacing
'                Sheets("sheet4").Cells(1 + i3, 9) = MinName
'                Sheets("sheet4").Cells(1 + i3, 10) = h
'                Sheets("sheet4").Cells(1 + i3, 11) = k
'                Sheets("sheet4").Cells(1 + i3, 12) = l
              End If 'end if 4
        End If 'end if 1

        Next 'end for 5 k loop
      Next 'end for 4 j loop
    Next ' end for 3 i loop


'==========================interplanar angles=========================
    'this calculates the angles measured in reciprocal space
    t1 = 0
    t2 = 0
    t3 = 0
    t4 = 0
    i4 = 0
    If i1 <> 0 And i2 <> 0 And i3 <> 0 Then ' if 5

      For i = 1 To i1 'for 6 i1 loop
        For j = 1 To i2 'for 7 i2 loop
          x11 = s11 * hkl1(i, 1) * hkl2(j, 1) + s22 * hkl1(i, 2) * hkl2(j, 2) + s33 * hkl1(i, 3) * hkl2(j, 3)
          x22 = s23 * (hkl1(i, 2) * hkl2(j, 3) + hkl2(j, 2) * hkl1(i, 3))
          x33 = s13 * (hkl1(i, 3) * hkl2(j, 1) + hkl2(j, 3) * hkl1(i, 1))
          x44 = s12 * (hkl1(i, 1) * hkl2(j, 2) + hkl1(i, 2) * hkl2(j, 1))
          z1 = dhkl1(i) * dhkl2(j) * (x11 + x22 + x33 + x44) / (vol ^ 2)

          If z1 = 1 Then 'if 6

          End If 'end if 6

          If Abs((z1 - 1)) < 0.00001 Then 'if 7
                  theta = 0
          Else
                  If Abs((z1 + 1)) < 0.00001 Then 'if 8
                    theta = 180
                  Else

                    If Abs(z1) > 1 Then  'if 9
                      z1 = Abs(z1) / z1
                      theta = Atn(-z1 / Sqr(-z1 * z1 + 1)) + 2 * Atn(1)
                      theta = theta2 * 180 / 3.14159265358979
```

```
            Else
               theta = Atn(-z1 / Sqr(-z1 * z1 + 1)) + 2 * Atn(1)
               theta = theta * 180 / 3.14159265358979
            End If 'end if 9
          End If 'end if 8
End If 'end if 7

If theta >= (angle12 - AngleErr) And theta <= (angle12 + AngleErr) Then 'if 10

   t1 = t1 + 1

   h3 = hkl1(i, 1) + hkl2(j, 1)
   k3 = hkl1(i, 2) + hkl2(j, 2)
   l3 = hkl1(i, 3) + hkl2(j, 3)

    w11 = h3 ^ 2 * astar + k3 ^ 2 * bstar + l3 ^ 2 * cstar
    w22 = 2 * h3 * k3 * adotb + 2 * k3 * l3 * bdotc + 2 * h3 * l3 * adotc
    dstar = w11 + w22

   spacing = 1 / Sqr(dstar)


    If spacing >= (d4 * (1 - DErr)) And spacing <= (d4 * (1 + DErr)) Then 'if 11
         i4 = i4 + 1
         hkl4(i4, 1) = h3
         hkl4(i4, 2) = k3
         hkl4(i4, 3) = l3
         dhkl4(i4) = spacing

         'calculating the angle between d4 and d1
         x11 = s11 * hkl1(i, 1) * h3 + s22 * hkl1(i, 2) * k3 + s33 * hkl1(i, 3) * l3
         x22 = s23 * (hkl1(i, 2) * l3 + k3 * hkl1(i, 3))
         x33 = s13 * (hkl1(i, 3) * h3 + l3 * hkl1(i, 1))
         x44 = s12 * (hkl1(i, 1) * k3 + hkl1(i, 2) * h3)
         z2 = dhkl1(i) * dhkl4(i4) * (x11 + x22 + x33 + x44) / (vol ^ 2)

         If Abs((z2 - 1)) < 0.00001 Then 'if 12
           theta2 = 0
         Else
            If Abs((z2 + 1)) < 0.00001 Then 'if 13                        theta2 = 180
            Else

               If Abs(z2) > 1 Then 'if 14
                  z2 = Abs(z2) / z2
                  theta2 = Atn(-z2 / Sqr(-z2 * z2 + 1)) + 2 * Atn(1)
                  theta2 = theta2 * 180 / 3.14159265358979
               Else
                  theta2 = Atn(-z2 / Sqr(-z2 * z2 + 1)) + 2 * Atn(1)
                  theta2 = theta2 * 180 / 3.14159265358979
               End If 'end if 14
            End If 'end if 13
         End If 'end if 12

         If theta2 >= (angle14 - AngleErr) And theta2 <= (angle14 + AngleErr) Then 'if 15
            t2 = t2 + 1
```

```
'checking angle between d2 and d4
x11 = s11 * hkl2(j, 1) * h3 + s22 * hkl2(j, 2) * k3 + s33 * hkl2(j, 3) * l3
x22 = s23 * (hkl2(j, 2) * l3 + k3 * hkl2(j, 3))
x33 = s13 * (hkl2(j, 3) * h3 + l3 * hkl2(j, 1))
x44 = s12 * (hkl2(j, 1) * k3 + hkl2(j, 2) * h3)
z3 = dhkl2(j) * dhkl4(i4) * (x11 + x22 + x33 + x44) / (vol ^ 2)


If Abs((z3 - 1)) < 0.00001 Then 'if 16
 theta3 = 0
Else
  If Abs((z3 + 1)) < 0.00001 Then 'if 17
    theta3 = 180
  Else

    If Abs(z3) > 1 Then 'if 18
      z3 = Abs(z3) / z3
      theta3 = Atn(-z3 / Sqr(-z3 * z3 + 1)) + 2 * Atn(1)
      theta3 = theta3 * 180 / 3.14159265358979
    Else
      theta3 = Atn(-z3 / Sqr(-z3 * z3 + 1)) + 2 * Atn(1)
      theta3 = theta3 * 180 / 3.14159265358979
    End If 'end if 18
  End If 'end if 17
End If 'end if 16


If theta3 >= (angle24 - AngleErr) And theta3 <= (angle24 + AngleErr) Then 'if 19
  t3 = t3 + 1

End If '19a

  For m = 1 To i3 'for 8 m loop
     'checking angle between d1 and d3
    x11 = s11 * hkl1(i, 1) * hkl3(m, 1) + s22 * hkl1(i, 2) * hkl3(m, 2) + s33 * hkl1(i,
    3) * hkl3(m, 3)
   x22 = s23 * (hkl1(i, 2) * hkl3(m, 3) + hkl3(m, 2) * hkl1(i, 3))
   x33 = s13 * (hkl1(i, 3) * hkl3(m, 1) + hkl3(m, 3) * hkl1(i, 1))
   x44 = s12 * (hkl1(i, 1) * hkl3(m, 2) + hkl1(i, 2) * hkl3(m, 1))
   z4 = dhkl1(i) * dhkl3(m) * (x11 + x22 + x33 + x44) / (vol ^ 2)


   If Abs((z4 - 1)) < 0.00001 Then 'if 20
    theta4 = 0
   Else
     If Abs((z4 + 1)) < 0.00001 Then 'if 21
       theta4 = 180
     Else

       If Abs(z4) > 1 Then 'if 22
         z4 = Abs(z4) / z4
         theta4 = Atn(-z4 / Sqr(-z4 * z4 + 1)) + 2 * Atn(1)
         theta4 = theta4 * 180 / 3.14159265358979
       Else
         theta4 = Atn(-z4 / Sqr(-z4 * z4 + 1)) + 2 * Atn(1)
```

```
           theta4 = theta4 * 180 / 3.14159265358979
         End If 'end if 22
       End If 'end if 21
     End If 'end if 20



 If theta4 >= (angle13 - AngleErr) And theta4 <= (angle13 + AngleErr) Then 'if 23

     t4 = t4 + 1


     v = v + 1
     For x = 1 To 3 'for 9 x loop
       combo1(t4, x) = hkl1(i, x)
       combo1(t4, x + 3) = hkl2(j, x)
       combo1(t4, x + 6) = hkl3(m, x)
     Next 'end for 9 x loop

     combo1(t4, 10) = h3
     combo1(t4, 11) = k3
     combo1(t4, 12) = l3


     dcomb1(t4, 1) = dhkl1(i)
     dcomb1(t4, 2) = dhkl2(j)
     dcomb1(t4, 3) = dhkl3(k)
     dcomb1(t4, 4) = dhkl4(i4)
     dcomb1(t4, 5) = theta
     dcomb1(t4, 6) = theta2
     dcomb1(t4, 7) = theta3
     dcomb1(t4, 8) = theta4

      ZA1(t4, 1) = combo1(t4, 2) * combo1(t4, 6) - combo1(t4, 5) * combo1(t4, 3)
     ' ZA1(t4, 2) = -1 * (combo1(t4, 1) * combo1(t4, 6) - combo1(t4, 4) * combo1(t4,
     3))
      ZA1(t4, 3) = combo1(t4, 1) * combo1(t4, 5) - combo1(t4, 4) * combo1(t4, 2)

      ZA1(t4, 1) = hkl1(i, 2) * hkl2(j, 3) - hkl2(j, 2) * hkl1(i, 3)
      ZA1(t4, 2) = -1 * (hkl1(i, 1) * hkl2(j, 3) - hkl2(j, 1) * hkl1(i, 3))
      ZA1(t4, 3) = hkl1(i, 1) * hkl2(j, 2) - hkl2(j, 1) * hkl1(i, 2)


      Sheets("sheet2").Cells(1 + v, 1) = DiffPatternName
      Sheets("sheet2").Cells(1 + v, 2) = stream
      Sheets("sheet2").Cells(1 + v, 3) = size
      Sheets("sheet2").Cells(1 + v, 4) = treatment
      Sheets("sheet2").Cells(1 + v, 5) = DErr
      Sheets("sheet2").Cells(1 + v, 6) = AngleErr
     Sheets("sheet2").Cells(1 + v, 7) = MinName
     Sheets("sheet2").Cells(1 + v, 8) = SG


      For l = 1 To 3 'for 10 l loop
          Sheets("sheet2").Cells(1 + v, 8 + l) = combo1(t4, l)
```

```
                                       Sheets("sheet2").Cells(1 + v, 11 + l) = combo1(t4, l + 3)
                                       Sheets("sheet2").Cells(1 + v, 14 + l) = combo1(t4, l + 6)
                                       Sheets("sheet2").Cells(1 + v, 17 + l) = combo1(t4, l + 9)
                                       Sheets("sheet2").Cells(1 + v, 20 + l) = dcomb1(t4, l)
                                       Sheets("sheet2").Cells(1 + v, 23 + l) = dcomb1(t4, l + 3)
                                       Sheets("sheet2").Cells(1 + v, 28 + l) = ZA1(t4, l)
                                 Next 'end for 10

                                 Sheets("sheet2").Cells(1 + v, 27) = dcomb1(t4, 7)
                                 Sheets("sheet2").Cells(1 + v, 28) = dcomb1(t4, 8)
                              End If 'end if 23
                              Next ' end for 8 - i3 loop
'                          End If 'end if 19

                          End If 'end if 15

                  End If' end if 11




               End If 'end if 10

            Next 'end for 7 - i2 loop
        Next 'end for 6 - i1 loop

     End If 'end if 5
'   w = w + 1
'
'       Sheets("sheet4").Cells(1 + w, 1) = DiffPatternName
'       Sheets("sheet4").Cells(1 + w, 2) = stream
'       Sheets("sheet4").Cells(1 + w, 3) = size
'       Sheets("sheet4").Cells(1 + w, 4) = treatment
'        Sheets("sheet4").Cells(1 + w, 5) = DErr
'       Sheets("sheet4").Cells(1 + w, 6) = AngleErr
'       Sheets("sheet4").Cells(1 + w, 7) = MinName
'       Sheets("sheet4").Cells(1 + w, 8) = SG
'      Sheets("sheet4").Cells(1 + w, 9) = i1
'Sheets("sheet4").Cells(1 + w, 10) = i2
'Sheets("sheet4").Cells(1 + w, 11) = i3
'Sheets("sheet4").Cells(1 + w, 12) = i4
'Sheets("sheet4").Cells(1 + w, 13) = t1
'Sheets("sheet4").Cells(1 + w, 14) = t2
'Sheets("sheet4").Cells(1 + w, 15) = t3
'Sheets("sheet4").Cells(1 + w, 16) = t4
   Next 'end for 2 - mineral loop
Next 'end for 1 diff pattern loop
End Sub
```

Allowed reflection checker

```
Sub TitaniumSGcheck()
Application.ScreenUpdating = False


Dim rows As Integer
Dim hkls As Integer
Dim h As Integer
Dim k As Integer
Dim l As Integer
Dim check1 As Boolean
Dim check2 As Boolean
Dim check3 As Boolean
Dim special1 As Boolean
Dim special2 As Boolean
Dim mineral As String
Dim nrows As Integer
Dim SG As Integer


nrows = Application.InputBox(prompt:="enter the number of rows", Type:=1)
MsgBox nrows

For rows = 2 To nrows
   mineral = Sheet2.Cells(rows, 7)
   SG = Sheet2.Cells(rows, 8)


    For hkls = 1 To 4
      h = Sheet2.Cells(rows, (8 + (hkls * 3) - 2))
      k = Sheet2.Cells(rows, (8 + (hkls * 3) - 1))
      l = Sheet2.Cells(rows, (8 + (hkls * 3)))




      If SG = 61 Then

         check1 = False
         check2 = False
         check3 = False
         special1 = False
         special2 = False

         If h = 0 Then
            If k Mod 2 = 0 Then
               check1 = True
            End If
         Else
            check1 = True
         End If

         If k = 0 Then
         If l Mod 2 = 0 Then
```

```
          check2 = True
    End If
  Else
   check2 = True
  End If

  If l = 0 Then
  If h Mod 2 = 0 Then
      check3 = True
    End If
  Else
  check3 = True
  End If

  If (h + k) Mod 2 = 0 Then
      special1 = True
    End If

  If (k + l) Mod 2 = 0 Then
      special2 = True
  End If


  If check1 And check2 And check3 = True Then
   If special1 And special2 = True Then
     Sheet2.Cells(rows, 52 + hkls) = "all met"
    Else
     Sheet2.Cells(rows, 52 + hkls) = "general met"
  End If
  Else
    Sheet2.Cells(rows, 52 + hkls) = "failed"
  End If
End If

If SG = 62 Then
  check1 = False
  check2 = False
  check3 = False
  special1 = False
  special2 = False

  If h = 0 Then
    If (k + l) Mod 2 = 0 Then
      check1 = True
    End If
  Else
    check1 = True
  End If

  If l = 0 Then
  If h Mod 2 = 0 Then
      check2 = True
    End If
  Else
  check2 = True
  End If
```

```
   If (h + l) Mod 2 = 0 Then
           special1 = True
       End If

   If k Mod 2 = 0 Then
           special2 = True
   End If


   If check1 And check2 = True Then
     If special1 And special2 = True Then
        Sheet2.Cells(rows, 52 + hkls) = "all met"
       Else
        Sheet2.Cells(rows, 52 + hkls) = "general met"
    End If
    Else
     Sheet2.Cells(rows, 52 + hkls) = "failed"
    End If
End If

If SG = 63 Then

    check1 = False
    check2 = False
    check3 = False
    special1 = False
    special2 = False


     If (h + k) Mod 2 = 0 Then
         check1 = True
     End If


    If k = 0 Then
    If l Mod 2 = 0 Then
            check2 = True
        End If
    Else
    check2 = True
    End If

    If l Mod 2 = 0 Then
            special1 = True
        End If

    If h Mod 2 = 0 And l Mod 2 = 0 Then
            special2 = True
    End If


    If check1 And check2 = True Then
      If special1 And special2 = True Then
         Sheet2.Cells(rows, 52 + hkls) = "all met"
        Else
        Sheet2.Cells(rows, 52 + hkls) = "general met"
    End If
    Else
     Sheet2.Cells(rows, 52 + hkls) = "failed"
    End If
End If

If SG = 136 Then
   check1 = False
    special1 = False
    special2 = False

 If h = 0 Then
        If (k + l) Mod 2 = 0 Then
            check1 = True
        End If
     Else
        check1 = True
     End If

 If (h + k) Mod 2 = 0 And l Mod 2 = 0 Then
         special1 = True
      End If

 If (h + k + l) Mod 2 = 0 Then
             special2 = True
         End If


     If check1 = True Then
       If special1 And special2 = True Then
          Sheet2.Cells(rows, 52 + hkls) = "all met"
         Else
             If special1 = True Then
             Sheet2.Cells(rows, 52 + hkls) = "general + special 1 met"
             End If

             If special2 = True Then
             Sheet2.Cells(rows, 52 + hkls) = "general + special 2 met"
             End If
          Sheet2.Cells(rows, 52 + hkls) = "general met"
         End If
     Else
       Sheet2.Cells(rows, 52 + hkls) = "failed"
     End If

  End If

  If SG = 141 Then
       check1 = False
       check2 = False
       check3 = False
      special1 = False
      special2 = False
      special3 = False
      'Some Special conditions missing
      If (h + k + l) Mod 2 = 0 Then
            check1 = True
       End If


       If l = 0 Then
          If h Mod 2 = 0 Then
          check2 = True
          End If
       Else
       check2 = True
       End If

        If h = k Then
          If (2 * h + l) Mod 4 = 0 Then
          check3 = True
          End If
       Else
       check3 = True
       End If

       If (2 * k + l) Mod 2 <> 0 Or (2 * k + l) Mod 4 = 0 Then
       special1 = True
       End If

     '
     '   If Application.WorksheetFunction.IsOdd(h + k) = True Or
Application.WorksheetFunction.IsOdd(l) = True Or (2 * k + l) Mod 4 = 0 Then
     '  special2 = True
     '  End If

       If check1 = True And check2 = True And check3 = True Then
           If special1 = True Then
             Sheet2.Cells(rows, 52 + hkls) = "all met"
          Else
     '       If special1 = True Then
     '       Sheet2.Cells(rows, 52 + hkls) = "general + special 1 met"
     '       End If
     '
     '       If special2 = True Then
     '       Sheet2.Cells(rows, 52 + hkls) = "general + special 2 met"
     '       End If
           Sheet2.Cells(rows, 52 + hkls) = "general met"
          End If
        Else
        Sheet2.Cells(rows, 52 + hkls) = "failed"
        End If
     End If


     If SG = 148 Then
       check1 = False

       If (-h + k + l) Mod 3 = 0 Then
             check1 = True
        End If
```

```
   If check1 = True Then
         Sheet2.Cells(rows, 52 + hkls) = "general met"

   Else
    Sheet2.Cells(rows, 52 + hkls) = "failed"
   End If

End If


If SG = 167 Then
  check1 = False
    check2 = False
   special1 = False

  If (-h + k + l) Mod 3 = 0 Then
         check1 = True
   End If


   If k = -h Then
      If l Mod 3 = 0 And l Mod 2 = 0 Then
      check2 = True
      End If
   Else
   check2 = True
   End If

   If l Mod 2 = 0 Then
   special1 = True
   End If

   If check1 = True And check2 = True Then
       If special1 = True Then
          Sheet2.Cells(rows, 52 + hkls) = "all met"
      Else
       Sheet2.Cells(rows, 52 + hkls) = "general met"
      End If
   Else
    Sheet2.Cells(rows, 52 + hkls) = "failed"
   End If

End If

If SG = 182 Then
  check1 = False
    special1 = False
    special2 = False
    special3 = False
    special4 = False

   If h = k = 0 Then
    If l Mod 2 = 0 Then
```

```
        check1 = True
 End If
Else
check1 = True
End If


 If h = k Then
    If l Mod 2 = 0 Then
    special1 = True
    End If
 Else
    special1 = True
 End If

 If h = -k Then
    If l Mod 2 = 0 Then
    special2 = True
    End If
 Else
    special2 = True
 End If

 If (h - k) Mod 3 = 0 Then
    If l Mod 2 = 0 Then
    special3 = True
    End If
 Else
    special3 = True
 End If

 If l Mod 2 = 0 Then
 special4 = True
 End If


 If check1 = True Then
     If special1 = True And special2 = True And special3 = True And special4 = True Then
       Sheet2.Cells(rows, 52 + hkls) = "all met"
    Else
       If special1 = True Then
       Sheet2.Cells(rows, 52 + hkls) = "general + special 1 met"
       End If

       If special2 = True Then
       Sheet2.Cells(rows, 52 + hkls) = "general + special 2 met"
       End If

       If special3 = True Then
       Sheet2.Cells(rows, 52 + hkls) = "general + special 3 met"
       End If

       If special4 = True Then
       Sheet2.Cells(rows, 52 + hkls) = "general + special 4 met"
       End If
     Sheet2.Cells(rows, 52 + hkls) = "general met"
```

```
      End If
    Else
     Sheet2.Cells(rows, 52 + hkls) = "failed"
    End If
End If


If SG = 225 Then
          check1 = False
      special1 = False

    If (h + k) Mod 2 = 0 And (k + l) Mod 2 = 0 And (l + h) Mod 2 = 0 Then
    check1 = True
    End If

    If h Mod 2 = 0 And k Mod 2 = 0 And l Mod 2 = 0 Then
    special1 = True
    End If

    If check1 = True Then
          If special1 = True Then
             Sheet2.Cells(rows, 52 + hkls) = "all met"
         Else
             Sheet2.Cells(rows, 52 + hkls) = "general met"
         End If

    Else
    Sheet2.Cells(rows, 52 + hkls) = "failed"
    End If

End If

If SG = 227 Then
    check1 = False
    check2 = False
    special1 = False

        If (h + k) Mod 2 = 0 And (k + l) Mod 2 = 0 And (l + h) Mod 2 = 0 Then
      check1 = True
      End If

         If h = 0 Then
            If k Mod 2 = 0 And l Mod 2 = 0 And (k + l) Mod 4 = 0 Then
            check2 = True
            End If
         Else
         check2 = True
         End If


       If (h + k + l) Mod 2 <> 0 Or (h + k + l) Mod 4 = 0 Then
       special1 = True
       End If


       If check1 = True And check2 = True Then
```

```
            If special1 = True Then
              Sheet2.Cells(rows, 52 + hkls) = "all met"
            Else
              Sheet2.Cells(rows, 52 + hkls) = "general met"
            End If

        Else
        Sheet2.Cells(rows, 52 + hkls) = "failed"
        End If

    End If
  Next
Next

End Sub
```

Smallest planes checker

```
Sub planeCheck()

Application.ScreenUpdating = False

Dim rows As Integer
Dim hkls As Integer
Dim h As Integer
Dim k As Integer
Dim l As Integer
Dim check1 As Boolean
Dim check2 As Boolean
Dim check3 As Boolean
Dim special1 As Boolean
Dim special2 As Boolean
Dim mineral As String
Dim gcd(3) As Integer

nrows = Application.InputBox(prompt:="enter the number of rows", Type:=1)



For rows = 2 To nrows
mineral = Sheet1.Cells(rows, 7)
SG = Sheet2.Cells(rows, 8)

  For hkls = 1 To 3

      h = Sheet2.Cells(rows, (8 + (hkls * 3) - 2))
      k = Sheet2.Cells(rows, (8 + (hkls * 3) - 1))
      l = Sheet2.Cells(rows, (8 + (hkls * 3)))
      gcd(hkls) = Sheet2.Cells(rows, 48 + hkls)

      If gcd(hkls) = 1 Then '=================================GCD
check==========================
        Sheet2.Cells(rows, 58 + hkls) = "gcd pass"

      Else
        h = h / gcd(hkls)
        k = k / gcd(hkls)
        l = l / gcd(hkls)

          If SG = 61 Then

          check1 = False
          check2 = False
          check3 = False
          special1 = False
          special2 = False

          If h = 0 Then
            If k Mod 2 = 0 Then
              check1 = True
            End If
          Else
```

```
     check1 = True
  End If

  If k = 0 Then
  If l Mod 2 = 0 Then
              check2 = True
     End If
  Else
    check2 = True
  End If

  If l = 0 Then
  If h Mod 2 = 0 Then
        check3 = True
     End If
  Else
  check3 = True
  End If

  If (h + k) Mod 2 = 0 Then
        special1 = True
     End If

  If (k + l) Mod 2 = 0 Then
        special2 = True
  End If


  If check1 And check2 And check3 = True Then
     Sheet2.Cells(rows, 58 + hkls) = "gcd fail"
  Else
     Sheet2.Cells(rows, 58 + hkls) = "gcd pass"
  End If
End If

If SG = 62 Then
   check1 = False
   check2 = False
   check3 = False
   special1 = False
   special2 = False

   If h = 0 Then
      If (k + l) Mod 2 = 0 Then
         check1 = True
      End If
   Else
      check1 = True
   End If

   If l = 0 Then
   If h Mod 2 = 0 Then
         check2 = True
      End If
   Else
   check2 = True
```

```
    End If

    If (h + l) Mod 2 = 0 Then
          special1 = True
       End If

    If k Mod 2 = 0 Then
          special2 = True
    End If


    If check1 And check2 = True Then
     Sheet2.Cells(rows, 58 + hkls) = "gcd fail"
    Else
      Sheet2.Cells(rows, 58 + hkls) = "gcd pass"
    End If
End If

If SG = 63 Then

    check1 = False
    check2 = False
    check3 = False
    special1 = False
    special2 = False


     If (h + k) Mod 2 = 0 Then
        check1 = True
     End If


    If k = 0 Then
    If l Mod 2 = 0 Then
          check2 = True
       End If
    Else
    check2 = True
    End If

    If l Mod 2 = 0 Then
          special1 = True
       End If

    If h Mod 2 = 0 And l Mod 2 = 0 Then
          special2 = True
    End If


    If check1 And check2 = True Then
     Sheet2.Cells(rows, 58 + hkls) = "gcd fail"
    Else
      Sheet2.Cells(rows, 58 + hkls) = "gcd pass"
    End If
End If
```

```
If SG = 136 Then
  check1 = False
   special1 = False
   special2 = False

 If h = 0 Then
      If (k + l) Mod 2 = 0 Then
         check1 = True
      End If
   Else
      check1 = True
   End If

 If (h + k) Mod 2 = 0 And l Mod 2 = 0 Then
       special1 = True
    End If

 If (h + k + l) Mod 2 = 0 Then
         special2 = True
      End If


    If check1 = True Then
     Sheet2.Cells(rows, 58 + hkls) = "gcd fail"
    Else
      Sheet2.Cells(rows, 58 + hkls) = "gcd pass"
    End If

 End If

 If SG = 141 Then
     check1 = False
     check2 = False
     check3 = False
    special1 = False
    special2 = False
    special3 = False
    'Some Special conditions missing
    If (h + k + l) Mod 2 = 0 Then
          check1 = True
     End If


     If l = 0 Then
        If h Mod 2 = 0 Then
        check2 = True
        End If
     Else
     check2 = True
     End If

     If h = k Then
        If (2 * h + l) Mod 4 = 0 Then
        check3 = True
        End If
     Else
```

```
      check3 = True
      End If

      If (2 * k + l) Mod 2 <> 0 Or (2 * k + l) Mod 4 = 0 Then
      special1 = True
      End If

    '
    '   If Application.WorksheetFunction.IsOdd(h + k) = True Or
Application.WorksheetFunction.IsOdd(l) = True Or (2 * k + l) Mod 4 = 0 Then
    '   special2 = True
    '   End If

      If check1 = True And check2 = True And check3 = True Then
      Sheet2.Cells(rows, 58 + hkls) = "gcd fail"
      Else
        Sheet2.Cells(rows, 58 + hkls) = "gcd pass"
      End If
    End If

    If SG = 148 Then
      check1 = False

      If (-h + k + l) Mod 3 = 0 Then
            check1 = True
      End If



      If check1 = True Then
      Sheet2.Cells(rows, 58 + hkls) = "gcd fail"
      Else
        Sheet2.Cells(rows, 58 + hkls) = "gcd pass"
      End If

    End If


    If SG = 167 Then
      check1 = False
        check2 = False
       special1 = False

      If (-h + k + l) Mod 3 = 0 Then
            check1 = True
       End If


       If k = -h Then
         If l Mod 3 = 0 And l Mod 2 = 0 Then
         check2 = True
         End If
       Else
       check2 = True
       End If
```

```
  If l Mod 2 = 0 Then
  special1 = True
  End If

  If check1 = True And check2 = True Then
      Sheet2.Cells(rows, 58 + hkls) = "gcd fail"
  Else
    Sheet2.Cells(rows, 58 + hkls) = "gcd pass"
  End If

End If

If SG = 182 Then
 check1 = False
   special1 = False
   special2 = False
   special3 = False
   special4 = False

  If h = k = 0 Then
   If l Mod 2 = 0 Then
           check1 = True
   End If
  Else
  check1 = True
  End If


   If h = k Then
      If l Mod 2 = 0 Then
      special1 = True
      End If
   Else
      special1 = True
   End If

    If h = -k Then
      If l Mod 2 = 0 Then
      special2 = True
      End If
    Else
      special2 = True
    End If

    If (h - k) Mod 3 = 0 Then
       If l Mod 2 = 0 Then
       special3 = True
       End If
    Else
       special3 = True
    End If

    If l Mod 2 = 0 Then
    special4 = True
    End If
  If check1 = True Then
    Sheet2.Cells(rows, 58 + hkls) = "gcd fail"
   Else
     Sheet2.Cells(rows, 58 + hkls) = "gcd pass"
   End If
End If


If SG = 225 Then
          check1 = False
      special1 = False

   If (h + k) Mod 2 = 0 And (k + l) Mod 2 = 0 And (l + h) Mod 2 = 0 Then
   check1 = True
   End If

   If h Mod 2 = 0 And k Mod 2 = 0 And l Mod 2 = 0 Then
   special1 = True
   End If

   If check1 = True Then
       Sheet2.Cells(rows, 58 + hkls) = "gcd fail"
   Else
     Sheet2.Cells(rows, 58 + hkls) = "gcd pass"
   End If

End If

If SG = 227 Then
   check1 = False
   check2 = False
   special1 = False

        If (h + k) Mod 2 = 0 And (k + l) Mod 2 = 0 And (l + h) Mod 2 = 0 Then
      check1 = True
      End If

         If h = 0 Then
            If k Mod 2 = 0 And l Mod 2 = 0 And (k + l) Mod 4 = 0 Then
            check2 = True
            End If
         Else
         check2 = True
         End If


       If (h + k + l) Mod 2 <> 0 Or (h + k + l) Mod 4 = 0 Then
       special1 = True
       End If


       If check1 = True And check2 = True Then
          Sheet2.Cells(rows, 58 + hkls) = "gcd fail"
       Else
         Sheet2.Cells(rows, 58 + hkls) = "gcd pass"
```

```
                End If

            End If
         End If
      Next
   Next
   End Sub
```

Plotable pattern checker

```
Sub plotcheck()
Application.ScreenUpdating = False

Dim hkl(3) As String
Dim rows As Integer
Dim hkls As Integer
Dim gcd(3) As String

nrows = Application.InputBox(prompt:="enter the number of rows", Type:=1)


For rows = 2 To nrows
fail = 0
For hkls = 1 To 3
   hkl(hkls) = Sheet2.Cells(rows, 52 + hkls)
   If hkl(hkls) = "failed" Then
      fail = fail + 1
   End If

Next

For hkls = 1 To 3
   gcd(hkls) = Sheet2.Cells(rows, 58 + hkls)
  Next



If fail > 1 Then
Sheet2.Cells(rows, 57) = "failed"
Else
Sheet2.Cells(rows, 57) = "pass"
End If
'
If gcd(1) = "gcd pass" And gcd(2) = "gcd pass" And gcd(3) = "gcd pass" Then
Sheet2.Cells(rows, 58) = "gcd pass"
Else
Sheet2.Cells(rows, 58) = "gcd fail"
End If

Next
End Sub
```

Zone axes type definer

```
Sub ZAtype()

Dim rows As Integer
nrows = Application.InputBox(prompt:="enter the number of rows", Type:=1)
MsgBox nrows

For rows = 2 To nrows
    mineral = Sheet2.Cells(rows, 7)
     ZA = Sheet2.Cells(rows, 36)
     HexZa = Sheet2.Cells(rows, 47)

   If mineral = "brookite" Or mineral = "Goethite" Or mineral = "pseudobrookite" Or mineral =
"Lepidocrocite" Or mineral = "ferro pseudobrookite" Then
         Sheet2.Cells(rows, 48) = ZA
   End If

   If mineral = "Ilmenite" Or mineral = "Hematite" Or mineral = "siderite" Or mineral = "pseudorutile"
Then
      Sheet2.Cells(rows, 48) = HexZa
   End If

   If mineral = "rutile" Or mineral = "anatase" Then
      h = Abs(Sheet2.Cells(rows, 33))
      k = Abs(Sheet2.Cells(rows, 34))
      l = Abs(Sheet2.Cells(rows, 35))
      newh = WorksheetFunction.Max(h, k)
      newk = WorksheetFunction.Min(h, k)
      Sheet2.Cells(rows, 48) = "<" & newh & newk & l & ">"
   End If

  If mineral = "wustite" Or mineral = "magnetite" Then
      h = Abs(Sheet2.Cells(rows, 33))
      k = Abs(Sheet2.Cells(rows, 34))
      l = Abs(Sheet2.Cells(rows, 35))
      newh = WorksheetFunction.Max(h, k, l)
      newl = WorksheetFunction.Min(h, k, l)
      newk = 0

      If h < newh And h > newl Then
         newk = h
      End If

      If k < newh And k > newl Then
         newk = k
      End If

      If l < newh And l > newl Then
         newk = l
      End If

      If newk = 0 Then
         newk = newl
      End If
      Sheet2.Cells(rows, 48) = "<" & newh & " " & newk & " " & newl & ">"
   End If
Next
End Sub
```